FATIGUE BEHAVIOUR OF SURFACE CRACKS IN BUTT-WELDED JOINTS

by

Shahram Parsapour Moghadam BSc (Eng), MSc

A thesis submitted for the degree of
Doctor of Philosophy of the
University of London, and for the
Diploma of Membership of Imperial College

February 1984



Department of Mechanical Engineering
Imperial College of Science and Technology
University of London
London SW7 2BX

ABSTRACT

The growth of surface cracks with resulting, possibly catastrophic, failure in welded joints used for offshore purposes has been of considerable concern in recent years. The present thesis attempts to describe how such failure can be predicted using linear fracture mechanics. The approach requires fatigue crack growth data for the materials associated with a butt-welded joint, weld metal, HAZ, and parent material as well as a correlation for the stress intensity factor of semi-elliptical crack propagation both on the surface and in the through-thickness direction.

These and other properties were found for BS4360-50D, class 6 weld metal, and HAZ associated with the parent metal and weldment, as currently used for construction of North Sea oil platforms. The effects of stress ratio, loading frequency, specimen geometry, and salt-water environment were investigated. The stress intensity factor calibration for semi-elliptical cracks that gave the best correlation with the data from through-thickness cracks was found from the literature.

To obtain basic crack propagation data, tests were conducted on standard compact type specimens. Fatigue crack growth tests were also performed on surface-notched plates in bending. These tests covered the full subcritical range of growth rates from ΔK_{th} to high values of ΔK. The results showed that the growth rates of surface cracks in the

weldment were higher than for the parent plate and that in general the fatigue crack growth rates increase with increase in stress ratio and decrease in frequency. The use of an A.C. potential drop microgauge for crack depth measurements was also investigated. It was found that the variation of the digital voltage with crack depth is linear, and that increasing the gain results in a corresponding increase in sensitivity without affecting the linearity.

A model which can accommodate the fatigue crack propagation on the surface as well as for the crack in the through-thickness direction was developed to predict the growth of semi-elliptical cracks. The influence of initial flaw size on the shape and size of growing fatigue cracks was investigated, together with the effect of different width and thickness, using this model.

Finally an attempt was made to suggest ways to improve the fatigue properties of butt-welded joints. Preliminary tests showed that the technique developed to fabricate the butt-welded specimens reduced the rate fatigue crack growth when compared to the weldments fabricated by conventional methods.

To my Mother

ACKNOWLEDGEMENTS

The author wishes to thank his supervisor, Dr. J.C. Radon, whose approachability during the course of this work is particularly appreciated.

Special thanks are due to Dr. T.J. Baker of the Department of Metallurgy for his comments on fractographs and the metallurgy of welds, to Mr. C.E. Noad for his perfectionism in the final preparation of this work, and also to members of the technical staff in the laboratories and in the departmental workshop.

Finally, the author is indebted to his parents for their endless forbearance and encouragement.

CONTENTS

	Page
Title Page	1
Abstract	2
Acknowledgements	4
Contents	5
Nomenclature	11
CHAPTER 1: INTRODUCTION	
1.1 Background	15
1.2 Objectives	16
1.3 Outline of the Work	17
1.3.1 Crack Growth Behaviour of BS4360-50D Welded steel	17
1.3.2 Growth of Semi-Elliptical Surface Cracks in BS4360-50D Welded Steel	17
1.3.3 Computer Simulation of Surface Crack Propagation	17
1.3.4 An Attempt to Improve Fatigue Strength of Butt-welded Joint	18
CHAPTER 2: SURVEY OF PREVIOUS RESEARCH	
2.1 Introduction	19
2.2 Linear Elastic Fracture Mechanics	22
2.2.1 Application of Fracture Mechanics to Fatigue Crack Propagation	28
2.2.2 The Crack Growth Curve	30
2.3 Theoretical Analysis of Fatigue Crack Propagation	31
2.3.1 The Effect of Stress Ratio	33

Page

2.3.2 The Effect of Frequency of Cyclic Loading 37

2.3.3 The Effect of Salt Water Solution 38

2.3.3.1 Frequency effect 40

2.3.3.2 Stress Ratio effect 41

2.4 Threshold of Fatigue Crack Growth 41

2.4.1 Criteria for Non-Propagating Cracks 41

2.4.2 Effect of Stress Ratio on ΔK_{th} 43

2.4.3 Effect of Specimen Geometry on ΔK_{th} 45

2.4.4 Effect of Environment on ΔK_{th} 45

2.5 Factors Affecting Fatigue Crack Growth in Butt-welded Joints 48

2.5.1 Weld Defects 50

2.5.2 Residual Stresses 53

2.5.2.1 Fatigue crack growth through Residual Stress Field 55

2.6 Fatigue Crack Propagation in Weld Metal 58

2.7 Fatigue Crack Propagation in the Heat Affected Zone (HAZ) 63

Figures 2.1 to 2.3 66

CHAPTER 3: EXPERIMENTAL DETAILS AND DATA PROCESSING TECHNIQUES

3.1 Material and Test Specimens 67

3.2 Testing Machines 70

3.3 Crack Length Measurements During Fatigue Tests 72

3.3.1 Crack Depth Measurements using Potential Drop Microgauge 73

Page

3.3.1.1 Effect of crack front shape on digital meter reading 76

3.3.1.2 Effect of gain setting on digital meter reading 77

3.4 Scanning Electron Microscope (SEM) 77

3.5 Analysis of the Results 78

3.5.1 The Graphical Method 79

3.5.2 Finite Difference or Secant Method 79

3.5.3 Modified Difference Method 80

3.5.4 The Incremental Polynomial Method 80

3.5.5 The Total Polynomial Method 81

3.5.6 Discussion of Data Processing Methods 81

3.6 Determination of Stress Intensity Factors 84

3.6.1 Compact Type Specimen 84

3.6.2 Semi-Elliptical Surface Cracks 85

Figures 3.1 to 3.14 93

CHAPTER 4: CRACK GROWTH BEHAVIOUR OF BS4360-50D WELDED STEEL

4.1 Introduction 109

4.2 Experimental Procedures 110

4.3 Results 114

4.3.1 Base Metal 114

4.3.2 Weldment 116

4.3.3 Weldment in Salt Water Environment 118

4.4 Fractography 120

4.5 Discussion 122

Page

4.5.1 The Effect of Stress Ratio and Frequency in Air on Parent Metal 122

4.5.2 The Effect of Stress Ratio and Frequency in Air on Weldment 127

4.5.3 The Effect of Salt Water Environment on Weldment 134

4.6 Conclusions 141

Figures 4.1 to 4.38 144

CHAPTER 5: SURFACE CRACK GROWTH OF BS4360-50D WELDED STEEL

5.1 Introduction 179

5.2 Experimental Procedures 181

5.3 Results 184

5.3.1 Base Metal 184

5.3.2 Weldment 187

5.3.3 Heat-affected Zone 191

5.4 Discussion 192

5.4.1 Base Metal 192

5.4.2 Weldment 205

5.4.3 Heat-affected Zone 213

5.5 Conclusions 216

Figures 5.1 to 5.41 220

CHAPTER 6: COMPUTER SIMULATION OF SURFACE CRACK PROPAGATION

6.1 Introduction 259

6.2 Fatigue Crack Growth Model 260

Page

6.3 Prediction of Surface Crack Growth Under Bending Loads in Steel and Weld Metal 262

6.3.1 Effect of Geometry 265

6.3.2 The Influence of Initial Flaw Size and Shape 265

6.4 Discussion 268

6.5 Conclusions 273

Figures 6.1 to 6.19 274

CHAPTER 7: IMPROVEMENT OF FATIGUE STRENGTH OF BUTT-WELDED JOINTS

7.1 Introduction 293

7.2 Some Methods of Improving the Fatigue Strength of Weldments 294

7.2.1 Prior Overloading 295

7.2.2 Peening 295

7.2.3 Spot Heating 296

7.3 Experimental Procedures 297

7.4 Results 297

7.5 Fractography 299

7.6 Discussion 301

7.7 Conclusions 304

Figures 7.1 to 7.21 305

CHAPTER 8: CONCLUSIONS AND RECOMMENDATIONS

8.1 Introduction 322

8.2 General Conclusions 323

8.3 Recommendations for Future Work 329

Page

References 332

NOMENCLATURE

A	Constant
A_1, A_2	Empirical material constants
a	Crack depth
a_{eff}	Effective crack depth
a_p	Critical crack depth
a_i	Crack depth at the i^{th} cycle
Δa	Crack depth increment
Δa_i	Crack depth increment after the i^{th} cycle
B	Specimen thickness
B_f	Correction factor
B_0	Constant
B_1	Constant in the crack growth rate expressions
b	Constant in the crack growth rate equations
b_0, b_1, b_2	Constants
$C, C_1, C_2, \ldots$	Constants in the crack growth rate expressions
C_{N1}, C_{N2}	Constants
c	Crack length
c_i	Crack length at the i^{th} cycle
Δc_i	Crack length increment after the i^{th} cycle
da/dN	Crack growth rate of deepest point of semi-ellipical crack
dc/dN	Crack growth rate of semi-ellipical crack at the free surface
E	Young's modulus
$E(k)$	Elliptical integral of the second kind

f	Frequency
H	Specimen height
K	Stress intensity factor
K_I, K_{II}, K_{III}	Stress intensity factor for modes I, II and III
K_a	Stress intensity factor at the deepest point of semi-elliptical crack
K_{app}	Applied stress intensity factor
K_c	Stress intensity factor at the free surface of semi-elliptical crack
K_c'	Critical value of K for unstable crack growth
K_{1c}	Minimum value of K_c'
K_{CL}	Level of K required to open the fatigue crack
K_{eff}	Effective stress intensity factor
K_f	Fatigue strength reduction factor
K_{ISCC}	Threshold value of K in stress corrosion
$K_{max}, K_{min}, K_{mean}$	Maximum, minimum and mean value of K during load cycling
$K_{max,th}$	Value of K_{max} at threshold
K_R	Residual stress intensity factor
K_t	Theoretical elastic stress concentration factor
ΔK	Range of K in a loading cycle
ΔK_a	Range of K at the deepest point of semi-elliptical crack

ΔK_{app}	Applied ΔK
ΔK_c	Range of K at the surface point of semi-elliptical crack
$\Delta K_{c',th}$	Critical range of ΔK at threshold
ΔK_{eff}	Effective stress intensity factor range
ΔK_{res}	Range of residual stress intensity factor
ΔK_{th}	Threshold value of ΔK
ΔK_{Oth}	Value of ΔK_{th} at zero stress ratio (R=0)
M_1, M_2, M_3, M_{12}	Stress intensity correction factors for semi-elliptical cracks
$m, m_1, m_2, \ldots$	Exponents in the crack growth rate
N	Number of cycles
N_i	Number of cycles at the i^{th} cycle
N_t	Total number of cycles
ΔN	Increment of number of cycles
P	Applied load
R	Stress ratio
r	Radial coordinate at the crack tip
r_p	Radius of plastic zone
U_1	Ratio of the effective to total value of ΔK
u	Displacement
v	Crack opening displacement
w	Specimen width
x,y	Cartesian coordinates

Y	Geometric factor in the stress intensity factor expression
α	Constant of state of stress
β	Constants in the crack growth rate expression
θ	Angular coordinate at the crack tip
ρ	Monotonic plastic zone size at the crack tip
ρ'	Crack tip radius
ρ^*	Microstructural dimensions
λ_1	Constant
ν	Poisson's ratio
σ	Level of stress
σ_f	Fracture stress
σ_h	Stress reduction due the hydrogen environment action
σ_{RAVE}	Average value of redistributed residual stress
σ_y	Tensile yield stress
τ	Shear stress
COD	Crack opening displacement
J	A contour integral

CHAPTER 1

INTRODUCTION

1.1 BACKGROUND

Because of the recent expansion in sea-based development work, there has been a corresponding growth in the numbers and types of offshore construction built . Such constructions must be safely designed with respect to a number of possible failure modes due to the forces acting on them, as the structural integrity of offshore installations and equipment is one of prime importance with regard to danger to human life.

The service loading which a welded steel offshore structure experiences derives from a large number of sources, and consists of a combination of static, dynamic and cyclic loads. Among these, the cyclic stress caused by wind or waves can cause failure by fatigue. The main oilfields in the North Sea are located in areas which experience some of the worst weather conditions in the world, where in winter water temperatures fall to around 4°C and prolonged air temperatures to well below freezing, and where in stormy conditions there are gusts of wind exceeding 160 km/hr and waves rise to heights of 20m. It is therefore very important to have sufficient information on the fatigue behaviour of structural steel and welded joints, as used in structures operating under these conditions.

In such offshore structures, which are welded during construction, small crack-like defects are invariably present from the beginning of their commissioning. The majority of the data on the fatigue strength of welded joints have been obtained by using axially loaded specimens, and relatively little work has been done with types of specimen which contain realistic residual stress systems and which would give the designer some idea of the influence of such residual stresses.

Considerable effort is now being expended, in different centres for offshore research throughout the United Kingdom, in obtaining basic fatigue data under various loading and environmental conditions relevant to the North Sea. The present work is part of this major programme.

1.2 OBJECTIVES

The main objective of the present work was to generate data for fatigue of surface cracks in BS4360-50D low alloy structural steel and its weldment, as used in the North Sea. The aim was to investigate the effect of such variables as stress ratio, frequency and a corrosive environment on the growth of semi-elliptical cracks as well as the relationship between crack growth on the surface and in the through-thickness direction.

1.3 OUTLINE OF THE WORK

The work was carried out in four stages:-

1.3.1 Crack Growth Behaviour of BS4360-50D Welded Steel

The aim was to obtain basic fatigue data for threshold, low and intermediate stress intensities and to investigate the effect of stress ratio, frequency and salt water environment. The results showed that the fatigue crack growth rates in the weldment were lower than those in the base material.

1.3.2 Growth of Semi-elliptical Surface Cracks in BS4360-50D Welded Steel

The main objective was to obtain fatigue crack growth data for such cracks and investigate the correlation between the results from the previous stage. The results showed that the growth rates of semi-elliptical cracks in the weldment were higher than for the parent plate. The development of the shape of these cracks led to the third stage of the present work.

1.3.3 Computer Simulation of Surface Crack Propagation

The effect of geometry and of the initial flaw size were factors investigated by computer simulation.

1.3.4 An Attempt to Improve Fatigue Strength of Welded Joints

A new method which has been named sandwich welding was developed and its effectiveness was investigated in a series of tests carried out on compact type and surface-notched plate specimens.

CHAPTER 2

SURVEY OF PREVIOUS RESEARCH

2.1 INTRODUCTION

The fatigue phenomenon and the consequent material failure of a component have been topic of intense research during the past century. The traditional method used to predict the life of a component has been through the use of S-N curves, where the life of a component is plotted against the applied stress amplitude.

It is now well known that fatigue failure occurs in three phases. The crack initiates at the surface or a blunt notch and propagates until a critical size is reached, whereafter fracture of the remaining section occurs. The fatigue life of a component is determined by the sum of the time required to initiate a fatigue crack and the time for the crack to grow from a subcritical dimension to the critical size before fracture occurs. The relative proportion of times occupied by these two phases of crack growth may depend on surface finish, residual stresses, material microstructure, such as inclusions, or the presence of small cracks introduced during fabrication.

The introduction of welding as a method of fabrication of structures has resulted in severe fatigue problems. Defects within the weld and stress concentrations due to the

weld geometry are influential factors in fatigue failure. Such defects can take many forms, such as cracks due to residual stresses in the weld region, lack of penetration, inclusions and porosity, and it is these which are detrimental in terms of fatigue. It is not therefore suprising that many laboratory fatigue tests have shown that fatigue resistance of welded specimens is considerably reduced. This is because the period normally required for the crack to initiate is virtually absent and consequently the total fatigue life is taken up with crack propagation. Thus an accurate life prediction can be made on the basis of the time taken to grow a fatigue crack from an initial defect to a critical size which causes unstable fracture. Hence the essence of the integrity of a welded structure or joint is that a crack should not grow, under the influence of cyclic loading, from the initial defects to a critical size during the design life. The critical size will depend on the criterion of failure, which in turn depends on the structure and the material used.

Two techniques have been proposed to determine the required life for a joint or structure subjected to fatigue. These are safe-life and fail-safe. Neither can be applied in its original form to the problem of fatigue of large welded structures. Safe-life is formulated basically as an extension of the S-N approach, the working stresses being arranged such that the service life is less than the predicted fatigue life (i.e., cracking does not occur). In contrast, the fail-safe approach has always accepted that

cracking will occur, but provides sufficient structural redundancy to allow for detection and repair before large-scale failure can take place. An alternative approach is also based on the safe-life criterion except that the life is a propagation life rather than overall fatigue life. Thus, the design should be such that if a fatigue crack does occur, it will propagate at a rate slow enough to ensure that either the complete failure condition is not reached in the service life, or, if the fatigue-sensitive areas are accessible, then the inspection and repair can be carried out. If viewed in terms of practical problems of fabrication, the criterion becomes a question of how large a defect can be tolerated in the structure before failure.

The prediction of fatigue life based on crack growth lies on the ability to calculate the rate at which the crack will grow in a given position in a structure. This is an extremely complex task because the rate of propagation of a crack is dependent on its size and shape, the stress field around the crack, the environment and the material into which the crack is growing. Fracture mechanics is particularly suited to describing fatigue crack propagation and fracture, and its use is therefore becoming increasingly widespread. The basis of fracture mechanics is that a flaw or a defect, such as fatigue crack growth, can produce a stress concentration within a material and that in turn can lead to the creation of intensified stresses at the crack tip. Providing the nominal stress acting upon a material is less than 0.8 of the yield strength, and also providing that

the region of plastic deformation ahead of the crack tip is small relative to the total component size, the component can be considered as a macroscopically elastic body. The state of stress ahead of the crack is then determined by linear elastic fracture mechanics [1]. In this case the stress intensity factor, K, can be used as a single parameter to describe the elastic stress field in the vicinity of the crack tip. A detailed description of the fundamental concepts of fracture mechanics is given in the next section.

2.2 LINEAR ELASTIC FRACTURE MECHANICS

Descriptions of elementary fracture mechanics can be found in a variety of texts (see for example [1] and [2]); the following pages present only those fundamentals of the theory needed to understand the subsequent text.

The presence of a crack in a stressed solid can cause it to fracture at a stress much lower than the ultimate strength of the material. Early attempts to predict the fracture strength of cracked solids were based on an energy-balance approach [3,4]. However, a more successful approach to the problem may be based on the elastic stress field around the crack tip [5].

A crack in a solid can be categorized according to its mode, as illustrated in Fig. 2.1. Normal stress gives rise

to the "opening mode" (Mode I) in which the displacements of the crack surfaces are perpendicular to the plane of the crack. In-plane shear stress causes the "sliding mode" (Mode II), in which the displacement of the crack surfaces is in the plane of the crack and perpendicular to the leading edge of the crack. The "tearing mode" (Mode III) is caused by out-of plane shear stress; crack-surface displacements are in the plane of the crack and parallel to the leading edge of the crack.

For an infinite plate subjected to a remote stress, σ, (i.e., Mode I) the stress field displacements at the tip of a sharp crack with length 2a at a point $P(r,\theta)$ were derived by Irwin [5], and Williams [6], and can be written in the form:

$$\begin{bmatrix} \sigma_{xx} \\ \sigma_{yy} \\ \tau_{xy} \end{bmatrix} = \frac{K_I}{\sqrt{2\pi r}} \begin{bmatrix} \cos\theta/2\ (1 - \sin\theta/2 \sin 3\theta/2) \\ \cos\theta/2\ (1 + \sin\theta/2 \sin 3\theta/2) \\ \cos\theta/2 \sin\theta/2 \cos 3\theta/2 \end{bmatrix} \quad ,(2.1)$$

$$\begin{bmatrix} u \\ v \end{bmatrix} = \frac{K_I}{8\alpha} \left(\frac{2r}{\pi}\right)^{\frac{1}{2}} \begin{bmatrix} (2\alpha - 1) \cos\theta/2 - \cos 3\theta/2 \\ (2\alpha + 1) \sin\theta/2 - \sin 3\theta/2 \end{bmatrix}, (2.2)$$

where $\alpha=3-4\nu$ in plane strain and $\alpha= (2 - \nu)/(1 + \nu)$ in plane stress, and r and θ are the radial coordinates centred at the crack tip.

The parameter K_I is designated the "stress intensity factor" and is independent of r and θ . It dictates the magnitude but not the distribution of the stress fields in different crack configurations. For an infinite plate containing a crack of length 2a, subjected to a remote tensile stress field, σ , the Westergaard [7] solution gives

$$K_I = \sigma\sqrt{\pi a} \qquad .(2.3)$$

In the case of finite bodies, the expression for K_I becomes more complex and is expressed as follows

$$K_I = Y\sigma\sqrt{\pi a} \qquad ,(2.4)$$

where Y is a dimensionless parameter which varies according to the geometry of the specimen, location of the crack, proximity of a free surface, distribution of load, etc., and is often found using the Griffith [3] energy criterion which relates the energy required to increase the crack length by an infinitesimal increment, Δa, to the elastic energy released as a result of that crack growth. K_I can be related to the elastic stress concentration factor K_t by

$$K_I = \lim_{\rho\to 0} \frac{K_t\sigma\rho^{\frac{1}{2}}}{2} \qquad ,(2.5)$$

where ρ' is the radius of curvature. The above equation, which was derived by Irwin [4], implies that K_I is valid only when a sharp crack is considered.

Thus far attention has been focused on the case of a crack in a tensile stress field. Results analogous to equations (2.1) and (2.2) can be obtained for the case of a crack subjected to in-plane shear, i.e.,

$$\begin{bmatrix} \sigma_{xx} \\ \sigma_{yy} \\ \tau_{xy} \end{bmatrix} = \frac{K_{II}}{\sqrt{2\pi r}} \begin{bmatrix} -\sin \theta/2 \ (2+\cos \theta/2 \cos 3\theta/2) \\ \sin \theta/2 \cos \theta/2 \cos 3\theta/2 \\ \cos \theta/2 \ (1-\sin \theta/2 \sin 3\theta/2) \end{bmatrix} , \quad (2.6)$$

and out-of-plane shear

$$\begin{bmatrix} \tau_{xz} \\ \tau_{yz} \end{bmatrix} = \frac{K_{III}}{\sqrt{2\pi r}} \begin{bmatrix} -\sin \theta/2 \\ \cos \theta/2 \end{bmatrix} . \quad (2.7)$$

K_I , K_{II}, and K_{III} are referred to as the mode I, mode II and mode III stress intensity factors. The subscript I will, however, be omitted from the symbol K since only the opening mode is assumed throughout this work.

Once the stress intensity factor is known, the stress fields at the crack tip in a purely linear elastic body are completely specified. On the assumption that the fracture is governed by conditions at the crack tip, it must be expected that fracture will occur when K reaches a critical value, K_c, which latter may be obtained from a laboratory test. The difficulty in applying linear elastic fracture mechanics (LEFM) lies in ensuring that K_c is obtained under crack-tip conditions which are reproduced in the structure to be analysed. For purely elastic behaviour this is no problem, since the stress field at the crack tip is completely specified by K for all configurations. However, for a real material perfect elasticity is never completely realised.

Equation (2.6) indicates that as $r \longrightarrow 0$, crack tip stresses will become infinite for any value of the applied stress. Hence, plastic deformation will occur at the crack tip. The order of magnitude of the plastic zone, r_p, can be estimated from Equation (2.6) by setting $\sigma_{yy}=\sigma_y$, the yield stress of the material leading, to

$$r_p = \frac{1}{2\pi} \left(\frac{K}{\sigma_y}\right)^2 \qquad (2.8)$$

for plane stress conditions.

An elastic stress distribution with a singularity at the crack tip characterises the stress field ahead of the crack where the plastic yielding occurs. If the extent of the plastic zone is small in comparison with the dimensions of the elastically stressed region of the structure, the elastic model will closely represent the real conditions. Since LEFM provides a method of measuring the fracture strength of a brittle material, one must ensure that errors introduced by plastic yielding are minor or can be corrected. For plasticity effects to be negligible the plastic zone must be small compared with the crack length and remaining ligament. At the onset of fracture, at which $K=K_c$, the error introduced by plastic yielding may be estimated from

$$\frac{r_p}{a} = \frac{1}{2\pi a}\left(\frac{K_c}{\sigma_y}\right)^2 = \frac{1}{2}\left(\frac{\sigma_f}{\sigma_y}\right)^2 \quad ,(2.9)$$

where σ_f is the gross-fracture stress. Thus the LEFM approach is acceptable as long as the gross fracture stress is small compared to the yield stress of the material. To correct the small-scale plastic yielding effect it was suggested by Irwin [4] that the physical crack be increased by an amount r_p to obtain an effective crack length, a_{eff}, i.e.,

$$a_{eff} = a + r_p \quad .(2.10)$$

The fracture toughness, K_c, is dependent on, among other factors, the thickness of the specimen. The role of thickness is to provide a triaxial stress field ahead of the crack, which increases the hydrostatic stress component and thus reduces the plastic zone size. Experimentally it has been verified that K_c decreases as the thickness increases, attaining a minimum value, K_{1c}, corresponding to plane strain conditions. The major effect which explains the above trend is that the tensile stress rises as the thickness is increased. This favours the cleavage mode of fracture over the shear mode, which consequently reduces K_c.

2.2.1 Application of Fracture Mechanics to Fatigue Crack Propagation

Linear elastic fracture mechanics was originally developed to analyse static fracture, and the technique has been applied most widely to brittle fracture. Since fatigue crack propagation is also a fracture process, it seems reasonable to assume that the stress intensity factor is a suitable parameter for describing the influence of loading and geometry on fatigue crack growth rates. However, the successful application of growth data, analysed using the stress intensity factor, depends on the solution of K being available for the complicated geometry of real structures.

The fatigue crack growth data, da/dN, where N is the number of fatigue cycles, can in general be expressed as a function of stress intensity range, ΔK, stress ratio, R,

temperature, type of environment, residual stress, loading history, etc. Hence

$$\frac{da}{dN} = f(\Delta K, R, \text{temperature, environment,...,}) \quad .(2.11)$$

Recent studies have also confirmed that da/dN is primarily controlled by the stress intensity factor range, ΔK, through Paris's expression [8]

$$\frac{da}{dN} = C\ (\Delta K)^m \quad ,(2.12)$$

where C and m are constants. Deviations from this form occur at very low crack growth rates close to threshold ΔK_{th} values, and at rates approaching fracture. Experimental investigations on a wide range of materials have reported values of m lying in the range of 2 to 20. This range of values is found because the expression (2.12) is not in general obeyed over a wide range of growth rates. These investigations, however, have shown that the expression (2.12) adequately describes the fatigue behaviour in the mid-range of growth rates, i.e., 10^{-6} mm/cycle < da/dN < 10^{-3} mm/cycle, but underestimates them at higher, and overestimates them at lower, growth rates. However, an important factor in fatigue crack grow which could invalidate this approach is whether or not fracture takes

place under every cycle of applied stress. If certain features of the material inside the crack tip plastic zone, such as microstructure, cause significant irregular delays or accelerations in crack growth then the stress intensity would not provide sufficient information on the state of stress at the crack tip. If the same behaviour occurs as a result of changes in the plastic zone, then the stress intensity factor should be modified to take account of this influence.

Crack tip yielding is a major limitation to this statement as yielding should be small compared with other relevant dimensions if LEFM is to be used. This limitation may be particularly important in the context of propagation of very small fatigue cracks, especially when the applied stress and resulting plastic zone are large. Moreover, it may well be the case that the factors which control very small increments of crack propagation are not described by the stress intensity factor alone.

2.2.2 The Crack Growth Curve

The variation of crack growth rates with stress intensity factor can be illustrated by a sigmoidal curve of log da/dN versus log ΔK as shown for steels in [9], Fig. 2.2.

To explain the sensitivity of stress ratio, thickness, microstructure, environment, etc., on the sigmoidal

variation of growth rate with ΔK, Lindley et al [9] analysed the problem on the basis of a primary crack growth mechanism. It is shown that in steels, for the mid-range of growth rates (regime II), failure generally takes place through a transgranular ductile striation mechanism [10,11] and that the rate of crack growth is largely insensitive to stress ratio, thickness, frequency, microstructure, etc. The influence of these factors may, however, predominate in the high and low growth-rate regimes (III and I, respectively). At high growth-rates, the effect of the above factors can be described in terms of superimposed static modes of fracture such as cleavage, or intergranular, $\Lambda_{fracture}$ and microvoid coalescence accompanying or replacing striation growth [12,13]. The mechanism of low growth rates has been observed to be microstructurally sensitive to stress ratio, involving the occurrence of induced fracture modes, such as intergranular fracture in steels [14].

2.3 THEORETICAL ANALYSIS OF FATIGUE CRACK PROPAGATION

Fatigue crack growth laws are numerous and a comprehensive discussion of them is beyond the scope of the present work. However, a brief review will be presented here.

Paris and Erdogan [8] concluded that such a law could be expressed in the form of (2.12) and presented experimental data, which favoured an exponent value of m=4 . Barsom [15] based his model on strain energy release and

COD, and predicted a value of m=2. Liu [16], who also predicted a value of m=2, used dimensional analysis together with the concept of total energy absorption to failure.

Weertman [17] applied an improved version of the dislocation model proposed by Bilby et al [18] to fatigue crack growth, using the criterion that fracture occurs when accumulated plastic displacement reaches a critical value which is a characteristics of the material. He found a value of m=4. Rice[19] and McCartney [20] used a similar approach and also obtained a value of m=4.

Lardner [21] predicted a value of m=2 based on the changes of crack-tip opening displacement during cyclic loading. Schwalbe [22] has developed a theory of fatigue crack growth based on crack tip displacement, and obtained a value of m=2.

Recently Majumdar et al [23] and Antolovich et al [24] predicted a value of m=2 using Coffin-Manson low cycle fatigue correlation as a failure criterion at the crack tip, though, using the same criterion, Duggan [25] obtained a value of m of about 3.

From the above short review it is apparent that the theoretical crack growth laws predict values of m in the

range 2 to 4. However, experimental observations show that values of m in the medium growth rates may vary between 2 and 8. This limitation of the theoretical growth laws has led many investigators to use empirical laws for fatigue crack-growth prediction.

The theoretical models for fatigue crack-growth briefly discussed above do not take into account the effect of such factors as stress ratio, frequency, environment, etc. These factors are known to affect the fatigue crack-growth rates as observed in numerous experimental results. In the following section a review of these effects will be presented.

2.3.1 The Effect of Stress Ratio

Fatigue crack-growth models which have been proposed to account for the effect of stress ratio on crack growth rates are all modifications of Paris's [8] expression (2.12).

Roberts and Erdogan [26] modified Paris's expression to include the influence of K_{max} , and therefore R, at high growth rates and suggested an expression of the form:

$$\frac{da}{dN} = C_1 \, \Delta K^{m_1} \, K_{max}^{m_2} \qquad ,(2.13)$$

where m_1 and m_2 were both found to be 2. Forman et al [27] considered the consequence of K_{max} approaching the fracture toughness, K_c, and proposed the following:

$$\frac{da}{dN} = \frac{C_2 \Delta K^{m_3}}{\{(1-R)K_c - \Delta K\}\beta} \qquad ,(2.14)$$

where β is unity. Expression (2.14) has been successfully applied to growth behaviour in aluminium alloys [28-31]. However, in mild steel [32], and other alloy steels [33] which are less sensitive to stress ratio, it over-predicts the exaggerated growth at high ΔK.

Klesnil and Lukas [34] proposed an expression to account for the behaviour observed at low growth rates. They introduced the threshold stress intensity factor below which no growth occurs:

$$\frac{da}{dN} = C_3\left\{\left[\frac{\Delta K}{(1-R)^{\gamma}}\right]^{m_4} - K_{th}^{m_5}\right\} \qquad ,(2.15)$$

where γ is a material constant.

Branco et al [32] proposed a general expression which

includes ΔK_{th} and K_{max} effects at low and high growth-rates respectively of the form:

$$\frac{da}{dN} = \frac{C_4 \ (1-R^2)(K_{max} - K^2_{max,th})}{K^2_c - K^2_{max}} \quad .(2.16)$$

Recently Dover and Hibberd [35] proposed a generalized expression correlating random loading data:

$$\frac{da}{dN} = C_5(\Delta K)^{m_5}\left(\frac{K_{max} - K_{max,th}}{K_{max}}\right)^{m_6}\left(\frac{K_{max}}{K_c - K_{max,th}}\right)^{m_7} . (2.17)$$

Other growth models proposed are based on the effective stress intensity factor range, ΔK_{eff}. In these models the crack closure phenomenon is used. Elber [36] detected physical crack closure in specimens subjected to tensile loads, and assumed that damage does not occur when the stress singularity is destroyed by closure. He modified the Paris expression thus:

$$\frac{da}{dN} = C_6 \ (\Delta K_{eff})^{m_8} \quad ,(2.18)$$

where

$$K_{eff} = U_1 \ \Delta K$$

and

$$U_1 = \frac{K_{max} - K_{CL}}{K_{max} - K_{min}} \quad .(2.19)$$

K_{CL} is the stress intensity factor at which the crack opens during the tensile part of the load cycle. Elber also proposed a simple relationship between U_1 and R for an aluminium alloy 2024-T3 which was experimentally tested:

$$U_1 = 0.5 + 0.4R \qquad .(2.20)$$

Maddox et al [33] attempted to develop a simple relationship between U_1 and R for some structural steels, but, though fairly successful for R<0, the results for R>0 were scattered. Subsequent studies have revealed that crack closure is a complicated phenomenon and is influenced by some additional metallurgical factors in a highly complex manner [37]. Recent results by Ohta et al [38], who measured strains in the proximity of the crack tip, showed that damage does occur even when the crack is closed. Thus these observations have cast some doubt on the understanding of the effect of crack closure based on Elber's proposals.

Judging from the results reported in the literature on the effect of stress ratio, fatigue crack growth in aluminium alloys and high strength steels appears to be highly sensitive to stress ratio whilst in low alloy steels it is not. Recently, there have been a number of advances to explain the effect of mean stress in mechanistic terms. Richards and Lindley [9] have discussed at length the stress ratio effect and the different fatigue crack growth

mechanisms, and concluded that crack growth by a pure, ductile, striation-forming mechanism was insensitive to stress ratio. Other growth mechanisms, such as microcleavage, void coalescence or intergranular separation, were found to be significantly influenced by stress ratio.

2.3.2 The Effects of Frequency of Cyclic Loading

The results reported in the literature suggest that the speed of cyclic loading has little effect on fatigue crack growth in mild environments over the range of frequencies between 4 and 100Hz [39]. At higher frequencies crack-tip heating results in residual stress relaxation as well as softening of the material, and causes a reduction in the crack-growth rates. At lower frequencies environmental effects due to water vapour in the air tend to increase growth rates.

Schij ve [40] in his early tests showed that the crack growth rates were about 30% faster at 0.33Hz than at 33Hz in 2024-T3 aluminium alloy. Hertzberg et al [41] also tested this material and also found that growth rates were higher at lower frequencies (0.5Hz–133Hz).

Yokobori and Sato [42] have shown that decreasing frequency results in an increase in growth rates and proposed an empirical formula to correlate their data:

$$\frac{da}{dN} = C_7 \ (\Delta K)^{m_9} \ f^{-\lambda_1} \qquad ,(2.21)$$

where f is the frequency (0.016Hz-140Hz) and λ_1 is a material constant which is 0.08-0.09 for 2024-T3 aluminium alloy and 0.12-0.14 for SM50 steel as tested.

Recently Musuva and Radon [43] have reported growth rates increasing with decreasing frequency only at a high stress ratio for mild steel.

2.3.3 The Effect of Salt Solution

The effect of a salt solution on fatigue crack growth has been studied by many investigators [44-45] and is generally known as corrosion fatigue, which implies the presence of an environment which influences the fatigue properties of the material by means of a chemical attack.

The exact mechanism of corrosion fatigue is not clear since most proposed models fail to account for all experimental observations reported. It is possible that no single mechanism is responsible for the corrosion fatigue behaviour for all metal environment systems.

Early investigators of corrosion fatigue [46] assumed

that cracks were initiated in the bases of large hemispherical pits created by the corrosion process on the metal surface. Cyclic loading accelerated corrosion-pitting and caused the development of crevices or fissures. Duquette [47] proposed a crack-initiation mechanism based on preferential load dissolution of the metal at emerging slip steps. The dissolution unlocks the otherwise blocked slip process, accelerating the extrusion-intrusion process which results in premature crack nucleation and growth. Evans [48] applied an electrochemical theory, describing the corrosive attack on a specimen in a wet environment as an electrochemical process in which the whole surface was considered to be divided between anodes and cathodes.

Other suggestions concerning corrosion fatigue are based on hydrogen embrittlement [49]. This mechanism is encountered in steels and titanium alloys due to hydrogen being absorbed from such sources as cathodic reduction during aqueous corrosion which diffuses to regions within the material where it can be accommodated by producing less distortion of the crystal lattice and may result in a build-up of hydrogen at internal microcracks. Hydrogen creates hydrostatic pressure within the cracks so that the stresses acting upon the growing crack are increased resulting in accelerated growth rates.

The crack growth behaviour of steel in salt water is affected by several factors such as frequency and stress

ratio. A brief review of these is presented below.

2.3.3.1 Frequency effect

Barsom [50] investigated the effect of environment and loading variables on 12Ni-5Cr-3Mo maraging steel in a 3% NaCl solution and showed that in an air and salt water solution at room temperature the crack growth rates could be represented by

$$\frac{da}{dN} = F(t)\ (\Delta K)^2 \qquad ,(2.22)$$

where F(t) is a function varying inversely with frequency, attaining a constant minimum value for the frequency at which crack growth is sufficiently fast for it to be unaffected by the environment. He plotted logda/dN versus log ΔK for the data obtained at different frequencies. The plot gave parallel straight lines by which the lowest frequency produced the highest growth rates.

However, data obtained by other investigators [51-53] do not show such a tendency for parallel curves as Barsom's. Vosikovsky [51] conducted tests on X-65 maraging steel, which showed high frequency dependence at ΔK values above K_{ISCC}, but no significant effect at low ΔK values. Austen and Walker [52] reported similar results for 835M30 steel which further show lower growth rates in NaCl solution than in air at 64Hz frequency. Atkinson and Lindley [53] in their study of two steels (En56C and A533B-1) over a wide range of

frequencies (0.001-10Hz) showed that for a given ΔK, there was a critical frequency at which maximum environmental attack occurred for both steels. This critical frequency increased with increasing temperature.

2.3.3.2 Stress ratio effect

The most significant factor affecting crack growth in a salt water environment is stress ratio. The fatigue crack growth through almost the entire range of ΔK is significantly increased at higher mean stresses. Scott and Silvester [54] have conducted tests on BS4360-50D steel immersed in sea water. The data obtained showed that high R ratios (0.7-0.85) increase the crack growth rates compared to low stress ratio (0.1) in a way which was not observed in tests conducted in air. Similar results have been reported for pressure vessel steels A533-B and A508 in water environments typical of water-cooled nuclear reactors [55,56]. Bamford [57] has obtained some data on stainless steel in a similar water-cooled reactor environment, but his results showed no effects of stress ratio. Hibberd and Dover [58] have reported increased growth rates with increase in R-ratio in two alloy steels, Q1(N) and HY100, tested in sea water under random loading.

2.4 THRESHOLD OF FATIGUE CRACK GROWTH

2.4.1 Criteria For Non-Propagating Cracks

The earliest criterion for a non-propagating crack was

put forward by Frost [59] in the form:

$$\Delta\sigma^3 a > A_1 \qquad ,(2.23)$$

where A_1 is an empirical material constant which is obtained from plots of $\Delta\sigma^3 a$ against log of endurance cycles for a value of $\Delta\sigma^3 a$ at which the curve becomes horizontal.

Frost [60] reanalysed the problem using the fracture mechanics approach, and obtained values of ΔK_{th} for different materials. An important observation from these results was the lower value of ΔK_{th} found for shorter cracks (0.025-0.25mm) as compared with that obtained for longer cracks (0.5-5mm).

Sadananda and Shahinian [61] proposed a model which predicts the existence of a ΔK_{th} which is expressed in the form:

$$\Delta K_{th} = A_2 \sqrt{\pi\rho^*}\ \sigma_f \qquad ,(2.24)$$

where ρ^* is the minimum distance that the dislocation can exist away from the tip (taken as the Burgers vector), σ_f is the minimum stress to nucleate a dislocation at the crack tip, and A_2 is numerically equal to $\sqrt{3/2}$. Equation (2.24) does not predict any variation of ΔK_{th} with mechanical, microstructural and environmental factors, which

is consistent with the experimental data available.

Ritchie [62] has recently suggested that the fracture stress σ_f in equation (2.24) can be reduced by σ_h in the presence of a hydrogen-producing environment, and has obtained:

$$\Delta K_{th} = \sqrt{\frac{3}{2}\pi\rho^*}\,(\sigma_f - \sigma_h) \qquad .(2.25)$$

σ_h was calculated in terms of yield strength, stress ratio and other parameters of temperature, hydrogen concentration and gas constant. However, Ritchie has pointed out that it is probably premature to utilise this expression in a predictive capacity because of uncertainty in the magnitude of the various parameters in the final expression for ΔK_{th}.

2.4.2 Effect Of Stress Ratio on ΔK_{th}

A low rate of crack growth is generally sensitive to stress ratio. Research on a wide range of steels and non-ferrous materials, tested in air under ambient conditions, shows that the value of ΔK_{th} markedly decreases as the stress ratio is raised from zero to a high value.

Klesnil and Lukas [34] have related the stress ratio, R, and ΔK_{th} in the form:

$$\Delta K_{th} = \Delta K_{Oth}\,(1-R)^{\gamma} \qquad ,(2.26)$$

where ΔK_{Oth} is the threshold at R=0 and γ is a material constant varying from 0.5 to 1 for different steels. Values of γ close to 1 indicating a linear relationship between R and ΔK_{th} have been measured for most medium carbon steels [63,64].

Vosikovsky [65] established a linear relationship between ΔK_{th} and R for HY130. He proposed and tested an expression of the form

$$\Delta K_{th} = \Delta K_{Oth} - B_{OR} \qquad ,(2.27)$$

and later it was applied successfully to data for a wide range of steels [66].

Further expressions without such material constants as are used above have been suggested by McEvilly [67] and Branco et al [32] in the form:

$$\Delta K_{th} = \Delta K_{Oth} \left[\frac{1-R}{1+R}\right]^{\frac{1}{2}} \qquad ,(2.28)$$

and

$$\Delta K_{th} = \Delta K_{Oth} \left[1-R^2\right]^{\frac{1}{2}} \qquad ,(2.29)$$

respectively.

Recently, Davenport and Brook [68] proposed an expression which also included the fracture toughness, $K_{c'}$, and obtained a satisfactory correlation for a 0.15%C, 1.5%Mn steel. Their expression was of the form:

$$\Delta K_{th} = \Delta K_{Oth} \left[\frac{K_{c'} - K_{max}(1-R)}{K_{c'} - K_{Oth}} \right]^{1/3} \quad .(2.30)$$

2.4.3 Effect of Specimen Geometry on ΔK_{th}

To date no specific results have been reported on the effect of specimen geometry on ΔK_{th}. It has usually been assumed that the effects of specimen geometry are those associated with changes in the state of stress at the crack tip which are taken account of by the stress intensity factor. However, small differences in the growth rates between specimens of different geometry can arise because of crack closure effects and the complexity of the stress field ahead of the crack tip.

2.4.4 Effect of Environment on ΔK_{th}

A large proportion of published data on the influence of the environment on the threshold has been concerned with aluminium alloys [45,69], mainly because the aircraft industry has been most active in this field. Tests performed

on mild steel immersed in brine, tap water and oil [70,71] showed that for zero-tension loading in mild steel at ambient temperatures, the value of ΔK_{th} was reduced from 7.3 $MN/m^{3/2}$ in SAE30 oil to 6.0 $MN/m^{3/2}$ in air, and significantly reduced to 2 $MN/m^{3/2}$ in brine. Paris et al [72,73] observed no change in ΔK_{th} between an air and a distilled water environment on low strength steel, a result later confirmed by Branco [32] on mild steel in air and salt-water environments.

Mantz and Weiss [74] performed tests on 7050-T73651 aluminium alloy and D6ac steel in air, dry argon and wet argon. For the D6ac steel room air produced the lowest ΔK_{th} while dry and wet argon produced identical values of ΔK_{th} but higher than in air. The effect on the aluminium alloy was, however, more significant, i.e., ΔK_{th} was much lower in air than in dry or wet argon.

Usami and Shida [75] have recently obtained results on 13%Cr cast steel. They showed that salt water did not affect ΔK_{th} at high R-values but caused a substantial decrease on ΔK_{th} at low stress ratios.

However, there are other results which show a significant decrease in ΔK_{th} when comparing crack growth data in vacuum and in air. Cooke et al [76] obtained threshold data for EN24 steel and found an increase in

ΔK_{th} from 5 to 7 $MN/m^{3/2}$ at R=0.1 and from 3 to 7 $MN/m^{3/2}$ at R=0.7 in vacuum compared to air. Similar results have been reported by Irving and Kurzfeld [77] who tested BS817M40 and SAE4340 steels. More recently, Kirby and Beevers [78] obtained other, similar results for three commercial aluminium alloys.

From the above results it is apparent that the environmental effect on ΔK_{th} depends on the nature of the reference environment used for comparison. If dry argon is used as the reference environment, then there is no significant effect on ΔK_{th}, at least for steels. However, when data for a vacuum environment were compared to data in air then significant changes in ΔK_{th} are observed. It should be pointed out that rewelding effects have been reported to occur for cracks in a vacuum [79].

There is also an added complication in that in hostile or wet corrosive environments ΔK_{th} may be raised compared with more inert environments. This may arise from the "wedging" effect, where the presence of thick corrosion products in the crack may prevent further access for environmental elements or from certain environments which promote crack-branching. These effects may also lead to crack-tip blunting which may in some cases cause crack arrest [69].

2.5 FACTORS AFFECTING FATIGUE CRACK GROWTH IN BUTT-WELDED JOINTS

For a simple butt weld with the weld reinforcement intact, fracture occurs at the weld toe, because the stress concentration, caused by the change of cross-section, is at a maximum at that point [80]. Newman and Dawes [81] found that a significant improvement in fatigue properties can be obtained by machining or grinding the weld toe. They used this technique on some defective welds, to ensure that the failure was initiated by the defect and not at the weld toe. A similar finding has been reported by Mindlin [82]; he concluded that the fatigue strength of transverse butt welds increases in proportion to the included angle between the weld reinforcement and the base plate.

Welter and Choquet [83] performed tests on ASTM-E373-58T steel and observed that grinding the weld reinforcement produced a large decrease in the fatigue strength, particularly if the grinding scratches were parallel to the weld and therefore transverse to the direction of applied stress. In such cases the scratches act as stress raisers and therefore as sites for crack intiation either in the weld or the heat-affected zone (HAZ).

Munse [84] investigated the effect of edge preparation on the fatigue strength of butt-welded joints and concluded that single-Vee and single-U welded joints have rather higher fatigue strengths than the double-Vee welded joints.

He believes that, that is the result of the stress concentration at the weld toes being in different planes. However, Newman and Gurney [85] carried out a series of tests on 1/2-inch welded mild steel specimens with 60° single-Vee, single-U, double-Vee and close square-butt preparations. Very significant differences in strength were obtained, and they attributed this variation to the differences in reinforcement shape. They also tested three series of specimens which were prepared for welding by machining, manual gas cutting and machine gas cutting, all other variables, such as geometrical shape of preparation and welding conditions being the same. They obtained a better fatigue strength for the series with a machine weld preparation, which they considered was due to the absence of the undercuts remaining after welding which was a result of the comparatively smoother surface of the preparation.

Munse [84] has summarized the effect of the base metal strengths on the fatigue properties of butt-welded joints for steels with UTS of up to 758 $MN/m^{3/2}$. A considerable amount of scatter exists in his data from which it can be concluded that the fatigue strengths of welds in high-strength steels are no better than those of similar welds in mild steel.

There are a further two variables associated with welded joints which lead to extremely high local stresses, and each contributes to the poor fatigue properties of

welded joints. These are discussed in detail below.

2.5.1 Weld Defects

Defects in the weldments induce stress concentrations. Internal crack-like defects in weldments may be classified into two groups:

i) defects which result from the design of the weldment, i.e., fillet or partial penetration welds;

ii) defects due to poor material properties or inadequate welding procedures, i.e., lack of side wall or interrun fusion, hydrogen cracking, lamelar tearing, etc.

Internal weld defects may provide sites for crack initiation. Examples of such defects are porosity, slag inclusions and lack of penetration.

Weld defects are also significant in fatigue failures which are initiated at the external stress concentration of the weld toe. These defects are non-metallic intrusions which remain embedded in the weld after it cools [86]. Normally, non-metallic material such as weld slag floats to the surface of the liquid weld metal before it has cooled sufficiently to solidify. However, at the boundary of the parent plate and the weld pool, where the solid base plate and liquid weld exist side by side, some of the weld metal is not completely liquid and non-metallic materials cannot float to the surface.

In a sound weld, surface cracks will originate from the weld toe. This is partly due to the stress concentration in the toe region, and partly due to sharp microscopic slag intrusions which are found to be an inherent feature of welds, particularly when produced by manual arc methods [86].

If a weld reinforcement is removed from a butt weld the fatigue strength is raised and failure occurs in the weld metal. Examination of fracture surfaces has shown that failure is then initiated at the location of weld defects such as porosity, slag intrusions, undercutting and lack of penetration.

In general, the fatigue properties of a weld are much more sensitive to defects than the static tensile properties. Clough [87] showed that a 5% defective area in a mild steel butt weld with the reinforcement removed has a negligible effect on the ultimate tensile stress but reduces the fatigue strength by 30-45%. Munse [88] investigated the effect of small and large flaws on the fatigue strength of a butt weld in HY-80 steel. He showed that with the weld reinforcement removed, 5% porosity reduced the fatigue strength by 45%, and a flaw area as small as 0.1% reduced the fatigue strength by 18%.

Slag inclusions have long been recognised as possible sites for fatigue fracture initiation in welds. The first attempts to correlate fatigue strength with defect size did not isolate the effect of inclusions from the effects due to porosity and also could not deal with slag inclusions of irregular shape [89]. Newman and Gurney [90] have developed a technique for prediction of slag inclusions of reproducible shape and size, thus permitting systematic investigation of the effect of slag inclusions on fatigue strength. They tested butt welds in 1/2-inch thick mild steel and found a close correlation between the inclusion size and fatigue strength. Increasing the inclusion length by an order of magnitude resulted in a 20-30% reduction in fatigue strength, single inclusions giving slightly higher fatigue strengths than multiple inclusions of the same size.

Harrison [91] examined the effect of three 1/4-inch inclusions and one continuous slag line and found that the effect of slag inclusions depended upon their location. The effect of inclusions at the centre of the weld thickness was diminished by compressive residual stresses, large and small defects giving similar fatigue strengths. When the compressive residual stresses were relieved prior to testing, the fatigue strength increased when defects were discrete but decreased when the defect was a continuous slag-line. Harrison believed this was due to the stress relief treatment, removing hydrogen from the weld defects. Slag-inclusions near the welded surface reduced fatigue strength by approximately 40% compared with specimens having

inclusions in the centre of the weld.

In contrast, lack of penetration has a major effect on fatigue properties of butt-welded joints, as the applied stress is transverse to a partial penetration butt weld. Newman and Dawes [81] investigated the effect of inadequate joint preparation in 1/2-inch thick butt-welded mild steel. Partial penetrations were 3/4 and 1½ inches long. It had been intended to test these specimens with the weld reinforcement intact, but initial tests showed that, under these circumstances, failure was initiated at the weld toe. Consequently the edge reinforcement was ground flat so as to encourage failure initiation from the defect. They found a close correlation between the defect size and the fatigue strength. Increasing the defect length by half an order of magnitude resulted in a 20-30% reduction in fatigue strength.

Incomplete fusion has not been systematically investigated but may be expected to have a similar effect on fatigue properties of butt-welded joints to that of inadequate joint preparation, as both are essentially two-dimensional defects.

2.5.2 Residual Stresses

Residual stresses are produced in weldments by local thermal expansion, plastic deformation, and subsequent

shrinkage on cooling [92-94]. The residual stresses produced in this way are both normal to and in the direction of welding, as shown in Fig. 2.3. In the region of the weld the resulting tensile residual stresses may reach a level close to the yield strength [95,96]. In general, the magnitude of residual welding stresses will depend on the welding process, welding parameters, restraint on the joint, and dimensions of the parts being joined. In a summary published by Munse [84], it was noted that views expressed in the literature concerning the effect of residual bending stresses on fatigue differed markedly. There continues to be some disagreement on this subject although many investigators have reported that residual welding stresses do indeed affect the the fatigue strength [84,93,97,98].

Little work appears to have been done, however, to evaluate quantitatively the effect of residual stresses on fatigue crack intiation, and even less on fatigue crack growth rate. Furthermore, the conclusion that residual welding stresses do affect fatigue life is often based on a comparison with fatigue data obtained for weldments in which residual stresses have been relieved or modified by thermal or mechanical means. The stress-relief procedure may alter the microstructure and therefore affect the fatigue properties. The subject is further complicated because the magnitude and distribution of residual stresses are rarely reported and test specimens are often removed from the weldment in such a manner as to relieve all or most of the residual welding stresses [97,99].

2.5.2.1 Fatigue crack growth through a residual field

Even if the residual welding stresses in a component could be computed, this effect on fatigue crack propagation would be difficult to assess, mainly because the residual stress distribution is often very complex and its response to the presence of a growing crack is unclear. Underwood et al [100] investigated fatigue crack growth through a measured residual stress field in low alloy forged steel with a yield strength of 1210 $MN/m^{3/2}$. Residual stress in three-point bend specimens was produced by using a localised plastic deformation process. Although the probable residual stress distribution must satisfy the conditions of zero resultant force and moment, a stress distribution that remained linear across the full width of the specimen was assumed which allowed the stress distribution to be represented by superposition of pure bending and uniform tension. Fatigue crack growth data were obtained for both as-received and residual-stress relieved specimens.

An expression proposed by Underwood et al for ΔK which attempted to include the effect of residual stress took the form:

$$\Delta K_{eff} = (K_{max} + K_R) - (K_{min} + K_O) \qquad ,(2.31)$$

where ΔK_{eff} is the effective ΔK including effects of residual stress, K_{max} and K_{min} are the extreme values of

applied K, and K_R and K_O are the K-values which simulate the effect of residual stress at the points of maximum and minimum load during the cycle. In the case of a compressive residual stress, crack closure can occur, resulting in the delayed opening of the crack at some point in the cycle above the minimum load.

Underwood et al also considered both notched and cracked specimens with their idealised residual stress distributions. In the case of the notched specimen, the residual stress distribution is shifted to the end of the notch and is independent of the applied load. The cracked specimen, however, can close completely under the influence of a compressive residual stress and will transmit the load across its faces. When the cracked specimen is loaded, the residual stress distribution is similar to that of the notched case, and will therefore shift depending on whether the crack is open or closed. Using this argument they found the following relationships:

$$\Delta K_{eff} = \Delta K_{app} + K_R \qquad \text{for cracked specimens,} \quad (2.32)$$

$$\Delta K_{eff} = \Delta K_{app} + 2K_R \qquad \text{for notched specimens,} \quad (2.33)$$

where ΔK_{app} is the applied ΔK .

Two methods of obtaining K_R were suggested. The first method uses the simple expression

$$K_R = \sigma_{Rave}\sqrt{\pi a} \qquad ,(2.34)$$

where σ_{Rave} is the average value of the redistributed residual stress near the tip of a crack of length a . A superposition of a pure bending and a uniform tension stress intensity factor is used in the other approach. The latter does not take redistribution of residual stresses into account.

An analysis of results showed that the effects of residual stress remained significant, even at a/w=0.3 . When the redistribution of residual stress was taken into account a reasonable agreement with stress-free results was obtained. The results also seemed to indicate that the effect of residual stress is independent of crack length. The authors believe that this may have been due to the local closing effect on the crack tip which occurs over an area which is small relative to crack length.

Since residual stresses are often present in the weldment, some work on fatigue crack growth by means of residual stresses has been reported. In common with other work reviewed in this section, Glinka [101] used a superposition method, assuming that the effective stress intensity factor, ΔK_{eff} , can be computed as the sum of the residual stress intensity factor, $K_R = f(\sigma_R)$, and the applied stress intensity factor, $K_{app}=f(\sigma)$. It was assumed

that residual stresses do not diminish under fatigue loading. Glinka believed that this assumption overestimates the residual stress effect, but is reasonable from a practical point of view. For calculating K_R in a centre-cracked plate Kanazawa's [102] formula was used:

$$K_R = \int_{-a}^{a} \sigma_R(x) \left\{ \frac{2 \sin(\pi(a+x)/w)}{w \sin(\frac{2\pi a}{w}) \sin(\pi(a-x)/w)} \right\}^{\frac{1}{2}} dx \quad ,(2.35)$$

where a is the half-crack length, w is the plate width, and the x-axis lies in the crack plane with x=0 when a=0. The true residual stress distribution was approximated by simplified rectangular distribution. Forman's [27] equation which includes the stress ratio was used to obtain life predictions. Good agreement with experimental results was obtained. Glinka also notes that the effect of residual stress on fatigue crack growth rate depends on the magnitude of the applied load. The lower the applied load the higher the residual stress effect. Also, a higher applied load causes greater residual stress relaxation.

2.6 FATIGUE CRACK PROPAGATION IN WELD METAL

Fatigue cracks which are initiated at the sites of internal defects, such as slag-inclusions or lack of root fusion, may spend all their lives propagating in the weld metal. If a crack initiates at the toe of the weld, it spends the initial part of its life in weld metal and eventually propagates into the heat affected zone (HAZ) and

base plate.

Early workers assumed that low fatigue strengths associated with welded joints were a consequence of the metallurgical features of the weld metal and HAZ which were in some way inferior to those of the parent plate. However, Baxter et al [103] showed that the fatigue strengths of the basic materials Properties were at least as high as that of the parent metal, and the reason for the low fatigue strength of the joints was the presence of severe stress concentrations.

It is not suprising that conflicting theories about the fatigue properties of weldments should exist. The metallurgical features of a weld joint are complex and variable through the joint; also, different weld metals and welding processes will result in different features.

In order to be in a position to predict the fatigue behaviour of welded joints it is clearly desirable to know how much the varying metallurgical structure of a weld influences the rate of crack propagation.

Dawes and Richards [104] investigated fatigue crack propagation across weld and parent plates of mild and low alloy steel with particular emphasis on the rate of crack propagation across HAZ. The plates were butt-welded using a

K-preparation such that the weld and HAZ were at an angle of 75°to the direction of loading. Fatigue tests were carried out under a constant range of stress intensity factor. They observed that the rate of crack growth was virtually the same in both the parent and the weld metal.

Griffiths et al [105] investigated the influence of mean stress on fatigue crack growth in low alloy steel weld metal. They carried out constant-K tests and observed that high tensile mean stresses cause an increase in the rate of crack growth. They also carried out fractographic examination of the fatigue-fractured surfaces and observed typical ductile striations and areas of propagation by void coalescence type fatigue fracture which can only occur under plane stress conditions.

Parry et al [106] studied the fatigue crack growth in weldments, HAZ and parent plate of A514 steel using compact type and single edge notch specimens. They observed that the mean load had no effect on the crack growth rates in the weld and suggested that fracture mechanisms other than striation formations were also operative during the fatigue process so as to account for the growth rate differences (e.g., quasi-cleavage and void coalescence).

Shahinian et al [107] performed tests on types 304 and 316 stainless steel and submerged arc weldments at room

temperature. In general, the resistance to crack growth of weld metal was about the same as that of parent metal at room temperature, slightly greater at 427° C, and significantly greater at 593° C. They attributed the superiority of fatigue resistance of weld metal relative to that of base metal to microstructural differences. They observed at high temperatures the fine duplex delta ferrite-austenite microstructure of the weld metal with its many phase boundaries which they believed were more responsible for the resistance to crack growth than the larger grain, fully austenitic structure of the base metal.

The effect of load-cycling frequency and environment on fatigue crack growth of weldments was investigated by Poon and Hoeppner [108]. The material they used was ASTM A533 grade B class 1 weldment material in which weldments were fabricated by manual shielded metal arc welding procedures. They observed no effect of frequency in laboratory air, but reducing the frequency from 10Hz to 0.5Hz accelerated the crack growth rates in a distilled water environment. Fractographic examination of fatigue-fractured specimens revealed no significant differences in crack growth rates. This was because of the similar microstructure of the weld material in both laboratory air and distilled water.

Ohta et al [109] have recently reported on threshold and mid-range fatigue crack growth in butt-welded joints, and also investigated the effects of welding processes on

fatigue crack propagation. The material used was 20mm thick HT80 steel of which one series of specimens were butt-welded by a gas metal arc welding process, and the other series by submerged arc-welding. They compared the results to that of the base plate and concluded that the fatigue properties of welded joints were inferior to those of the base metal, no significant differences being found between the fatigue crack propagation properties of welded joints made by different welding processes.

Finally, fatigue crack propagation from surface flaws in austenitic type 316 butt-welds has been studied by Lloyd and Walls [110]. They investigated the effect of the position of the flaw, mean stress and weld heat treatments. A U-configuration weld preparation was used. The surface flaws were introduced wholly within the weld by a combination of spark-machining and fatigue. This preparation gave specimens with an approximate semi-elliptical crack with an initial a/2c of 0.2 and initial a/B ratio of 0.3. To study the influence of the surface flaw they employed different initial a/2c values. The tests were carried out at 1Hz which showed that at low values of ΔK an increase in stress ratio from 0.05 to 0.6 had little effect on the rate of crack propagation. From the variation of the crack depth-to-length ratio a/2c with position within the plate, they concluded that, irrespective of the initial starter defect configuration, the crack shape changed asymptotically towards a/2c=0.4 for tension-to-tension loading; moreover, heat treatment was not beneficial in their case. From the

comparison of the maximum rates of fatigue crack growth in the butt welds and wrought parent plate they concluded that fatigue crack propagation was fastest in the parent plate.

2.7 FATIGUE CRACK PROPAGATION IN THE HEAT-AFFECTED ZONE (HAZ)

Most researchers mentioned in the previous section discussed fatigue crack growth in HAZ as well as in weld metal. In a machined butt weld fatigue cracks are usually initiated in the base plate rather than the more brittle HAZ, even though in some materials (e.g., low alloy steel), HAZ may be more notch-sensitive [111].

Dowes and Richards [104] investigated crack propagation behaviour crossing the base plate and HAZ under constant ΔK. The mechanism of fracture was the same in both base plate and HAZ, i.e., ductile propagation with formation of striations, but the rates of crack growth were different. As the crack approached the HAZ from the base plate the rate of crack growth fell sharply until the crack reached the centre of HAZ; from there on the rate increased and eventually continued at the original rate into the weld. Hardness measurements showed that the welding produced a hard HAZ. Dawes and Richards suggested that reduction in the rate of propagation was due to the change in the yield Stress which was reflected in the variation in hardness.

Parry et al [106] measured the propagation rates for a crack growing in the HAZ. They observed that the crack growth rate was considerably lower in the HAZ than the growth rate in the base metal. The tests on stress-relieved specimens revealed that the growth rate in the HAZ increased considerably. From these observations they concluded that the HAZ was also under the infuence of residual stresses.

Poon and Hoeppner [108] investigated the crack growth in HAZ of an ASTM A533 grade B class 1 weldment which was fabricated by manual shielded metal-arc welding. They observed that the effect of frequency was slight in laboratory air when the data for 10Hz and 1Hz were compared. The crack growth rate data obtained in distilled water were compared for the weld metal and HAZ, showing that the crack growth per cycle for a weld is slightly higher than that for HAZ. It was also shown that the fatigue threshold, ΔK_{th}, for both HAZ and weldment differed only slightly.

Ishihara et al [112] measured the fatigue crack growth rate in an HT80 weldment and HAZ, and examined the fatigue-fractured surfaces by means of fractography. The lowest crack growth rate was obtained in the HAZ which was attributed to the welding residual stresses. They compared the macroscopic growth rate and the striation spacing and observed that for the base metal and HAZ, the growth rate coincided with the striation spacing almost completely, but for the weld metal the macroscopic growth rate did not

coincide with the striation spacing at all and was approximately twice as much as for the striation spacing corresponding to ΔK. This discrepancy they believed was due to the acceleration of macroscopic growth rate by dimple fracture.

Kitsunai [113] determined the fatigue crack growth rate in a steel plate 12mm thick with differing stress ratios in the weld metal, HAZ and base plate. He concluded that the fatigue crack growth rates in the base plate, weld metal and HAZ above the value of ΔK =15 $MN/m^{3/2}$were about the same regardless of stress ratio, but near threshold the growth rate was highest in the HAZ.

Maddox [114] investigated fatigue crack propagation in the HAZ and weld metal. His results showed that the crack growth rate in HAZ is similar to or slower than that of weld metal. Ohta et al [109] also carried out tests on HAZ. Their study showed that the fatigue properties of HAZ were inferior to those of base metal with a threshold stress intensity factor about a quarter that of base metal. They attributed this inferiority to the tensile residual stress around the crack tip.

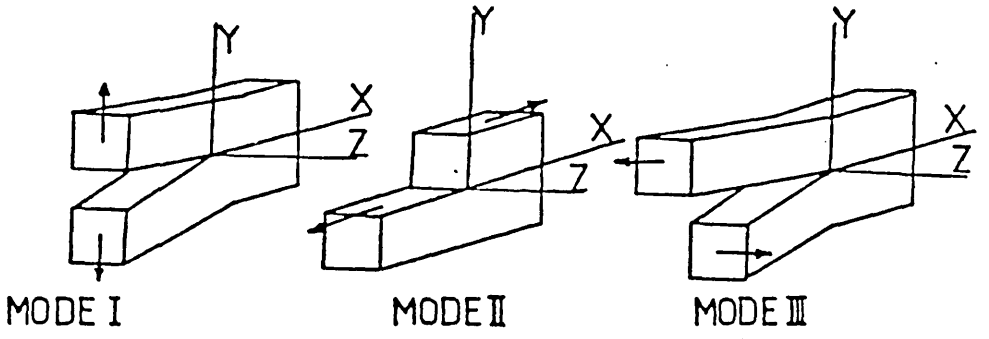


Figure 2.1 Loading modes

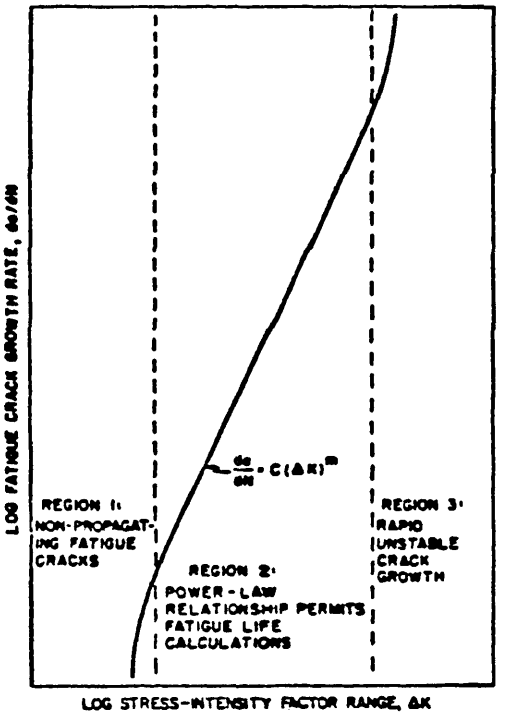


Figure 2.2 The sigmoidal nature of the crack propagation curve

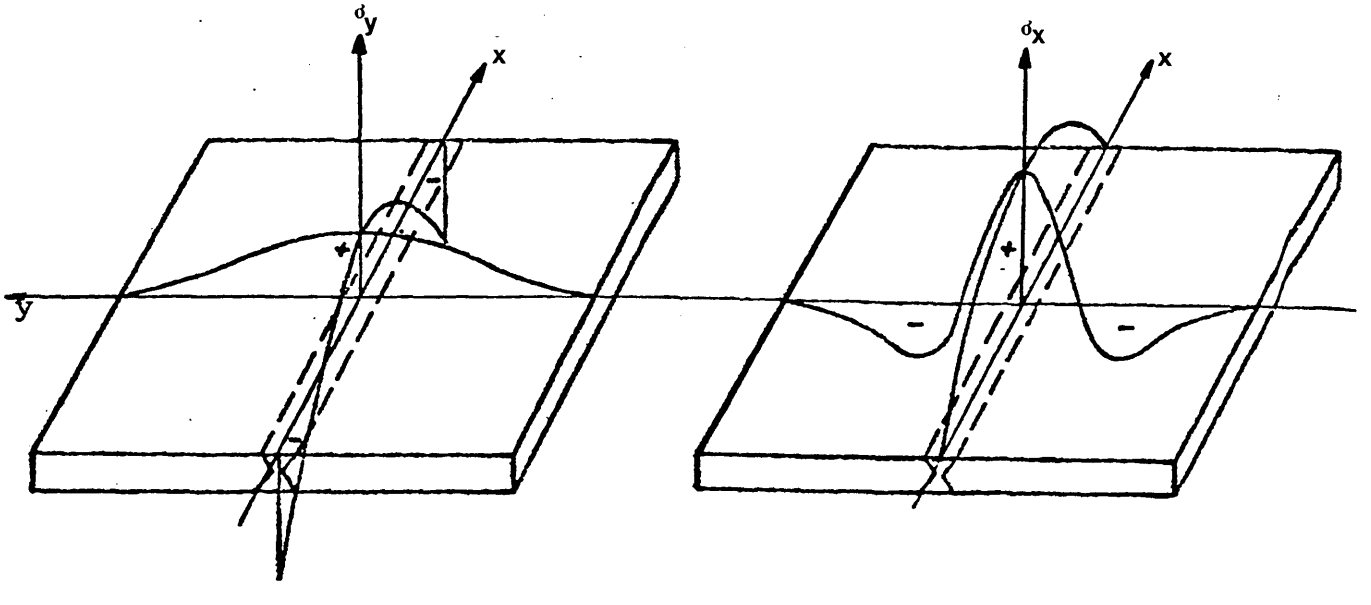


Figure 2.3 The residual stress pattern for two butt-welded plates

CHAPTER 3

EXPERIMENTAL DETAILS AND DATA PROCESSING TECHNIQUES

3.1 Material and Test Specimens

Although the present investigation is concerned with the fatigue cracks in butt-welded joints, it was necessary to obtain fatigue crack propagation data for the materials associated with welded joints.

The material used for this investigation was a low alloy steel, BS4360-50D, available in hot-rolled plates of 25mm thickness. The chemical and mechanical properties of the material are given in Table 3.1. No additional heat treatment was performed on either the plates or the machined specimens.

Two types of specimen were used in this investigation; the standard compact type (CT) and surface-notched plate (SNP) of dimensions as shown in Figs. 3.1 and 3.2. The steel specimens were manufactured from the supplied plates so that the fatigue crack propagated perpendicular to the rolling direction. In the case of SNP the notch was produced using a 30° circular cutter of 3 inches diameter.

The blanks for the butt-welded CT specimens were prepared by the butt-welding of two plates, each about 50mm

wide and 95mm long. For the case of SNP geometry, two plates 120mm wide and 210mm long with the butt-weld running across each plate were used (see Fig. 3.3). The joint preparation was a double "Vee" and incorporated a 2mm root gap which is shown in Fig. 3.4. Manual arc-welding and the wide weave technique were employed for manufacturing the butt-welded specimens using a C/Mn electrode of type BS639(1976):E4311R21. The chemical composition and mechanical properties of the weld metal are given in Table 3.2. The kind of prepared joint for the specimens where the crack was to grow in the HAZ was the "K" joint, in order to ensure that the crack stayed in HAZ during the test (see Fig. 3.5). Butt-welding of plates caused some angular distortion as shown in Fig. 3.6. This angular distortion was found to affect the results obtained for the weldment in a bending stress field. Two sides of the welded plates were identified and are referred to here as the "tensile" side and the "compressive" side (see Fig. 3.6). Therefore it was necessary to fabricate two kinds of SNP geometry: one where the notch was located on the tensile side; the other where the notch was located on the compressive side. This will be discussed in detail in Chapter 5.

The blanks for sandwich welded specimens were prepared as for the conventional welded specimens described above. Fabricating sandwich welds consists of using electrodes which have different mechanical properties for each pass and then stacking up a sandwich in which the outer layers are made of the same material but having a higher yield strength

than the middle layer, five-layer sandwich was used in fabricating this kind of specimen. The type of welding electrodes used were BS1719:E317, BS1719:E217, BS2926:20.9.3R. The arrangement of electrodes is shown in Fig. 3.7, and the chemical and mechanical properties are given Tables 3.3, 3.4, and 3.5.

All the welds were ground flat, and some of the welded joint specimens were stress relieved at 650°C for half an hour then furnace cooled to room temperature.

The surface of one side of each specimen in the case of CT geometry and the notch side for the case of SNP geometry were polished to facilitate optical observation of the crack tip. Both geometries were found to be satisfactory for the testing machines used and the results were sufficiently repeatable.

The specimens used for tests in salt water were specially prepared. For CT geometry the fluid was collected via channels made from thin aluminium plates and stuck around the specimen with Araldite adhesive (the Araldite was made by CIBA-Geigy & Additives Co., Cambridge). The bond was strong enough to hold the channels and yet flexible enough not to affect the specimen compliance. A transparent perspex strip was stuck to the channel on the side where optical viewing of the crack was made (see Fig. 3.8).

For the case of SNP geometry a rectangular reservoir was made of rubber and stuck around the crack with Evostick adhesive (the adhesive was made by Evode Ltd., Stafford). To facilitate the crack depth measurements ten pairs of probe terminals were spot-welded onto the face and across the notch, and ten reference probe terminals spot-welded approximately 1mm from the crack mouth (see Fig. 3.9). A piece of transparent perspex was stuck to the rubber to facilitate the optical viewing of the crack on the surface and to prevent the salt solution from splashing out of the reservoir. The salt water was introduced into the notch of the specimen via a thin plastic tube and the flow rate was controlled by gravity feeding and adjusted by means of a screw clip.

3.2 Testing Machines

The tests in the present investigation were carried out using Dowty Electro-Hydraulic and Mayes Servo-Hydraulic fatigue machines.

The Dowty fatigue machine type has a range of load cycling frequencies from 0.06 up to 100Hz depending on the applied load. The machine has three load cells of maximum load capacities of 15kN, 30kN, and 60kN, respectively (see Fig. 3.10).

The Mayes Servo-Hydraulic machine type has a range of frequencies from 0.1 to 200Hz and again the choice of frequecy depends on the applied load. The machine had a load cell of maximum capacity 100kN (see Fig. 3.11).

In all these machines, it is possible to adjust the load while the test is in progress, and automatic switch-off is provided when specimen failure occurs or when specimen deflection exceeds a prescribed amount. The machines are provided with facilities for choosing the shape of the input load control waveform (i.e., sinusoidal, triangular, etc.).

Both machines were provided with suitable grips for holding the compact type specimens. Also a four-point bend rig was designed to facilitate both the Mayes and Dowty machines for the use of surface notch geometry in the testing (see Fig. 3.12).

The Dowty and Mayes have facilities for feeding the load signal into an external recorder and also can take external load signals. They are equipped with a digital voltage display of the applied loads, enabling the mean, maximum, and minimum loads to be observed. The Dowty load display reads 10 volts at maximum load for the respective load cell, while that of the Mayes reads in a percentage of the load. The two-decimal place display enables these

machines to sense load changes of less than 0.01kN.

The load calibration of all machines used was checked and found to be within allowable limits. Some check fatigue crack growth tests were performed to ensure that the machines used gave similar results under identical conditions.

3.3 CRACK LENGTH MEASUREMENTS DURING FATIGUE TESTS

There are several methods which can be used to monitor crack length during a fatigue test. The most commonly used methods are the optical and the potential drop techniques. The optical method measures the crack length on the surface of the specimen but cannot detect the crack front configuration in the interior of the specimen. The potential drop technique can be used to measure through-thickness cracks [115]. In the present investigation both the optical and the potential drop technique were used.

Measurements of the surface crack length for both compact type and surface-notch plate geometries were made using microscopes mounted on travelling micrometric stages. These microscopes could measure crack increments of less than 0.01mm. The crack length measurements on the base metal compact type specimen were made on one side of the specimen since the crack growth was uniform across its thickness. However, with the welded compact type specimen the crack

growth was non-uniform across the specimen thickness with one side of the crack front leading the other; also, the crack front curvature was sometimes substantial. Thus the crack length measurements were made on both sides of the specimen and after each test the specimen was opened up and measured, and the crack length corrected for the curvature of the crack front as recommended in ASTM standards [116].

The crack depth measurements for the surface-notched specimens were carried out using an A.C. potential drop microgauge [117]. This instrument and its performance are briefly discussed below.

3.3.1 Crack Depth Measurement Using The Potential Drop Microgauge

The crack microgauge is designed to detect and measure the depth of cracks or other discontinuities in metallic components. It can be used on both steels and aluminium alloys with or without prior calibration depending on the application and the accuracy required. The principle upon which the instrument relies is that a steady current (A.C.) field of 2 amps is generated to flow approximately normal to the defect under examination. Due to the type of the field generated, the current path is limited to the skin of the sample under test. When a suitable measurement probe is placed on the sample, a very accurate measurement of the voltage drop between the probe electrodes is made. If a fatigue crack is present in the sample, the A.C. current

will follow the surface of the metal around the crack. By interpretation of the potential drop across the crack, either directly from the theory or using prior calibration, a measure of crack length or depth can be determined.

A digital meter, which can read from zero to $\pm$ 1999 volts is provided. Coarse and fine gain control adjustments can be set to give the most convenient reading on the panel meter depending on the accuracy required. The instrument also has an output facility to enable recording of the probe voltage on a chart recorder. This facility was not used in the present investigation.

The current terminals were supplied by RS components Ltd., London, (of type 4BA insulated terminal; 10 amps). They were screwed into 4BA taped holes, drilled symmetrically on either side of the specimen such that they were perpendicular to the notch. The current terminals were connected to the current leads using insulated bunch pin-plugs, also supplied by RS components. The current lead, which was cut from a twin-cored 6.2mm diameter screened cable with twisted core for hum reduction, was connected to the crack microgauge using a two-way cable socket.

For the tests in air a standard 10mm probe was used. A probe holder was made from perspex, which enabled the probe to slide along and across the crack, and also permitted a

direct view of the crack (see Fig. 3.10). One side of the holder was marked every 2mm so that the depth measurement could be carried out at the same position for successive readings. This also enabled measurements for different specimens to be compared. Twelve to twenty-five positions in the direction of the crack were used for the crack depth measurements.

For the tests performed in a salt water solution, where the standard probe could not be used, twenty pairs of probe terminals were spot-welded onto the face and across the notch and crack line, each pair having a pair of reference probe terminals (see Fig. 3.9). These terminals were made from soft iron wire of diameter 1mm. A spot-welding machine (made by Unitec corporation, U.S.A., model 1-048-03-02), provided with 1.6mm copper electrodes, was used for the spot-welding process. The machine was set at 65 watt/second for the best welding process.

The probe terminals were positioned 10mm apart equally spaced about the crack line. The reference terminals were also set at 10mm apart but to one side of the crack line and approximately 1mm from the notch and crack line. The distance between each pair of probe terminals was 5mm, and the first probe was positioned in the middle of the notch. The probe terminal wires were connected to the probe lead by soldering. The probe lead, cut from a single core of 2mm diameter screened cable, was connected to the crack

microgauge by means of a four-pin plug.

3.3.1.1 Effect of crack front shape on digital meter reading

The effect of crack front shape on the digital meter reading was investigated to see whether the reading needed any subsequent adjustment. Using a specimen with growing fatigue crack, crack depth measurements were made for different probe positions across the width of the specimen. After each crack depth reading the crack-front profile was marked by changing the amplitude of loading for approximately 10,000 cycles. At the end of the test the specimen was cooled in a liquid nitrogen bath and then broken under three-point bend loading. The crack profiles corresponding to the crack depth measurements were then recorded by means of a microscope. Fig. 3.13 shows the results, from which it can be observed that the digital meter reading consistently underestimated the crack depth whatever the position of the probe across the specimen width. This error was found to be about 10% for the deepest point and increased up to about 40% near the edge of the crack. The results from different specimens of the same material and also for welded specimens, with the same current and probe position, were found to be adequately repeatable.

The effect of salt-water environment on the digital meter reading was also investigated. The primary calibration

on a growing fatigue crack which was measured in air and then filled with salt water solution showed a very small decrease in digital meter reading. This slight difference which was also observed by Dover [118] is because water is a better conductor than air and some of the field will be transmitted through this medium as well as the steel. However, the differences are so slight that they really make no impact on the accuracy of the crack depth prediction.

3.3.1.2 Effect of gain setting on digital meter reading

The variation of digital voltage with crack depth was investigated to find any variation in sensitivity of the microgauge in measuring crack depth. A fatigue test was performed and crack depth measurements were made for different probe positions across the width of the specimen, and the gain settings were adjusted from minimum to high values. The results are shown in Fig. 3.14.

The variation of the digital voltage with crack depth is linear, and increasing the gain results in a corresponding increase in sensitivity without affecting the linearity.

3.4 SCANNING ELECTRON MICROSCOPE (SEM)

A Joel-T200 scanning electron microscope was used. The fracture surface was cut from one half of the broken test-piece to suitable dimensions for mounting on the SEM

specimen holder. After cleaning the specimen with acetone in an ultrasonic bath and allowing it to dry in the open, the fracture surfaces were then examined using a secondary electron image at an acceleration voltage of 25 kV, and working distances of 20 and 48 mm.

A small amount of conducting paint (made by Acheson Colloids Co., Plymouth) was applied between the specimen and the stage to improve conduction. This was necessary and sufficient to prevent charging when the specimen was examined in the scanning electron microscope. The specimen holder was able to move in two perpendicular directions (x and y) so that almost any orientation and position of the fracture could be examined. The exact position of the specimen to be examined was located with respect to some reference point (e.g., specimen edges) by means of two micrometers which control the movement along the x and y directions.

3.5 ANALYSIS OF THE RESULTS

The first step in the analysis of the test results was to obtain the rate of crack propagation from the measurements of the crack length or depth, made at the appropriate number of cycles. Various techniques have been used to analyse such data. A summary and brief description of some of these techniques is presented below.

3.5.1 The Graphical Method

This method involves drawing the best curve through the a versus N (i.e., crack length versus number of cycles) data and estimating the crack growth rate by measuring the slope of the tangent to this curve at the corresponding experimental point. Such visual analysis of data suffers from the error due to the individual's subjective choice of the best-fit curve and also the best tangent through a particular point on the curve for determination of the crack growth rate.

3.5.2 Finite Difference or Secant Method

This method involves calculating the slope of the straight line connecting two successive data points, (a_i, N_i) and (a_{i+1}, N_{i+1}), i.e.,

$$\frac{da}{dN} = \frac{a_{i+1} - a_i}{N_{i+1} - N_i} \qquad \text{.(3.1)}$$

This technique can result in erratic gradients at times because of the inherent scatter in the experimental fatigue data. It should, however, be noted that when a large number of data points are available, taken at suitable intervals of a_i and N_i, the scatter in da/dN data can be considerably reduced using the secant method in conjuction with a graphical method, as was observed in the present investigation.

3.5.3 Modified Difference Method

This method estimates derivatives of an unknown function from derivatives of either an nth-order polynomial passing through a number of adjacent pivotal points or by a Taylor's series expansion of unknown functions. This technique uses sets of successive data points over the range $a_{i-2}<a<a_{i+2}$ to calculate da/dN at the mid-point, a_i.

3.5.4 The Incremental Polynomial Method

This method estimates crack growth rates by fitting a second order polynomial to sets of seven successive data points. The form of the equation for the local fit is [119]:

$$a = b_0 + b_1 \left(\frac{N - C_{N1}}{C_{N2}}\right) + b_2 \left(\frac{N - C_{N1}}{C_{N2}}\right)^2 \quad ,(3.2)$$

where b_0, b_1 and b_2 are regression parameters which are determined by the least square criterion over the range $a_{i-3} \leq a \leq a_{i+3}$. The parameters $C_{N1}=(N_{i-3}+N_{i+3})$ and $C_{N2}=(N_{i+3}-N_{i-3})$ are used to scale the input data, thus avoiding numerical difficulties in determining the regression parameters. The rate of crack growth is obtained from the derivative of Equation (3.2) which is given by the expression

$$\frac{da}{dN} = \frac{b_1}{C_{N2}} + 2b_2 (N_i - C_{N1}) / C_{N1}^2 \quad .(3.3)$$

3.5.5 The Total Polynomial Method

This method involves fitting a high order polynomial to selected data points (typically 20 to 70) covering the entire range of data. The curve-fitting model is of the general form:

$$a = \sum_{i=1}^{N} B_i F_i (N) \qquad ,(3.4)$$

where the curve-fitting functions $F_i(N)$ are power functions whose exponents are determined by the min-max criterion, that minimises the maximum deviation between the observed and the fitted values of the crack length. The regression parameters, B_i, are subsequently determined by the least square criterion. The rate of crack growth at each data point is estimated from the derivative of the above expression.

3.5.6 Discussion of Data Processing Methods

The scatter of the crack growth rate data obtained using the various methods discussed above will depend on the degree of variability in the raw experimental data. If, for example, the data points lie on a smooth curve then the secant method may prove satisfactory. If, however, the experimental data are subjected to a great amount of scatter, a curve-fitting method is to be preferred.

Gurney [120] attempted to analyse his results with a computer, by fitting a curve to the crack propagation data

and obtaining da/dN by differentiation. However, the method failed because of scatter in the results.

Davies and Fedderson [121] attempted to present their experimental data using polynomial curve-fitting but observed that the fitted curves oscillated about the experimental data in such a way that the gradients estimated by differentiation were seriously in error. They also observed that the secant method in their case produced better results.

McCartney and Cooper [122] have developed a least square method of estimating growth rates by making use of a spline function (a piece-wise continuous polynomial). Though they obtained comparatively good results, nevertheless oscillation about some points was observed.

Wei et al [123] statistically compared crack growth rate data obtained by using the finite difference method and by some incremental polynomial techniques. They observed that the incremental polynomial method generally introduced a systematic bias into the da/dN data. However, in practice, the bias may not be significant in terms of probable errors in predicted fatigue lines. The finite difference (secant) method and parabolic curve-fitting procedure (Simpson's rule) did not show significant bias, although these methods produced greater scatter. The secant and the incremental

polynomial methods are recommended by ASTM standards [116].

In the present investigation, the raw data with a considerable amount of scatter were averaged out and the secant method was used. However, for the raw data with less scatter, the curve-fitting procedure was found satisfactory. The amount of scatter in crack growth rate data is also influenced by the interval of crack length measurements [123]. Although large measurement intervals might produce acceptable variations in da/dN data, they could severely limit the number of observations made during fatigue tests on a single specimen and affect the precision of computing ΔK . Therefore, the choice of measurement interval is important and depends on a realistic assessment of measurement precision, which should be established experimentally for individual situations. In the present investigation it was established that measurement intervals of the order of 0.5mm produced satisfactory results for crack growth rates using either the secant or the curve-fitting techniques. It is also observed that the scatter in the raw data could be significantly reduced by first averaging the data before calculating the crack growth rates using the secant method. Thus it was decided that the secant method for raw data with little or no scatter, or graphical averaging followed by the secant method, would be used to determine crack growth rate in the present investigation.

3.6 DETERMINATION OF STRESS INTENSITY FACTORS

The crack growth results, in the present investigation, have been analysed using the fracture mechanics approach. Thus, it was necessary to establish an expression for the stress intensity factor, K, for the particular geometry studied.

3.6.1 Compact Type specimen

For this geometry, K is given by [124]:

$$K = \frac{P}{Bw^{\frac{1}{2}}} f(a/w) \qquad ,(3.5)$$

where P is the applied load, B is the specimen thickness, w is the specimen width, a is the crack length and f(a/w) is a measure of the compliance of the specimen. For a constant ratio of specimen height, H, to specimen width, w, the function f(a/w) can be expressed in a polynomial form as a function of dimensionless crack length (a/w). The compact specimens have H/w equal to 1.2 and f(a/w) can be expressed by [124]:

$$f(a/w)=29.6(a/w)^{1/2}-185.5(a/w)^{3/2}+655.7(a/w)^{5/2}-1017.(a/w)^{7/2}+683.9(a/w)^{9/2} \qquad ,(3.6)$$

for

$$0.3<a/w<0.7 \quad .$$

Expression (3.6) covers a limited range of crack length, but calibrations covering a much broader range have recently been developed. Willson [125] has obtained an expression for

f(a/w) for lengths of a/w>0.8 of the form:

$$f(a/w) = \frac{2\,(1+a/w)}{1 - (a/w)^{3/2}} + \frac{1}{2\,(1-a/w)^{1/2}} \qquad .(3.7)$$

A K-calibration expression valid for 0.2<a/w<0.925 has been given by Srawely [126]:

$$f(a/w) = \frac{2 + a/w}{(1-a/w)^{3/2}} \left\{ 0.886 + 4.64(a/w) - 13.32(a/w)^2 + 14.72(a/w)^3 - 5.6(a/w)^4 \right\} \qquad .(3.8)$$

3.6.2 Semi-Elliptical Surface Cracks

Values of the stress intensity factor as the crack propagates through a plate are necessary for the reasonable prediction of the life and mode of failure of a structure. Since there exists a stress gradient across the thickness of a plate, and the shape of the crack is usually that of an ellipse, a three dimensional analysis is essential.

Much of the earlier effort has been confined to two-dimensional analysis because of the complexity of the three-dimensional case. Investigators have used experimental or approximate analytical methods to obtain stress intensity factors for surface cracks under tension or bending loads.

The surface flaw is the most prevalent type of flaw in many classes of structures, particularly welded structures. Weld defects are the usual origin of surface flaws in welded joints. It may be argued, however, that since most of the life of welded structures is spent at low stress intensity factors and with short cracks, estimated values derived from semi-elliptical cracks in a finite thickness plate subjected to bending will provide adequate results.

The solution of Irwin [127] provides a useful example of such an approach. For a semi-elliptical flaw in an infinite elastic plate subjected to uniform tension with major and minor axes 2c and 2a respectively (a being in the through thickness direction), the value for the stress intensity factor at an angle θ to the axis is given by:

$$K = 1.12 \frac{\sigma\sqrt{\pi a}}{E(k)} \left(\sin^2\theta + \frac{a^2}{c^2}\cos^2\theta\right)^{1/4} \quad ,(3.9)$$

where $E(k)$ is an elliptical integral of the second kind and may be approximated by

$$E(k) = \left[1 + 1.47(a/c)^{1.64}\right]^{0.5} \quad .(3.10)$$

The figure of 1.12 in (3.9) is a correction factor to allow for the presence of a free surface ahead of the crack tip and plasticity. The maximum error in the stress intensity factor from using (3.10) is about 0.13 percent for all values of a/c [128].

The surface crack in a finite plate is shown in Fig. 3.2 . The width of the plate, w, is usually large with respect to the crack length. The form of the stress intensity factor is given by:

$$K = \frac{\sigma\sqrt{\pi a}}{E(k)} \; F(a/t,\; a/c,\; c/w,\; \theta) \qquad ,(3.11)$$

where F is the boundary correction factor, which takes account of the influence of the front face, back face, and finite width on the stress intensity factor for a crack in an infinite solid. Many investigators have tried to determine the correct expression for F through approximation techniques.

Shah and Kobayashi [129] estimated the correction factors from an empirical front face magnification and an analytical back face magnification. They obtained a solution for an embedded elliptical crack approaching the free surface of a semi-infinite solid.

The alternating method was used by Smith and Sorensen [130] to calculate the variation of the stress intensity factor along semi-elliptical surface cracks in a finite thickness plate. They obtained the stress intensity factor as a function of position along the crack border for a variety of crack shapes and crack depths. They concluded that the effects of the front and back surfaces and the

interaction between them are all important in the analysis. They also found that the maximum stress intensity does not necessarily occur at the deepest point along the border of a shallow semi-elliptical surface crack.

Raju and Newman [131] obtained a correction factor by employing a finite element method with singularity elements for completely embedded elliptical cracks in large bodies and for semi-elliptical cracks with aspect ratios ranging from 0.2 to 2.0 in an infinite-thickness plate. To verify the accuracy of the finite element method, completely embedded circular and elliptical cracks were analysed. The stress intensity factors for these cracks were generally within 1.0 percent of the exact solution [132]. However, for the elliptical crack the calculated stress intensity factors in the region of sharpest curvature of the ellipse were about 3% higher than for the exact solution. Raju and Newman also found that for the semi-circular surface crack the maximum stress intensity factor occurred near the intersection of the crack with the free surface, but, for the semi-elliptical surface crack, the maximum stress intensity factor occurred at the deepest point, and for both the semi-circular and semi-elliptical surface cracks the stress intensity factors were larger for larger values of crack-depth to plate-thickness ratio. In a later publication [133] they reported stress intensity factors from a three-dimensional, finite element analysis for shallow and deep semi-elliptical surface cracks in finite elastic plates subjected to tension or bending loads which covered a wide

range of configuration parameters. The effect of plate-width on stress intensity factor variations along the crack front was also investigated. For ease of computation an equation for the stress intensity factor of a surface crack in a finite plate subjected to tension and bending loads was fitted to their finite element results. They claimed that for all configurations for which ratios of crack-depth to plate-thickness do not exceed 0.8, the equation was within ± 5 percent of the finite element results and single edge crack solution.

Hayashi and Abe [134] have recently proposed a solution for the stress intensity factor and compared their results with those from two other sources [135,136]. The agreement at the surface point for a semi-circular crack is suprisingly good. However, at the deepest point the disagreement between the authors is more marked.

McGowan et al [137] compared the results of some recent stress intensity factor studies on surface flaws in a plate under remote tension and bending. These results were of high precision because of the sophisticated numerical techniques used, and McGowen et al arrived at a best estimate of the stress intensity variation along the flaw border. The geometry of the semi-elliptical surface flaw examined had depth-to-length ratio of 0.25and25 and 75 percent relative crack depths (i.e., a/t =0.25, etc.). The derived best estimate curve for the stress intensity factor was believed

to be within 3 percent of the actual value along the crack front. The comparison of the best estimate curve with experimental data gave an error of ± 10 percent which they considered was largely due to the difference in geometry and Poisson's ratio.

Koterazawa and Minamisaka [138] estimated the stress intensity factors of semi-elliptical surface cracks in a plate of finite thickness subjected to bending by taking account of the free surface magnification factor for the stress intensity component due to linearly varying pressure, which they claimed was neglected in a calculation by Shah and Kobayashi [139]. The authors believed that the stress intensity factors obtained were somewhat smaller than those given by Shah and Kobayashi, and gave a reasonable estimate of the propagation rate of part-through cracks by fatigue.

Holdbrook and Dover [140] found a correlation factor for deep surface cracks under both tension and bending loads. They analysed the problem by first considering the variation of K around the perimeter of a surface crack and then obtained a correlation with standard fatigue crack growth data by applying simple correction factors to the existing infinite plate solution. It was possible to correlate fatigue crack growth data measured on surface crack plate specimens with conventional through-crack data.

In a recent review by Scott and Thorpe [141], the accuracy of several theoretical stress intensity solutions in predictive fatigue crack growth calculations was tested by using the development of the shape of the fatigue crack as a diagnostic tool. They have suggested that the stress intensity factor solutions for uniform tension by Raju and Newman [131] and that of Koterazawa and Minamisaka [138] for pure bending are the most accurate for the semi-elliptical cracks in finite thickness plates of infinite surface dimensions. It was also suggested by the authors that the correction factors evaluated by Holdbrook and Dover [140] for finite width plates made a significant contribution to crack tip stress intensity values calculated from the solutions identified (i.e., [131,138]) and that these corrections were essential for correlating crack propagation data for the same material with simple, through-thickness specimens such as the compact type.

Therefore, from the above brief review of stress intensity factor solutions, it can be observed that these solutions do not agree with each other particularly well and that the basis for the choosing which one is best has not been established. However, based on the judgement of Scott and Thorpe [141] the stress intensity factor solution of Koterazawa and Minamisaka [138] and the correction factors proposed by Holdbrook and Dover [140] have been used throughout this work and indeed, as is shown in subsequent chapters, this approach seems to give the best correlation with the through-thickness results obtained from compact

type specimens.

The equations used are as follows:

$$K_c = M_{12} \frac{\sigma\sqrt{\pi a}}{E(k)} \quad B_f \qquad ;(3.12)$$

$$K_a = M_2 M_3 \frac{\sigma\sqrt{\pi a}}{E(K)} \quad B_f \qquad ;(3.13)$$

where:

$$M_{12} = [M_1 (1-0.3\ a/B)(1-(a/B)^{12})] + [0.394E(k)(a/B)^{12}\sqrt{c/a}] \qquad ;(3.14)$$

$$M_1 = [1.21 - 0.1(a/c) + 0.1(a/c)^4] \sqrt{a/c} \qquad ;(3.15)$$

$$M_2 = [1-1.36\ (a/B)\ (a/c)^{0.1}] \qquad ;(3.16)$$

$$M_3 = 1.13 - 0.07\ (a/c)^{0.5} \qquad .(3.17)$$

The form of E(k) used is the same as in equation (3.10). The correction factor B_f proposed by Holdbrook and Dover is given by:

$$B_f = 1 + \frac{f(a/c)\ G\ (c/w)\ H\ (a/B)}{(0.2745)^2} \qquad ,(3.18)$$

$$F(a/c) = 0.381 - 0.141(a/c) - 0.366(a/c)^2 + 0.569(a/c)^3 - 0.248(a/c)^4 \qquad ;(3.19)$$

$$G(c/w) = -0.239 + 1.434(c/w) - 2.984(c/w)^2 + 7.822(c/w)^3 \qquad ;(3.20)$$

$$H(a/B) = -0.0113 + 0.323(a/B) + 0.749(a/B)^2 - 0.535(a/B)^3 \qquad .(3.21)$$

TABLE 3.1

STEEL BS4360-50D

(a) Chemical Composition (by weight)

Element	C	Si	Mn	P	S	Cr
%	0.180	0.36	1.40	0.018	0.003	0.11
Element	Mo	Ni	Al	Cu	Nb	
%	0.020	0.095	0.035	0.16	0.039	

(b) Mechanical Properties

	Direction		
	Longitudinal	Transverse	Through-Thickness
Yield strength (MN/m^2)	386	382	388
Ultimate tensile strength (MN/m^2)	560	551	563
% elongation (GL equals 3")	30	29	18
% reduction in area	74	68	61

(c) Fatigue properties

Cyclic yield strength, σ_{yc}	415 MN/m^2
Strain hardening exponent, n	0.19
True fracture strain (or fatigue ductility coefficient), ε_f	1.35

TABLE 3.2

Welding Electrode BS 639 : E 4311 R21

Chemical Composition (by weight)

Element	C	Mn	Si	S	P
%	0.06	0.58	0.43	0.02max	0.03max

Mechanical Properties

Yield strength N/mm^2	448
Ultimate tensile strength N/mm^2	510
% Elongation	22
% Reduction in area	50
Charpy V-notch at RT (20°C)	80 joules

TABLE 3.3 : Vortic Marine BS1719 : E317

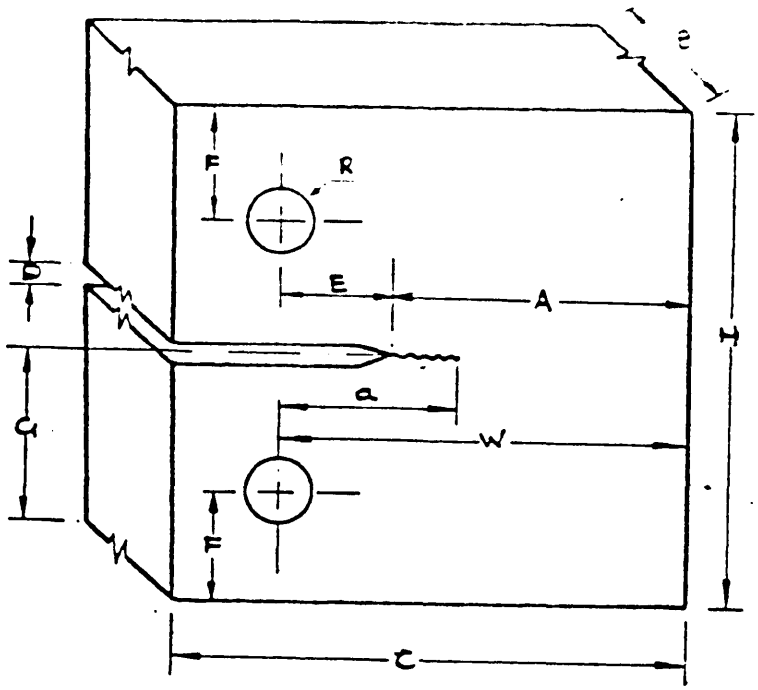
Composition		Mechanical Properties	
C	0.08	Yield strength	445 N/mm^2
Mn	0.44	UTS	508 N/mm^2
Si	0.10	Elongation	26%
S	0.02	Reduction of area	58%
P	0.03		

TABLE 3.4 : RADIAN BS1719 : E217

Composition		Mechanical Properties	
C	0.07	Yield strength	460 N/mm^2
Mn	0.46	UTS	514 N/mm^2
Si	0.12	Elongation	22%
S	0.02	Reduction of area	64%
P	0.03		

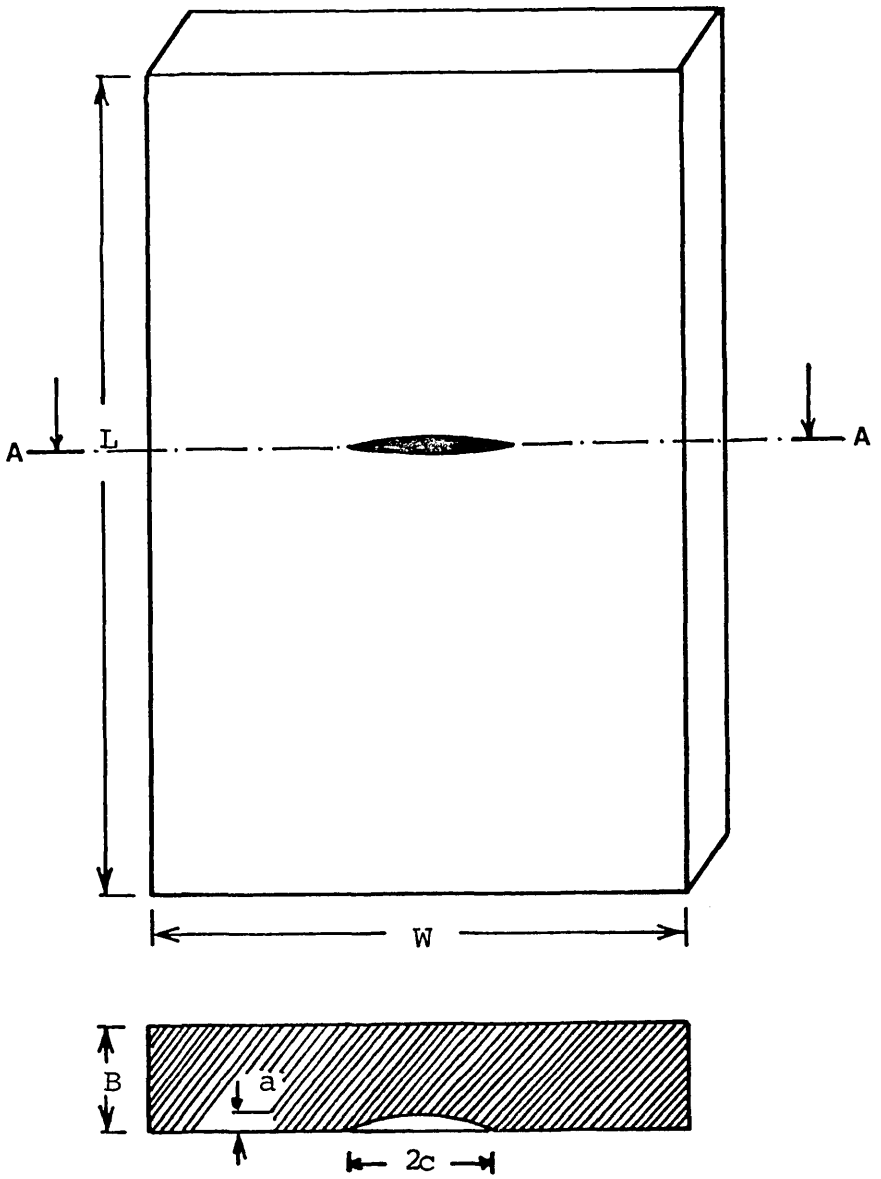
TABLE 3.5 : Armoid 1 BS 2926:20.9.3.R

Composition		Mechanical Properties	
C	0.08	Yield strength	587 N/mm^2
Mn	1.5	UTS	319 N/mm^2
Si	0.7	Elongation	30%
Cr	20.0	Reduction of area	43%
Ni	9.0		
Mo	3.3		
S	0.02		
P	0.03		



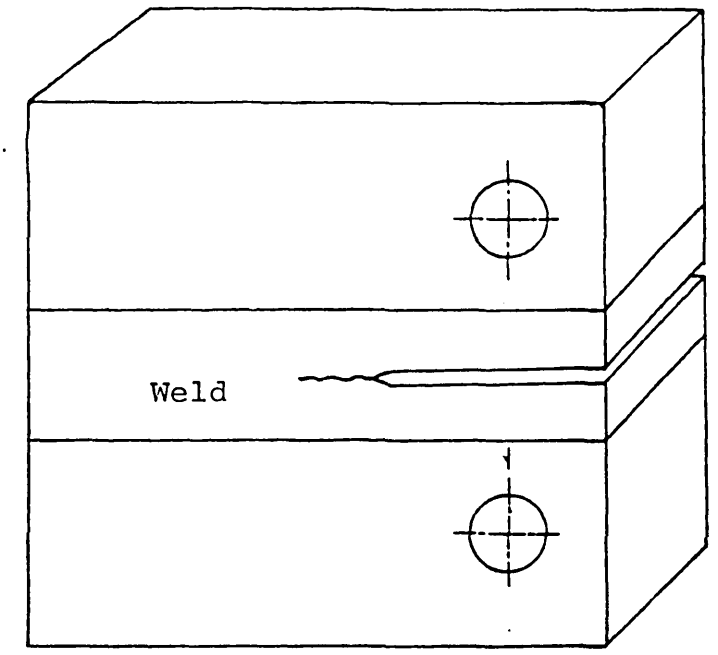
DIMENSION (mm)	A	B	C	D	E	F	G	H	R	W
SIZE	59.5	24	98.6	3.0	20.0	21.8	47.7	95.4	6.35	79.5

Figure 3.1 Compact type specimen geometry used in the experimental programme.



DIMENSION (mm)	L	W	B	2c	a
PARENT PLATE	415	115	24	40	5.5
WELDMENT & HAZ	415	115	24	28	2.51

Figure 3.2 Surface-notched plate specimen geometry used in the experimental programme.



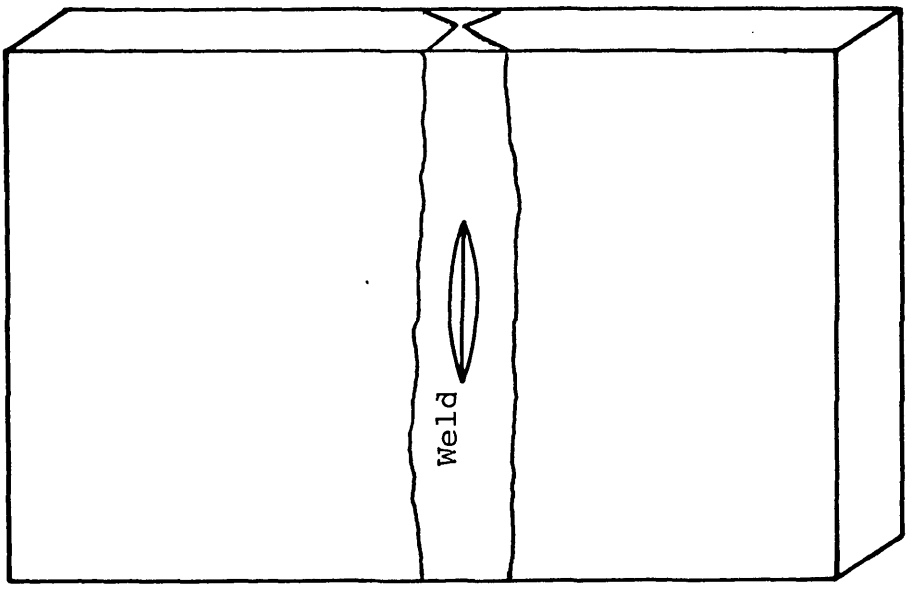


Figure 3.3 Welded joint specimens

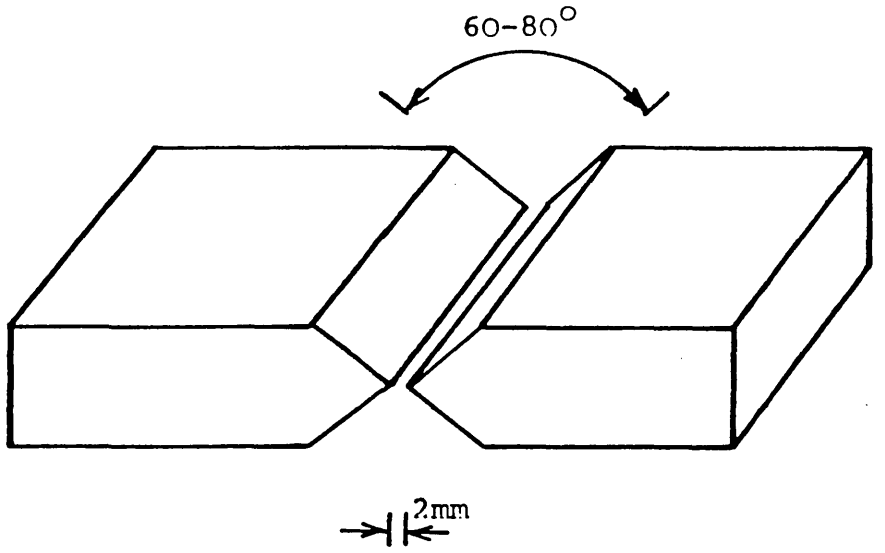


Figure 3.4 Double Vee joint

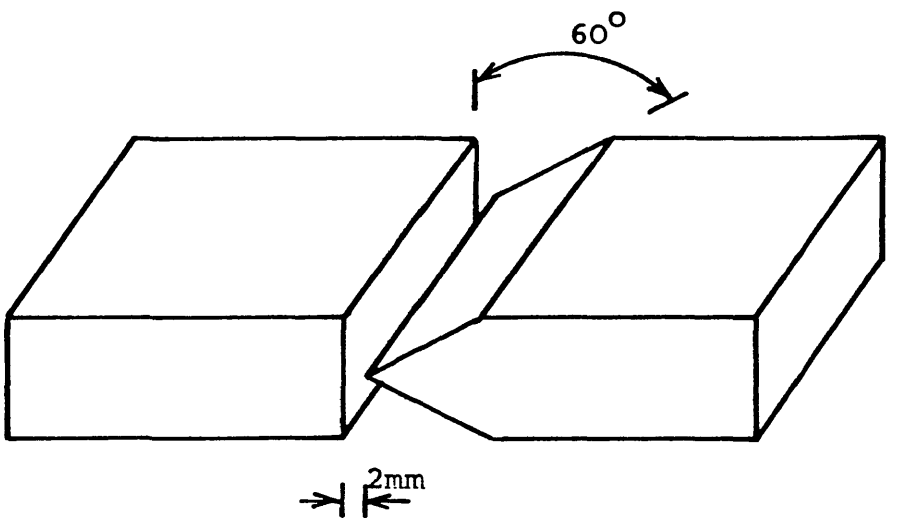


Figure 3.5 K joint

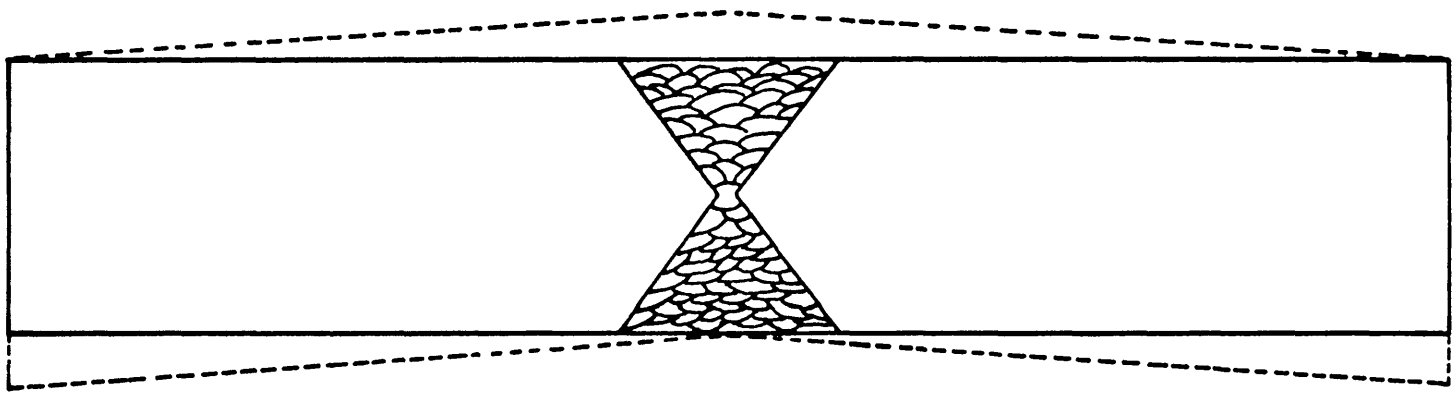


Figure 3.6 Original and final shape of the specimen

1.	Vortic Marine	BS1719:E317
2.	Radian	BS1719:E217
3.	Armoid 1	BS2926:20.9.3.R

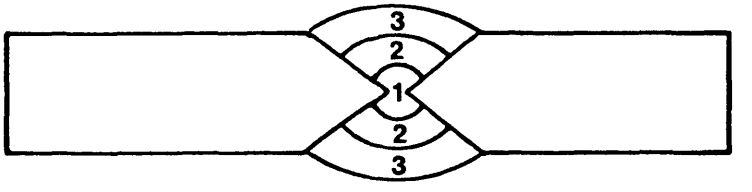


Figure 3.7 The arrangements of electrodes for sandwich weldment

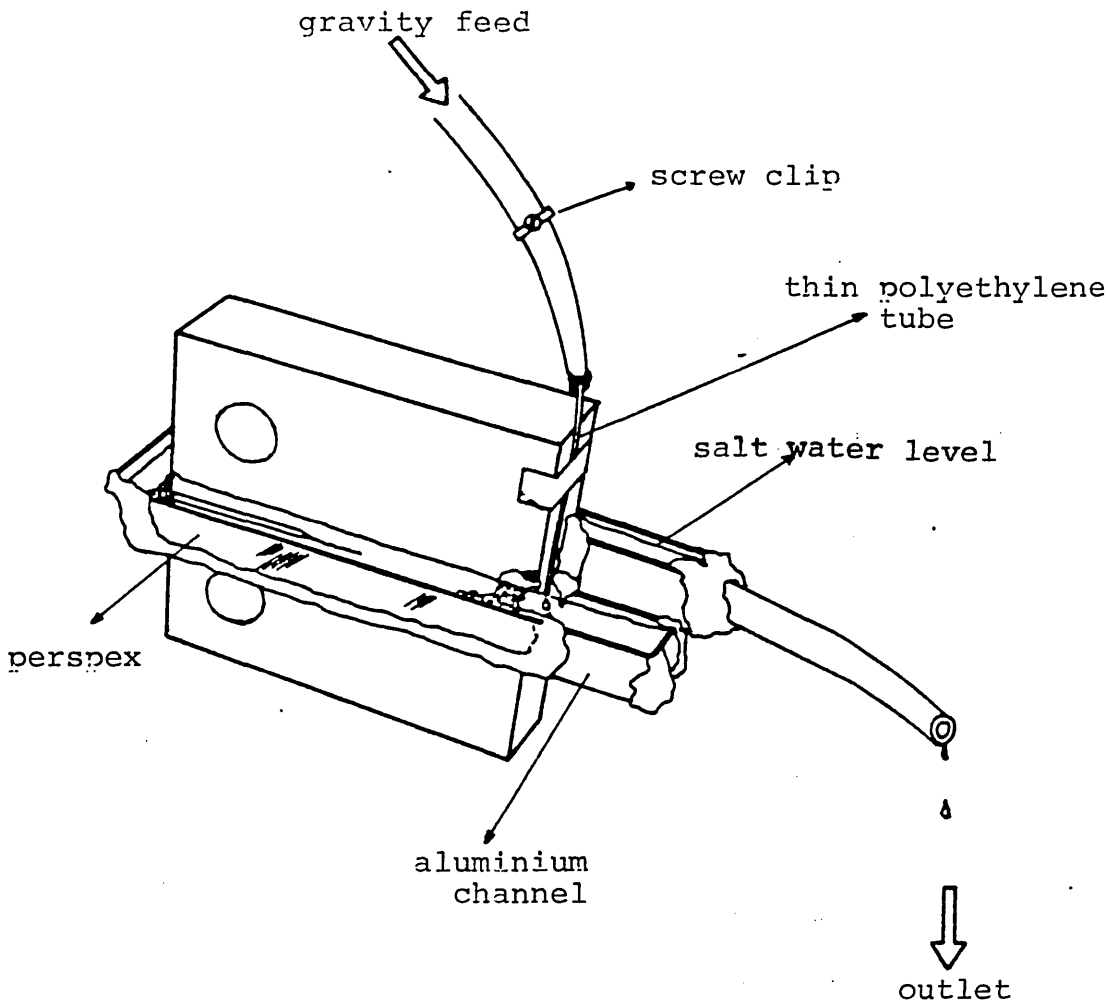


Figure 3.8 CT specimen with channels to accommodate salt water flow.

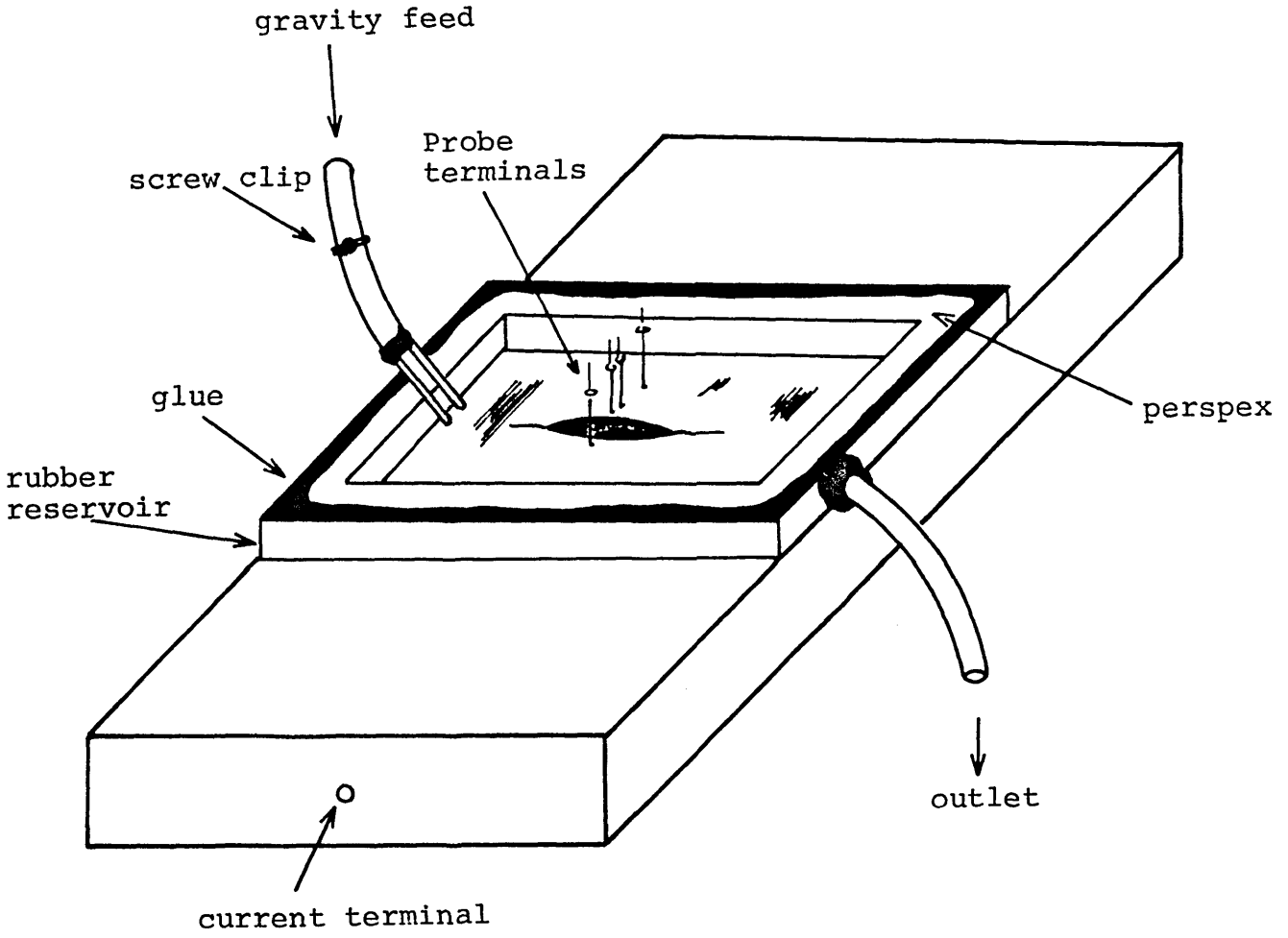


Figure 3.9 SNP specimen with a reservoir to accommodate salt water flow.

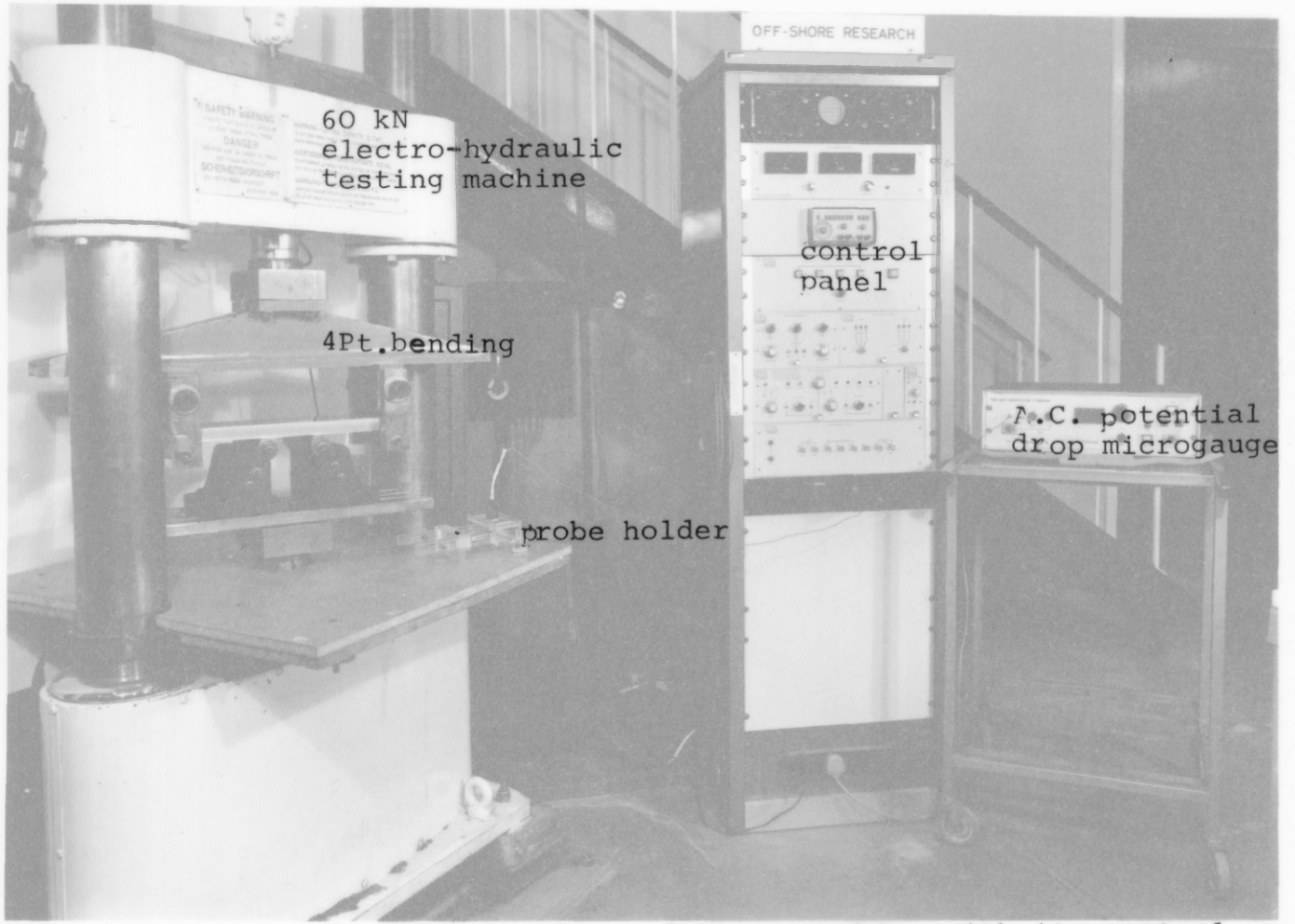


Figure 3.10 Dowty fatigue machine with its control system

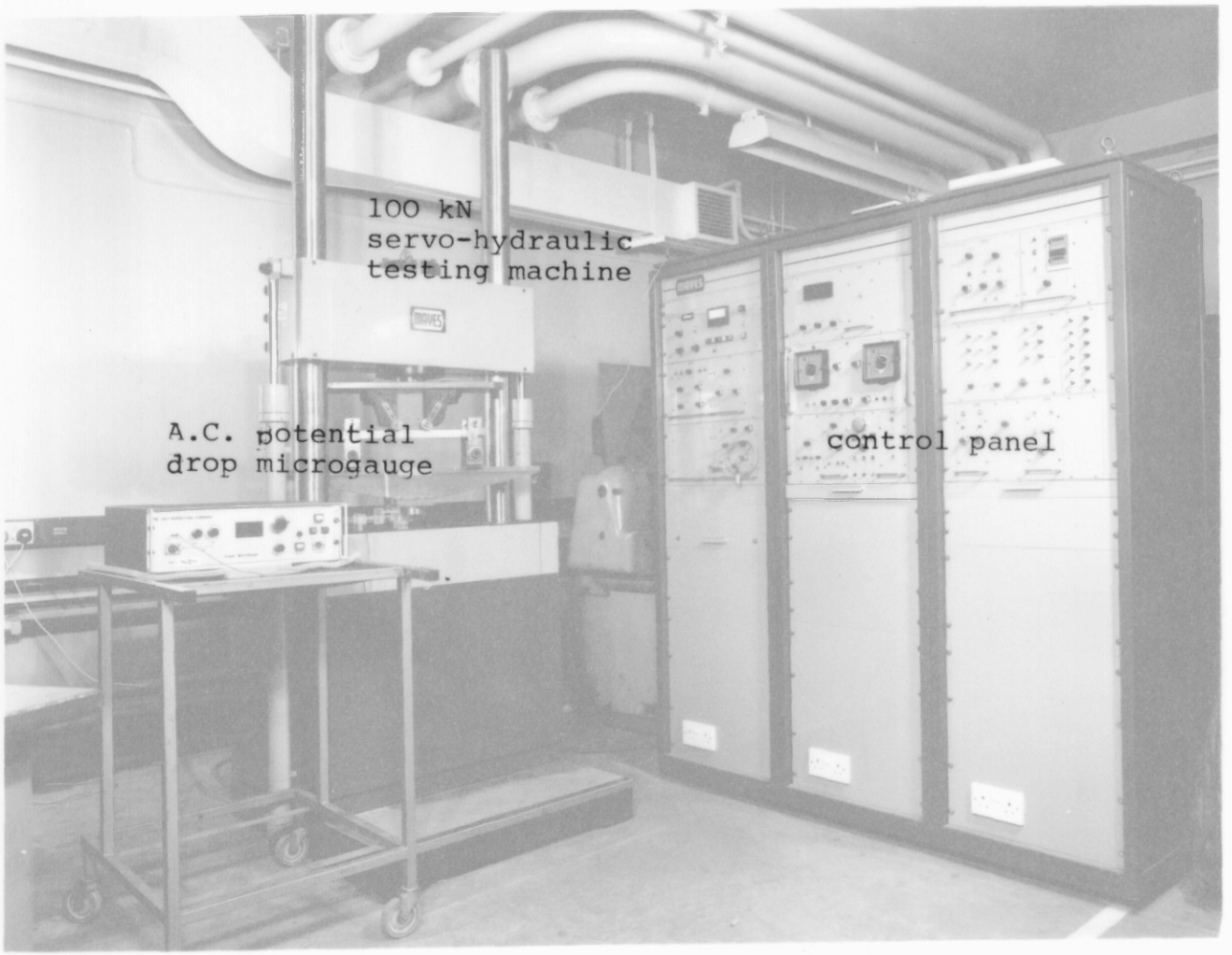


Figure 3.11 Mayes fatigue machine

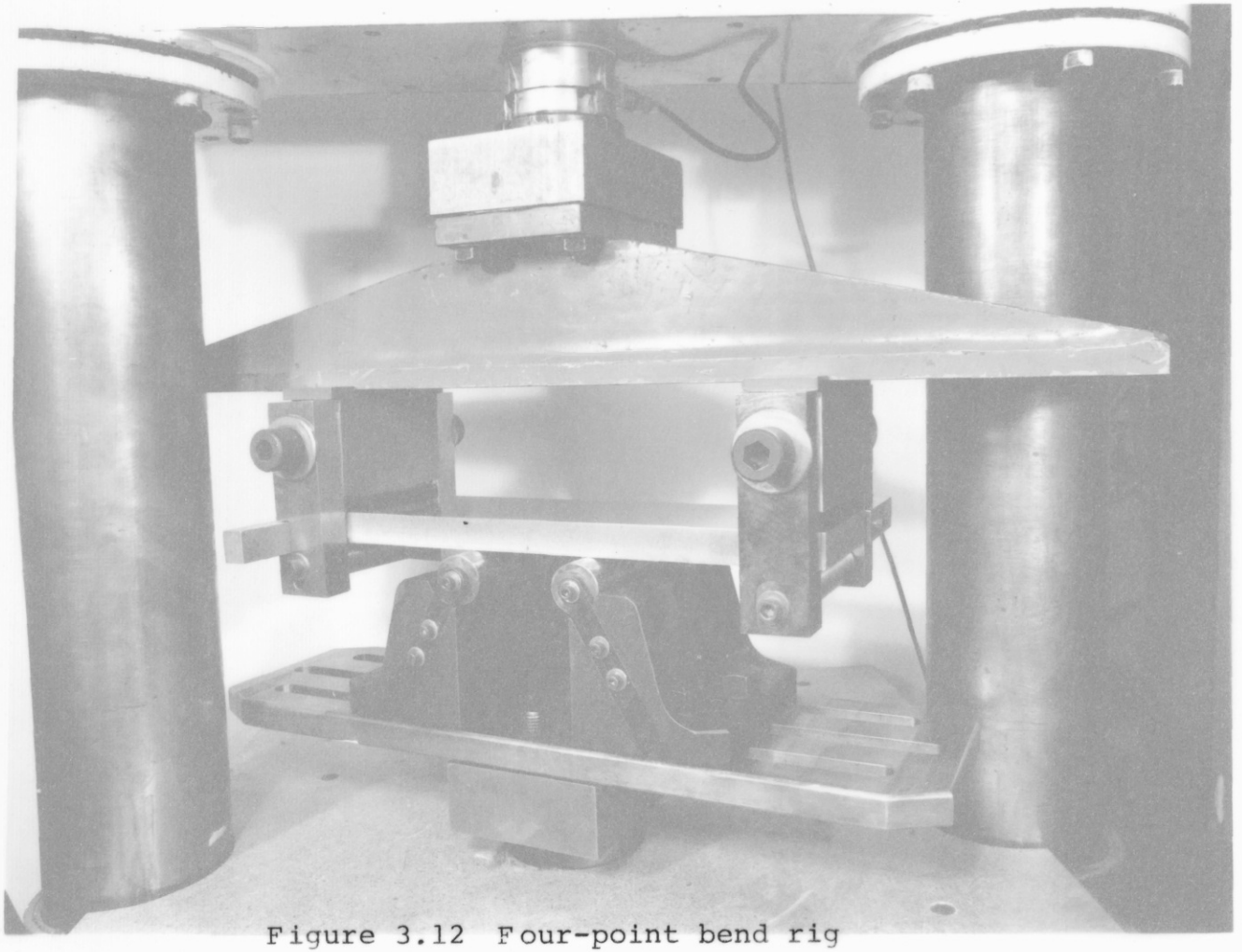


Figure 3.12 Four-point bend rig

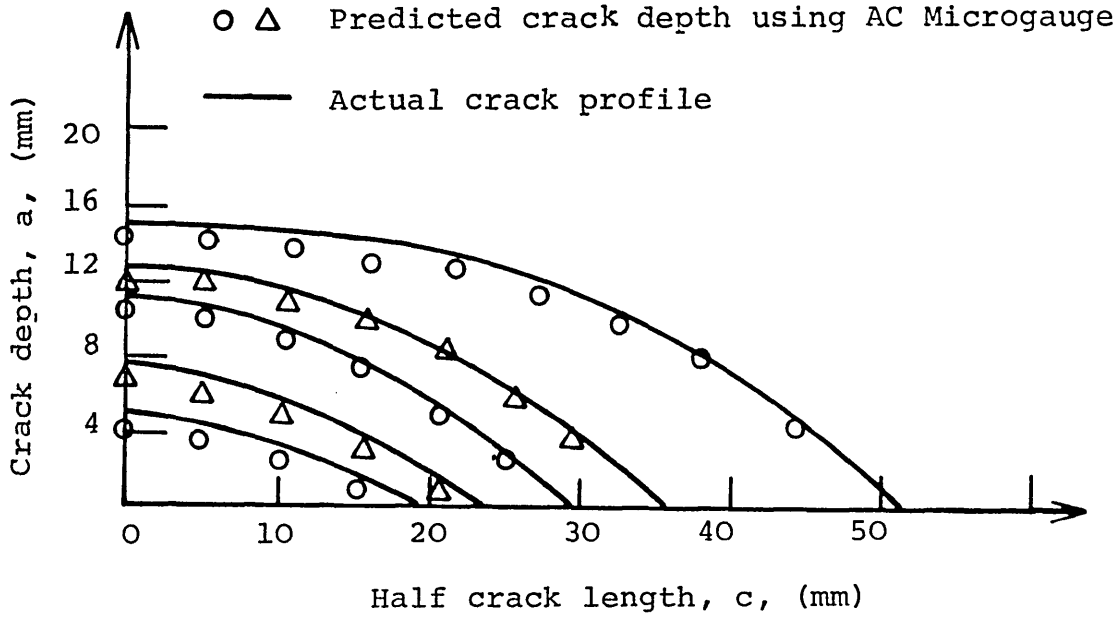


Figure 3.13 The effect of crack front on digital voltage reading of the crack microgauge

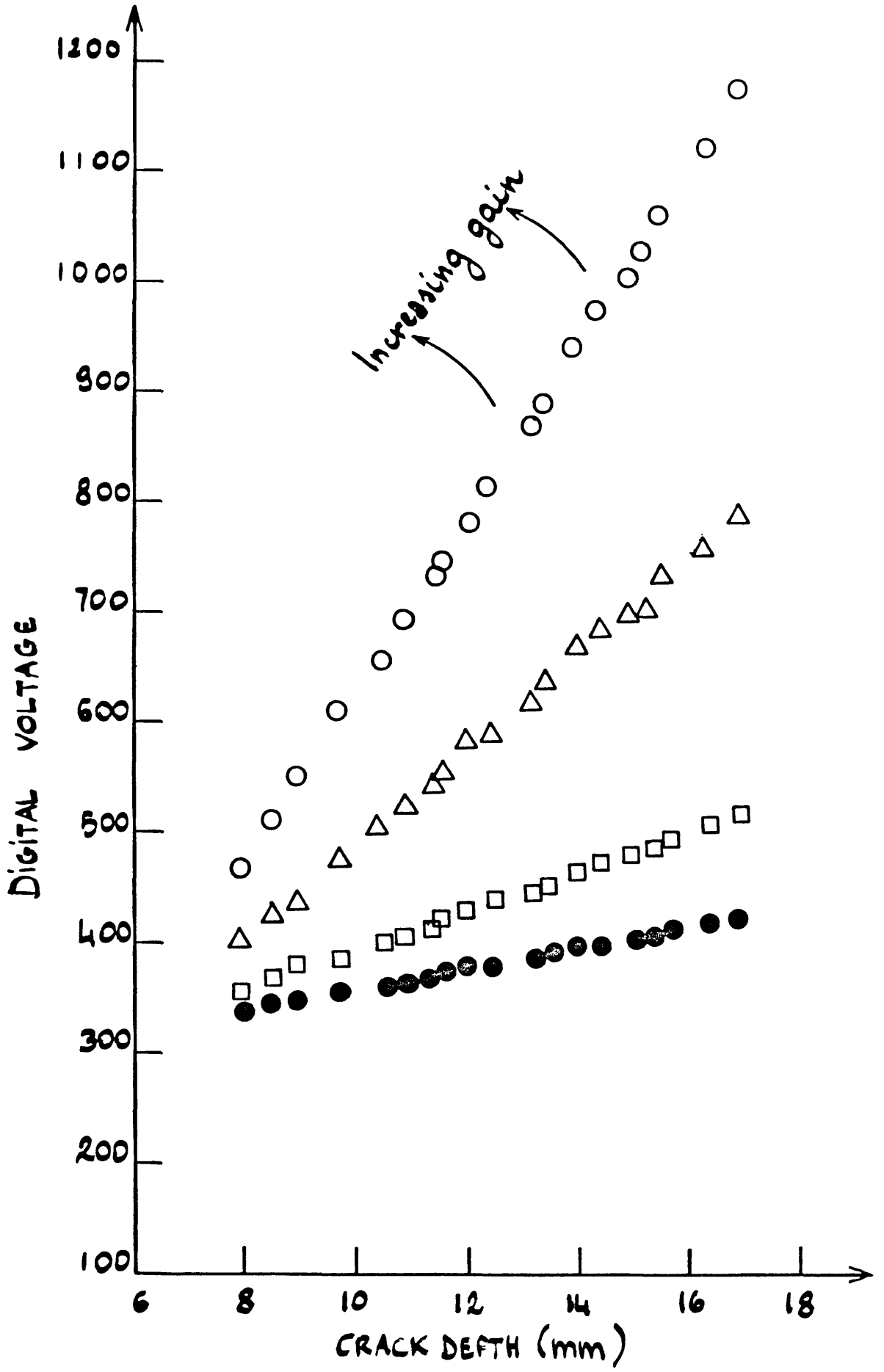


Figure 3.14 Variation of digital voltage with crack depth at various gain settings of the crack microgauge

CHAPTER 4

CRACK-GROWTH BEHAVIOUR OF BS4360-50D WELDED STEEL

4.1 INTRODUCTION

The analysis of fatigue crack growth developed by Paris [8], using linear elastic fracture mechanics, indicated that the fatigue crack growth rate, da/dN, is primarily controlled by the stress intensity range, ΔK , through the well-known Paris expression (Equation (2.12)). As has been described earlier, the actual situation is far more complicated than that represented by the Paris expression. It has been found that the Paris exponent m (see Equation (2.12)) is not constant but increases at high and low growth rates to give a sigmoidal shape to the crack growth curve. This sigmoidal relationship predicts the existence of a threshold, ΔK_{th}, for non-propagating cracks. Although this information is vital for determining safe non-destructive inspection intervals in certain engineering structures, most of the fatigue crack growth data, however, have been generated for growth rates greater than 10^{-5} mm/cycle.

The basic fatigue crack growth data for BS4360-50D steel and its welded joint were obtained using a compact type specimen. The effect of variables such as stress ratio, frequency, salt-water environment, and welding residual stresses were studied from threshold to the mid-range of crack growth rates, and the results are presented and discussed in this chapter. It has been established in

Chapter 2 that certain mechanical, environmental, and metallurgical factors affect fatigue crack growth rate, the role of R-ratio, frequency, environment, and welding residual stresses being of some significance. The test conditions in the present investigation were therefore varied to ensure that comprehensive results were obtained.

4.2 EXPERIMENTAL PROCEDURES

Tests were carried out using Dowty electrohydraulic and Mayes servohydraulic fatigue machines on both parent metal and weldment by means of CT geometry, details of which are given in the previous chapter. The tests were performed in laboratory air and, in the case of welded specimens, in 3.5% sodium chloride solution. All tests were performed under ambient conditions (i.e., at room temperature of 20° C and at about 50% relative humidity). As pointed out earlier some check results were made to ensure that all machines gave similar results under identical testing conditions.

The method used to obtain low crack growth rates and thresholds was what is referred to here as the "stepping-down load" technique. This method, which has been widely used for determing ΔK_{th} , involves the value of ΔK being progressively reduced by steps of 10% or less. During each ΔK step in the present case, the crack was allowed to grow past the plastic zone created by K_{max} of the previous step. Several readings of crack length against number of cycles were taken before making the next ΔK step. This procedure

was continued until threshold conditions were attained. The threshold value, ΔK_{th}, was considered to have been reached if, after the last ΔK-step, "no growth" was recorded in about 1 million cycles. This represented growth rates of the order 1×10^{-8} mm/cycle within the limits of accuracy of the crack length monitoring equipment (i.e., 0.01mm).

To investigate the effect of stress ratio, tests were performed at R equal to 0.08 and 0.7 at a cyclic frequency of 30Hz. Additional tests were performed on the weldment at R=0.5 and 30Hz to confirm the experimental trend.

To investigate the effect of frequency some other tests were performed at a loading frequency of 0.25Hz and stress ratios of 0.08 and 0.7 for both parent metal and weldment.

The effect of dressing on the fatigue crack growth rate of the weldment was investigated and additional tests were performed on specimens in "as-welded" condition at a loading frequency of 30Hz and stress ratio of 0.7.

The effect of a salt-water environment was investigated only for the weldment. Corrosion fatigue tests were performed at stress ratios, R, of 0.08 and 0.7 and at loading frequencies of 30Hz and 0.25Hz using a sinusoidal wave form. The fluid was introduced into the specimen at a

flow rate of approximately 1.5 ml/min.

To characterize the effect of residual stresses on fatigue crack propagation, tests were performed on stress-relieved specimens in both air and salt-water solution at a stress ratio of 0.7 and loading frequency of 30Hz.

In all the foregoing tests the specimen was prepared as described in the previous chapter. The specimens were precracked at a suitably higher frequency using a low load range giving a K_{max} not exceeding 20 $MN/m^{3/2}$ for the base metal and about 25 $MN/m^{3/2}$ for the weldment. Subsequently, the fatigue crack was propagated at the required loading conditions (i.e., stress ratio, frequency, etc.) for some 2 to 3mm before the actual test readings were started. This process ensured that uniform growth at the particular load range was attained and thus eliminated either the influence of short cracks at the original notch, or that of load histories on fatigue crack growth rate. All the tests were performed at fixed load limits, i.e., constant R-ratio allowing the crack to grow from its original length to the final length required. For some tests at low frequency (0.25Hz) and growth rates below $1x10^{-5}$ mm/cycle, the "step-up" or the "stepping-down load" techniques were used to shorten the investigation. For each step the value of ΔK was adjusted upwards or downwards by not more than 10% and the crack allowed to grow by more than the existing plastic zone produced by previous loading

conditions. Plastic zone size r_p can be calculated from:

$$r_p = \frac{1}{2\pi} \left(\frac{K_{max}}{\sigma_y}\right)^2 \qquad .(4.1)$$

At least two readings of the crack length and corresponding number of cycles were taken for each step before the first reading was taken. This process ensured elimination of load history effects.

Crack length measurements were made using a microscope mounted on a travelling micrometric stage as discussed previously. The experimental data were recorded in terms of crack length, a, and corresponding number of cycles, N.

To calculate the crack growth rate, da/dN, from the experimental data, a combination of graphical curve fitting and finite difference (secant) methods was used. When the readings showed little scatter of da/dN data, the raw experimental readings were used to calculate the growth rates. However, when the scatter was substantial, smooth curves were fitted (graphically) to the experimental data and points on these curves used to calculate da/dN using the secant method. This process reduced the scatter in the raw data. It was also observed that scatter was much reduced by taking readings at crack increments of between 0.5mm and 1mm, and hence these were used for all subsequent calculations of da/dN.

An attempt was made to apply the incremental polynomial method using least squares [142]. A computer program was developed from which da/dN and corresponding ΔK values could be calculated. This procedure was satisfactory when a large number of experimental points was available and/or scatter was minimal. However, this method was unsuitable for short tests and for results containing a considerable amount of scatter. Therefore, for consistency of results all the data reported here were analysed using only the secant method.

The stress intensity factor, K, was calculated using the appropriate standard expression for CT geometry, i.e., using Equations (3.5) and (3.6). The crack length, a, used to calculate K is the average of the two successive readings used to calculate the corresponding da/dN.

4.3 RESULTS

The experimental results are plotted in terms of da/dN versus the corresponding ΔK values for all the tests.

4.3.1 Base Metal

Fig. 4.1 shows a typical a versus N curve obtained during threshold tests using the stepping-down load technique.

The threshold and mid-range fatigue crack growth results in air have been represented in terms of da/dN versus ΔK as shown in Fig. 4.2, which shows the data obtained for a 24mm-thick specimen tested at stress ratios, R, of 0.08 and 0.7 and loading frequency of 30Hz. The results show the considerable influence of stress ratio on low crack growth rates and thresholds (i.e., growth rates increase with stress ratio, and ΔK_{th} values decrease with stress ratio). However, this effect diminishes with increase of crack growth rates.

Figs. 4.3 and 4.4 show the present results at 30Hz in air compared with the mean line through Musuva's and Radon's [144] results obtained in air for a 25.4mm-thick specimen of the same material. The authors used the "increasing R" technique at 30Hz. Their results compare very well with the present results.

For $K_{max,th}$ values of 6.25 $MN/m^{3/2}$ and 11.33 $MN/m^{3/2}$, correspondig to R-values of 0.08 and 0.7, respectively, were found.

Results at a cyclic frequency of 0.25Hz are shown in Fig. 4.5. These results show an increased effect of stress ratio at lower frequency when compared to the corresponding

data at 30Hz, and also show that only growth rates at high stress ratio are significantly affected by the change in frequency.

Figs. 4.6 and 4.7 show the present results at 0.25Hz in air compared with the mean line through Musuva's [143] results obtained in air for a 25.4mm-thick specimen of the same material at 0.25Hz. His results compare very well with the present results.

The effect of frequency was evaluated by drawing the best fit lines through the results of Figs. 4.2 and 4.5, which are shown in Fig. 4.8. The crack growth rates seem to be affected by the frequency change from 30Hz to 0.25Hz at R=0.08, apart from the region of low crack growth rates. However, at R=0.7 the growth rates are much higher at low frequency, and here the influence is appreciable.

4.3.2 Weldment

Fatigue crack growth of the weldment at the threshold and in the mid-range in air have been represented in terms of da/dN versus ΔK, as shown in Fig. 4.9. This shows the data for a 24mm-thick welded joint specimen tested in air at stress ratios, R, of 0.08 and 0.7 and loading frequency of 30Hz. Additional tests were performed on the weldment at R=0.5 and 30Hz loading frequency to confirm the experimental trend and are shown in Fig. 4.10. The results show a

significant effect of stress ratio on crack growth rates for both threshold and mid-range.

Figs. 4.11 and 4.12 shows a comparison between the results obtained for weldment and parent plate tested at 30Hz. The crack growth rates in the weldment were, however, lower than the growth rates in the parent material, probably due to favourable residual stresses.

For $K_{max,th}$, values of 14.75 $MN/m^{3/2}$, 17.0 $MN/m^{3/2}$, and 22.33 $MN/m^{3/2}$, corresponding to R-values of 0.08, 0.5 and 0.7, respectively, were found. The relationship between stress ratio and ΔK_{th} is shown in Fig. 4.13.

Fig. 4.14 represents the effect of as-not dressing on the fatigue crack propagation rate of the weldment. The test was conducted in air at stress ratio, R, of 0.7 and loading frequency of 30Hz.

The results at a loading frequency of 0.25Hz in air at stress ratios, R, of 0.08 and 0.7 are shown in Fig. 4.15. The effect of frequency in this case is more pronounced, when compared to the corresponding data at 30Hz. The results show that the growth rates are significantly affected by the change of frequency at R-value of 0.08, as shown in Fig. 4.16.

Figs. 4.17 and 4.18 show the results for the weldment compared with the results for the parent plate tested at 0.25Hz. They clearly indicate that the crack growth rates in the weldment are slower than or similar to the crack growth rates in the parent metal.

The results of tests in air on stress-relieved specimens are shown in Figs. 4.19 and 4.20. Fig. 4.19 shows a comparison of results obtained for a stress-relieved weld, and for an as-received weld tested at R=0.7 and 30Hz loading frequency, indicating that the crack growth rate is accelerated in the stress-relieved specimen for values of ΔK between approximately 6 $MN/m^{3/2}$ and 14 $MN/m^{3/2}$. Fig. 4.20 is a comparison of results for the stress-relieved weld and the parent plate and it shows that the crack propagation rate in the stress-relieved weld is still lower than for the parent metal at ΔK values above 8 $MN/m^{3/2}$. Fig. 4.21 illustrates the effect of residual welding stresses on fatigue crack propagation and was evaluated by drawing the best line through the results obtained for the parent metal, as-received weld and stress-relieved weld.

4.3.3 Weldment in Salt-Water Environment

Typical a versus N curves for a salt-water environment are illustrated in Figs. 4.22 and 4.23. Fig. 4.24 shows the effect of stress ratio on a weldment in a salt-water

environment at cyclic frequency of 30Hz and stress ratios of 0.08 and 0.7.

Fig. 4.25 shows corresponding in-air data. The results at both stress ratios (0.08, 0.7) indicate lower growth rates in salt-water solution as compared to in-air results. ΔK_{th} for R=0.08 was observed to increase from 13.75 $MN/m^{3/2}$ in air to approximately 22 $MN/m^{3/2}$, and for R=0.7 from 6.70 MN/m $3/2$ to 9.5 $MN/m^{3/2}$ in salt-water. It was found that introduction of salt-water into a crack previously growing in air at ΔK values below 14 $MN/m^{3/2}$ at R=0.08 and 7.0 $MN/m^{3/2}$ at R=0.7 caused a rather unexpected arrest in crack growth. The crack stopped very suddenly, for example, after a very short growth.

The results of tests conducted in a salt solution at 0.25Hz and two stress ratios (i.e., at 0.08 and 0.7) are shown in Fig. 4.26. These results show that, like the results obtained in air at the same frequency, stress ratio has a significant effect on crack growth rates. The results are again compared with those obtained in air which are shown in Fig. 4.27.

The effect of frequency is shown in Fig. 4.28 at stress ratios, R, of 0.08 and 0.7. These results show that reducing the frequency from 30Hz to 0.25Hz gives similar fatigue crack growth rates at ΔK values below 35 $MN/m^{3/2}$ and 18.5

$MN/m^{3/2}$ for R of 0.08, 07 Λ', respectively. Above these ΔK values the growth rates tend to increase with decrease in frequency.

The results of tests performed on stress-relieved specimens at R=0.7 and 30Hz loading frequency in salt solution are compared with the corresponding results obtained for as-received specimens and are shown in Fig. 4.29. These results are also compared with the data obtained for the stress-relieved weld in air, see Fig. 4.30. They indicate that the growth rates for a stress-relieved weld in a salt-water environment are lower than in air at ΔK values below 8 $MN/m^{3/2}$.

Finally, a combination of results for stress-relieved and as-received welds in air and salt-water environments is presented in Fig. 4.31.

4.4 FRACTOGRAPHY

The weldment fracture surfaces of fatigue cracked specimens in air were sectioned and mounted for observation in the scanning electron microscope (SEM).

All the variations of the fracture surfaces were examined; it was found in particular that dendritic formations might be responsible for the differences in the crack lengths as measured on the sides of the specimen. This

was attributed to the difference in the cooling rate of the weld beads. Fig. 4.32 shows a typical surface close to the specimen's side.

The cracks showed a tendency to branching (Fig. 4.33). It can be seen that these branches were random in direction, but there is no evidence to show that the main crack path was a result of a series of random paths. Also, a high proportion of secondary cracks was often found in a more brittle fracture observed at low ΔK values.

The failure surfaces showed a number of welding defects which may have a bearing on the results obtained. The most common was of worm-holes originating from the root of the weldments. The size of these defects varied from a pin-hole to a gross defect (Fig. 4.34). Some of these defects arose from porosity (Fig. 4.35).

The fracture mechanisms observed in the Paris regime were microvoid coalescence and striations. A microvoid coalescence area is shown in Fig. 4.36 and a typical striated area at ΔK=20 $MN/m^{3/2}$, R=0.7 and 30Hz is presented in Fig. 4.37. Transgranular cleavage-like fracture was observed at very low values of ΔK (7 to 10 $MN/m^{3/2}$) close to the near threshold region as shown in Fig. 4.38.

4.5 DISCUSSION

4.5.1 The Effect of Stress Ratio and Frequency in Air on Parent Metal

It is generally believed [145] that stage II fatigue crack propagation is largely independent of the stress ratio, R, or mean stress. A greater such dependency, however, in the threshold or stage I region has been observed by various authors and their results are reviewed in Section 2.4.1.

Tests at constant stress ratio, R, have been conducted [38,146-148] in investigating the effect of mean stress on fatigue crack propagation, while, in contrast, tests at constant mean stress have been made [32-35] to investigate the effect of stress ratio. The results of constant stress ratio can be easily transformed into the other (i.e., constant K_{mean}) using the following equation:

$$K_{mean} = \frac{1}{2} \frac{(1+R)}{(1-R)} \Delta K \qquad .(4.2)$$

Tests at constant stress ratio are more easily performed on the specimen geometry used in this investigation and also they are more appropriate to life-span calculations for non-redundant structures where the R-value remains constant with increasing crack length.

The present investigation has shown that crack growth

rates generally increase with stress ratio at low stress intensities. The stress ratio effect at low growth rates obtained in the data shown in Fig. 4.2 is similar to that reported by Cook et al [76], Paris et al [72,73], and Mackey [149] for other steels.

The effect of stress ratio on low growth rates has usually been explained in terms of either environmental interactions or crack closure phenomena [36]. The reported data for different kinds of environment are not conclusive as to the actual contribution of the environment to the effect of stress ratio observed in steels. Nevertheless, by examining fatigue crack growth behaviour of high strength steels, where the primary mechanism of environmental attack during fatigue crack growth in moist air and salt-water environments is hydrogen embrittlement [49], some seemingly consistent explanations have been put forward [62] which are supported by certain data obtained in inert environments (such as vacuum) and show a lack of, or at least a markedly reduced, effect of stress ratio at low growth rates [76-78]. It is also argued by the above authors that the lack of stress ratio effect at higher stress intensities, where the crack velocities are too fast for environmental factors to have any effect, is consistent with the above explanation. However, such an explanation of fatigue crack growth behaviour in low strength steels at low stress intensities, solely in terms of hydrogen embrittlement, may be questioned. In these steels, and especially at low stress intensities, the hydrogen enrichment ahead of the crack tip,

as predicted by Ritchie [62], would be very small owing to the lower magnitude of hydrostatic tension.

Musuva and Radon [144], who tested the same material (i.e., BS4360-50D) in salt-water, reported no significant environmental influence. The decrease in growth rates at low stress ratios they observed was attributed to the possible effects of fluid corrosion and corrosion products at the crack tip. Their results seem to support the general view [32,45,70-73] that, in low alloy steels, low growth rates and ΔK_{th} are not strongly affected by the environment. Although exceptions have been reported [69,71,150] where a corrosive environment was found to enhance the growth rates, more data is needed before any general conclusions can be drawn on the precise influence of the environment.

In view of the above results on both air and corrosive environments no firm conclusion could be drawn and environmental arguments alone cannot adequatly explain the observed effects of stress ratio. Therefore an alternative explanation, namely the crack closure concept, is advanced.

The crack closure concept was first reported by Elber [36] who proposed that closure of the crack surface may occur at tensile loads during the loading cycle as a result of plastic deformation left in the wake of a growing crack at high stress intensities. This phenomenon reduces the

effective stress intensity factor causing crack growth. Since then the concept has been used to explain the effect of stress ratio [36,39,72,144].

Most of the initial experimental work on crack closure was performed on thin sheet metal where crack tip conditions approximated to plane stress [36,151]. Lindley and Richards [152] sectioned SEN specimens parallel to the loading axis to reveal the crack profile in the thickness of the specimen. This demonstrated that under plane strain conditions in the centre of the specimen, the crack was open, but was locally closed at the surface, where conditions will approximate to plane stress. Closure therefore at low stress intensities and under plane strain conditions, which are the conditions prevailing at low fatigue crack growth rates, should be insignificant. However, Fleck and Smith [153] in a recent study developed a new compliance technique which was capable of monitoring the crack closure response at the centre of the specimen, and they conducted tests on the compact type specimens of a low alloy steel. From these tests they concluded that the crack closure was not just a surface phenomenon, could also occur in the body of a test-piece (i.e., plane strain regions). In particular, for the material they tested, fatigue cracks were closed for a significant portion (20%) of the load cycle.

Hence it appears that a simple application of the

closure concept to explain stress ratio effects during fatigue crack growth must be made with caution, as these effects are most marked in the low ΔK region, where it is most usual for plane strain conditions to exist.

In laboratory air at low stress ratios, clear evidence has been found for the build-up of a corrosive oxide product on the fracture surfaces of cracks growing close to ΔK_{th} [154]. The presence of such a layer of oxide particles in the crack will also increase the load in the fatigue cycle at which crack closure occurs [72]. Hence the effective ΔK will be lower than that applied, leading to lower crack growth rates and higher apparent threshold values. Further evidence of the importance of fretting corrosion debris is provided by the work of Paris et al [72] who found a similar dependence of ΔK_{th} on stress ratio in laboratory air with A533B and A508 steels. In distilled water, however, ΔK_{th} was greater than in air, an increase which they also suggested may be due to corrosion products limiting cyclic stress intensities.

The present results have shown that stress ratio can greatly influence fatigue growth rates at near-threshold stress intensities. However, its effects are considerably reduced at higher cyclic stress intensities ($\Delta K > 10$ $MN/m^{3/2}$).

The effect of stress ratio on growth rates observed at lower frequencies (0.25Hz) in air may be explained in terms of the hydrogen embrittlement mechanism. It is known that hydrogen in moist air can cause embrittlement at the crack tip, this resulting in increased growth rates. Hydrogen atoms in steel can diffuse to the regions of maximum hydrostatic tension ahead of the crack tip, thereby lowering the cohesive strength of the lattice [49]. This process, causing faster crack growth rates, is more significant in high strength steels.

It is possible that fatigue crack growth rates could be caused by the increase in stress ratio, since the higher value of K_{max} creates a large stress gradient to promote hydrogen diffusion. However, tests at high frequency (such as 30Hz) and high crack growth rates would not provide a favourable condition for hydrogen to diffuse to the crack tip in time to cause embrittlement, since the crack is advancing at a high velocity. This argument is supported by comparing Fig. 4.2 with Fig. 4.5, and is presented in Fig. 4.8.

4.5.2 The Effect of Stress Ratio and Frequency in Air on Weldment

In most of the welded joint specimens the crack deviated slightly from the plane of symmetry. However, it stayed within the weld for the total crack length (about 40mm), and the maximum deviation from the plane of symmetry

was about 1mm. The influence of a slightly curved path on the stress intensity was considered to be insignificant and was consequently ignored.

In order to achieve low growth rates and true thresholds unaffected by load history effects, it was necessary to make sufficiently small load changes and to test for sufficiently long periods. The present tests were performed on specimens with relatively short cracks (i.e., $0.3<a/w<0.45$), where the change in specimen compliance with crack length was small, and performed also to allow an adequate number of crack increments between load steps without too great a change in the value of the stress intensity factor. In the present investigation it was observed that reducing ΔK by more than 10% at higher growth rates, and more than 5% at low growth rates, caused long crack growth delays and sometimes arrest resulting in a false threshold value due to load history effects.

Although it is widely accepted that the fatigue of weldments is insensitive to mean stress, such a conclusion is not applicable to all weld details and stress ratios. For a weldment containing severe stress-raisers and subjected to pulsating tension, the fatigue properties are insensitive to mean stress [155]. However, fatigue of weldments can be sensitive to stress ratio, especially negative stress ratios [156].

The present results illustrate that crack growth rate increases with stress ratio. This effect is most pronounced at low stress intensities and diminishes with increase in growth rate. The stress ratio sensitivity for weld material at low growth rates and high frequency is presented in Fig. 4.10. The present ΔK_{th} results are compared with some recently reported investigations on steel and weldments (see Fig. 4.13). These results indicate that no simple relationship between ΔK_{th} and R seems to exist. However, it appears that for ferrite-pearlite steel [72,75] and HT80 steel welded joints [109], the results tend to point towards a limiting value of ΔK_{th}, $\Delta K_{c',th}$, reached at a high positive stress ratio. Although this trend contradicts the present results the data obtained by Branco et al [32], Davenport and Brook [68] and the suggestion by Blacktop and Brook [157] that ΔK_{th} can be extrapolated to zero at an R-value of 1 seems to support the present results but is not correct since ΔK_{th} losses its meaning.

As discussed previously the crack closure phenomenon has often been used to explain the observed effect of stress ratio on fatigue crack growth rate . According to this concept, at low stress ratios, the crack closure stress intensity factor, K_{CL}, is greater than the minimum applied stress intensity factor, K_{min}, and thus the effective stress intensity factor range responsible for the crack growth is substantially reduced. At high stress ratios, the crack remains open for the whole or for the larger part of the load cycle and thus the crack-closure effect becomes less

pronounced.

Following this argument it would seem reasonable to say that crack closure can be significant in weldments depending on the magnitude of residual welding stresses which exist in welded joints. The stress intensity factor, K, is a characteristic parameter for stresses and strains in the crack tip region only if tensile stresses and strains are produced by the applied load. Fatigue crack growth rates, when characterized by K, can be assumed to exist when they are caused by that part of ΔK which, when applied, results in tensile stresses and strains at the crack tip. Applying this strain characterization analogy to crack closure, the minimum stress intensity factor corresponding to zero stresses and strains will be defined as the crack closure stress intensity factor, K_{CL}.

Thus, the effective stress intensity factor range responsible for crack growth in a material with negligible residual stresses is given by

$$\Delta K_{eff} \doteq K_{max} - K_{CL} \quad \text{for } K_{min} < K_{CL} \qquad ,(4.3)$$

$$\Delta K_{eff} = K_{max} - K_{min} \quad \text{for } K_{min} > K_{CL} \qquad .(4.4)$$

The stress intensity factor range for a welded joint with compressive residual stresses is given by

$$\Delta K = \Delta K_{app} - \Delta K_{res} \quad ,(4.5)$$

or

$$\Delta K = K_{max} - K_{min} - \Delta K_{res} \quad .(4.6)$$

The effective stress intensity factor range responsible for the crack growth in a butt-welded joint with compressive residual stress field is of the form:

$$\Delta K_{eff} = K_{max} - (K_{CL} + K_{res}) \quad \text{for } K_{min} < K_{CL} \quad ,(4.7)$$

$$\Delta K_{eff} = K_{max} - (K_{min} + \Delta K_{res}) \quad \text{for } K_{min} > K_{CL} \quad .(4.8)$$

The comparison of the present data obtained for the parent material, Figs. 4.11 and 4.12 at 30Hz and Figs. 4.17 and 4.18 at 0.25Hz, indicated the existence of a compressive residual stress field, thereby suggesting the weld metal to be superior than base metal in terms of crack growth rate. To verify this, tests were performed on stress-relieved welded specimens, from which it was observed that the crack growth rate was significantly increased and became comparable to the crack growth rates in the parent metal (see Figs. 4.17-4.19). It follows from this argument that it is reasonable to assume that the crack closure in butt-welded joints is primarily due to compressive residual stresses induced in the plate during the welding process.

The above analysis shows that, depending on the magnitude of the compressive residual stress, it tends to maximise the crack closure effect at low growth rates,

although at high growth rates this effect diminishes apparently because of redistribution of these residual stresses.

At this point in the discussion, it is important to note that most researchers have attributed the decrease in fatigue crack growth rate in the weldment to favourable residual stresses normal to the crack [109,158,159]. This is discussed futher below.

Fig. 2.3 shows a simplified pattern of residual stresses for a butt-welded test section. The most significant residual stress component in the weld is the longitudinal component σ_x which can reach the magnitude of yield strength. The transverse stress component σ_y is usually substantially smaller, although no measurement of the residual stress was made. A qualitative discussion of the influence of the residual stress follows.

Although transverse stresses (i.e., parallel to the crack plane) do not influence the stress intensity factor, they have been shown to influence the plastic flow around the crack tip [160]. A tensile stress component parallel to the crack will decrease the plastic flow and a compressive stress component parallel to the crack will increase the plastic flow around the crack tip upon loading. The net effect over one cycle is not easily predicted. The

redistribution of longitudinal residual stresses in the direction perpendicular to the crack may induce a closing moment which will resist the opening of the crack and therefore tend to decrease the crack growth rates.

In some specimens, especially at low ΔK (7-15 $MN/m^{3/2}$), the crack growth is faster on the side of the specimen where the first bead was deposited. On that side the transverse residual stresses ought to be lower than on the side where the second bead was deposited. Also, when grinding the specimen, some of the transverse residual stresses may be released and therefore the crack growth rates should be lower (see Fig. 4.14).

Observations of frequency effects in the weldment confirmed the general trend discussed in Section 2.3.2. Increasing the loading frequency from 0.25Hz to 30Hz caused a reduction in crack growth rates above ΔK values of 22 $MN/m^{3/2}$ and 15 $MN/m^{3/2}$ at R=0.08 and 0.7, respectively (see Fig. 4.16).

Yokobori's formula (Equation (2.21)) implies a reduction of about 30% over the same frequency range and a further 6% reduction in changing from 10Hz to 30Hz. However, the reduction in crack growth rate with increasing frequency is a relatively minor effect in the low growth rate regime, but it serves as a warning against accelerated tests at high

growth rates and frequency, which may not give consistent results.

The increase in crack growth rate with decreasing frequency was explained by Bradshaw and Wheeler [161] as being caused by an environmental effect obtained in the reaction between the surrounding air and freshly exposed metal at the crack tip. Thus at lower frequency there is more time available for the reaction between constituents of ordinary air such as oxygen, nitrogen, and water vapour, and the metal. Therefore, this effect should be more pronounced at lower ΔK levels. Although there is considerable evidence in support of environment-controlled processes causing the frequency effect, the concept of a simple time-dependent or cycle-dependent interaction may be misleading. The present results do not support the above conclusion. Indeed, for ΔK values below 22 $MN/m^{3/2}$ and 15 $MN/m^{3/2}$, corresponding to stress ratios of 0.08 and 0.7, respectively, at 0.25Hz the crack growth rate appears to be the same as at the higher frequency (i.e., 30Hz). Therefore for a weldment in air the sensitivity to frequency is less at low ΔK values. The environmental influence is more likely to be related to dislocation-transport of hydrogen [162], which is a rate-sensitive process, rather than to any active path corrosion.

4.5.3 The Effect of Salt-Water Environment on Weldment

The phenomenon of crack growth delay is normally related either to a residual stress field present at the

crack tip [163], crack closure [36], or to a combination of these mechanisms. This effect has been widely investigated by means of applying overload/underload cycles in the constant amplitude test. The effect of the overload cycle is to introduce a relatively large plastic zone ahead of the crack tip which in turn produces a compressive residual stress field into which growth must proceed for a number of cycles before the crack "breaks free" of this compressive field. Underloads are not suitable as a means of building up residual stresses because of the relatively small plastic zone they produce.

There are other factors which can contribute to this retardation behaviour, in particular the interaction effect of corrosive media . Previous work by Rhodes and Radon [164] suggested two distinct processes by which crack propagation may occur. One is due to chemical action at the crack tip, enhanced by the presence of a tensile stress, referred to as "stress-assisted dissolution". The other is due to local mechanical failure, enhanced by the presence of an adverse environment, "environment-assisted fracture". These two processes are mutually competitive. Stress-assisted dissolution, by the action of microbranching and blunting, actually inhibits mechanical fracture. Conversely, if mechanical failure proceeds sufficiently rapidly, there is no time for dissolution to take place before the crack tip passes any particular point in the material. Thus the two processes are not simply superimposed. Either one or the other will dominate crack propagation. Both mechanisms will

influence the rate of crack growth.

Under actual working conditions, some structures will experience alternating environmental conditions. For example, as a result of tidal wave action, part of a supporting offshore structure will be alternately exposed to air and immersed in sea water. The effects of this alternate wet-and-dry environment have been the subject of several investigations.

Barsom and Novak [165] investigated this effect on A514 steel. First, the specimen was stressed at 0.2Hz under full immersion conditions in a 3% NaCl solution, then the NaCl bath was removed and the specimen was left to dry in air at room temperature overnight. The specimen was then replaced in the former salt solution and the test continued as before. Barsom and Novak observed that the life of the specimen was doubled due to delay equivalent to 115000 cycles.

Johnson et al [166] conducted tests on BS4360-50D steel specimens subjected to an environmental cycle of 6 hours immersed in sea water followed by 6 hours in air. Crack growth delay was also observed during the drying period. They suggested that partial drying out of the specimen would concentrate the level of salt in the crack and hence lead to an increase in temperature. Both effects might combine to

increase the corrosion rate and to cause plastic blunting of the crack tip, which effectively lowers the effective ΔK values.

Morgan and Bretherton [167] also performed tests on BS4360-50D steel specimens subjected to intermittent immersion. The results they obtained indicated that in situations where the temperature in the vicinity of the notch rose significantly during the "dry" periods, crack retardation and even total arrest occurred. They attributed this retardation to a reduction in effective stress intensity at the crack tip due to crack tip blunting by increased corrosion. They also concluded that increasing the "dry" to "wet" time ratio appears to delay the onset of accelerated growth, and that large "dry" to "wet" time ratios could cause total crack arrest.

Other experiments conducted by Hodgekiess [168] showed similar retardation under extremely low or negligible fatigue loading in place of exposure to a dry environment.

During such experiments, it is often necessary to stop tests overnight. The effect of a rest period in an environmental fatigue test is to blunt the crack so that crack growth may be delayed when load cycling restarts. After re-initiation, the crack, however, progresses eventually as if nothing had happened. In the present

investigation, this rest period did not seem to affect the growth rate severely; however, after such a period the corrosion fatigue crack was propagated for some 2-3mm before the actual readings were taken.

Fig. 4.22 shows a versus N at R=0.08 and loading frequency of 30Hz. It is interesting to note that there was a delay period of about 1.5 million cycles. At a crack length of about 22.25 mm, the crack was suddenly arrested for no apparent reason (i.e., no overload or other transient influences were noted or introduced prior to arrest). Although no fractographic evidence is available, it appears that either microstructural inhomogeneity and/or excessive micro-crack branching occured. Fig. 4.23 also shows a delay of approximately 2 million cycles at R=0.7 and cyclic frequency of 30Hz. This delay may be attributed to the deposited salt in the crack when the specimen was left to dry during shackle replacement (approximately 5 hours). Drying out the specimen will obviously increase the salt concentration at the crack tip. The retardation behaviour would most probably be caused by blunting of the crack tip.

The results obtained at loading frequencies of 30Hz and 0.25Hz and two stress ratios (i.e., 0.08 and 0.7) showed a considerable decrease of crack growth rates when compared to the corresponding air data (see Fig. 4.25). The retardation observed in a salt-water environment could be explained in terms of solution chemistry and the mechanical interaction

between fluid and crack tip geometry [169]. It is possible that due to the nature of the channels used to collect the fluid, the slow flow rate resulted in a rapid mixing of the crack and bulk solution. This could result in a difference in pH between the successive solutions at the crack tip and/or the possibility of the used fluid and corroded products being deposited at the crack tip and causing blunting which in turn reduces the growth rates. At lower values of ΔK , the crack growth rate is low, and blunting could occur as a result of general corrosion. However, at higher values of ΔK the growth rates are higher and it is possible that in this range the environmental action complements the mechanical stresses to enhance growth rates.

Tu and Seth [170] explained the retardation of fatigue cracks in corrosive environments at low ΔK values in terms of the effects of deposited corrosion products at the crack tip which form a protective film and effectively reduce the amount of further corrosion agents entering the crack tip, thus causing a slower crack growth rate at low values of ΔK and thresholds. At high values of ΔK where the growth rate is higher the corrosion products do not have enough time to pile up, and corrosive agents can enter the fresh fracture surfaces created during the loading cycle to cause further embrittlement without delay.

Radon et al [171] suggested a dissolution process which leads to crack blunting, the same mechanism responsible for

the lower crack growth rate in sodium chloride solution than in air at low test frequencies. The dissolution process contributes mainly by increasing the radius of curvature at the crack tip, for which at high growth rates a longer time will be necessary, since a larger volume of material will have to be removed. Thus, high growth rates do not favour crack tip blunting. This explanation agrees well with the present results, as there is less retardation at high growth rates.

A stress-assisted dissolution model proposed by Rhodes and Radon [164] suggested the occurrence of extensive microbranching and crack tip blunting as a result of metal dissolution. Both mechanisms, which have been previously discussed, will influence the rate of crack growth. In the present investigation, it appears that stress-assisted dissolution dominated the process of crack growth. However, no fractographic examination was made, and hence the mechanism of micro-branching cannot be confirmed in the present study.

It is interesting to note that where crack growth continues at a reduced rate, a critical value of ΔK exists, irrespective of loading frequency, beyond which rapid growth ensues. This was observed for "as-received" welds. These ΔK values are approximately 32 $MN/m^{3/2}$ at R=0.08, and 20 $MN/m^{3/2}$ at R=0.7; however, more tests are needed on stress-relieved welds in order to come to a general conclusion.

The data summarized in Fig. 4.27 show that the frequency effect occurs only at high growth rates. At near threshold and intermediate growth rates the data tend to bunch together. This observation confirms those of other investigators [43,51]. The results suggest two distinct regions which are identified [51] as "frequency-independent" and "frequency-dependent", regions I and II, respectively. In region I, where the growth rate is only ΔK-dependent, the exposure of clean metal surface at the crack tip is a rate-controlling mechanism. In region II, where the crack growth rate is only frequency-dependent, it is likely that some reaction-step in hydrogen-metal interaction at the crack tip controls the growth rate.

4.6 CONCLUSIONS

The linear elastic fracture mechanics approach was used to characterize the effects of stress ratio, frequency, and salt-water environment on fatigue crack behaviour in BS4360-50D steel butt-welded joints tested under ambient conditions at 21°C. From the results obtained in the threshold and medium growth rates (3×10^{-8} mm/cycle $<da/dN<2\times10^{-3}$ mm/cycle), the following conclusions may be drawn:-

1) Stress ratio and frequency of loading significantly affect crack growth rates both in the parent material and the weldment for the load range investigated. In general,

the fatigue crack growth rate increases with increasing positive stress ratio and/or with decrease in cyclic frequency for both parent plate and the weldment tested in air at a given value of ΔK. The effect of frequency is more pronounced at high stress ratios for the parent plate. The effects of stress ratio and frequency can be adequately described in terms of the crack closure concept and the environmental effect of moist air.

2) A comparison of rates of fatigue crack growth in both the "as-received" and "stress-relieved" weld material and the parent plate in air suggest that fatigue crack propagation will be faster in the parent plate due to favourable residual stresses in the weldment.

3) Fatigue crack growth in a weldment is highly sensitive to change of ΔK, as shown in the data obtained (e.g., Fig. 4.10) by the narrow range of stress intensity factor.

4) Salt-water solution does not enhance fatigue crack growth rates in the weld material at low values of ΔK. The salt-water enhancement of growth rates occurs only at mid and high ΔK values (i.e., $\Delta K > 30$ MN/m$^{3/2}$ at R=0.08 and $\Delta K > 20$ MN/m$^{3/2}$ at R=0.7). High testing frequency and stress ratio in welded joint specimens and in salt-water environment produces transient effects showing characteristics of stress corrosion in the region of $9 < \Delta K < 12$ MN/m$^{3/2}$. Corrosion fatigue crack growth rates increase with increase of stress ratio and decrease of frequency. However, frequency produces no effect at low ΔK values. A reasonable and conservative

estimate of the fatigue crack growth rate in the weldment can be made using growth rate results in the base material as an upper bound and is represented by:

$$\frac{da}{dN} = 9.0 \times 10^{-8} (\Delta K)^{3.0}$$

5) The decrease in crack growth rates of weld material in salt solution at low values of ΔK can be explained by a dissolution process as discussed in Section 4.5.3 which leads to crack tip blunting.

6) Stress-relieving does not change the shape of the curves in both air and salt-water environments, but only reduces the stress intensity factor range, ΔK, showing characteristics of compressive residual stress acting at the crack tip.

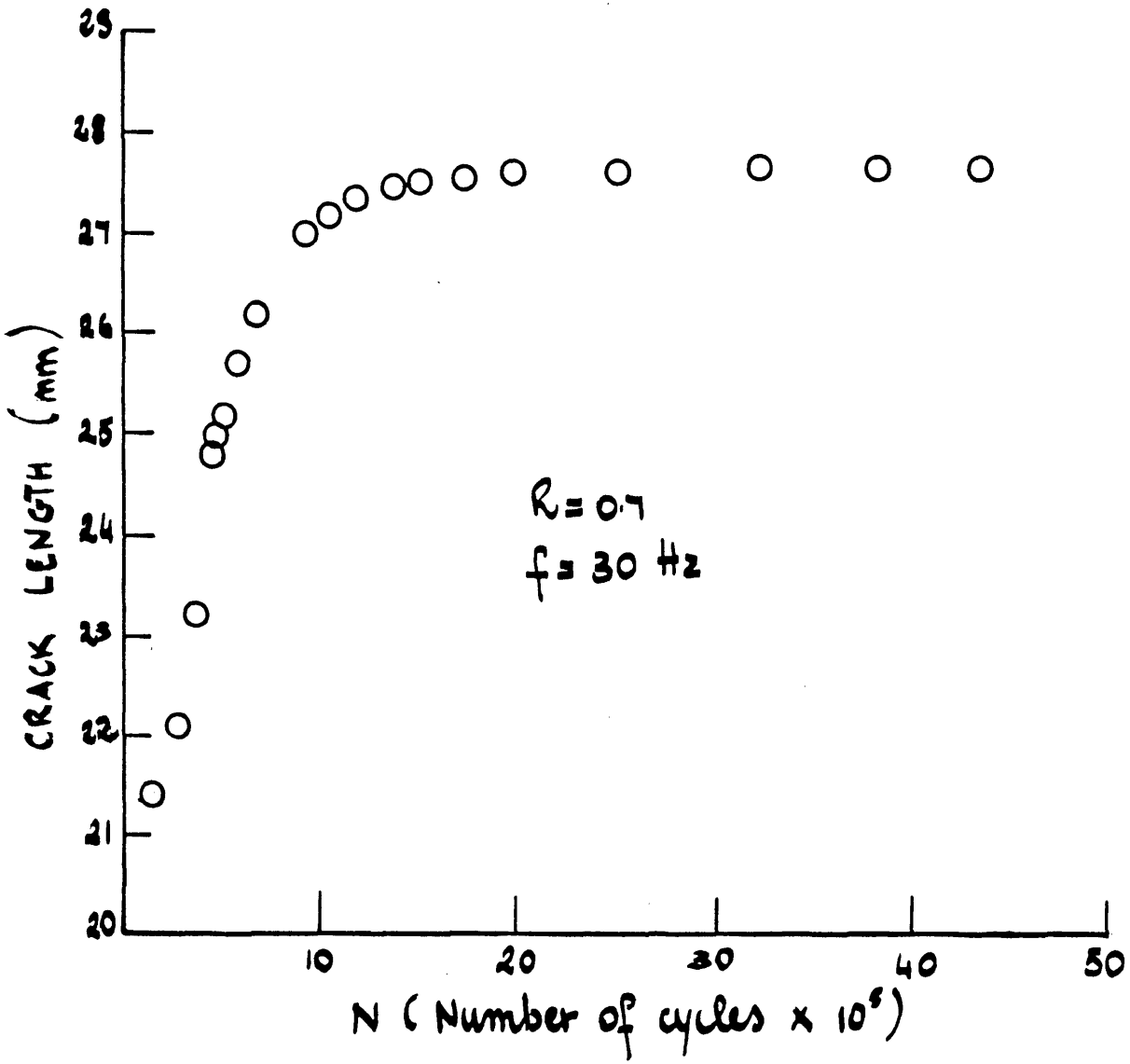


Figure 4.1 Crack length a versus N during threshold tests

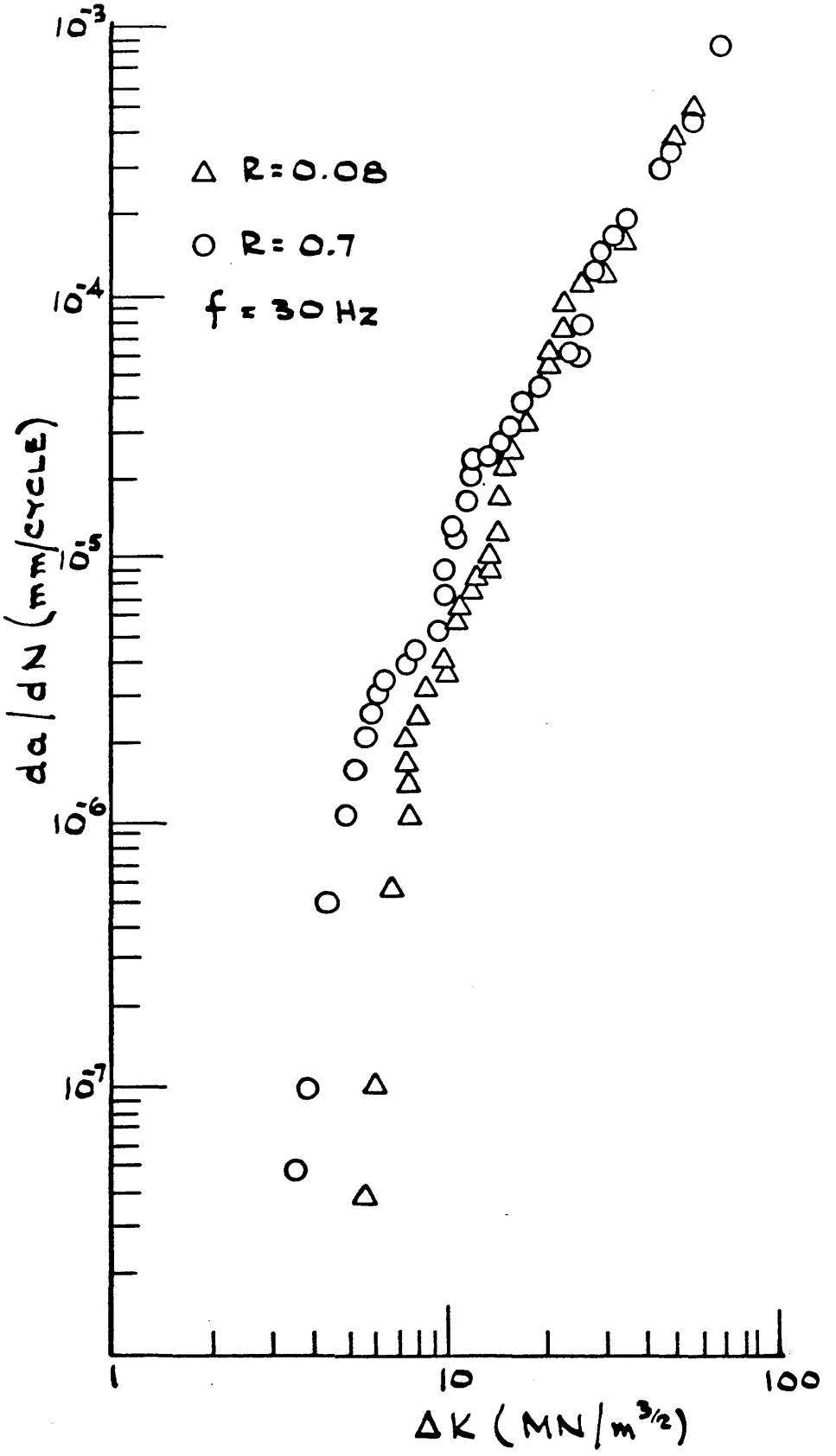


Figure 4.2 Effect of stress ratio on fatigue crack growth of BS4360-50D steel using CT specimen in air.

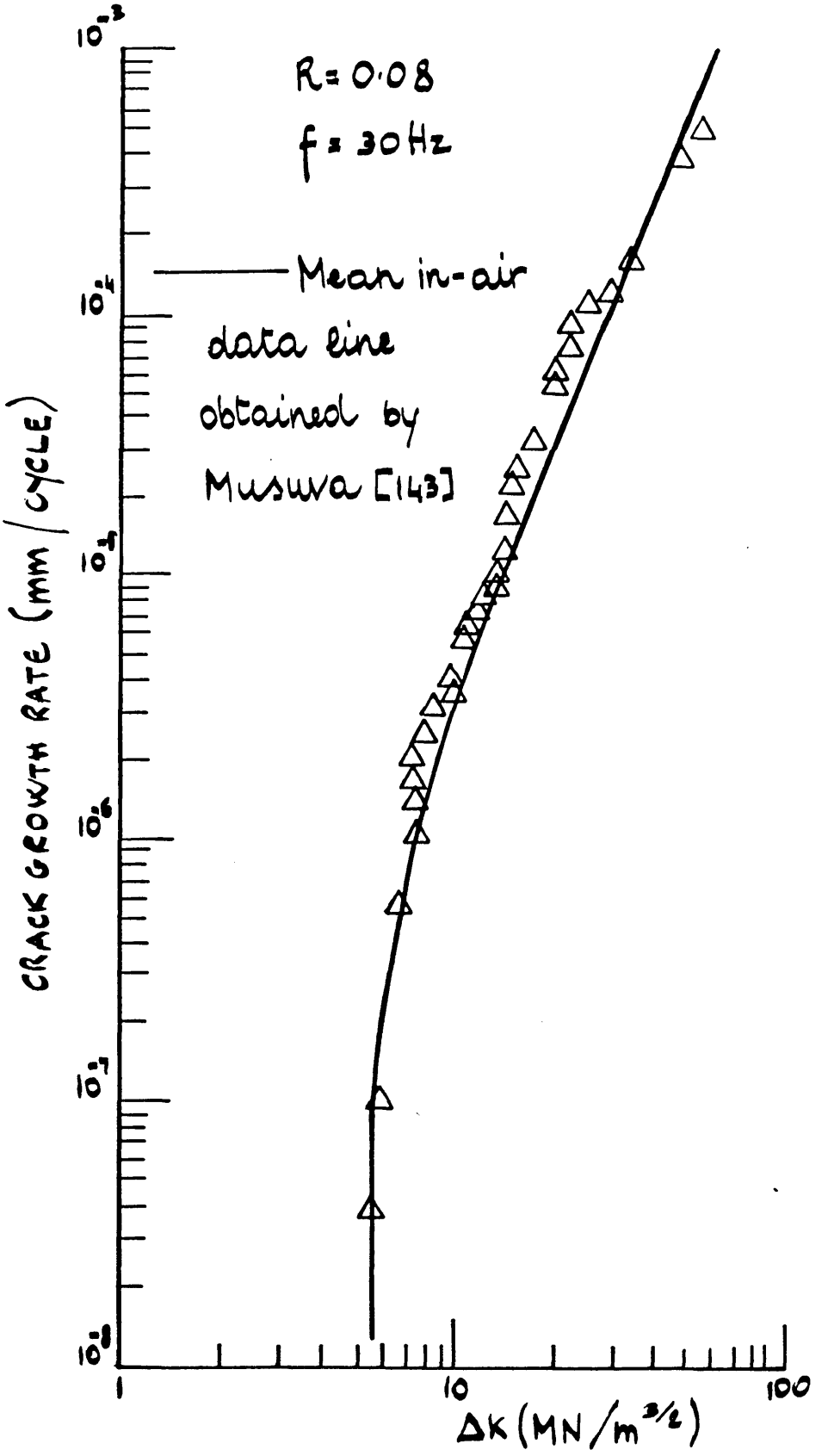


Figure 4.3 Comparison of results obtained from the present study and those of Musuva [143].

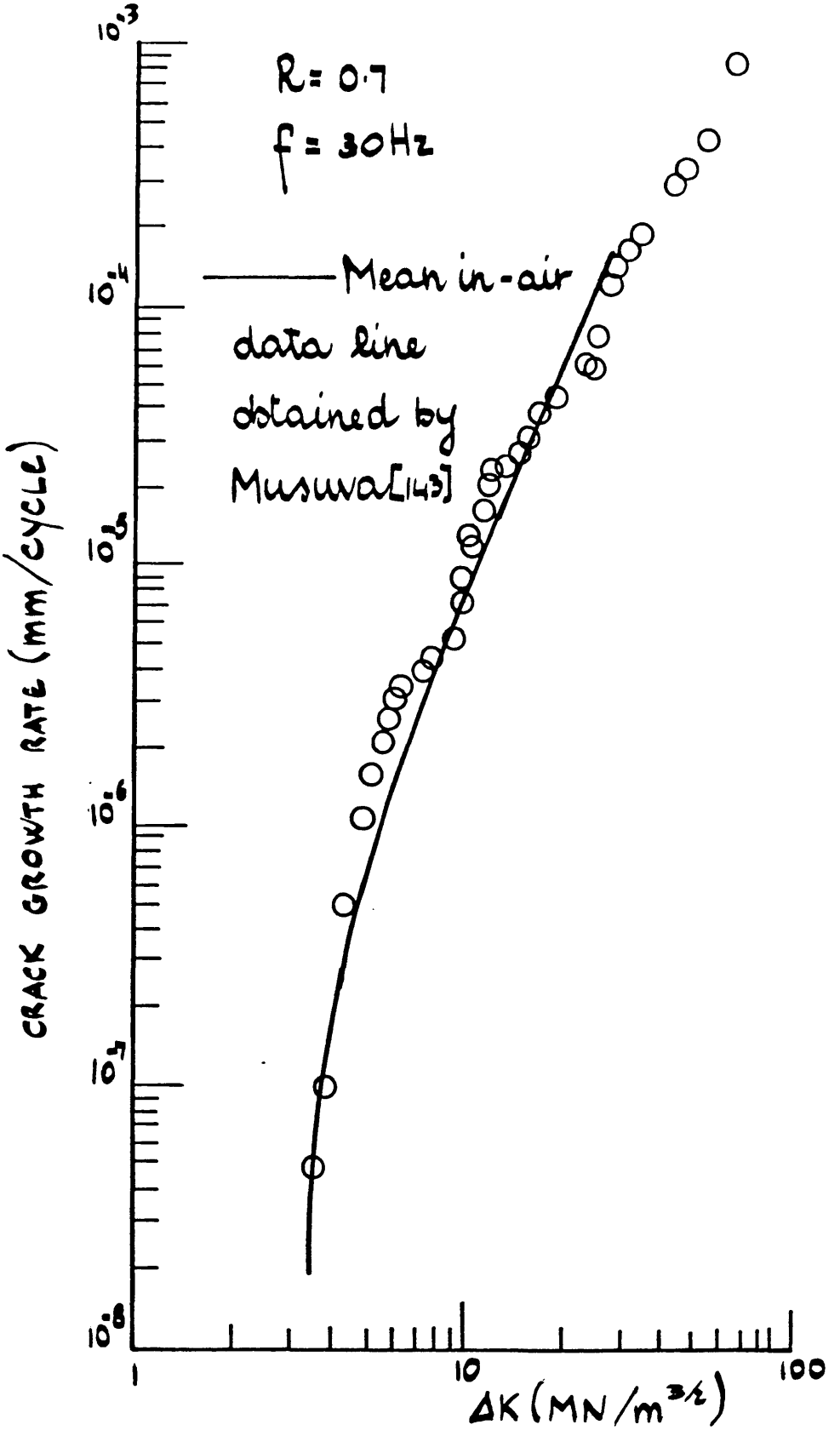


Figure 4.4 Comparison of results obtained from the present study and those of Musuva [143].

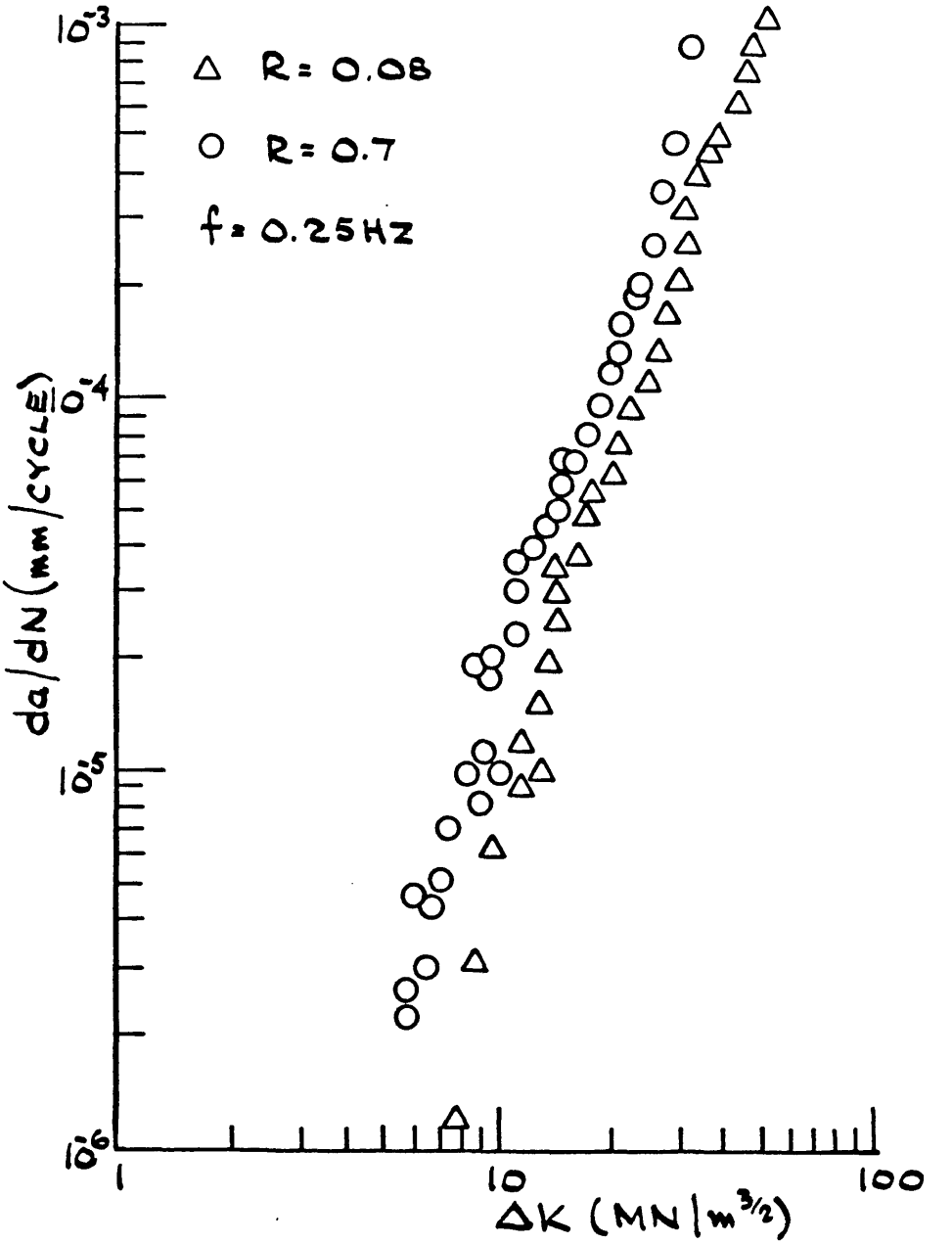


Figure 4.5 Effect of stress ratio on fatigue crack growth of BS4360-50D steel using CT specimen in air.

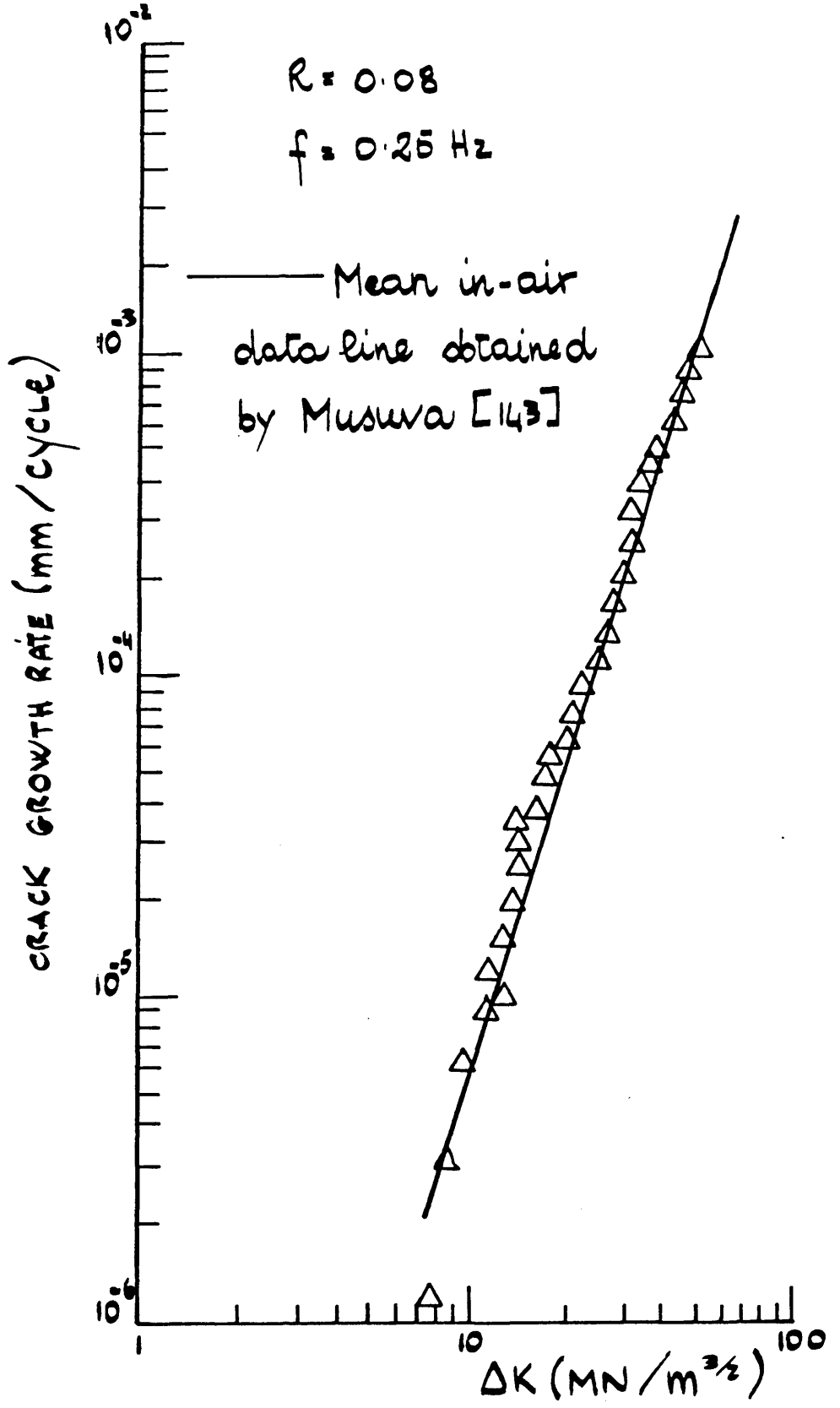


Figure 4.6 Comparison of results obtained from the present study and those of Musuva [143].

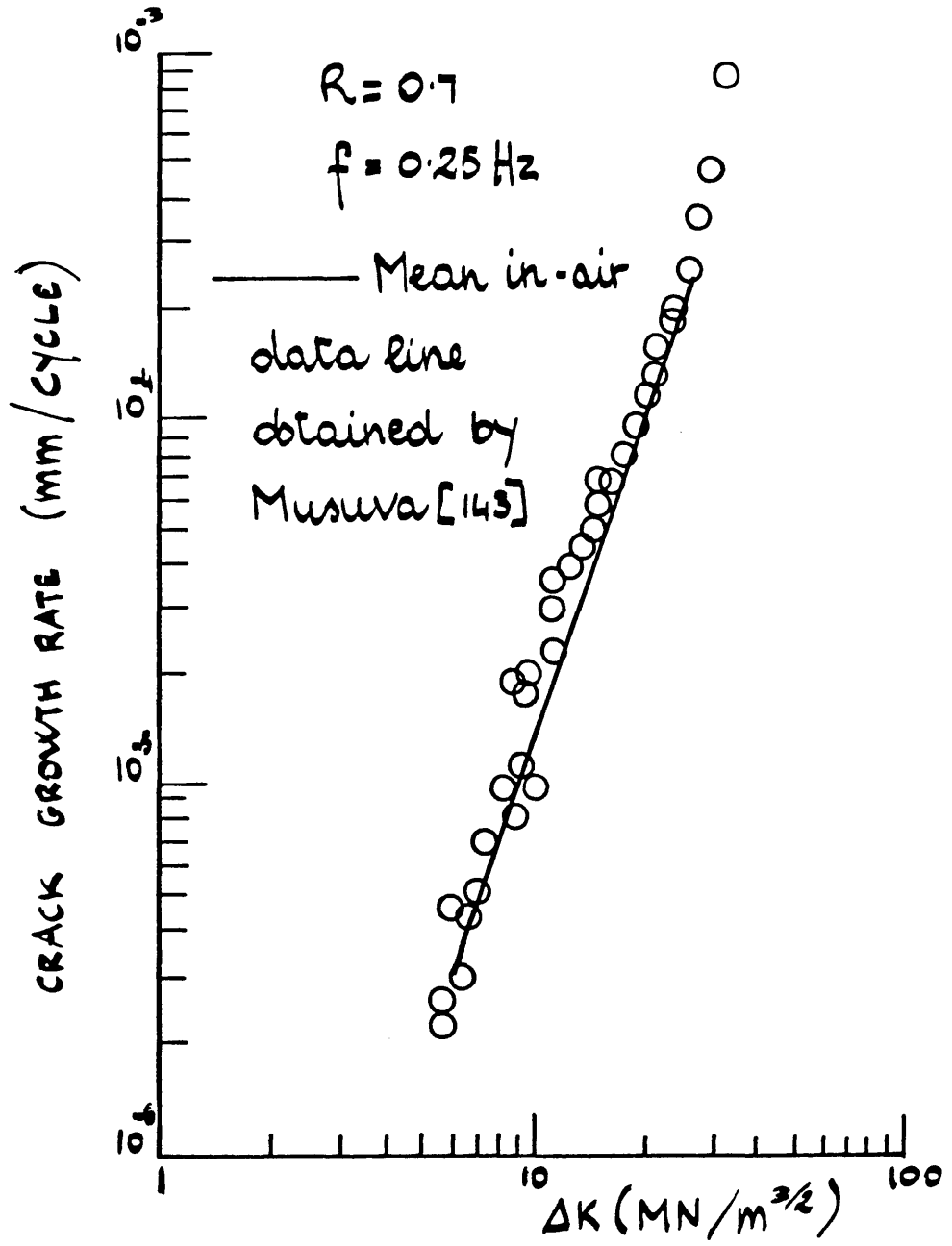


Figure 4.7 Comparison of results obtained from the present study and those of Musuva [143].

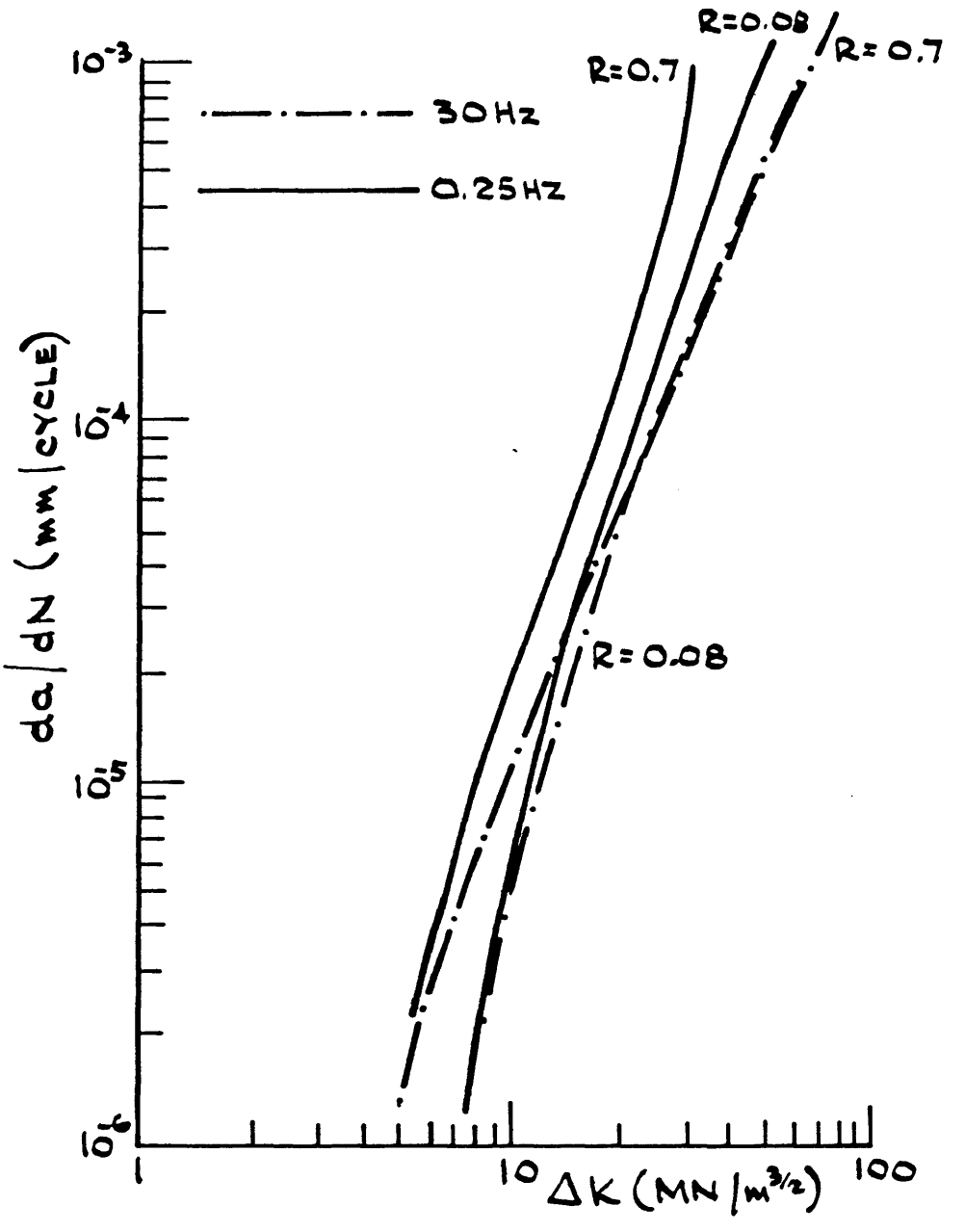


Figure 4.8 Effect of frequency on crack growth rate of BS4360-50D steel using CT specimen in air.

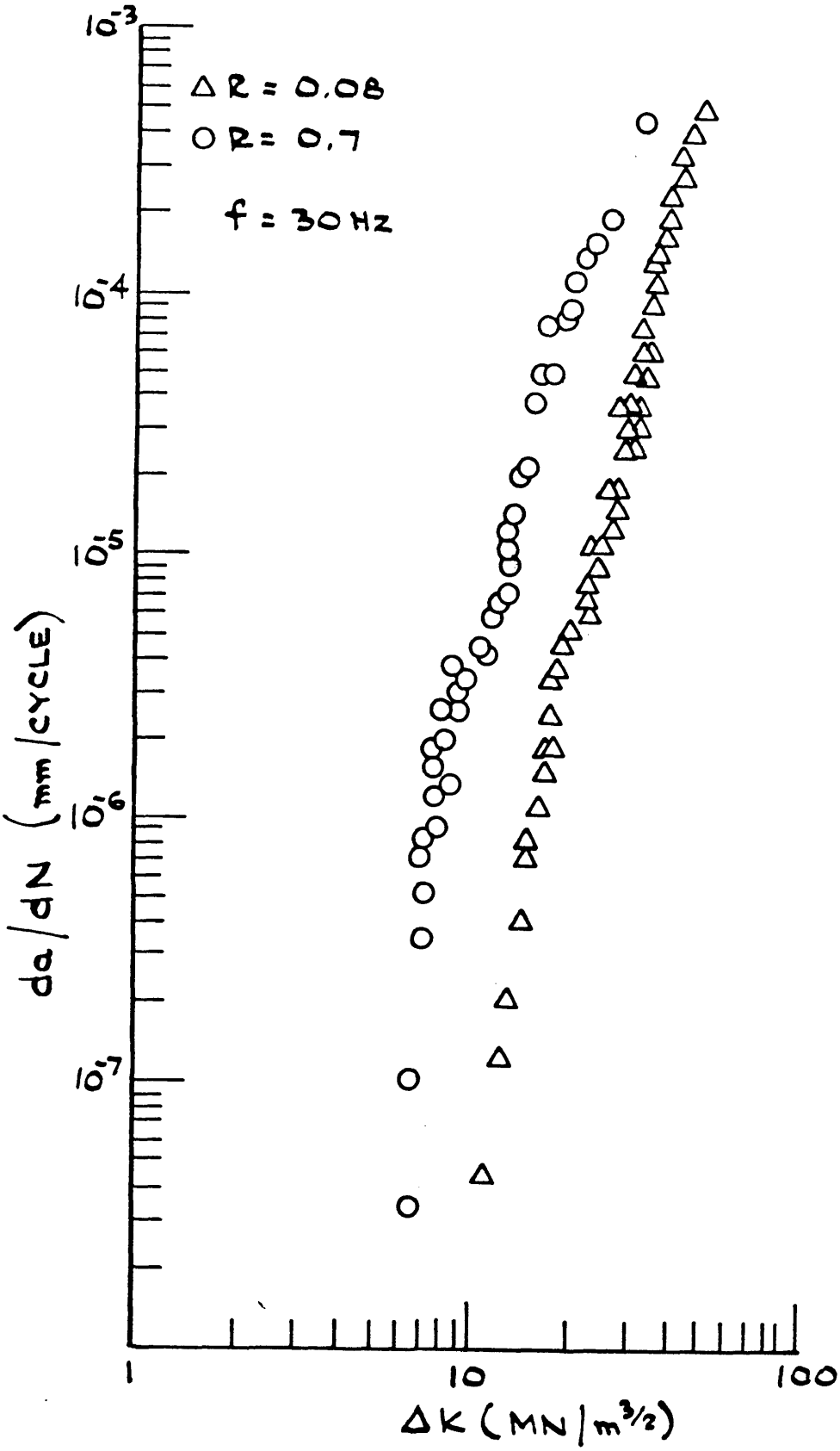


Figure 4.9 Effect of stress ratio on fatigue crack propagation in weldment using CT specimen in air.

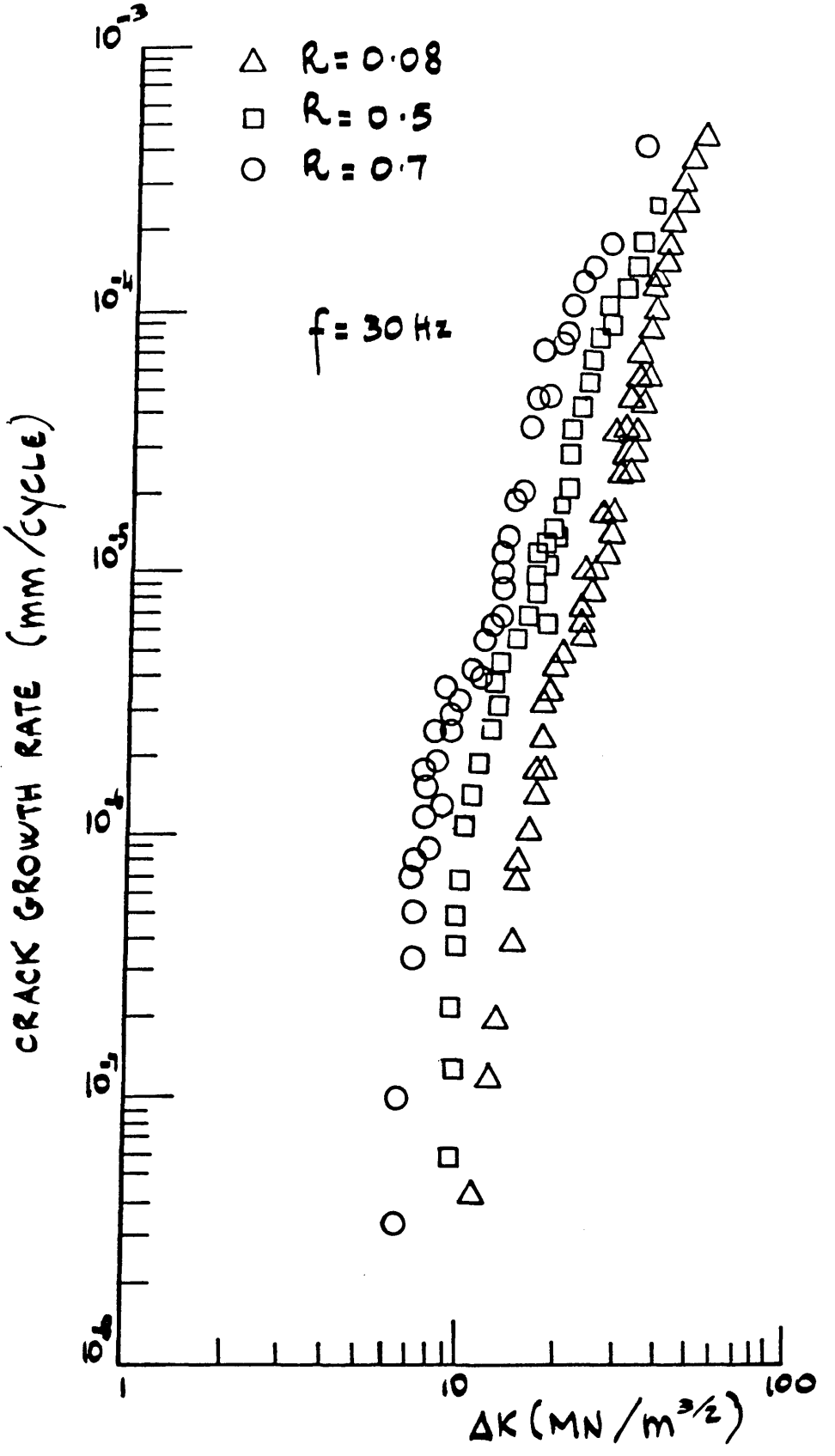


Figure 4.10 Effect of stress ratio on fatigue crack propagation in weldment using CT specimen in air.

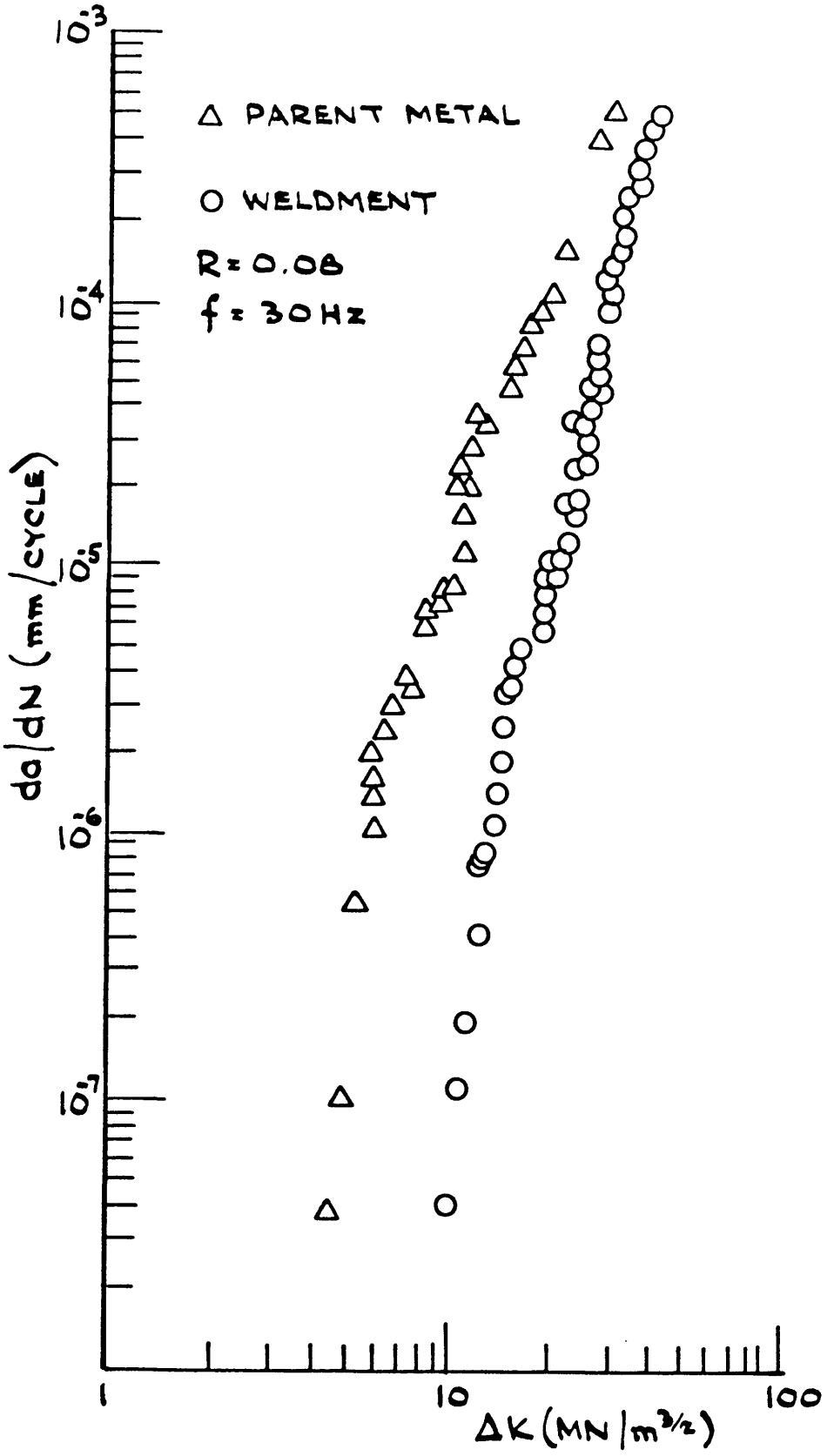


Figure 4.11 Comparison of fatigue crack growth curves obtained for BS4360-50D and weldment using CT specimen in air.

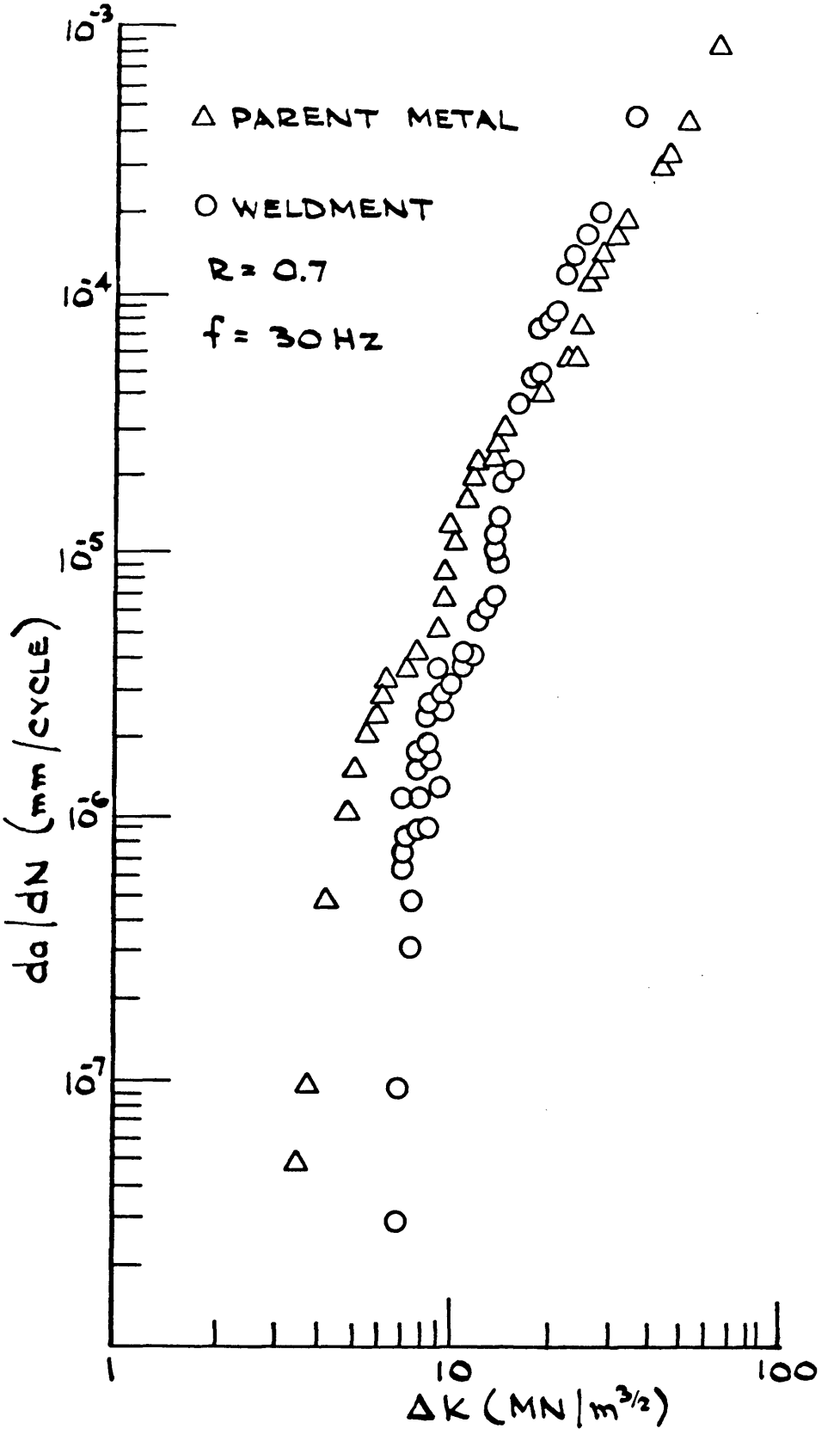


Figure 4.12 Comparison of fatigue crack growth curves obtained for BS4360-50D and weldment using CT specimens in air.

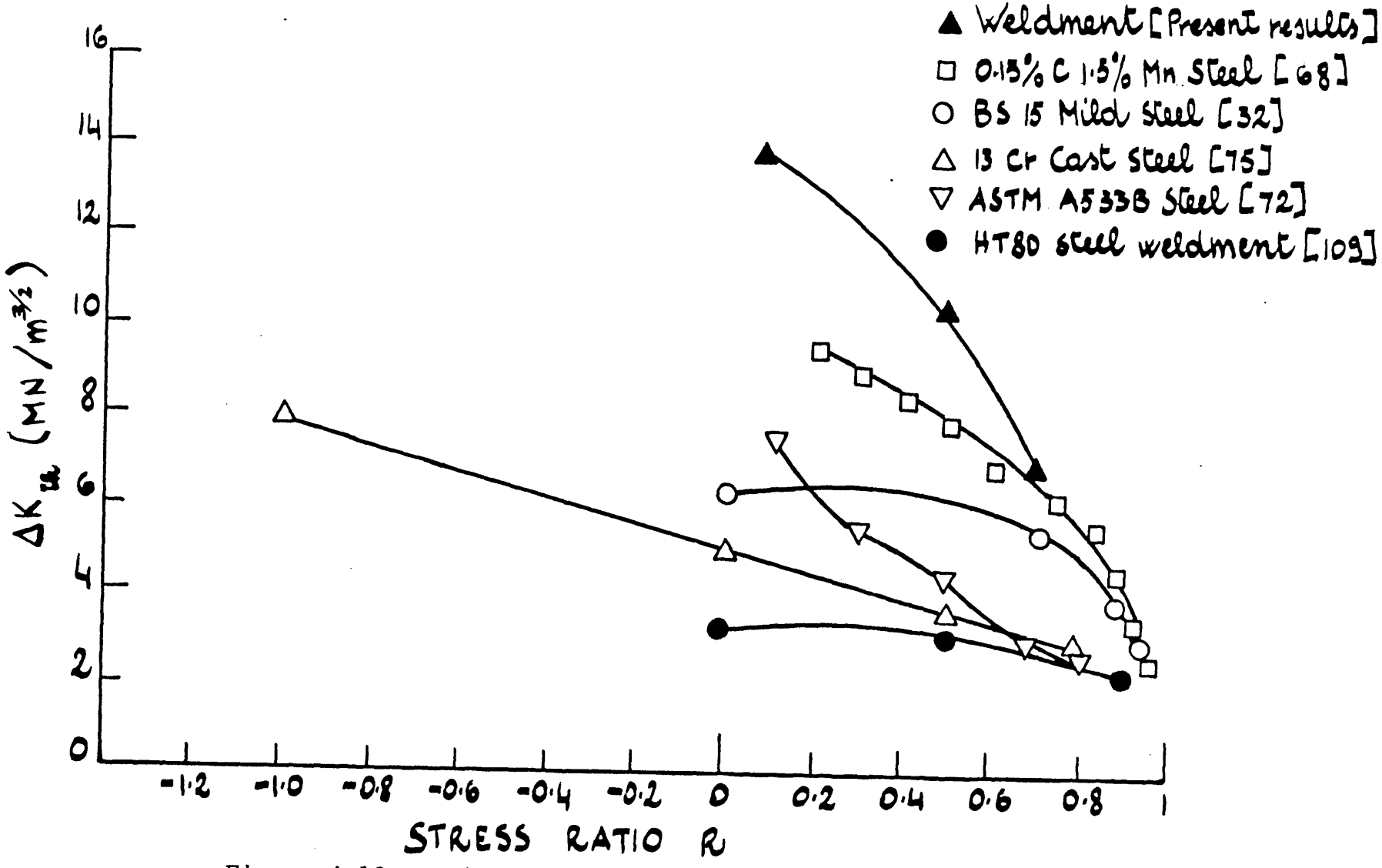


Figure 4.13 Variation of ΔK_{th} with R for different steels and weldment

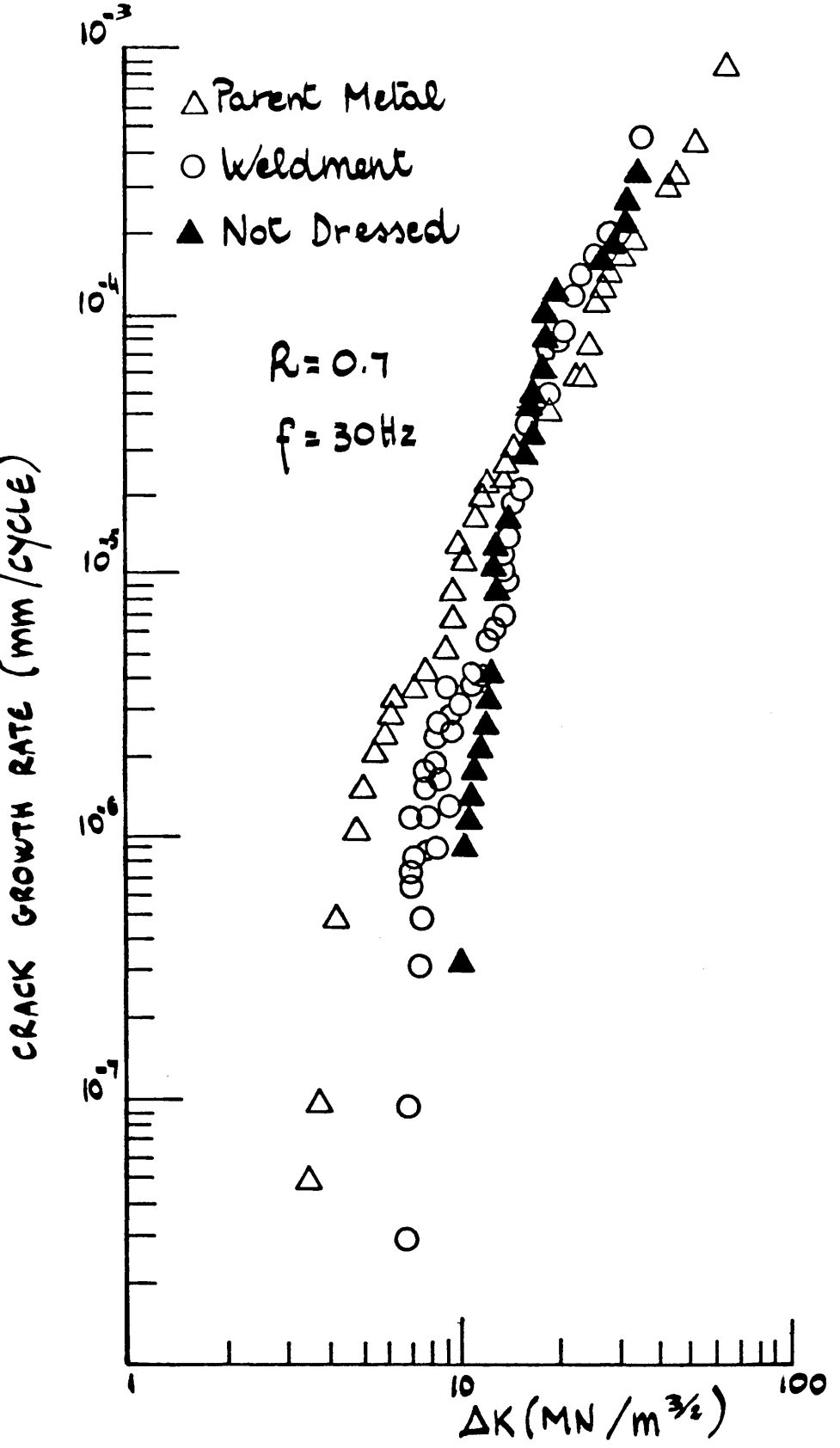


Figure 4.14 Effect of dressing on fatigue crack propagation of weldments tested using CT specimen in air.

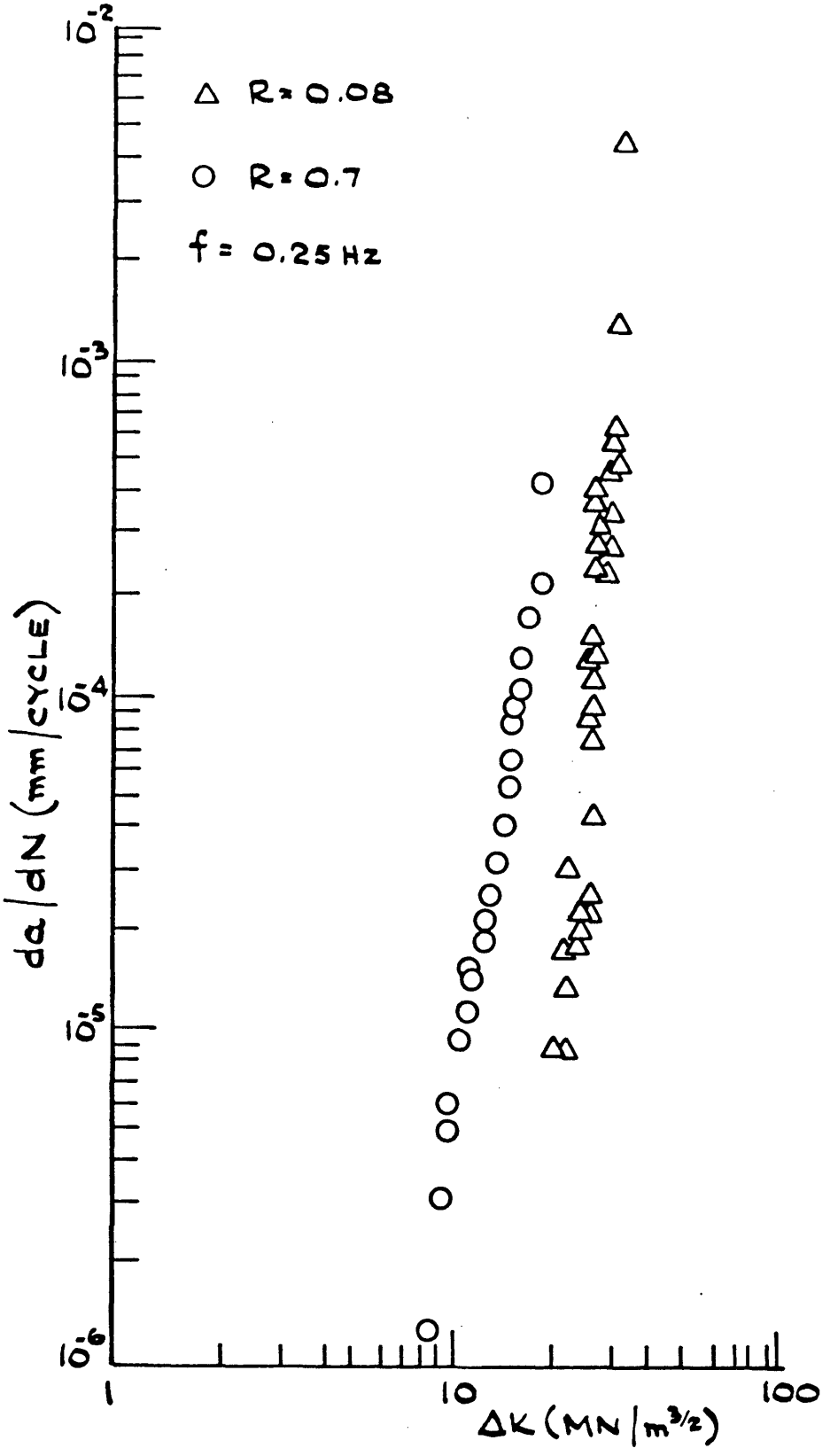


Figure 4.15 Effect of R on fatigue crack propagation of weldment using CT specimens in air.

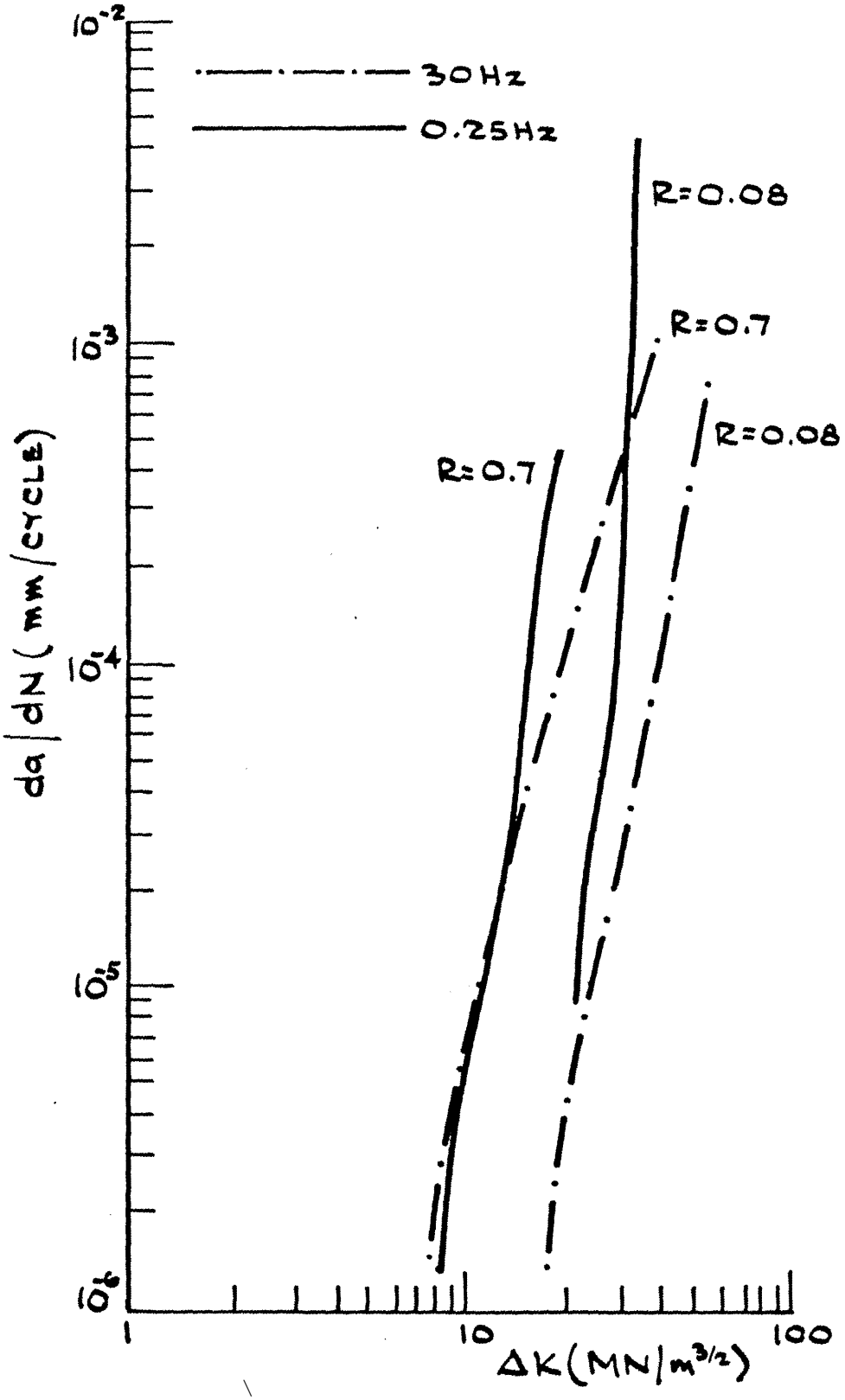


Fig 4.16

Effect of frequency on weldment"eia»ent

fig 4.i frequent

E«ect ot

b

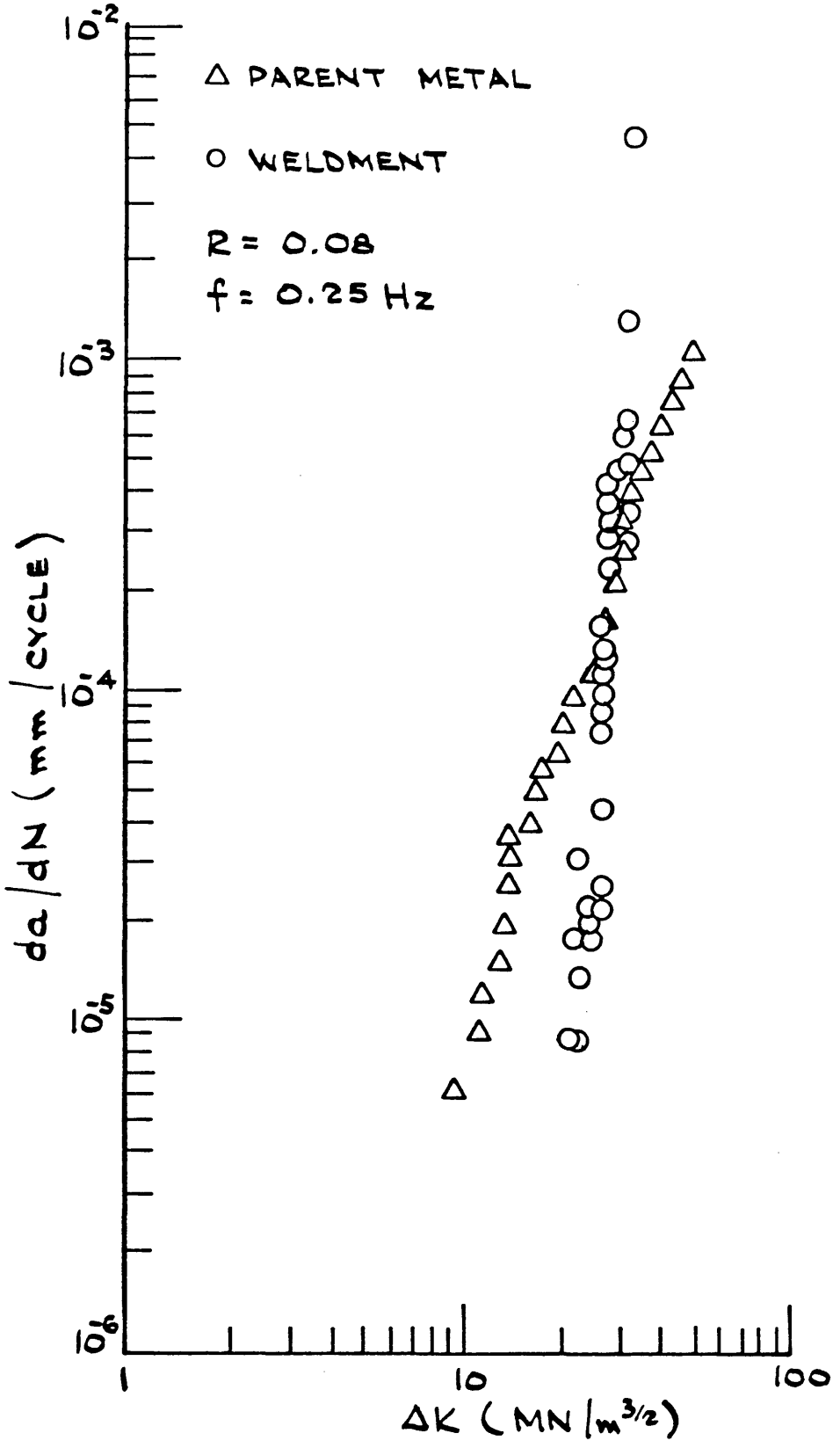


Figure 4.17 Comparison of the results obtained for BS4360-50D steel and weldment using CT specimen in air.

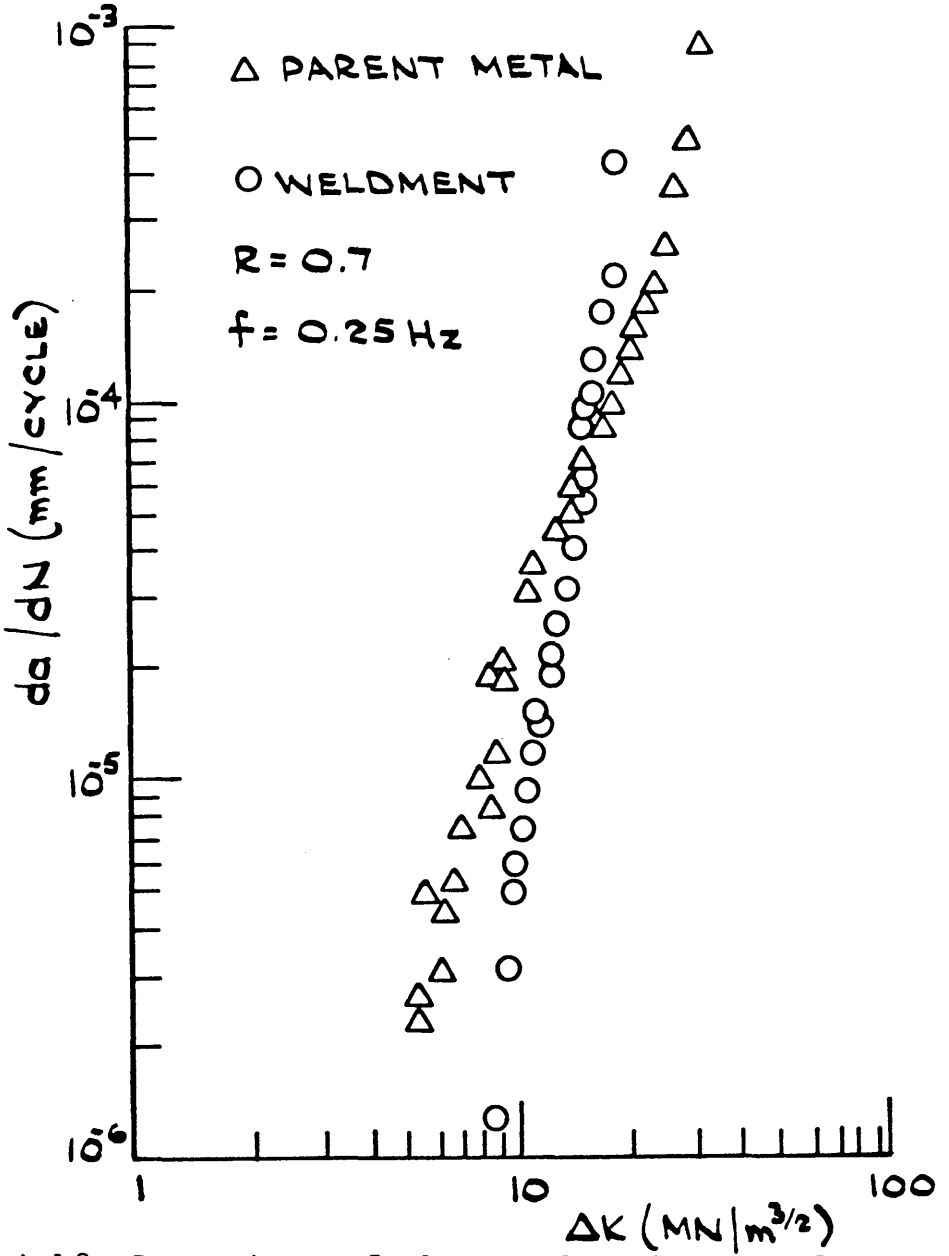


Figure 4.18 Comparison of the results obtained for BS4360-50D steel and weldment using CT specimens in air.

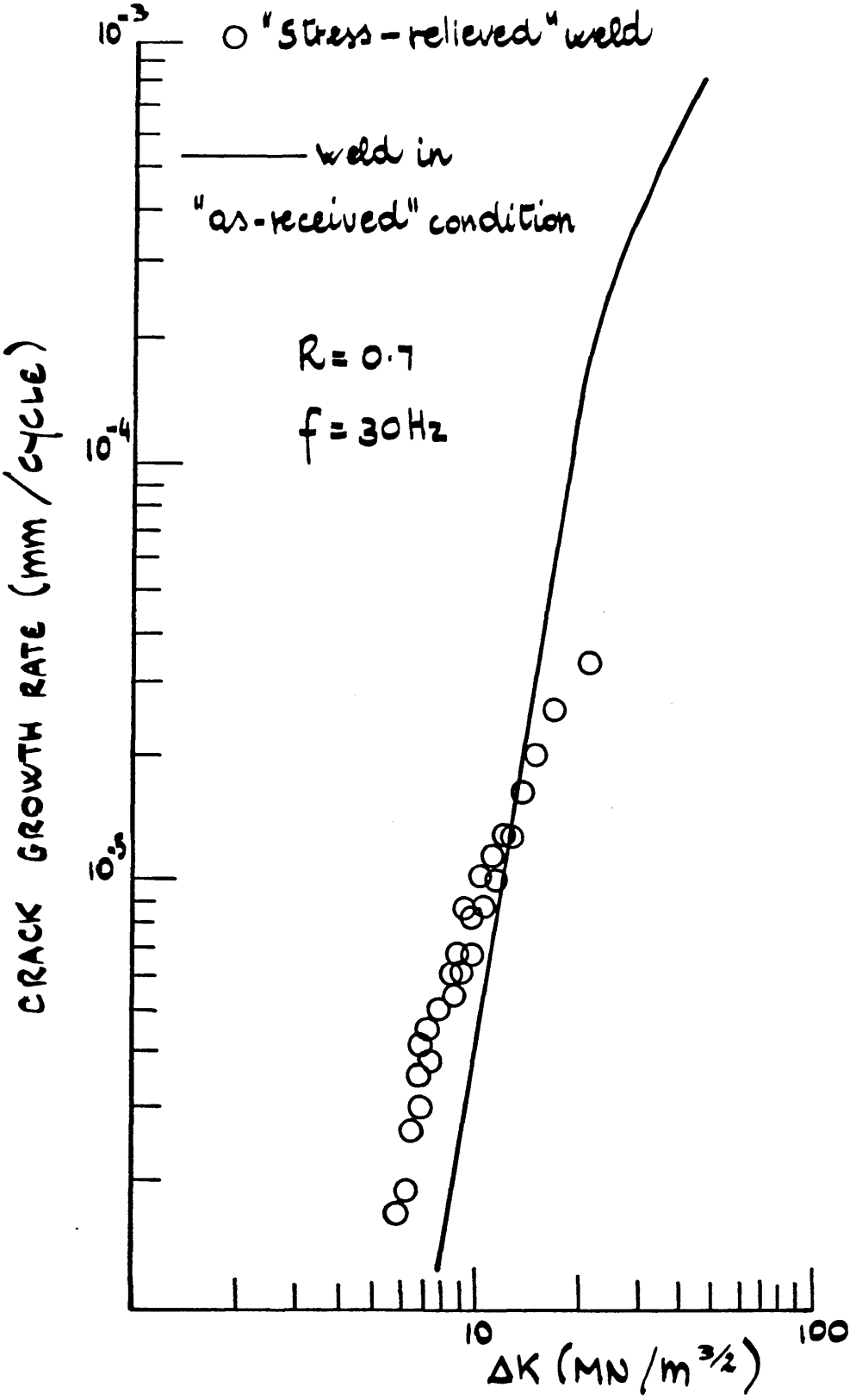


Figure 4.19 Comparison of the results obtained for stress-relieved weld and as-received weld using CT specimen in air.

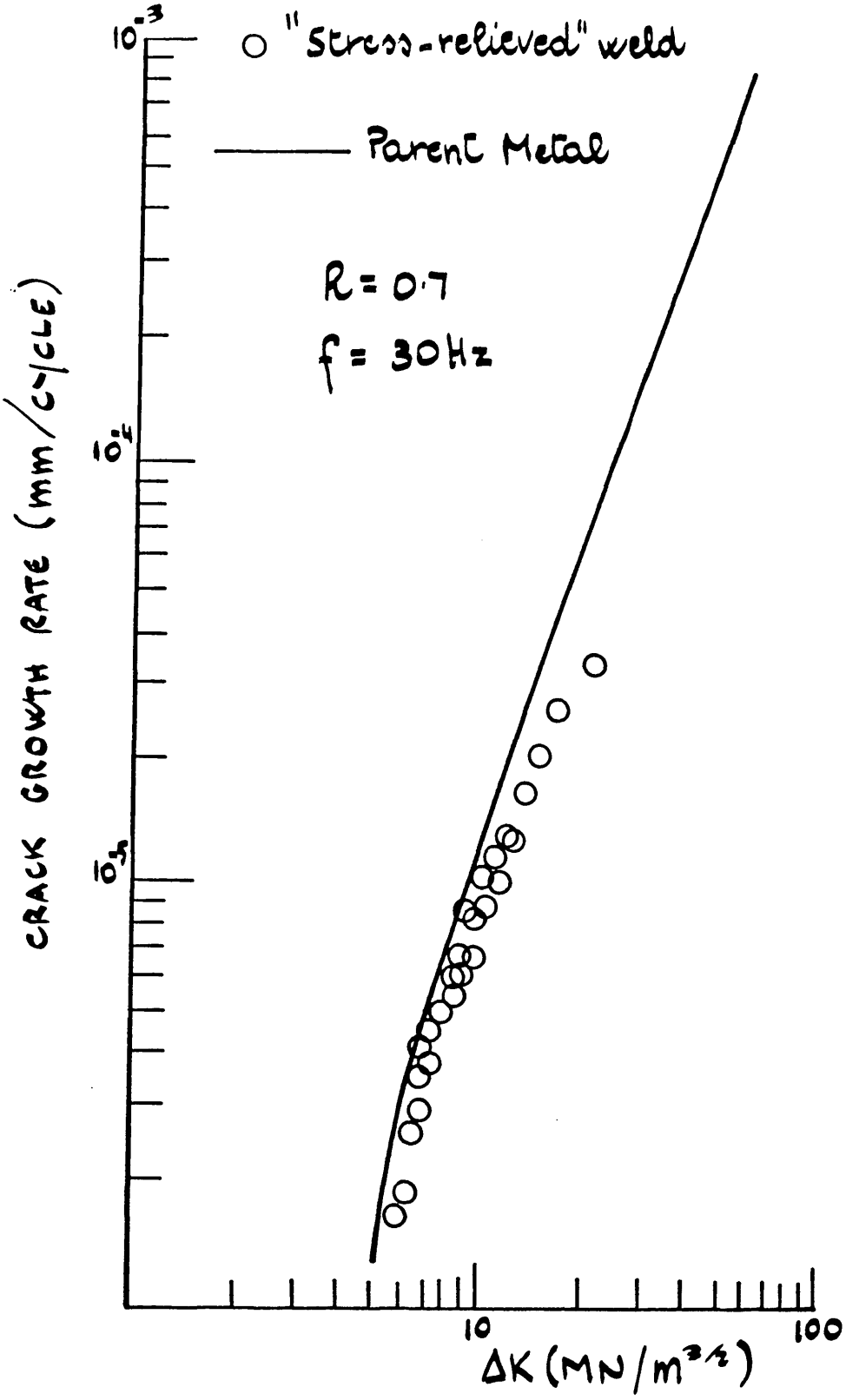


Figure 4.20 Comparison of the results obtained for stress-relieved weld and parent plate using CT specimen in air.

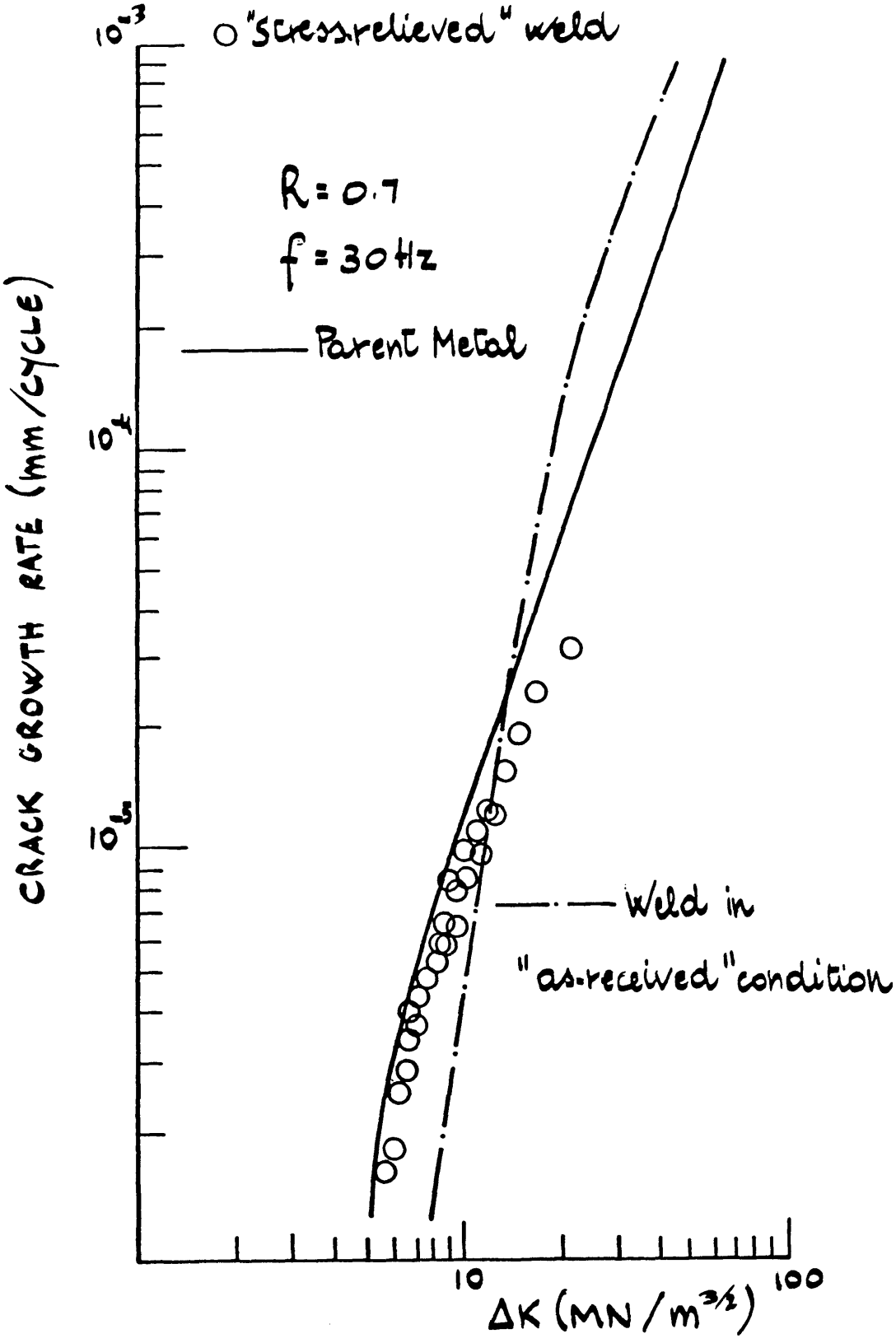


Figure 4.21 Effect of welding residual stress on fatigue crack propagation.

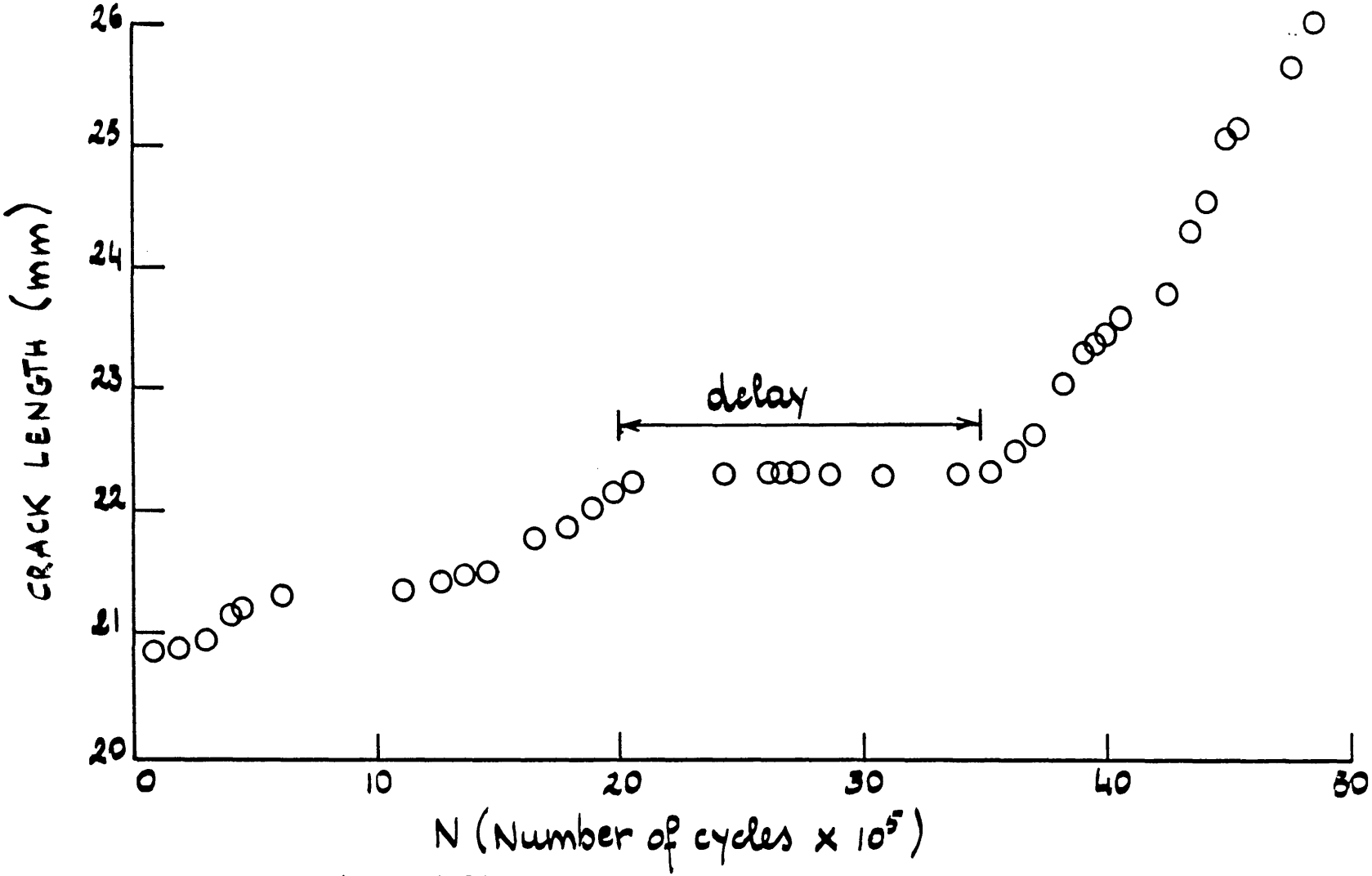


Figure 4.22 Crack length a versus N ; f=30Hz, R=0.08

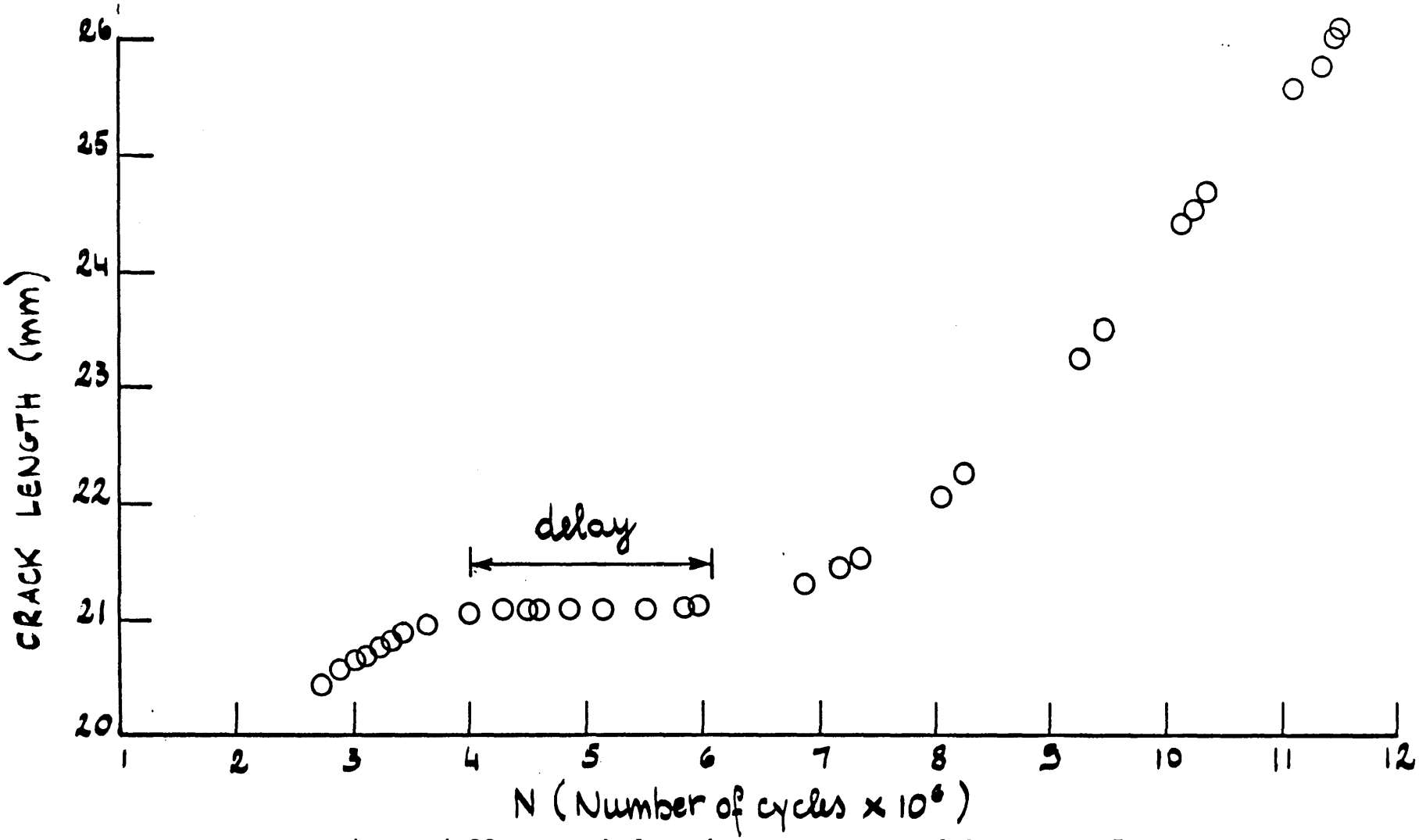


Figure 4.23 Crack length a versus N ; f=30Hz, R=0.7

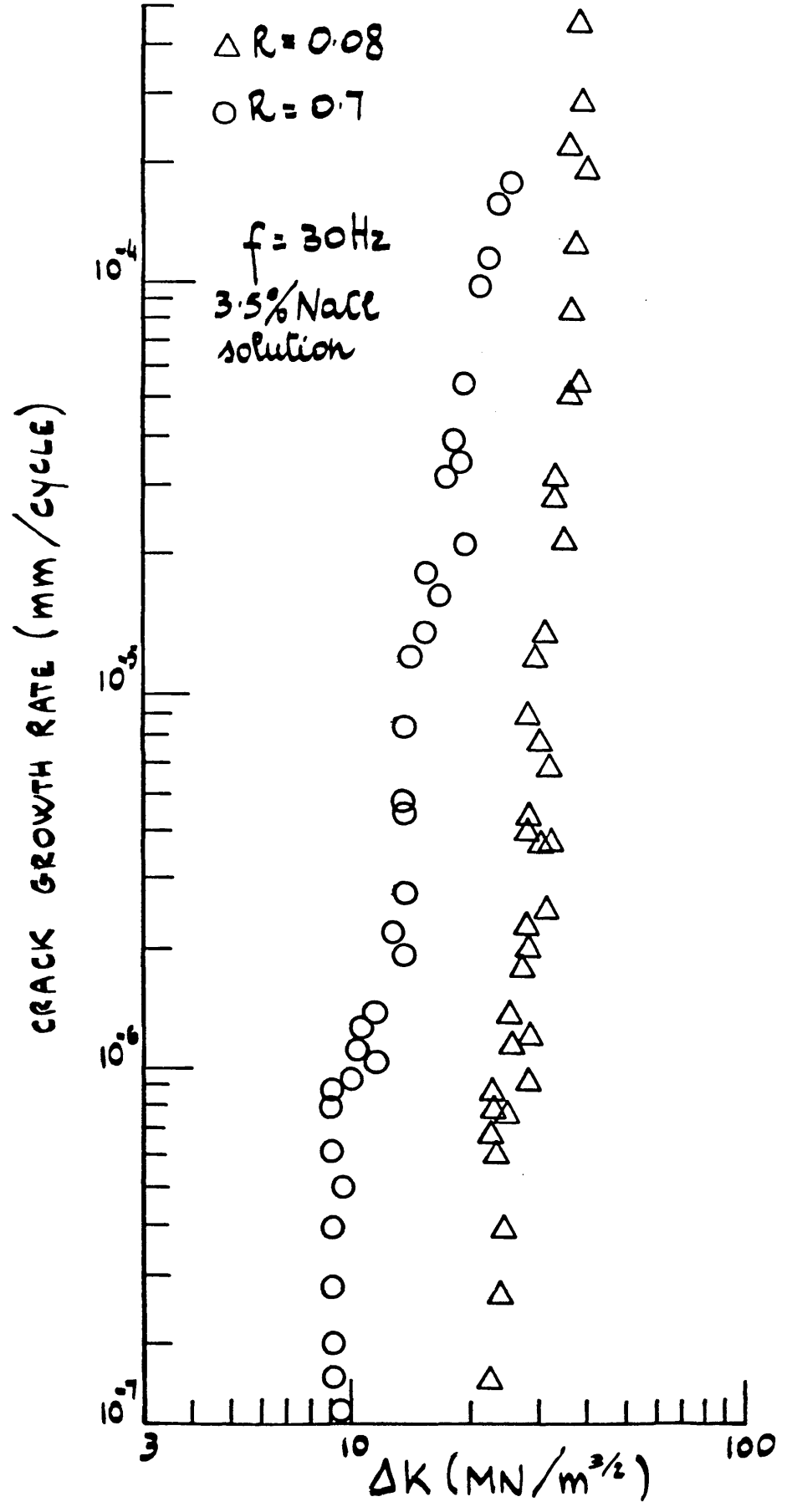


Figure 4.24 Effect of stress ratio on weldment using CT specimen in salt solution.

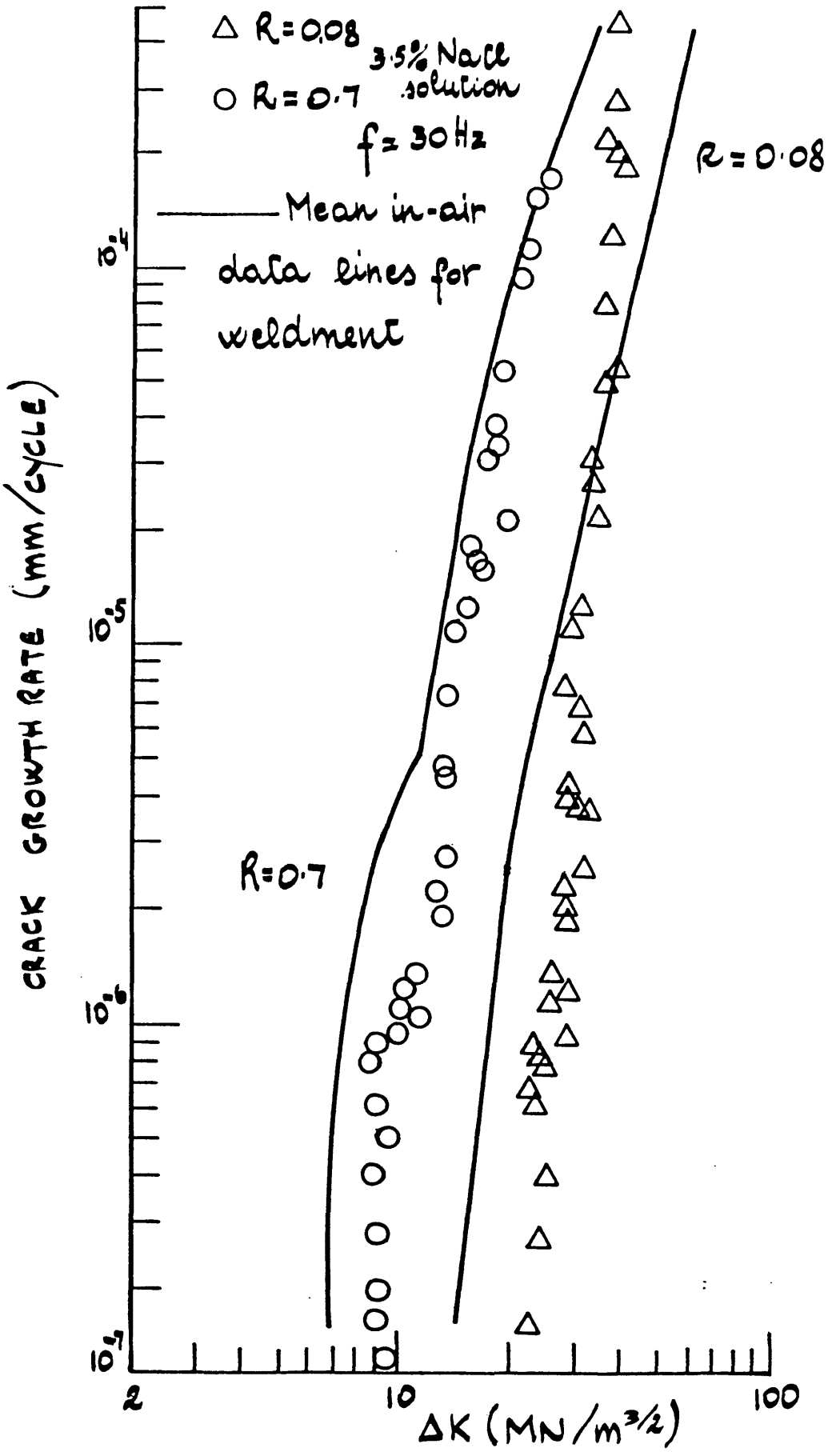


Figure 4.25 Comparison of the stress ratio effect for weldment using CT specimens in air and salt water environments.

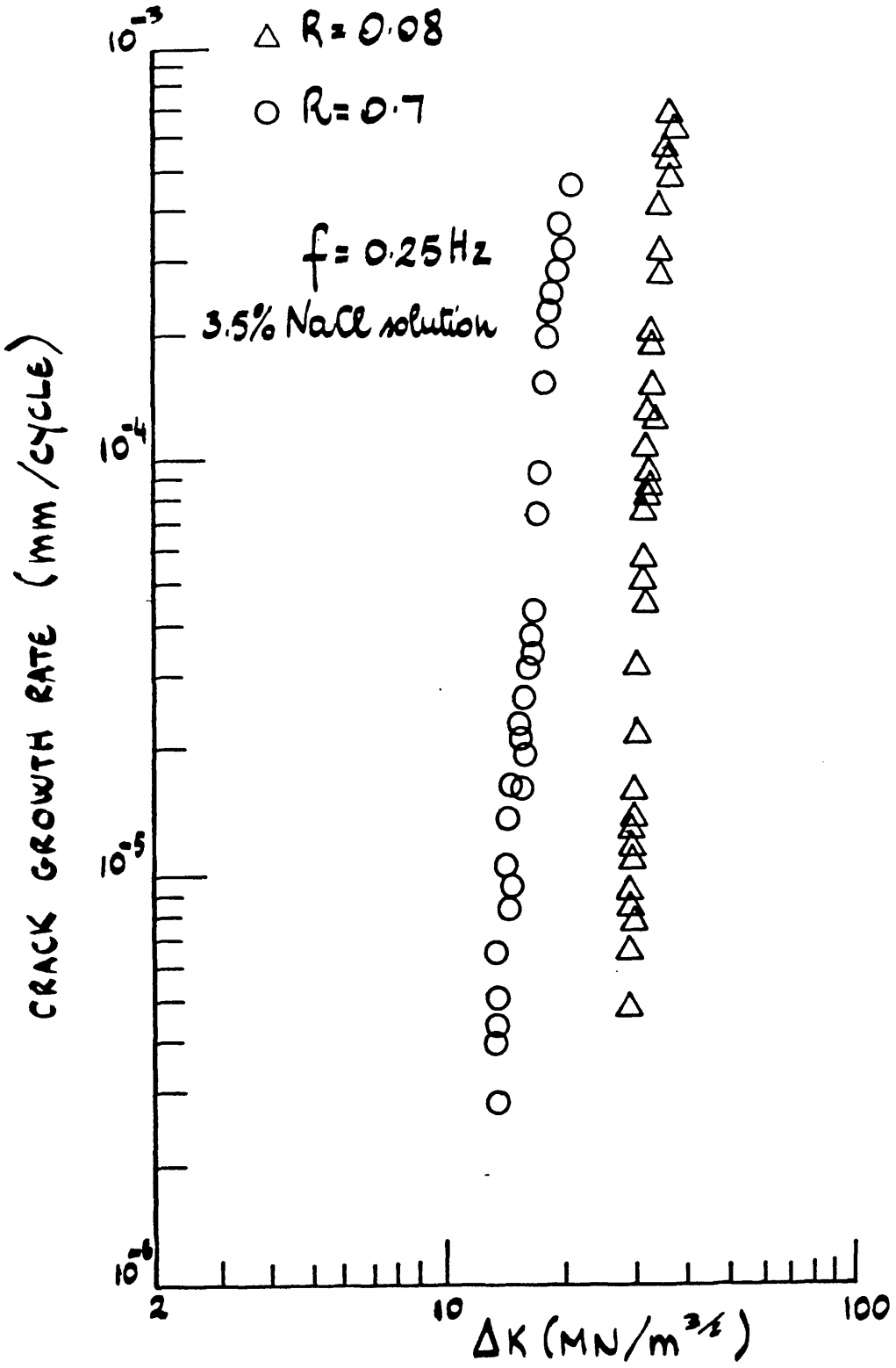


Figure 4.26 Stress ratio effect on weldment using CT specimen in salt solution.

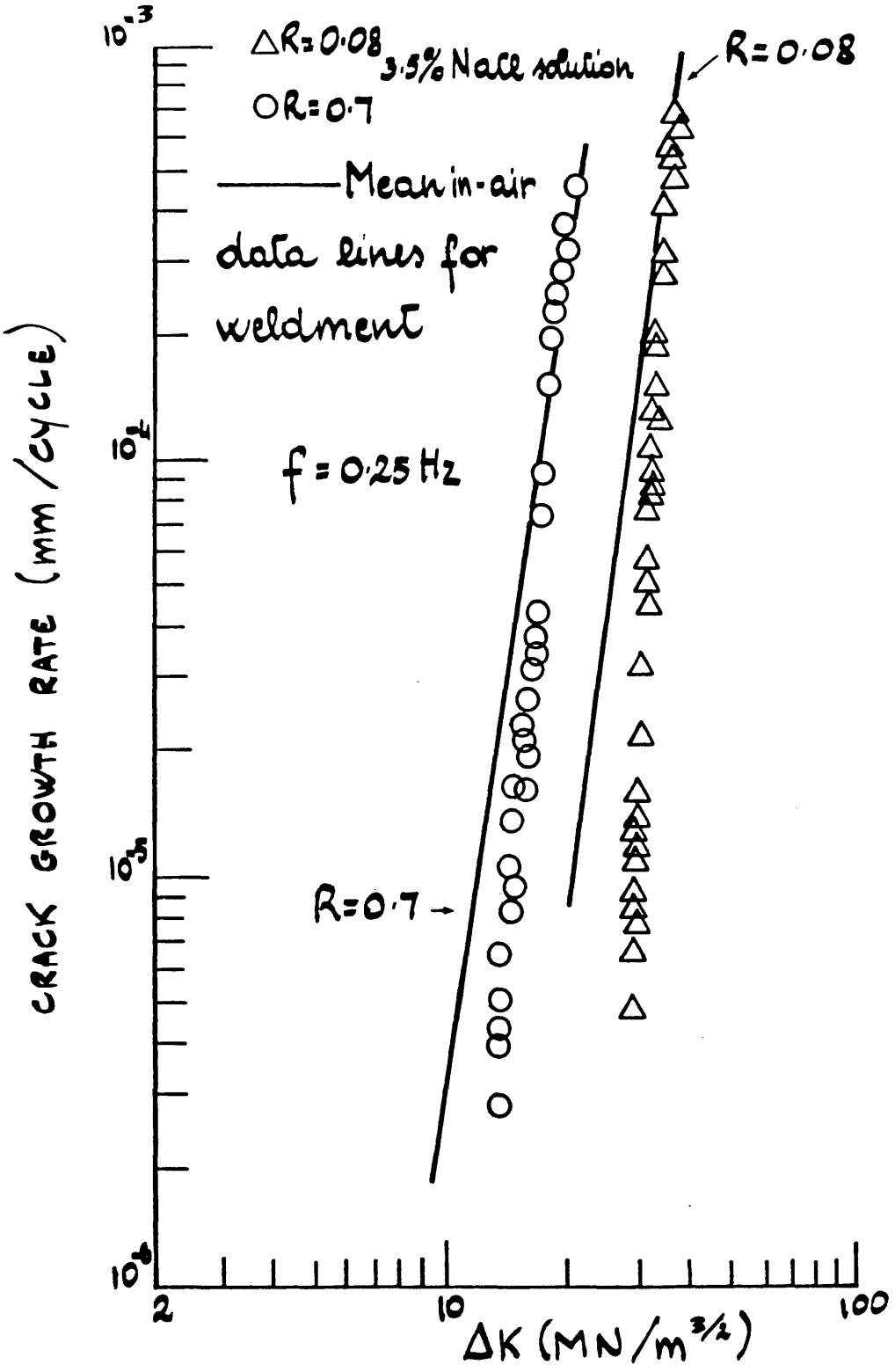


Figure 4.27 Comparison of the effect of stress ratio for weldment using CT specimen in air and salt solution.

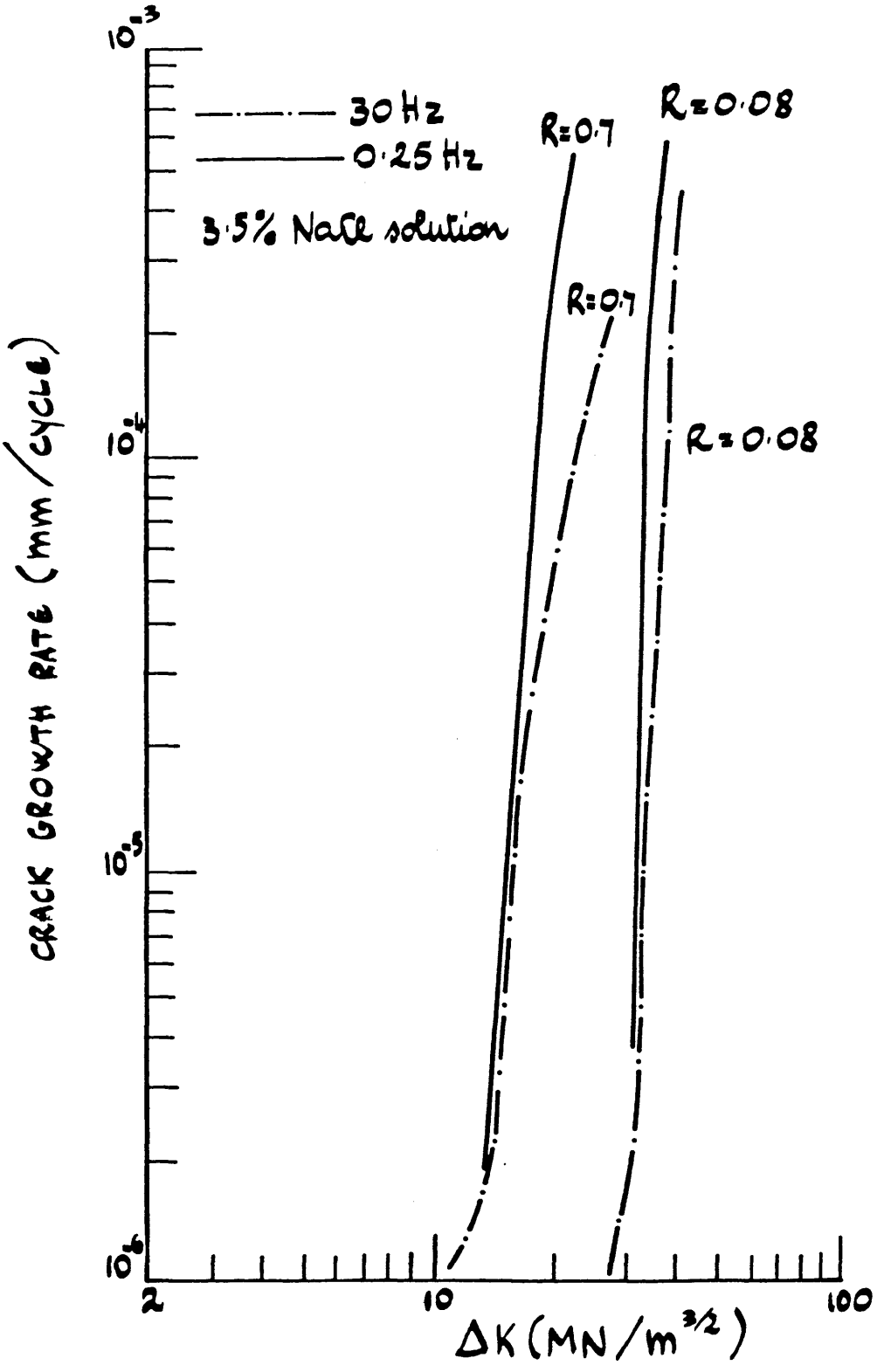


Figure 4.28 Frequency and stress ratio effects on weldment using CT specimen in salt solution.

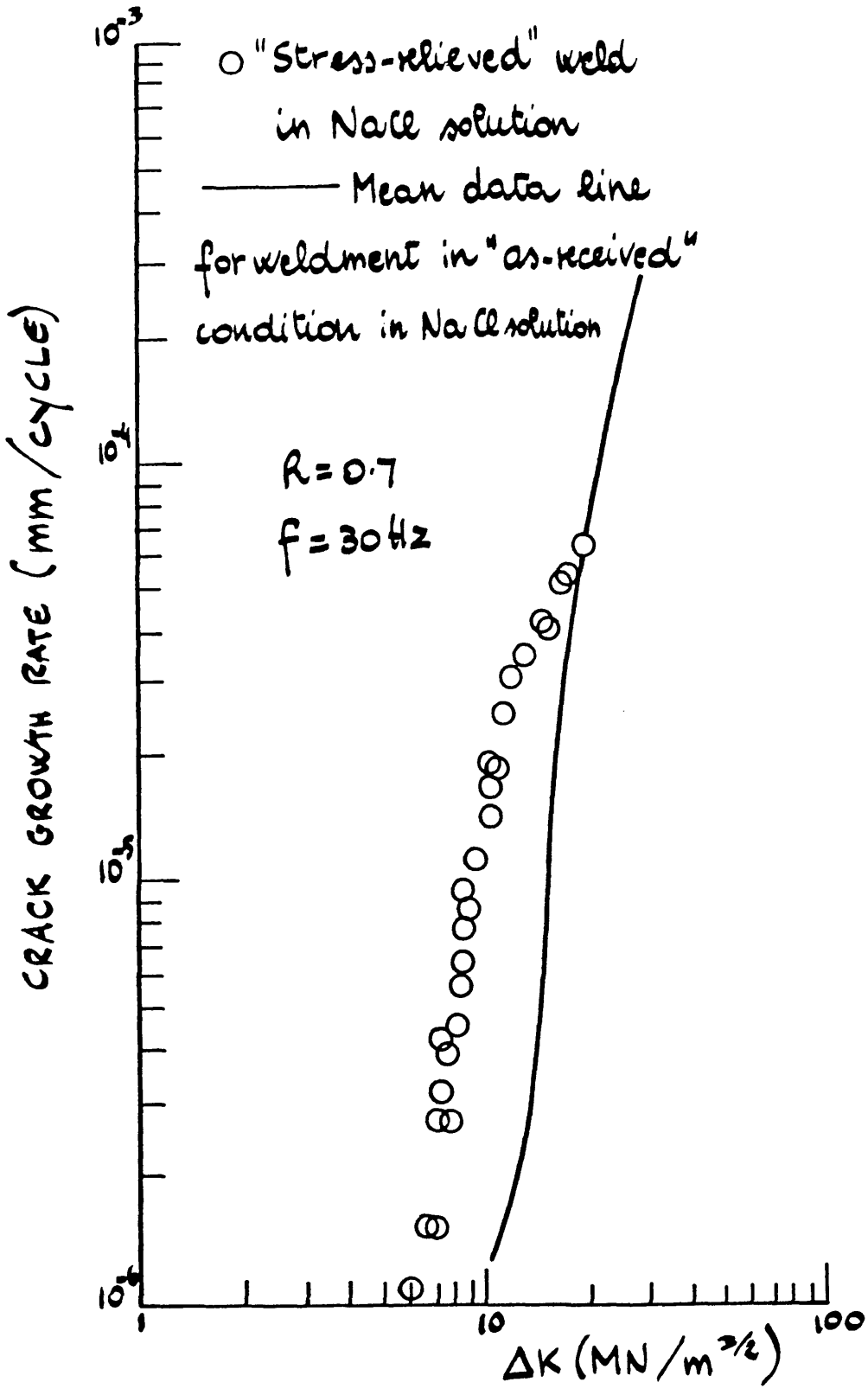


Figure 4.29 Comparison of results obtained for as-received and stress-relieved weldment using CT specimen in salt solution.

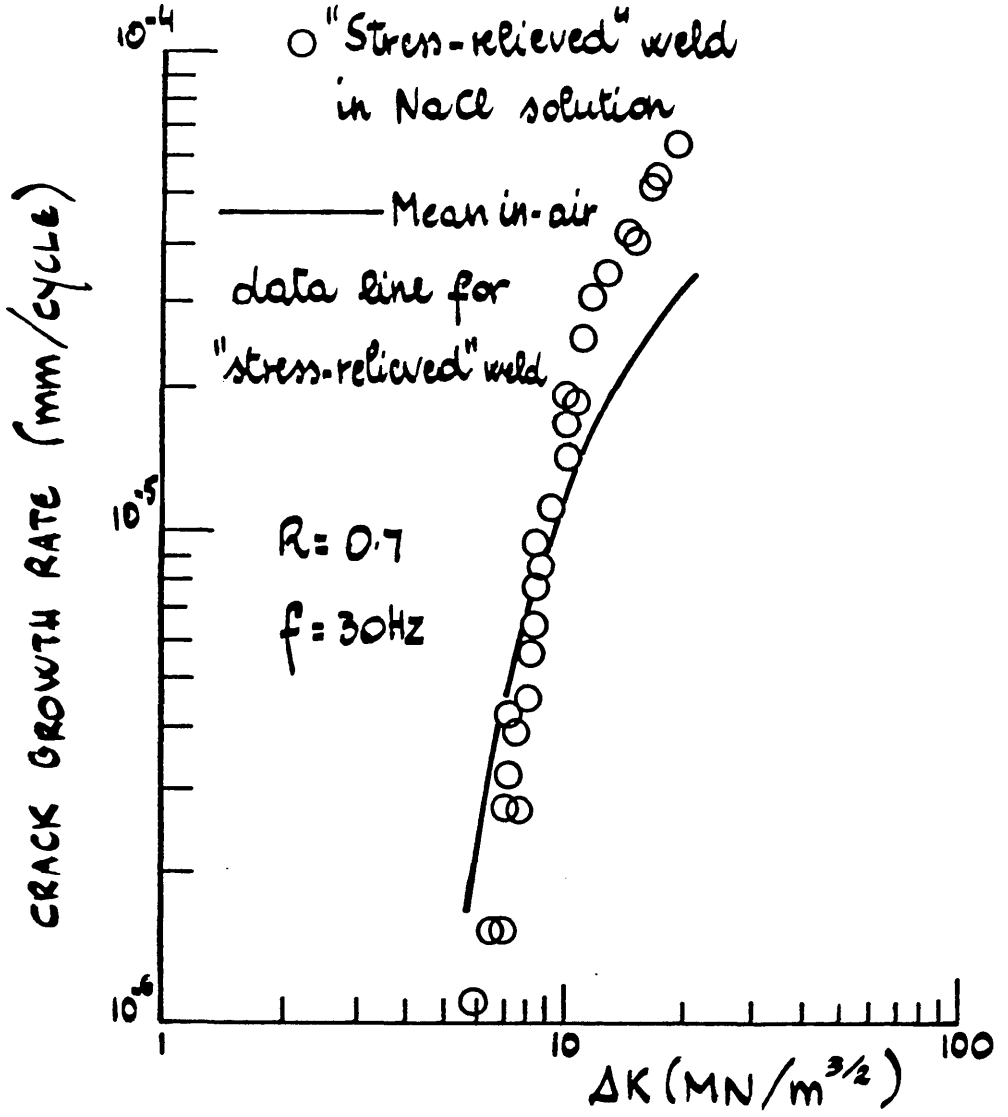


Figure 4.30 Comparison of results obtained for stress-relieved weldment using CT specimen in air and salt solution.

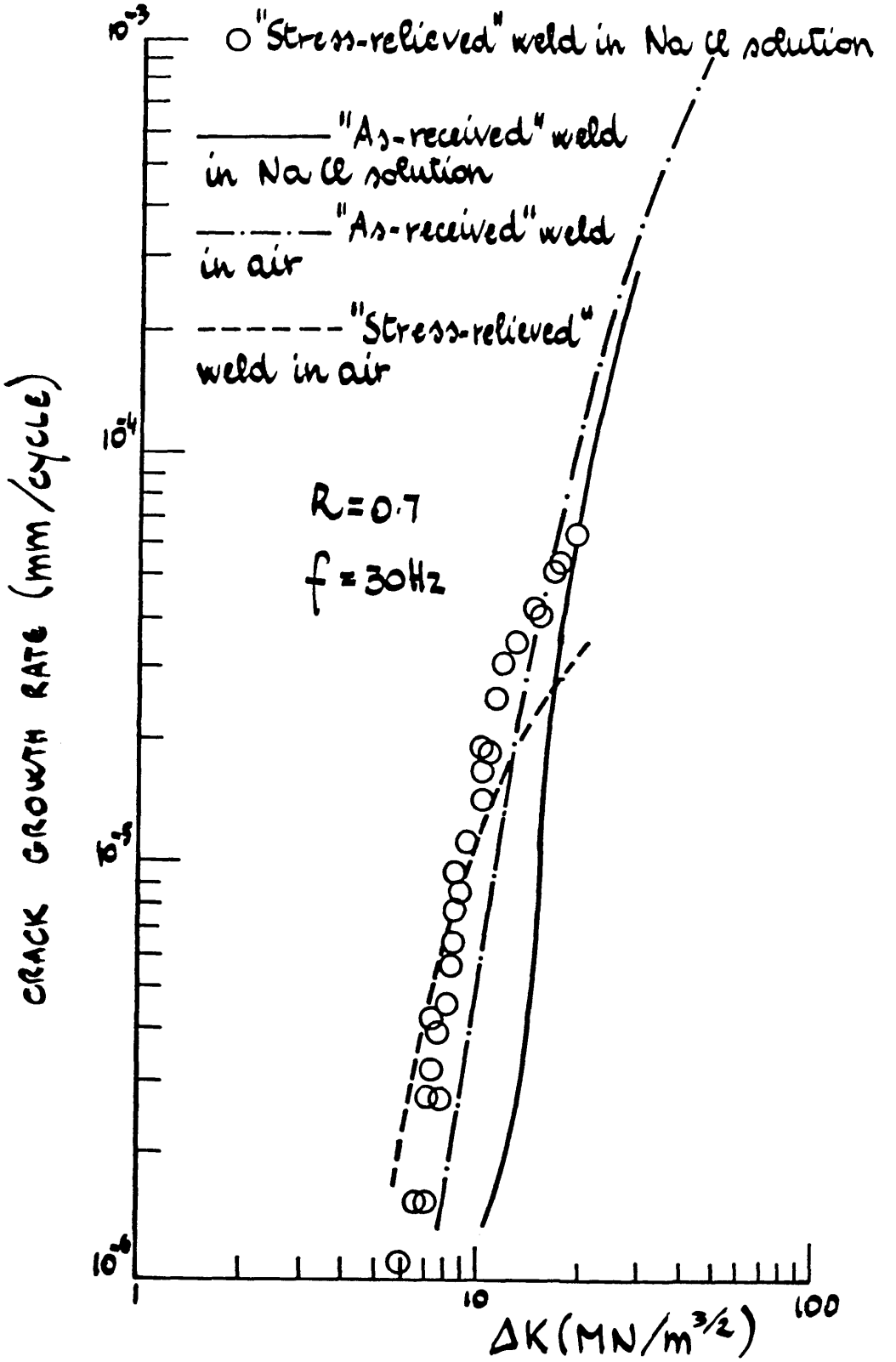


Figure 4.31 Comparison of results obtained for stress-relieved and as-received weld by using CT specimen in air and salt solution.

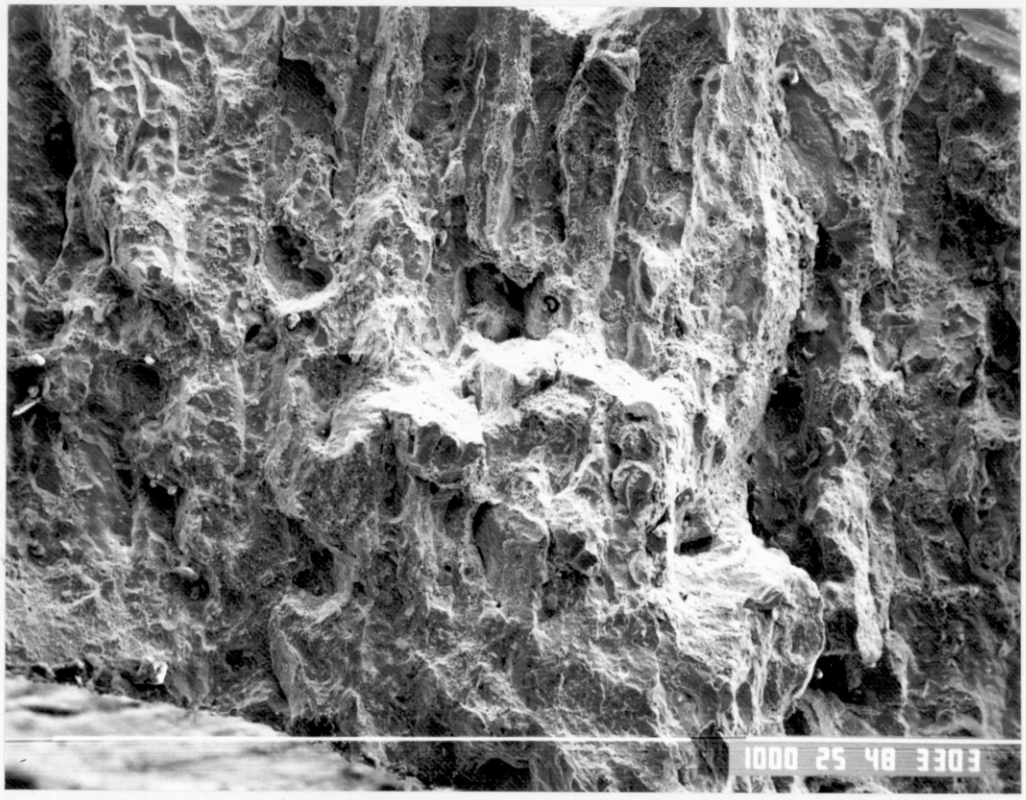


Figure 4.32 Dendritic formations with columnar grains

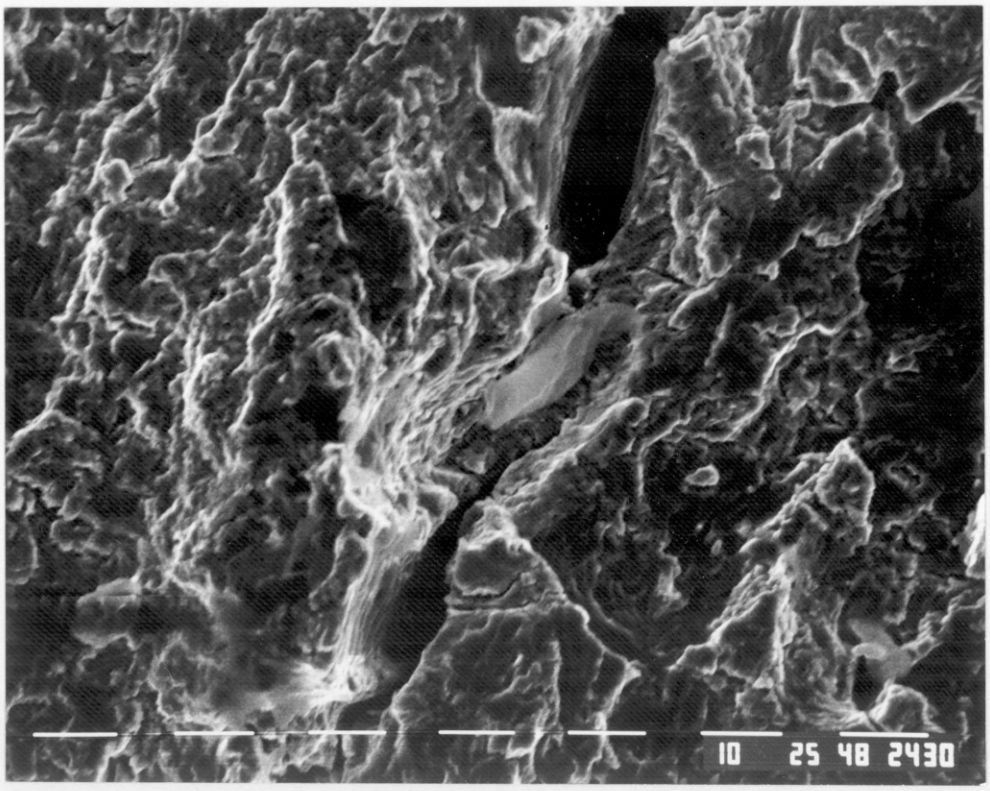


Figure 4.33 SEM Photograph showing secondary cracking

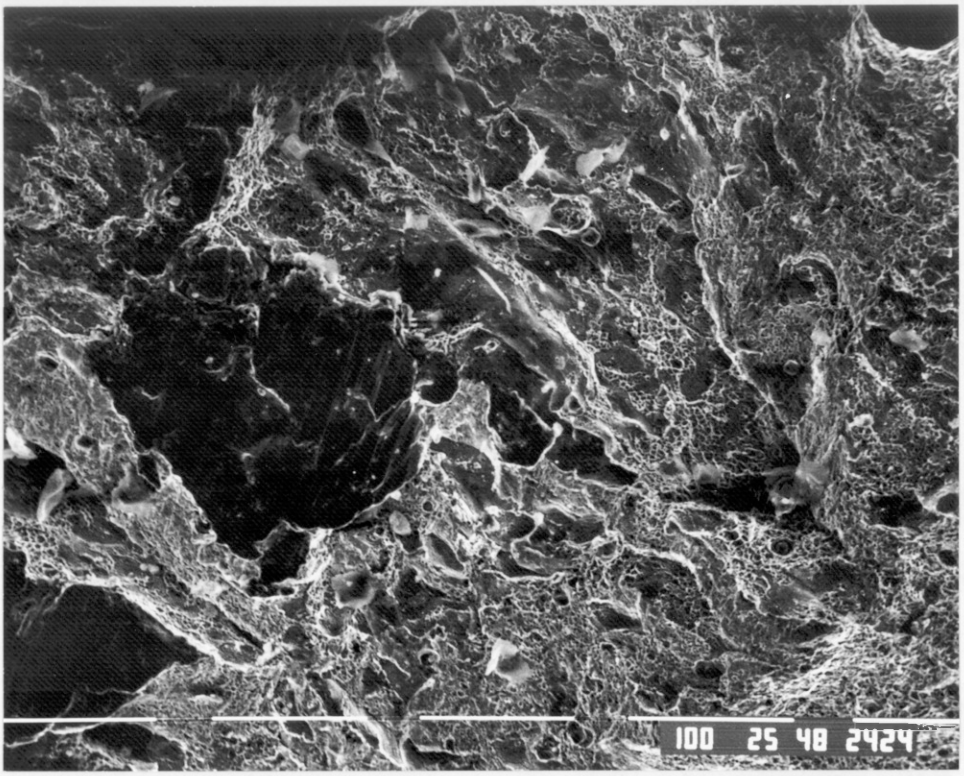


Figure 4.34 Weldment fracture surfaces showing a number of defects

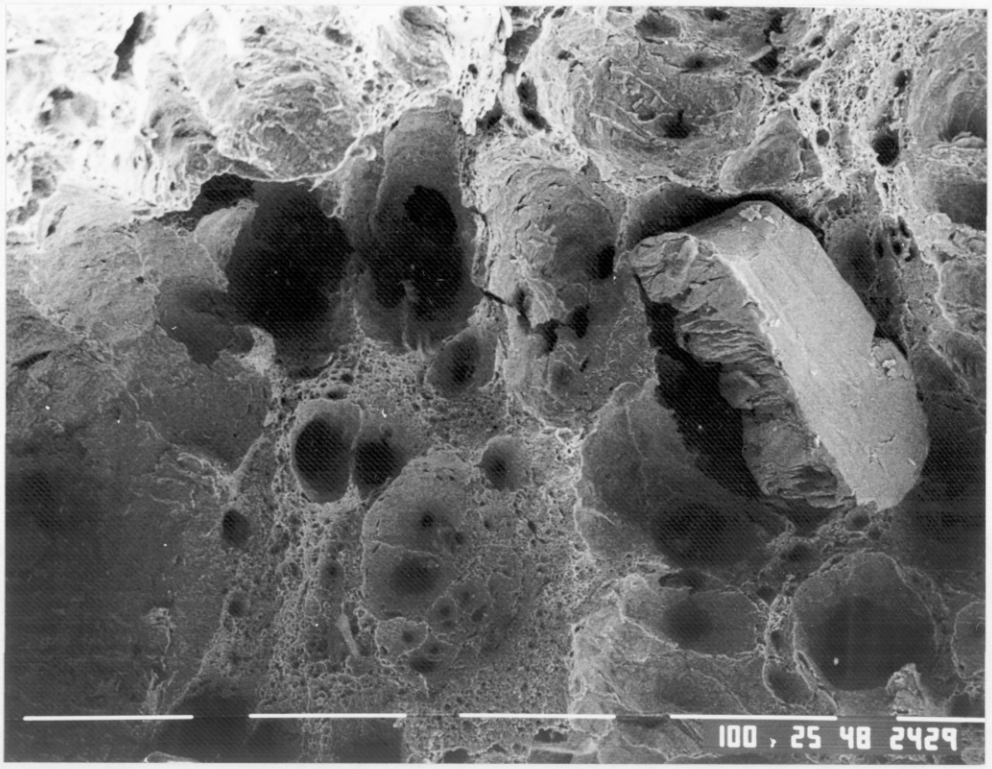


Figure 4.35 Fatigue fracture in welded specimen across a region of porosity

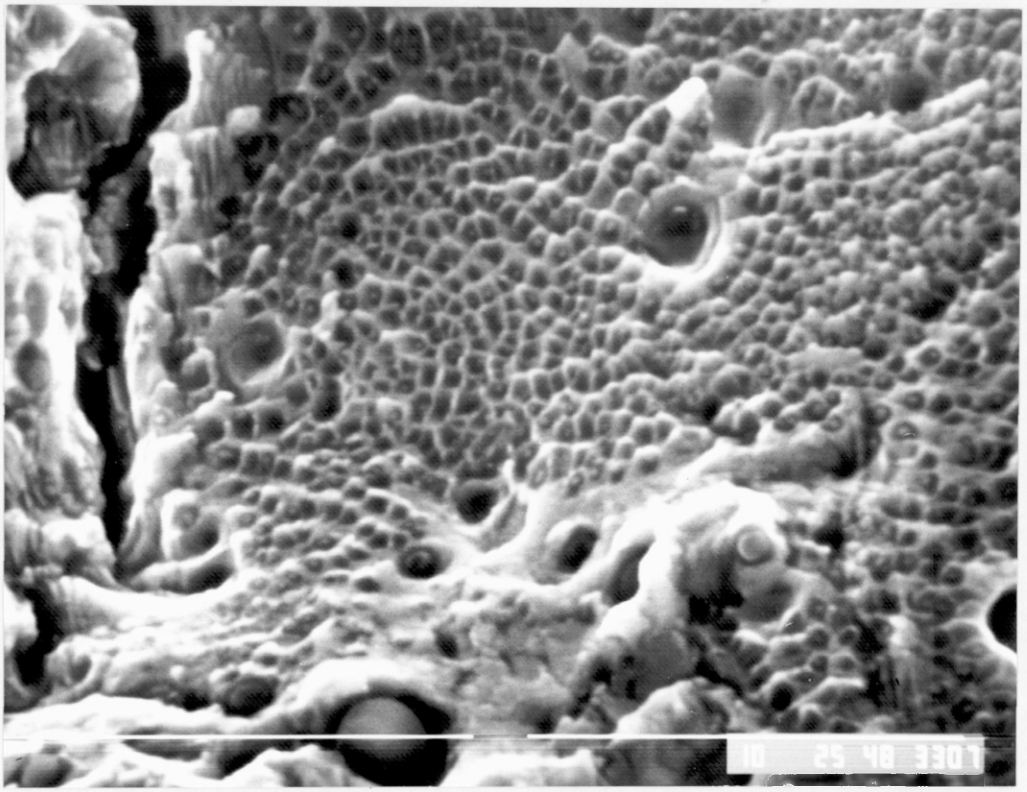


Figure 4.36 SEM photograph showing area of microvoid coalescence in the Paris regime

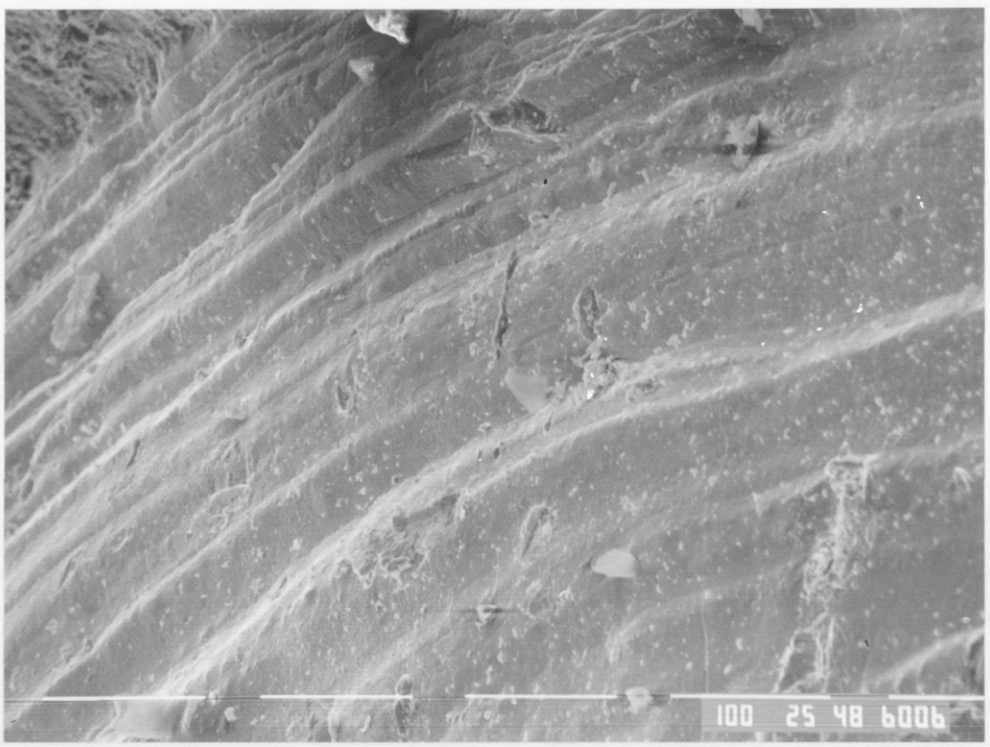


Figure 4.37 A typical striated area in the Paris regime $\Delta K=20$ MN/m$^{3/2}$, R = 0.7, f = 30Hz

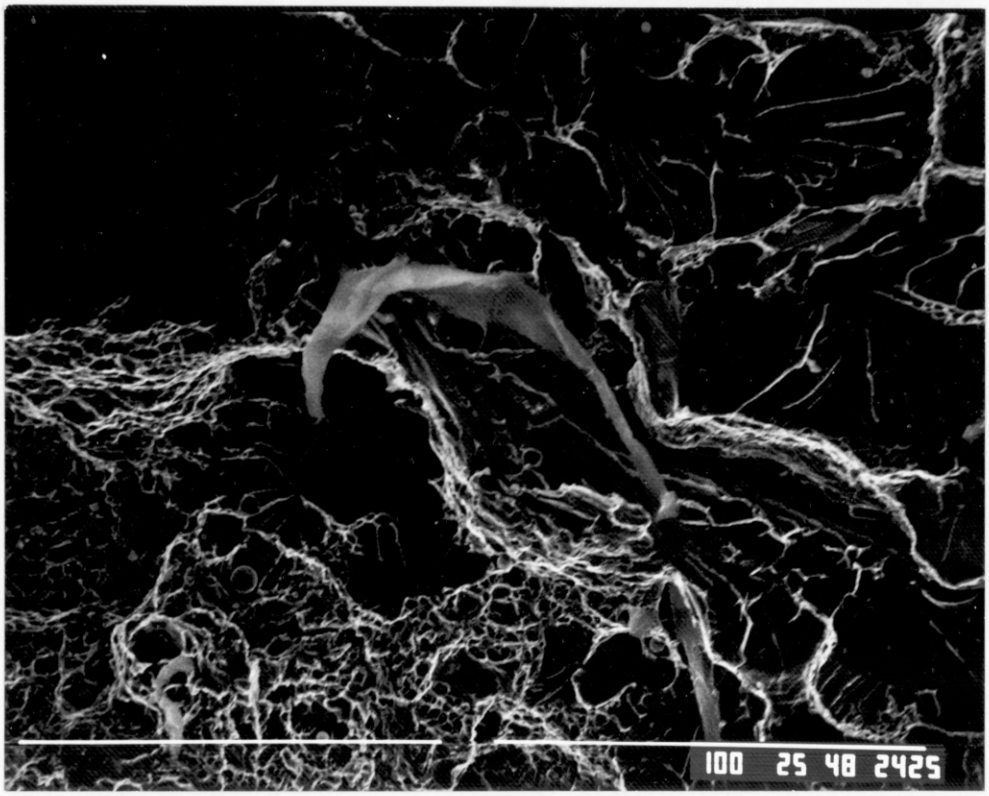


Figure 4.38 SEM photograph in the threshold region illustrating transgranular cleavage-like fracture

CHAPTER 5

SURFACE CRACK GROWTH OF BS4360-50D WELDED STEEL

5.1 INTRODUCTION

It has been increasingly widely recognized that defects in welded structures introduced during fabrication or developed in service may become potential sources of catastrophic failure. During the last decade much analytical and experimental research has been accomplished on the fatigue growth and fracture of surface flaws and the development of accurate stress intensity calibrations for semi-elliptical cracks in structures. This effort was undertaken because the surface flaw has been the most prevalent type of flaw in many classes of structure, particularly in welded structures. Weld defects are the common origin of surface flaws in welded joints. Other origins of surface flaws are inclusions, arc strikes, corrosion pits, weld-border cracks, tool marks, etc.

A surface flaw may be completely embedded in a structure or it may have grown to one surface or have originated at a surface. Surface crack propagation is an important problem which involves the development of flaws just after their initiation. In many cases it can be shown that a major part of the propagation time elapses while the crack is a part-through crack. Analysis of fatigue crack growth from a surface flaw of any configuration is usually performed by considering the flaw to be a semi-elliptical

crack for the sake of simplicity. The fatigue crack growth properties are generally measured with specimens containing through-thickness cracks, due to the fact that with them it is easier to make crack length measurements and to characterize the stress intensity factor, as well as to the relatively low cost. It is important to confirm that the same laws can be applied in the case of crack growth in specimens containing surface cracks.

To investigate the characteristics of crack growth, surface crack propagation should be studied, and variations in the shape of the crack and type of loading must be carefully considered. Unfortunately, the fatigue data of surface cracks is difficult either to analyse or to obtain. The problem lies, analytically, in the crack tip stress intensity factor solution as described in Section 3.6.2 and, experimentally, in the fact that crack propagation inside the specimen cannot be measured directly since such propagation is not visible to the naked eye.

Initial measurement of the growth rate of surface cracks was made by surface observation using an optical technique. Evaluation of crack depth, and therefore the crack shape, was done by a heat tinting procedure [172], or by an overload technique [173] which marks successive fronts. It has been established that the load level can influence the crack shape and subsequent rate of fatigue crack growth [174]. The development of potential drop

calibration [117] facilitates the continuous monitoring of the crack depth without interruption of the desired fatigue loading. The present work employs the potential drop technique to monitor the growth of cracks in the through-thickness direction and to verify the validity of the stress intensity solution recommended [138] for surface cracks in a bending stress field. The emphasis of the analysis has been on establishing a correlation between these growth rates and those obtained from compact-type specimens.

5.2 EXPERIMENTAL PROCEDURES

Four-point bend tests were carried out using Dowty electrohydraulic and Mayes servohydraulic fatigue machines on parent metal, weldment, and heat affected zone (HAZ). These tests used SNP geometry, details of which are given in Chapter 3. All the tests were performed in laboratory air at 20 $^{\circ}$ C under ambient conditions. In the case of welded-joint specimens and parent metal, some tests were performed in a 3.5% sodium chloride solution.

The method used to obtain low crack growth rates and thresholds has been described in Chapter 4. It is, however, worth pointing out here that, for the notch geometry used in this investigation, the deepest point of the crack front was in a higher stress state than that at the surface since the state of deformation for semi-elliptical surface cracks varies from plane strain at the deepest point of the crack front to conditions approaching plane stress where the crack

front intercepts the free surface. It was assumed that a higher stress state at the deepest point together with plane strain conditions would produce a plastic zone size comparable to the one on the surface where the conditions are those of a lower stress state and plane stress, which implies more extensive yield regions. Thus, the calculation of the plastic zone size was based on the K_{max} experienced at the surface point.

The effect of stress ratio on surface cracks was investigated, and tests were performed at R-values equal to 0.08 and 0.7 at a cyclic frequency of 30Hz. To investigate the effect of frequency, some other tests were carried out at 0.25Hz and stress ratios of 0.08 and 0.7 for parent metal, weldment, and heat affected zone.

To evaluate the effect of residual stresses on fatigue crack growth, tests were performed on stress-relieved specimens at a stress ratio of 0.7 and cyclic frequency of 30Hz. The effect of residual bending stresses was investigated, the tests being performed on welded joint specimens with the notch located on both the compressive and the tensile sides as discussed in Section 3.1.

Corrosion fatigue tests were performed on the parent metal, and on both as-received and stress-relieved weldments at R-values of 0.08 and 0.7 and a loading frequency of 30Hz

in a 3.5% salt-water solution. The fluid was introduced into the specimen notch at a flow rate of approximately 1.5 ml/min.

The details of specimen preparation and the rig used are discussed in Chapter 3. All the specimens were pre-cracked at a cyclic frequency of 30Hz using a low load range giving K_{max} not exceeding 20 $MN/m^{3/2}$ for the base metal, and about 15 $MN/m^{3/2}$ for the weldment and heat affected zone. The propagated fatigue crack was allowed to grow for some 2 to 3mm at the required loading conditions (i.e., stress ratio, frequency, etc.) before the actual test readings were taken. This process ensured the elimination both of the influence of short cracks at the original notch and of that of load history on fatigue crack growth rate. All the tests were performed at fixed load limits, i.e., constant load amplitude, thereby allowing the crack to grow from its original length to the final length as required.

The crack along the surface was measured using a microscope mounted on a travelling micrometric stage, and depth measurements (i.e., crack length in through-thickness direction) were made using an A.C. potential drop microgauge as discussed in Chapter 3. The experimental data were recorded in terms of crack length, 2c, crack depth, a, and corresponding number of cycles, N.

A finite difference (secant) method was used to calculate the crack growth rates, da/dN, dc/dN, from the raw experimental data, which was possible because they showed little scatter.

The stress intensity factors, K_c and K_a, were calculated using the solution proposed by Koterazawa and Minamisaka [138] in conjunction with the correction factor proposed by Holdbrook and Dover [140]. The half-crack length, c, and crack depth, a, as used to calculate K_c and K_a, were derived from the average of two successive readings as required to calculate the corresponding crack growth rate.

5.3 RESULTS

The experimental results are plotted in terms of crack growth rates, da/dN and dc/dN, versus the corresponding ΔK values for all the tests.

5.3.1 Base Metal

Figs. 5.1 and 5.2 show typical a or c versus N curves for the tests conducted in air at stress ratios, R, of 0.08 and 0.7, respectively, and loading frequency of 30Hz.

The threshold and mid-range surface crack growth results in air are presented in Fig. 5.3. This shows the results obtained for an SNP specimen tested at stress

ratios, R, of 0.08 and 0.7 and loading frequency of 30Hz. The results reveal the critical effect of stress ratio on low crack growth rates and thresholds. However, at higher growth rates there appears to be only a slight stress ratio effect (i.e., the effect of stress ratio decreases with increasing growth rates). From these results it is also apparent that lowering the crack growth rate at the free surface results in lower growth rates at the deepest point.

Fig. 5.4 shows the results obtained at a cyclic frequency of 0.25Hz for R-values equal to 0.08 and 0.7. The effect of stress ratio is slightly more pronounced at this frequency at high growth rates than those of 30Hz. The effect of frequency is illustrated in Fig. 5.5, which shows that the growth rates increase with decrease in frequency. From these results it is evident that the effect of stress ratio increases inversely with loading frequency.

Figs. 5.6 and 5.7 show the present results at 0.25Hz in air compared with the mean line through the Thorpe et al [175] results obtained from tests performed on a 38mm thick SNP geometry specimen of the same material. These authors used a three-point bend rig and a cyclic frequency of 0.1Hz at stress ratios, R, of 0.1 and 0.7. Their results compare very well with the present results at 0.25Hz and an R-value of 0.08, but not with those for 0.25Hz and stress ratio of 0.7 in which the differences between the results are manifest.

The present results are also compared with the results obtained for CT geometry and are shown in Figs. 5.8 and 5.9 for loading frequencies of 30Hz and 0.25Hz and stress ratios of 0.08 and 0.7, respectively. The results generally compare very well, especially the low frequency tests, indicating that the K-calibration used yields accurate data. However, the tests at 30Hz, the low crack growth rate regime and thresholds (i.e., the SNP results), indicate higher ΔK_{th} values. These ΔK_{th} values were found to be 4.1 $MN/m^{3/2}$ and 8.2 $MN/m^{3/2}$ at stress ratios of 0.08 and 0.7, respectively, and are average values of ΔK_{th} at the surface and deepest point of the crack.

Fig. 5.10 shows the results of tests conducted in a 3.5% salt-water solution at 30Hz and R-values of 0.08 and 0.7. It indicates that, unlike the results obtained in air, stress ratio has no significant effect on crack growth rates in a salt-water environment at a loading frequency of 30Hz for the load range investigated. These results are compared with those obtained in air, Fig. 5.11. This clearly shows that crack growth rates are higher in salt-water than in air at both low and high stress ratios for ΔK values above 18 $MN/m^{3/2}$ at R=0.08, and 15 $MN/m^{3/2}$ at R=0.7. However, extrapolating the data obtained in the salt-water environment below 1 x 10^{-5} mm/cycle indicates that the crack growth rate is the same and/or lower in a salt-water environment compared to air. For example, at R=0.7, it

appears that the crack growth rate is approximately three times slower in a salt-water solution than in air (- see Fig. 5.11).

Fig. 5.12 shows the present results for a salt-water environment compared with the mean line through Musuva's [144] results. He performed tests with the same material in a salt-water environment using a 25.4mm-thick CT specimen under identical loading conditions. His results for low stress ratio compare very well with the present results. However, at high stress ratios the present results indicate a higher growth rate (about four times at ΔK=20 MN/m$^{3/2}$).

5.3.2 Weldment

The threshold results for welded joint specimens tested in air at stress ratios of 0.08 and 0.7 and a loading frequency of 30Hz are shown in Fig. 5.13. As with the base plate, this also illustrates the effect of stress ratio on low crack growth rates and thresholds, which appears to diminish at higher crack growth rates.

$K_{max,th}$ values of 6.52 MN/m$^{3/2}$ and 14.33 MN/m$^{3/2}$ corresponding to R-values of 0.08 and 0.7, respectively, were found (-see Fig. 5.13). These $K_{max,th}$ values are the averages of $K_{max,th}$ obtained for the surface and deepest point of the crack.

The results obtained at a cyclic frequency of 0.25Hz in air at stress ratios, R, of 0.08 and 0.7 are shown in Fig. 5.14. The effect of frequency is illustrated in Fig. 5.15 by drawing the mean line through the results of Figs. 5.13 and 5.14. The results show the general trend observed, that is, a decrease in frequency results in an increase in growth rate at ΔK-values above 5 $MN/m^{3/2}$. Below this value the frequency does not seem to have any effect on growth rate.

To evaluate the effect of bending residual stresses, tests were performed on welded joint specimens with the notch orientated on the "compressive" side at R=0.08 and cyclic frequency of 30Hz. This is shown, together with results obtained from the specimens with the notch on the "tensile" side, in Fig. 5.16. As can be seen the crack growth rates in the specimen with the notch orientated on the tensile side are higher than those in the specimen with the notch orientated on the compressive side. This makes clear that the notch orientation has a significant effect on fatigue crack propagation in welded joints, and can result in considerably different fatigue data when compared with those of the parent plate. This can be seen in Fig. 5.17, where there is no difference in fatigue crack propagation of the base plate and of the welded joint specimen with the notch located on the "compressive" side, suggesting that the compressive bending stresses reduced the effective stress intensity factor at the crack tip.

The comparison of growth rates in weld and base metal given in Figs. 5.18 and 5.19 shows that, generally, cracks grew more slowly in the parent material than in the weld metal. The faster growth of cracks in the weld metal suggests the presence of tensile residual stresses. The difference in growth rates between the weld metal and parent plate seems to increase inversely with frequency.

The present results are also compared with the results obtained for CT specimens (see Chapter 4), as shown in Figs. 4.20 and 4.21 for loading frequencies of 30Hz and 0.25Hz, respectively. These results do not agree with each other, unlike the results for the base plate obtained for different geometries. Nevertheless they indicate the important role of residual stresses in fatigue crack propagation of butt-welded joints.

Hardness measurements across the welded specimens in "as-received" condition revealed the existence of a very hard HAZ, with V.H.N.s of 232 at the centre of the weld and approximately 360 in the HAZ. Hardness measurements were also taken across the "stress-relieved" welded specimens. These results are shown in Fig. 5.22, and indicate that stress-relieving did cause slight softening of the parent material.

The results of tests on "stress-relieved" welds at R=0.7 and 30Hz are compared to the corresponding results obtained for "as-received" welds and are presented in Fig. 5.23. The beneficial influence of stress-relieving, when $\Delta K < 10$ MN/m $^{3/2}$ must be attributed to the lowering of the tensile residual stresses.

The effect of a salt-water environment on crack growth rates at stress ratios of 0.08 and 0.7 and a cyclic frequency of 30Hz is illustrated in Fig. 5.24. A comparison with the corresponding in-air data is presented in Fig. 5.25, which indicates a salt-water enhancement of growth rates at ΔK values above 10 MN/m$^{3/2}$. These data are also compared with the results obtained from CT geometry in a salt-water environment and are shown in Fig. 5.26.

The effect of salt-water on "stress-relieved" welds was also investigated and is presented in Fig. 5.27, together with the corresponding in-air data and, in Fig. 5.28, is compared with the results for "as-received" welds in salt-water solution. As can be seen from the summary graph in Fig. 5.29, the salt-water enhancement only occurs after a certain ΔK value is reached, but the effect of stress-relieving increases this value of ΔK to 16 MN/m$^{3/2}$, while for the case of welded joint specimens in "as-received" condition, it is found to be 10 MN/m$^{3/2}$, probably due to the nature of the residual stresses acting at the crack tip.

5.3.3 Heat-Affected Zone

Fatigue crack growth results for HAZ in air are presented in Figs. 5.30 and 5.31 for stress ratios of 0.08 and 0.7 and loading frequencies of 30Hz and 0.25Hz, respectively. These results indicate a considerable effect of stress ratio on crack growth at low crack growth rates and thresholds at 30Hz. This effect becomes less marked with increase in crack growth rate. However, the effect of stress ratio appears to increase with a decrease in frequency. For R values of 0.08 and 0.7 at 30Hz, $K_{max,th}$ values of 6.52 $MN/m^{3/2}$ and 14.3 $MN/m^{3/2}$, respectively, were obtained.

The effect of frequency is illustrated in Fig.5.32, which confirms the general trend observed, that is, decreasing frequency resulting in higher crack growth rates.

These results are compared with the corresponding results obtained for the base metal and the weldment and are shown in Figs. 5.33 and 5.34 for a loading frequency of 30Hz, and in Figs. 5.35 and 5.36 for 0.25Hz, at two stress ratios, 0.08 and 0.7, respectively. These results indicate that the growth rates are generally higher in HAZ than the base metal after a certain ΔK is reached, below which the growth rates appear to be the same. These ΔK values are 10 $MN/m^{3/2}$ and 6 $MN/m^{3/2}$ at 0.25Hz and 30Hz corresponding to R-values of 0.08 and 0.7, respectively.

A comparison of results for HAZ with those for the weldment indicates that the crack growth rates in HAZ are in general similar to those for the weldment at a cyclic frequency of 30Hz. At low cyclic frequency (0.25Hz) and low stress ratio, the curves for both HAZ and weldment tend to run parallel, with the crack growth rates in HAZ being the lower. However, at a stress ratio of 0.7 the growth rates in HAZ and weldment are the same for ΔK values less than 5 $MN/m^{3/2}$.

5.4 DISCUSSION

The primary task of the present investigation has been to obtain accurate values of surface fatigue crack propagation data for weldment in conjunction with suitable computer simulation of such cracks. The descriptions of such simulation and of the characterization of the shape of a growing crack are given in Chapter 6, and the present chapter is accordingly limited to a discussion of the results presented.

5.4.1 Base Metal

The results for crack growth in air are plotted for both surface and in-depth crack growth in Figs. 5.3 and 5.4. The crack growth rates show good agreement with the results of the CT tests, although there appears to be a slight over-estimate of the threshold stress intensity factor range ΔK_{th}(see Figs. 5.8 and 5.9). This would seem to indicate a

slight load history effect. The plastic deformation associated with a crack tip exposed to mode I loading is generally more extensive in plane stress than when a state of plane strain prevails. In plane stress the absence of lateral constraint creates more extensive yield regions [176]. In the case of a semi-elliptical surface crack, the state of deformation varies from plane strain at the deepest point of the crack front to conditions approaching plane stress where the crack front intercepts the free surface. This is so because, since the state of deformation varies along the crack front, so does the degree of plastic deformation. A number of models have been proposed for determination of the plastic zone size. A brief discussion of these models is given bellow.

Rice [177] estimated the plastic zone size under plane stress conditions and perfect plasticity for a semi-infinite crack in a large plate. The maximum dimension of the plastic zone involved, r_p , was found to be

$$r_p = \frac{\pi}{8} \left[\frac{K}{\sigma_y}\right]^2 \qquad ,(5.1)$$

where K is the stress intensity factor and σ_y the uniaxial yield strength. Under conditions of plain strain, the problem has been treated by Keer and Mura [178], who studied a circular crack of radius a subjected to a remote uniform tensile stress field. They found the plastic zone size to be given by

$$r_p = a\left\{\left[1-\left(\frac{\sigma}{\sigma_y}\right)^2\right]^{-\frac{1}{2}} -1\right\} \qquad .(5.2)$$

A number of other models have been proposed for estimating the plastic zone size under small scale yielding and plane strain conditions, among them that of Irwin [179]:

$$r_p = 0.053\ \left(\frac{K}{\sigma_y}\right)^2 \qquad ,(5.3)$$

and that of Liu [180]:

$$r_p = 0.13\ \left(\frac{K}{\sigma_y}\right)^2 \qquad .(5.4)$$

These models are based on a two-dimensional representation of the crack geometry and hence their applicability to the surface crack configuration, where free surface effects are predominant, is dubious.

Ayres [181] treated the problem using a finite-difference technique for determination of the three-dimensional stress and deformation field in the neigbourhood of a semi-elliptical surface crack in a thick plate. The material was assumed to be elastic and perfectly plastic. He showed that the plastic zone at the deepest point of a surface crack having an aspect ratio of 0.5 at a high applied stress of $0.88\,\sigma_y$ penetrates to the back surface. However, the critical crack depth when the plastic zone reaches the back surface can be approximated for semi-elliptical surface crack in bending stress field as follows.

Stress intensity factor at the deepest point of a surface crack is given by Koterazawa and Minamisaka [134] as

$$K = M_1 M_2 \frac{\sigma\sqrt{\pi a}}{E(k)} \quad ,(5.5)$$

where M_1 and M_2 are correction factors, a is crack depth and σ is the bending stress.

The elastic stress field ahead of the crack tip is given by:

$$\sigma = K / \sqrt{2\pi r} \quad ,(5.6)$$

where r is the distance from the crack tip. The plastic zone size can be written as

$$\rho = 2r_p \quad ,(5.7)$$

where r_p is the radius of the plastic zone and which can be calculated by substituting $\sigma = \sigma_y$ (yield stress) into Equation (5.6).

When the plastic zone reaches the back surface, the critical depth a_p is given by

$$a_p = B - \rho \quad .(5.8)$$

Substituting Equation (5.7) into (5.6), we obtain

$$\sigma_y = \frac{K}{\sqrt{\pi\rho}} \qquad ,(5.9)$$

$$K = \sigma_y \sqrt{\pi\ (B-a_p)} \qquad .(5.10)$$

From (5.5)

$$M_1\ M_2\ \frac{\sigma\sqrt{\pi a_p}}{E(K)} = \sigma_y \sqrt{\pi(B-a_p)} \qquad (5.11)$$

$$\therefore \quad \frac{M_1 M_2}{E(K)}\ \frac{\sigma}{\sigma_y} = \sqrt{\frac{\pi(B-a_p)}{\pi a_p}} \qquad (5.12)$$

$$\therefore \quad M_1 M_2\ \frac{\sigma}{\sigma_y E(K)} = \sqrt{\frac{B}{\sigma_Y} - 1} \qquad (5.13)$$

$$\text{or} \quad \left(\frac{B}{a_p} - 1\right)^{\frac{1}{2}} = M_1 M_2 \left(\frac{\sigma}{\sigma_y E(K)}\right) \qquad .(5.14)$$

Therefore, the required value of a_p can be numerically obtained from Equation (5.14).

Thus, from the foregoing brief discussion of the problem of plastic zone size, it can be seen that most of

the formulae estimate the size of plastic zone only in two dimensions. In the present investigation the threshold crack growth rate measurements were based on the crack at the surface of the specimen where plane stress dominates. The plastic zone size was calculated using Rice's formula (Equation (5.1)), which appears to underestimate the size of the plastic zone and hence resulted in high ΔK_{th} values.

These results also indicate a slight overestimation of the stress intensity factor at the deepest point of the crack. To reach the threshold stress intensity factor range, ΔK_{th}, the stepping-down load technique was used. It was expected that taking the crack at the surface to low growth rates and thresholds would have led to ΔK_{th} at the deepest point. However, as the crack increases in depth, the stresses at the crack depth become smaller because of the stress gradient due to the bending stress field, and the rate of growth becomes less; nevertheless, the crack length is not exposed to a change in stress as the applied stress at the surface is constant. Therefore, it is expected that the change in crack depth with respect to crack length will become smaller as the crack becomes larger, which would result in very low growth rates and a much higher threshold stress intensity factor. A simplified model of bending stress distribution would predict that the crack depth would asymptotically approach the mid-thickness where the stress is zero but compressive beyond the mid-thickness.

The crack growth data for semi-elliptical cracks appear to show a higher stress ratio dependence than those of the previous CT specimen. This can be discussed in terms of the crack closure concept. Although the detailed mechanism of the interactions between the growth of the crack and plastic flow is beyond the scope of present work a brief discussion follows.

Due to the ductility of the material used, cyclic loading produces a plastic zone at the crack tip. Rice [19] has subdivided this plastic zone into two parts: a forward plastic zone and a reverse plastic zone, with the tensile deformation in the forward plastic zone being compressed in the reverse plastic zone, and the reverse plastic zone containing most of the deformation generated during a load cycle. It is thought that the reverse plastic zone is mainly responsible for the residual tensile displacement at the crack's free surfaces, and for the compressive stresses which ultimately lead to crack closure at lower applied stresses. Increasing the R-value at constant σ_{max} leads to a reduction of crack growth rate and also decreases the size of the reverse plastic zone, since ΔK gets smaller. Thus the residual tensile displacement also decreases gradually with increasing crack depth (ΔK decreases gradually also with increasing crack depth due to the stress gradient in the bending stress field) until new appropriate zone sizes are obtained. Therefore, it is expected that blunting behind the crack tip increases at any constant R with increasing number of fatigue cycles and consequently

leads to more crack closure.

A change in growth rates depending on the test frequency was observed for both stress ratios between the two sets of results (see Fig.5.5), the crack growth rate at 0.25Hz being approximately two-and-half times faster than at 30Hz, for ΔK=15 MN/m$^{3/2}$ and stress ratio of 0.08, and three times at ΔK=8 MN/m$^{3/2}$ at R=0.7.

This reduction in crack growth rate as a result of increase in loading frequency was the same for all specimen types. However, this frequency dependence was more pronounced for surface cracks (see Fig. 5.5). Hydrogen embrittlement is often used to explain this effect. In this an extra active mechanism is necessary to rationalize the retention of the frequency dependence of growth rate to higher ΔK, despite the observed similarity of the growth rates obtained for different geometries. Such a mechanism, which produces uniformly accelerated growth with a decrease in frequency, has been ascribed at high temperature to an environmental interaction for which an activation energy can be measured [182]. It is therefore suggested that these observations can be rationalized in terms of further parameters which determine the crack growth rate in the intermediate and high regimes. Firstly, at high stress intensities, where crack extension is very rapid due to purely mechanical effort, static parameters such as yield strength and fracture toughness would be expected to

uniquely define a particular growth rate. Secondly, at low stress intensities, a further mechanism needs to be active to hinder the both inherently faster and environmentally enhanced crack growth rate that has been proposed for the intermediate range.

In this context it has been proposed by Walker and Beevers [183] that growth rates can be significantly modified by a "non-closure" mechanism arising from the combination of out-of-plane crack growth and a relative displacement between the fracture faces. Clearly, the degree of "non-closure" would be accentuated at low ΔK values where the crack-opening displacements are small. This model has been extended by Suresh et al [184] to include fretting-enhanced oxidation of the newly produced crack faces, leading to an accumulation of very fine debris and therefore increased contact at the minimum applied load, in particular adjacent to the crack tip. This would imply that the inherently faster, less out-of-plane, growth at 0.25Hz could be counter-balanced by increased non-closure resulting from oxidation products.

For growth rates below 1×10^{-6} mm/cycle, divergence of growth rates can be seen between the two crack configurations (i.e., CT and SNP). The occurrence of these reduced growth rates at low stress intensities, and therefore at necessarily short crack lengths and low stresses, suggests the possibility of an error in either the

stress intensity calibration or the correction factors used. However, threshold tests which were based on the surface position of the crack tip by varying the applied load range, resulted in very low growth rates. This low rate correlated well with the value to be expected from the subsurface position, ΔK_{th}, but the stress intensity calibration at this position decreases with respect to the surface value for long crack lengths. Hence, it might have been expected that taking the crack at the surface to low stress intensities and thresholds would have led to a decrease in growth rates at the deepest point. Therefore, the observed behaviour may be interpreted as representing an effective acceleration in growth rate followed by a deceleration of subsurface crack growth with increasing crack length at the surface position. This indicates that there is no systematic error in the stress intensity calibration, rather, the actual growth rate changes due to the stress gradient. It is likely that these changes could arise either from some feature of the crack front curvature or from the rates of plane stress to plane strain growth, which are greater for the surface notched geometry. It could also possibly be due to the fact that the mechanical properties in the transverse and through-thickness directions are different (see Table 3.1).

Hence, it is proposed that, even if the shape of the crack has an effect on crack growth rate, the greatest proportion of the high ΔK retardation at the deepest point of the crack as observed arises from the effect of the stress state on fatigue crack propagation. Moreover, should

the plane stress growth be brought about by a significantly different mechanism than that due to the bulk of the test-piece, then the degree of retardation produced could well be further increased.

Despite using standard A.C. potential drop microgauge monitoring probes, it was estimated that linearity and hence predictability in crack depth calibration was only achieved with crack depths in excess of 0.5mm. Nevertheless, the ability to measure crack depth without recourse to predictions based on such microgauge readings was considered highly desirable, particularly for threshold tests (i.e., very low growth rates).

The results of the present investigation are compared with those of investigations carried out by Thorpe et al [175] on the same material and specimen geometry under three-point bend tests. It is found that the results of both tests are comparable under similar test conditions (i.e., environment - see Figs. 5.6 and 5.7). However, Thorpe et al carried out tests on 38mm-thick plates and growth rates higher than $1x10^{-5}$ mm/cycle at R=0.1, and $1x10^{-6}$ mm/cycle at R=0.7 i.e., only over one order of magnitude. There is a considerable difference between the present results at R=0.7 for the deepest point of the crack front and the results of Thorpe et al, the present results giving much higher growth rates than those of the other authors; for example, at a ΔK of 10 $MN/m^{3/2}$ the growth rates of the deepest point of

the crack front in the present results are one order of magnitude higher than those obtained in the latter investigation. Although the authors used the same K calibration as in the present case, it appears that their measurements of crack depths were in serious error. However, as is shown in the next chapter, computer simulation of a surface crack predicts a much higher growth rate for a 38mm-thick section than for a 24mm, the present case. Ideally the crack growth rate data for a 38mm-thick section should be consistently higher than the present data.

The results of corrosion fatigue are shown in Fig. 5.12. They indicate that the BS4360-50D steel studied is slightly sensitive to a change in stress ratio in a salt-water environment and that the relationship describing the intermediate range of growth (i.e., Paris equation) has an exponent of 2.7, a value arrived at by other workers [143].

The results obtained at a frequency of 30Hz in salt-water solution showed increased growth rates for ΔK values above 15 $MN/m^{3/2}$ compared to in-air results. However, on the basis of extrapolating the growth curves there appears to be a lower growth rate for lower ΔK values (<15 $MN/m^{3/2}$). This indicates that the effect of the environment is more important in the intermediate stages than in the early stages of crack propagation. This viewpoint has been shared by many investigators [e.g., 185, 186], who are of the opinion that the predominant effect of environmental attack

is experienced when crack length, and hence growth rates, are comparatively large.

The role of the environment in producing enhanced crack growth rates has been viewed as essentially the same mechanism in both true corrosion fatigue and stress corrosion fatigue, but with differing effects in the latter [52]. In aqueous environments and in hydrogen-bearing environments, the mechanism of environmental enhancement of crack growth rates is seen as the result of hydrogen embrittlement. Briefly, a reaction takes place between the surrounding medium and the freshly exposed metal surface at the crack tip, leading to the absorption of atomic hydrogen. These hydrogen atoms diffuse into the metal to recombine at a suitable site within the plastic zone and hence cause embrittlement localised in the crack tip region. The production of hydrogen gas in specimens in which the metal surfaces were not completely dried has been reported previously [187], and indicates that a hydrogen embrittlement mechanism must be considered a valid proposition.

Holder [188] attributed the reduction in fatigue crack propagation rate in the presence of a corrosive environment to adsorption of salt-water molecules on the ultra-clean surface of the newly formed slip-steps. This adsorption model for corrosion fatigue requires a surface-active species of solution which becomes attached to a metal-metal

bond and reduces the total energy balance in the system [189], and is therefore thermodynamically favourable. This may be the source of the energy required to transport salt-water molecules adsorbed on the notch surface towards the active crack front.

Musuva [143], who conducted tests on BS4360-50D steel under identical mechanical and environmental conditions using CT geometry, did not observe any effects of stress ratio. His results compare well with the present results at ΔK values below 20 $MN/m^{3/2}$. However, the present results, for example at R=0.7, predict a crack growth rate three times faster than that which he predicted. This acceleration of the crack growth can be attributed to the types of specimen used under different loading conditions (i.e., tension and bending). Surface cracks in bending appear to be more sensitive to corrosion-product wedging and thus allow a more meaningful assessment of corrosion fatigue. However, once accelerated surface crack growth has been initiated, crack extension seems to be more rapid than for the through-thickness cracks, as the corrosion products can build up a higher stress intensity and consequently a higher effective stress intensity factor in the surface-notched specimens in bending, and hence give rise to a higher growth rate.

5.4.2 Weldment

The relationship of crack growth rate to ΔK for a surface notched weld specimen is shown in Figs. 5.13 and

5.14 for loading frequencies 30Hz and 0.25Hz. It may be clearly seen that, unlike the case for CT geometry, the fatigue crack propagation rate did not vary substantially despite the change in the stress ratio from 0.08 to 0.7 at 30Hz. These results suggest that the tensile residual stresses in welded joint specimens are large enough to pull the crack fully open but to induce no effects of tensile mean stress on the fatigue crack propagation properties.

This is in agreement with an investigation carried out by Maddox et al [33] on the effect of stress ratio on structural steel. They studied the crack-closure phenomenon by observing the behaviour of strain gauges fixed alongside the crack path. They found that it was not quite true to suppose that crack closure occurred at zero stress. For steels studied they observed that closure always occurred towards the bottom of the tensile part of the cycle, but while the applied stress was still tensile. By studying the closure stress they were able to propose an effective stress intensity factor range, ΔK_{eff} , which was that part of the ΔK range over which the crack tip remained open. Harrison [190] related this behaviour to the effect of residual stresses, and suggested that, if the residual stress is at yield in tension, there will be little effect of an externally applied R-ratio since the local stress ratio will be positive. However, if the local stress range is large (i.e., greater than yield), the local stress ratio could be negative. Therefore, for a welded specimen, if the applied stress range is small, the effective R-ratio is positive,

but, if the stress range increases, the effective R will decrease until, when the stress range is equal to yield, the effective R will be zero.

Observation of the effect of frequency in the present study (see Fig. 5.15) confirmed the general trends discussed above. Increasing frequency from 0.25Hz to 30Hz caused a reduction in crack growth rates.

As mentioned in Chapter 3, butt-welding of plates usually causes some angular distortion. The reasons for this angular distortion are these: the first run of weld cools, contracts, and draws the plates together; the second run has the same shrinkage effect, since the contraction forces are resisted by the solidified first run which acts as a fulcrum for angular distortion; however, subsequent runs increase this effect and are only slightly influenced by the counteraction of the capping welding.

Although the use of a double-Vee preparation is recommended [191] in order to balance the shrinkage stresses about the neutral axis of the section, with consequent elimination of angular distortion, some angular distortion will still be present. Such a joint preparation was used in this study, but it was found that most of the plates were still slightly distorted. Angular distortion suggests the existence of residual bending stresses. Grinding to make the

sides of the plate parallel would release some of these residual bending stresses. In fatigue tests under bending loads, the remaining residual bending stresses appear to have a considerable effect on crack growth rates, depending on the side measured (see Fig. 3.6) where the residual bending stress is either in the direction of the applied bending stress or in the opposite direction, referred to here as the "tensile" side and the "compressive" side, respectively.

In order to investigate the effect of these residual bending stresses on fatigue crack propagation, tests were performed on specimens with the notch located on either the "compressive" side or the "tensile" side. The results show the importance of these residual bending stresses and their effect on the fatigue crack growth (see Fig. 5.16). From these results it appears that when the notch is positioned on the "compressive" side the resultant bending stress is less than the applied stress, as the applied and residual bending stresses are in opposite directions. In contrast, the notch on the "tensile" side increases the resultant bending stress at the crack tip since both the applied and the residual bending stresses are in the same direction. An interesting feature of fracture surfaces of welded specimens with the notch located on the compressive side was the observation of a "turn-back zone" which is shown in Fig. 5.37. Curse et al [172] who studied the development of the shape of the semi-elliptical surface cracks by the heat-tinting method also observed the turn-back zone. They

attributed this effect to the residual compressive stresses at the specimen's free surface. The surface compressive stresses appear to keep the crack tip (at the free surface) closed during a part of the cyclic loading, thereby reducing the cyclic damage for a given amount of remote loading.

Burk and Lawrence [192] observed that small joint distortion resulting from welding can induce significant bending stresses. They calculated such stresses by partially straightening the specimen under load, and concluded that the induced bending stresses depend upon Young's modulus and the size of the joint distortion, and should be taken into account in the calculation of the fatigue crack propagation time.

To extend the safety margin for design, all the results reported here were obtained with the initial notch positioned on the "tensile" side, with the exception of those obtained in investigating the effect of residual bending stresses. Therefore, the results presented are somewhat conservative.

The inferiority of the fatigue properties of welded joints to those of base metal has been attributed to the tensile residual stress of the welded joint used in as-welded condition [109]. Many investigators [e.g., 109,193,194] have measured the welding residual stresses

parallel to the longitudinal direction of welding using an X-ray technique. They found that the residual stress was tensile near the middle but compressive near the edge of the test-piece. This trend persisted after machining the specimen. Ohta et al [109] also measured the crack closure and observed that the crack was fully opened during the whole range of loading in welded specimens and suggested that the effective stress intensity factor range, ΔK_{eff}, was equal to the stress intensity factor range, ΔK, in welded specimens, while ΔK_{eff} was smaller than ΔK in the base metal specimens. Since crack growth rates depend upon ΔK_{eff} raised to some power, these closure results explain why crack growth rates in the welded joints are larger than those in the base metal. The observation of crack closure also confirmed the suggestion that the stress ratio effect in the base metal will diminish in welded joints as discussed earlier.

A comparison of the weldment results with those for the parent metal indicated the presence of tensile residual stresses at the crack tip in the direction of the applied stress. These stresses were superimposed on the applied stress and increased the resultant stress at the tip of the growing crack which resulted in an increase in the rate of growth.

To confirm the assumption that the tensile residual welding stresses were the main cause of fatigue crack growth

change in the weld as compared with the base metal, the characteristics of fatigue crack growth in stress-relieved welds were determined. From the evaluated experimental results it follows that in the stress-relieved specimens the rate of fatigue crack growth decreased and approached the growth rates of the base metal. Further confirmation of high tensile residual stress and/or the combined effect of residual bending and tensile stresses is indicated by the observation of local yielding on the surface of welded joint specimens (see Figs. 5.38 and 5.39) which took place at applied stresses much lower than yield stress ($\sigma_{app} \approx 0.4\sigma_y$). Furthermore, to ensure that the local yielding was not caused by overloading but was indeed the result of residual tensile stress, a weld specimen was prepared with the notch located 40mm away from the weld axis and on the base plate. Fatigue tests were carried out under the same loading conditions, and it was observed that local yielding occurred around the weld, as shown in Fig. 5.39.

In the present investigation attempts were made to measure residual stresses; this proved to be difficult, however, the only reasonable conclusion that could be reached, based on the results from stress-relieved weld and from observation of local yielding, being that the residual stresses may be of the order of magnitude of the yield stress. Nevertheless, it would be worthwhile measuring such stresses since the observed differences in fatigue crack propagation rate might thus be quantified more accurately.

Comparison of the results obtained for SNP geometry with those for welded joint CT specimens demonstrated the fact that the residual stresses acting at the crack tip have differed, most probably by going in opposite directions, thereby resulting in the superiority of the fatigue crack propagation rate of CT geometry and the inferiority of SNP geometry to those of the base plate.

The introduction of a salt-water environment was found to have a significant effect on fatigue crack propagation rates in welded joints in a bending stress field for ΔK values greater than 8 $MN/m^{3/2}$; below this ΔK value the crack growth rate in the weldment appears to be the same as or lower than the in-air data. As with the results in air the stress ratio does not have a significant effect in a salt-water solution because of high tensile residual stresses. Higher crack growth rates in salt-water have been reported before [195], but there is evidence that at low stress intensity values (i.e., low values of crack depth, length and stress range), crack growth rates in air and salt-water do not differ substantially [196]. As low stress intensities account for the major part of fatigue life, there is only a negligible influence from the salt-water environment and this was confirmed in [197].

The effect of a salt-water environment on crack growth rates increases slightly with increasing stress ratio. At

R=0.08 the environmental acceleration of crack growth in the weldment is about the same as for the in-air data. However, at the highest stress ratio of 0.7, the crack in a salt-water environment grew faster than in air. This effect was also observed by Vosikovsky [198], who tested HY130 steel weldments in air and 3.5% NaCl solution.

5.4.3 HAZ

As indicated earlier, crack growth rates are higher in the HAZ than in the parent metal. For example, at ΔK =20 $MN/m^{3/2}$, the growth rates in HAZ are 3 times higher than the corresponding values in the base material. This trend holds true for tests at 30Hz, a fact which directs our attention immediately to two variables as possibly having a critical effect on growth rates in HAZ, namely, residual stress and microstructure, as discussed below.

The residual tensile stresses appear to interact with the applied opening loads, resulting in a considerably higher value for the critical crack tip stress intensity. Fatigue cracks in HAZ started from the machined notch at an angle of between 2° and 5° from the plane of symmetry away from the weld. This deviation appears to be caused by non-symmetric residual forces on both sides of the crack plane and a non-symmetric plastic zone at the crack tip which are caused by the different flow strengths of the weld metal and the base material. As the crack advances, the crack tip appears to deviate towards the softer regions. This results

in a greater rate of growth and a corresponding larger plastic zone [104]. Just how much of the deviation effect can be attributed to the variation of flow stress and how much to the residual stresses clearly needs further research.

The possible deleterious effect of microstructural changes during the welding process is highlighted by the extreme susceptibility of the hard HAZ structure developed in the steel investigated. It has been suggested that a very small heat input, such as if the weld bead were small, or in thick plates (i.e., the bulk of cold material surrounding the weld would have a higher cooling rate), will result in a very hard HAZ and a brittle microstructure [199]. However, it should be borne in mind that such unfavourable welding conditions can hardly be avoided in practice when fabricating large welded structures.

The dominant role of microstructure in determining the mechanism by which fatigue cracks propagate in HAZ and the associated material is clearly indicated in the results given in Fig. 5.22. The hardness of HAZ is attributed to the presence of large grains containing martensite. This is the hardest constituent found in steel and its presence accounts for the high hardness recorded. Its formation is due to the rapid fall in temperature of welded plate during cooling. The fracture surfaces of HAZ specimens were generally rougher and were crystalline in appearance.

Some authors [200] suggest that the fatigue crack growth rates in HAZ are independent of microstructure and are only influenced by the residual stresses. However, the fractography of the failed HAZ specimens revealed regions of intergranular and trangrsanular fracture (see Figs. 5.40 and 5.41). Fatigue cracks propagate more rapidly and over large distances mainly because of the intergranular fracture mechanism acting on large grains. Hence, it appears that the average rate of fatigue crack growth under a mixed intergranular and transgranular fracture mechanism will be higher than for a crack which propagates through the transgranular mechanism alone. This was also observed by Maddox [201] who studied crack growth behaviour of HAZ in BS968 steel. He found that the rate of crack propagation was reduced by thermally stress-relieving the HAZ. The fractography of fracture specimens showed some areas of intergranular fracture but the proportion of intergranular fracture was much less than that observed in the as-received specimens. He attributed the lower growth rate of the crack propagation obtained from stress-relieved specimens to the lower incidence of intergranular fracture. This was the case in the present investigation, which indicates that the variation in microstructure at a weld should be taken into account as well as the residual stresses when analysing fatigue in welded structures.

Although a limited amount of work has been carried out

and the conclusions are somewhat tentative, the evidence does point to the fact that fatigue safety in welded joints depends on the HAZ having a similar hardness to that of the base metal. Therefore, pre-heating precautions should be taken where possible, before welding such materials, to avoid hardened HAZ.

Due to the difficulty in determining the exact residual stress distribution in a structure, and also due to the inherent variability of such stresses in even strictly controlled welding processes, it seems reasonable to use the upper bound of the scatter band for the weldment as a conservative estimate for the fatigue crack growth rate in regime II of HAZ. This is given by

$$\frac{da}{dN} = 1.35 \times 10^{-8} (\Delta K)^{4.2} \qquad .(5.15)$$

5.5 CONCLUSIONS

1) The stress intensity factor solution used for surface cracks in 24mm-thick specimens gave a good correlation with the results obtained for specimens of the same thickness containing through-thickness cracks in the parent metal. However, at low values of ΔK there was a marked difference between the results, which was probably due to the failure of the correction factor at low values of ΔK and/or underestimation of plastic zone size due to the complexity

of plastic zone effects on surface cracks.

2) For the parent plate, crack growth both at the surface and in the through-thickness direction generally increased with stress ratio, this effect being most significant at low growth rates, can be explained in terms of crack closure. The comparison of growth rates for surface cracks and through-thickness cracks indicated that the surface cracks are more sensitive to stress ratio in regime II than through-cracks.

3) The effect of frequency in the 24mm-thick BS4360-50D steel was the same as observed in the CT geometry tested, that is, decreasing frequency results in increased growth rates. However, comparing the results obtained for different frequencies, it appears that frequency has no effect at low values of ΔK and thresholds.

4) A comparison of present results with those obtained by other investigators [175] on the same material showed a good agreement at low stress ratio(i.e., R=0.08); however, at high stress ratio of 0.7 the present results predict higher growth rates.

5) A salt-water solution (3.5% NaCl) enhanced fatigue crack growth rates for ΔK values above 18 $MN/m^{3/2}$ at R=0.08 and 15 $MN/m^{3/2}$ at R=0.7. Corrosion fatigue crack growth rates increase with stress ratio. However, from extrapolating corrosion fatigue curves it appears that for early stages of crack propagation in a salt-water environment ($<10^{-5}$

mm/cycle) the growth rates are lower than in air.

6) For butt-welded specimens the surface crack growth was faster than in the parent material due to the tensile residual stresses. This was confirmed by observation of local yielding which took place on the surface of welded specimens, suggesting the presence of tensile residual stresses. Moreover stress-relieved specimens showed better fatigue properties, and their surface crack growth rates were comparable to those of parent material for a given value of ΔK.

7) The crack growth rate data obtained for part-through cracks in butt-welded joints did not correspond to the results obtained from CT geometry. They showed much higher growth rates when compared to the latter. This indicates that the resultants of residual stresses acting on the crack tip were in opposite directions. It is therefore the case that the inferiority of the properties of butt-welded joints used in the investigation must be due to tensile residual stresses within the welded joint specimen used in as-received condition.

8) To obtain consistent data from fatigue tests on laboratory surface-notched butt-welded specimens under bending loads, it is important to use the same notch orientation for all specimens, as there exist bending residual stresses which are added to the applied bending stress (i.e., increasing the effective stress intensity at the crack tip) on one surface of the specimen, and

counteract the applied stress if the notch is located on the other surface of the specimen.

9) Enhancement of crack growth rates because of salt-water environment in welded joint specimens appears to occur at ΔK values above 7 $MN/m^{3/2}$, below which the growth rates seem to be lower in salt-water than in air. The same behaviour was observed for stress-relieved specimens in salt solution, but the cross-over from lower to higher growth rates occurs at ΔK values of approximately 10 $MN/m^{3/2}$.

10) There was no significant difference in crack growth rate data obtained for SNP geometry for the weld metal and HAZ at 30Hz. At cyclic loading of 0.25Hz, however, the crack growth rates in HAZ seem to be lower than in the weld metal. In general, crack growth rates in HAZ are higher than those in base metal at high frequency. However, at low frequency (0.25Hz) and low ΔK values (<9 $MN/m^{3/2}$ at R=0.08 and <4.5 $MN/m^{3/2}$ at R=0.7), the crack growth rates in HAZ approach those in the base material.

11) The higher crack growth rates in HAZ as compared with the base metal are attributed to the presence of tensile residual stresses and the microstructure of HAZ. The hardness test showed the presence of very hard HAZ, which is associated with large grains containing martensite. Fractography of the failed HAZ specimens revealed regions of both intergranular and transgranular fracture.

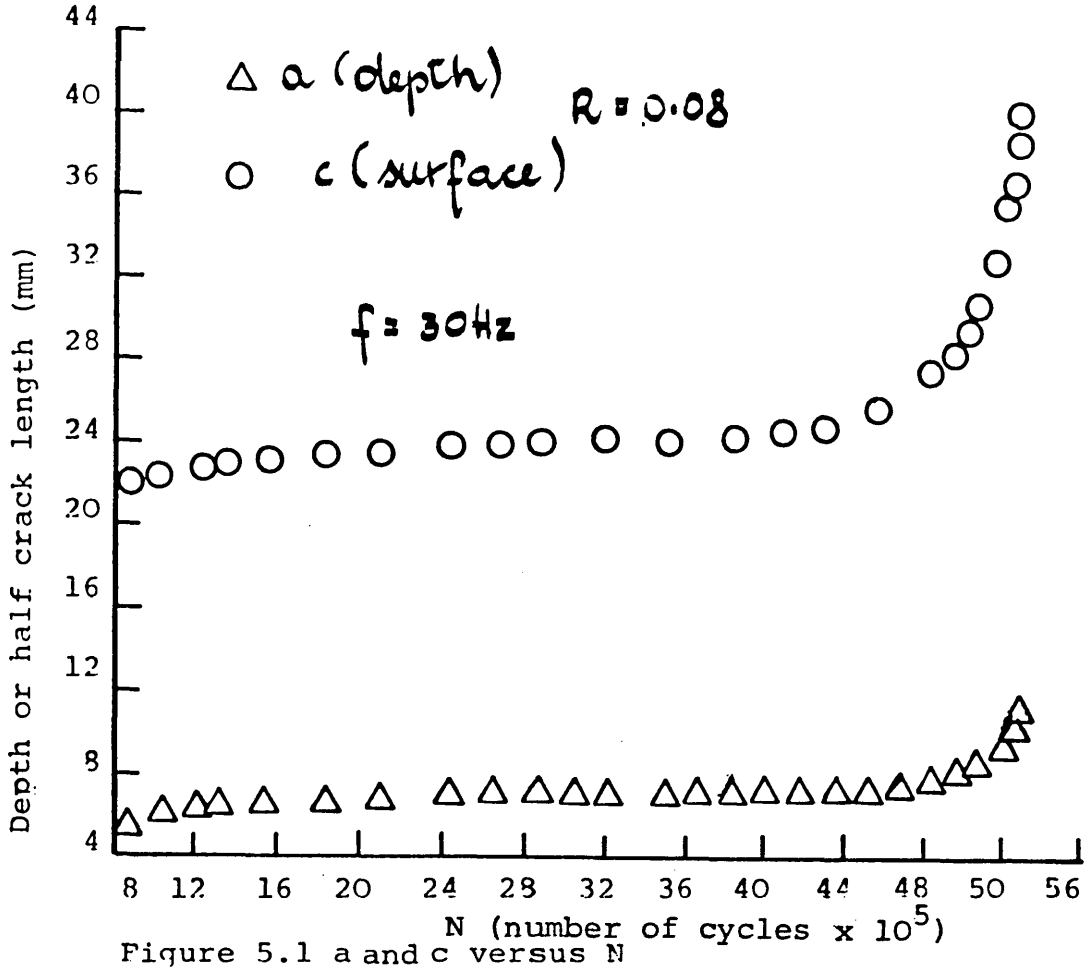


Figure 5.1 a and c versus N

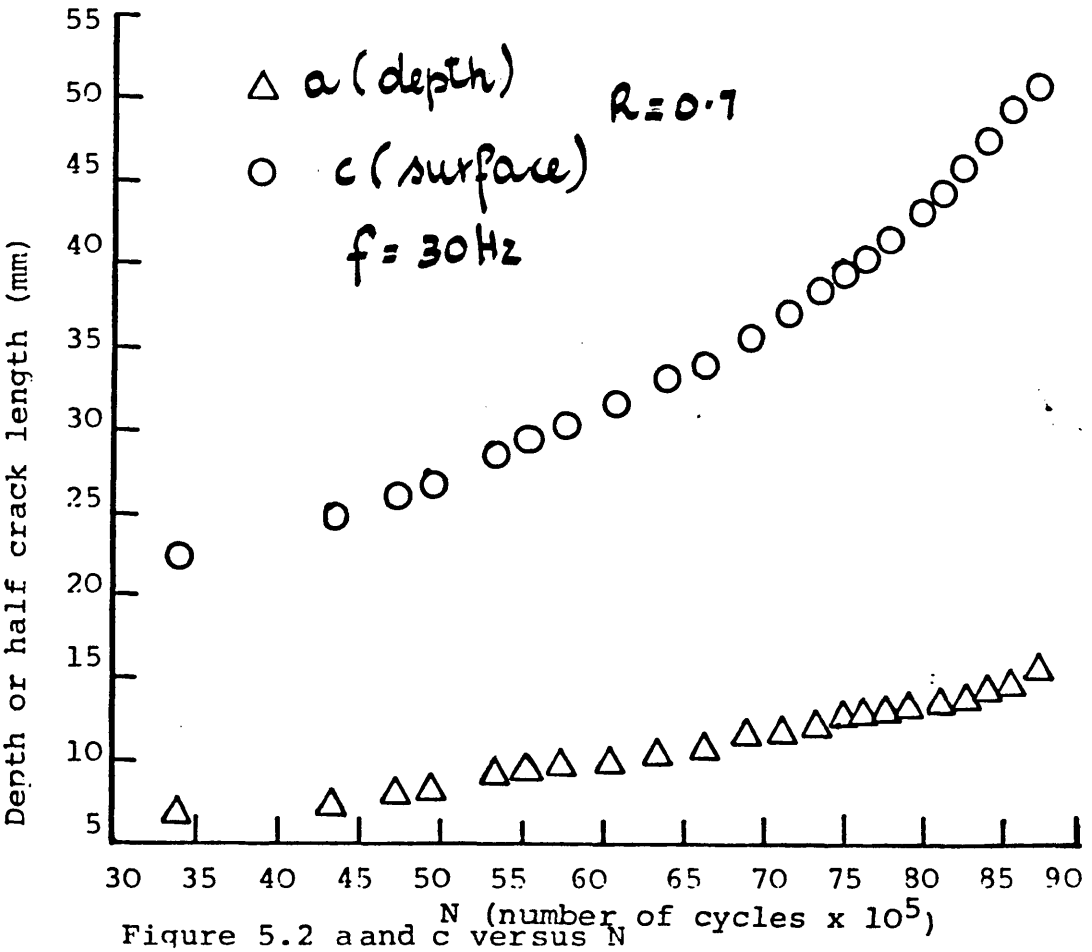


Figure 5.2 a and c versus N

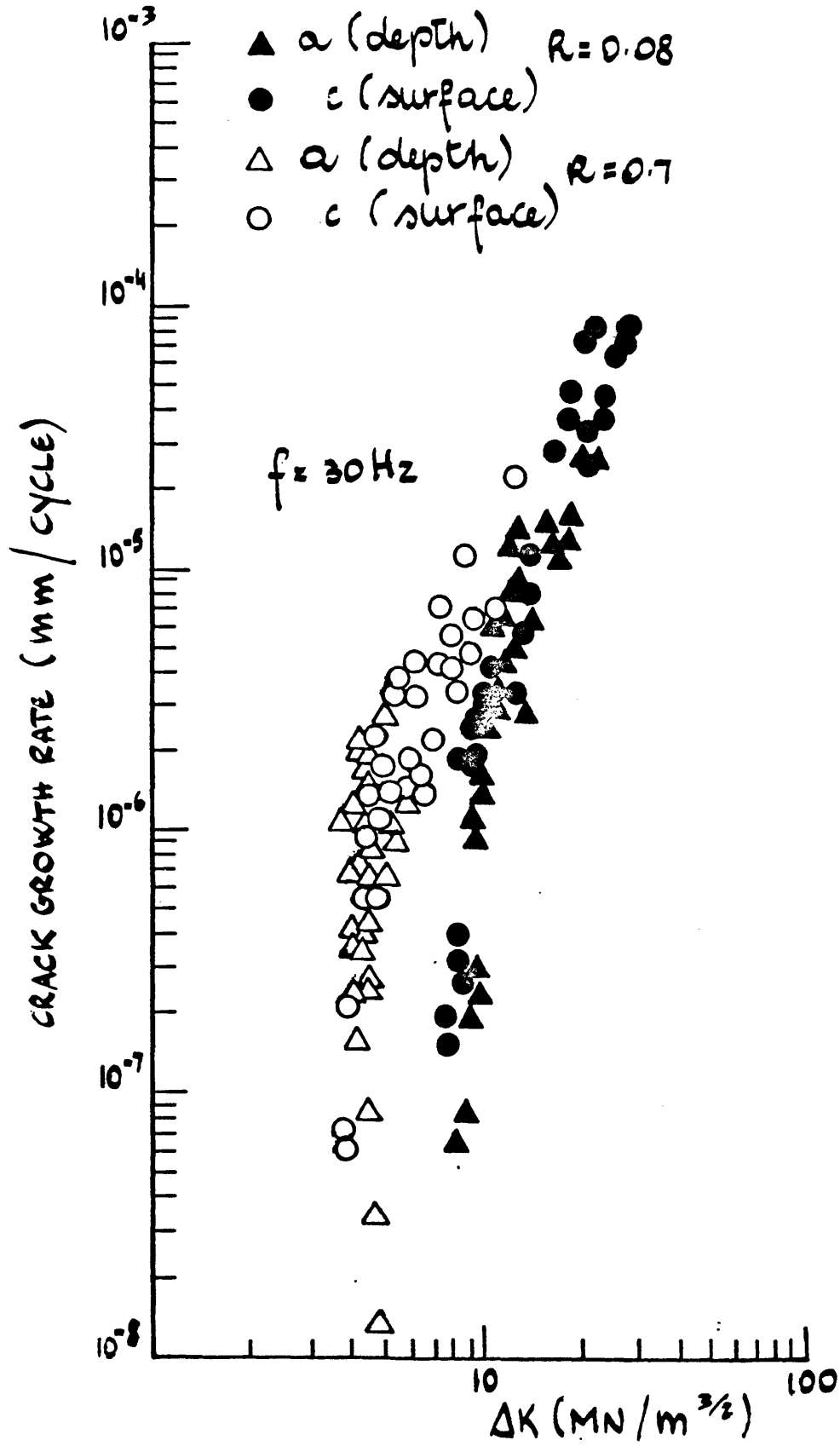


Figure 5.3 The effect of stress ratio on surface crack growth of BS4360-50D steel in air.

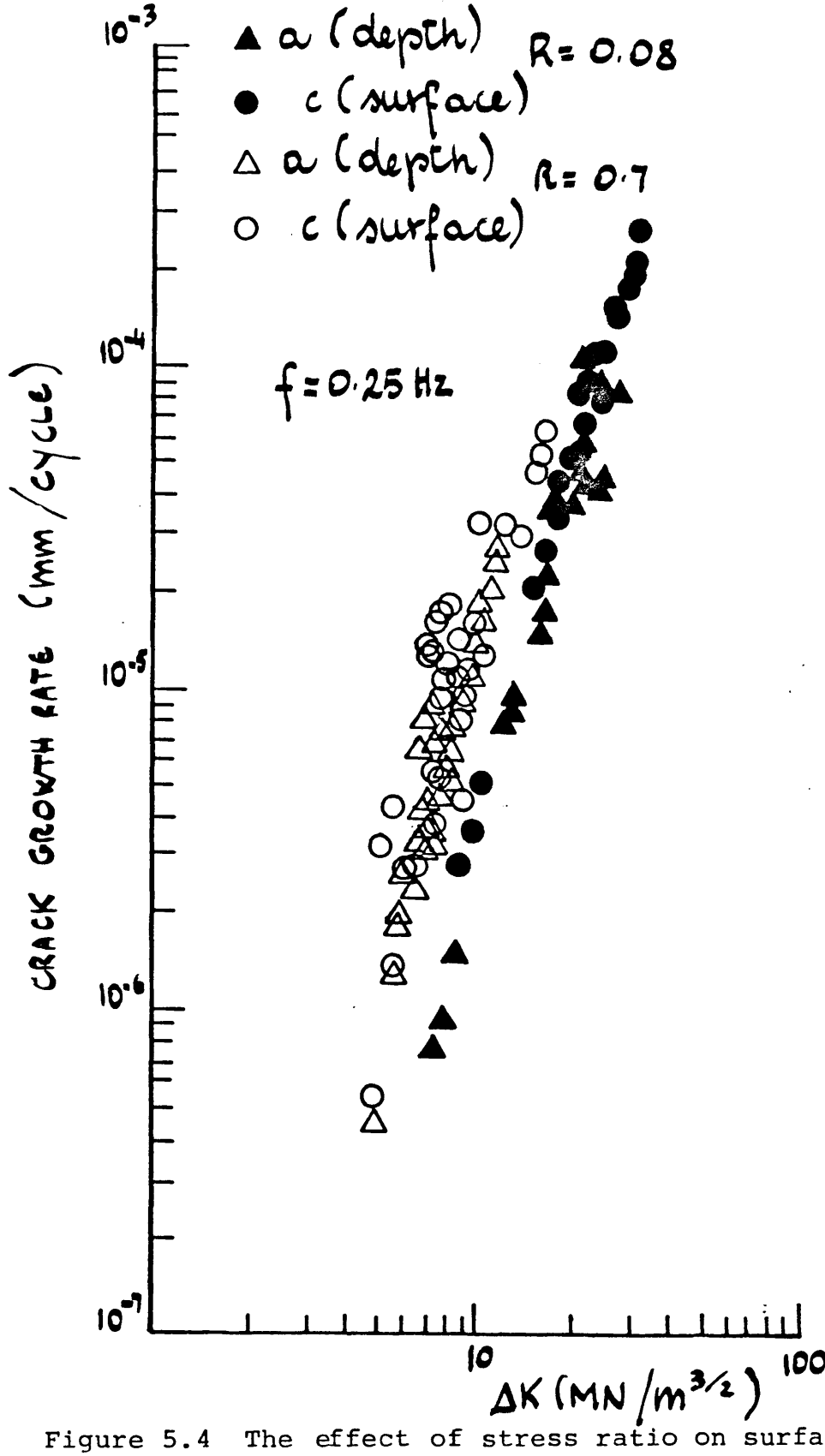


Figure 5.4 The effect of stress ratio on surface crack growth of BS4360-50 steel in air.

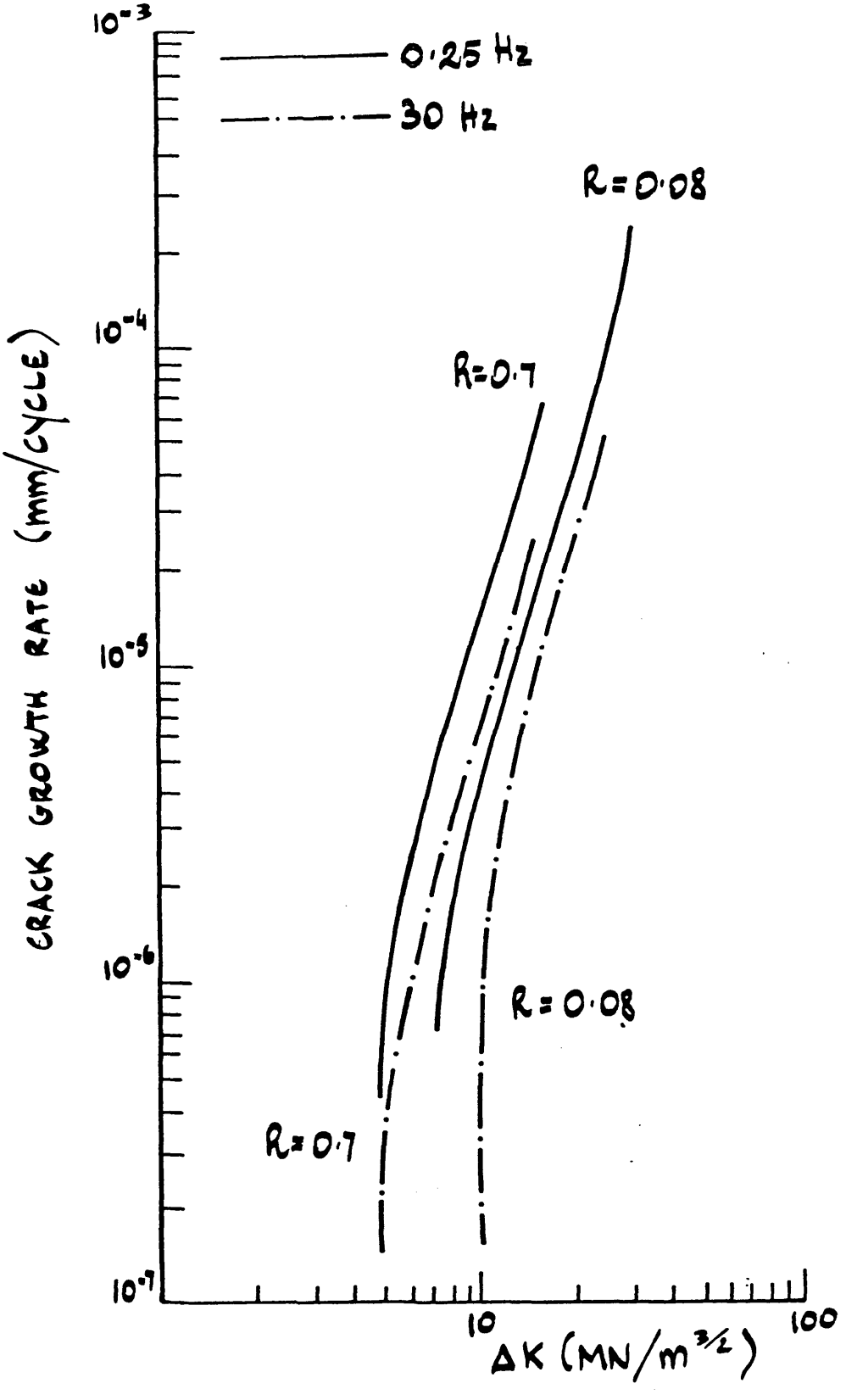


Figure 5.5 The effect of frequency on surface crack growth of BS4360-50D steel in air.

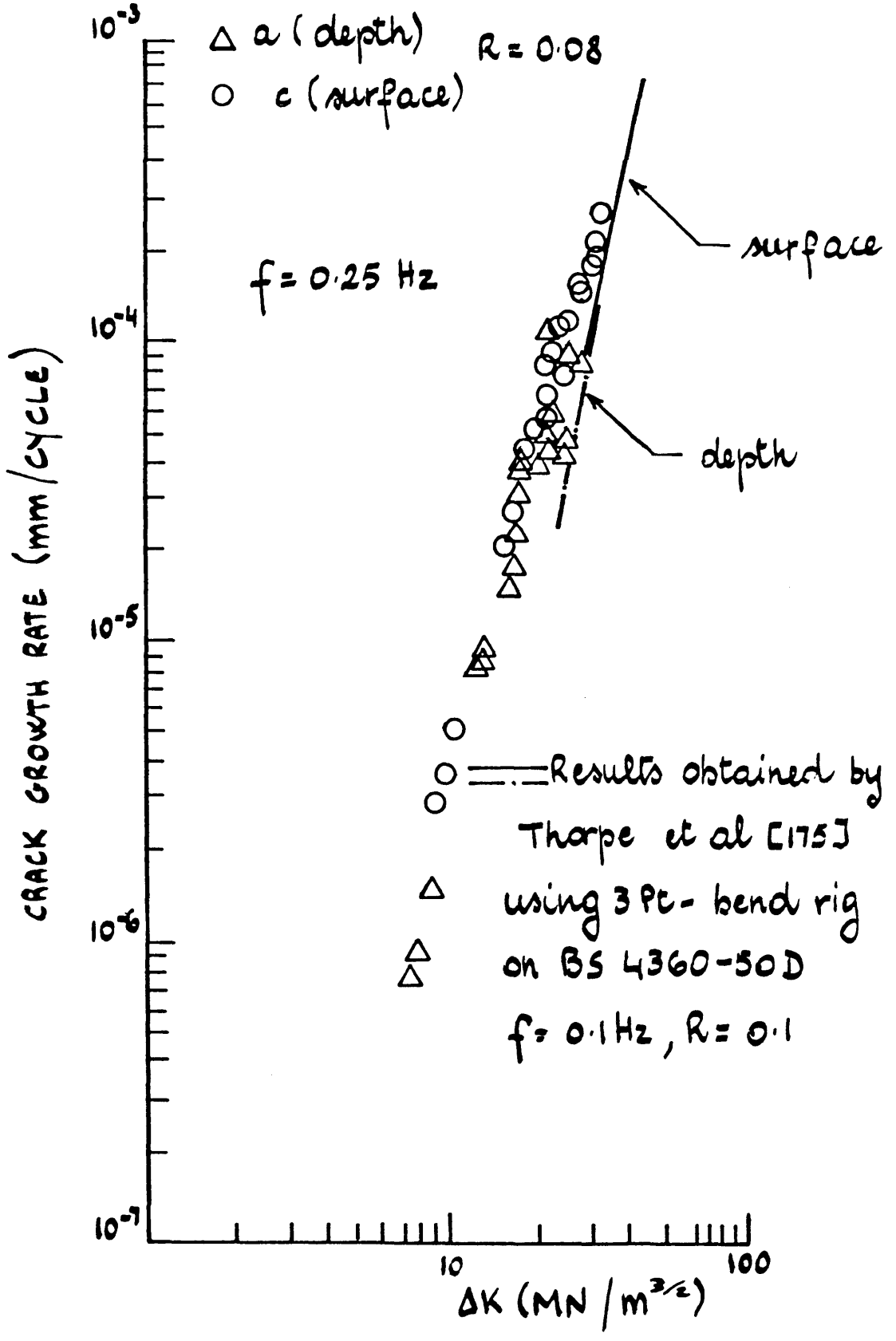


Figure 5.6 Comparison of results obtained in the present investigation with those obtained by Thorpe et al.

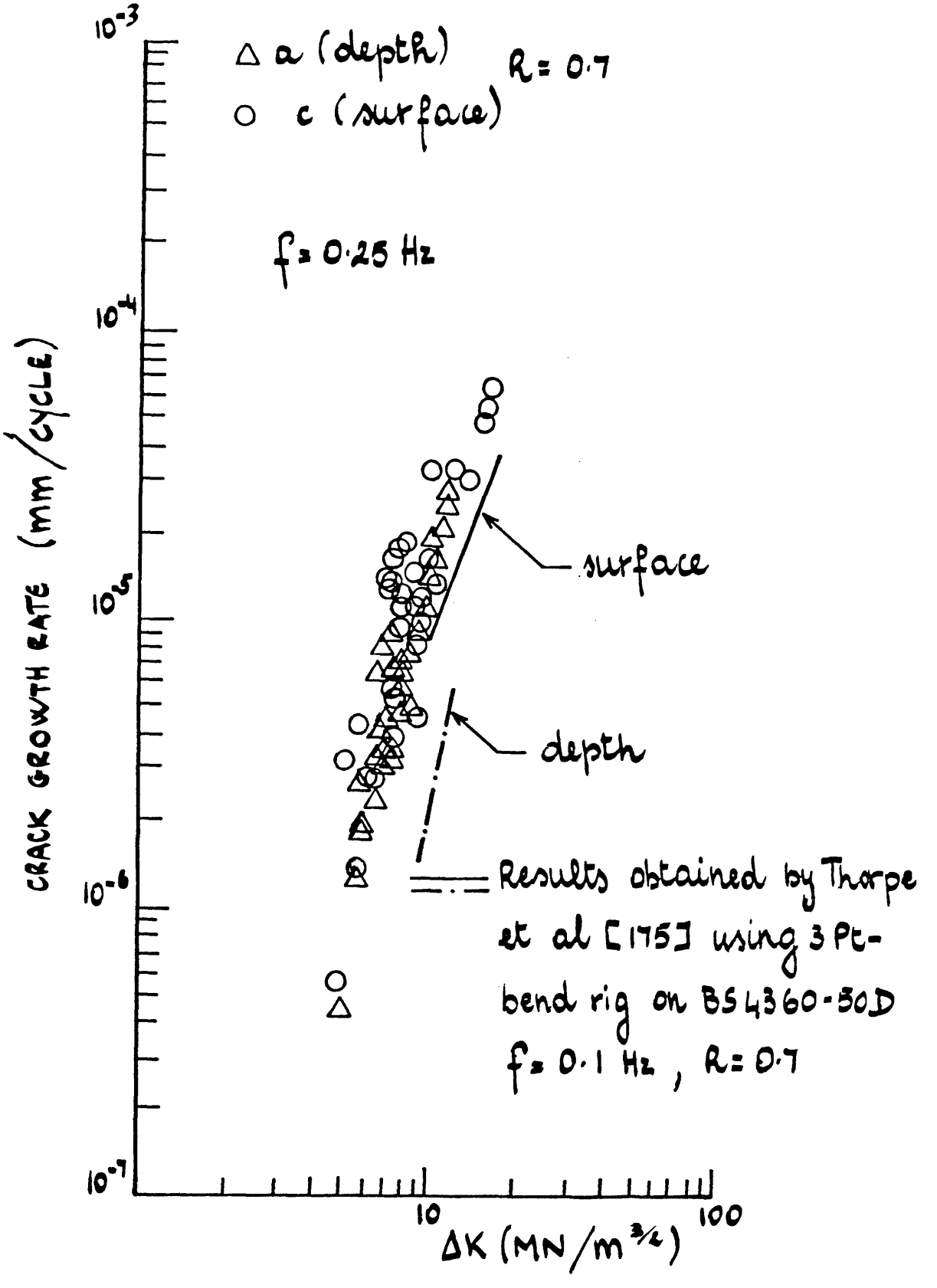


Figure 5.7 Comparison of results obtained in the present investigation with those obtained by Thorpe et al.

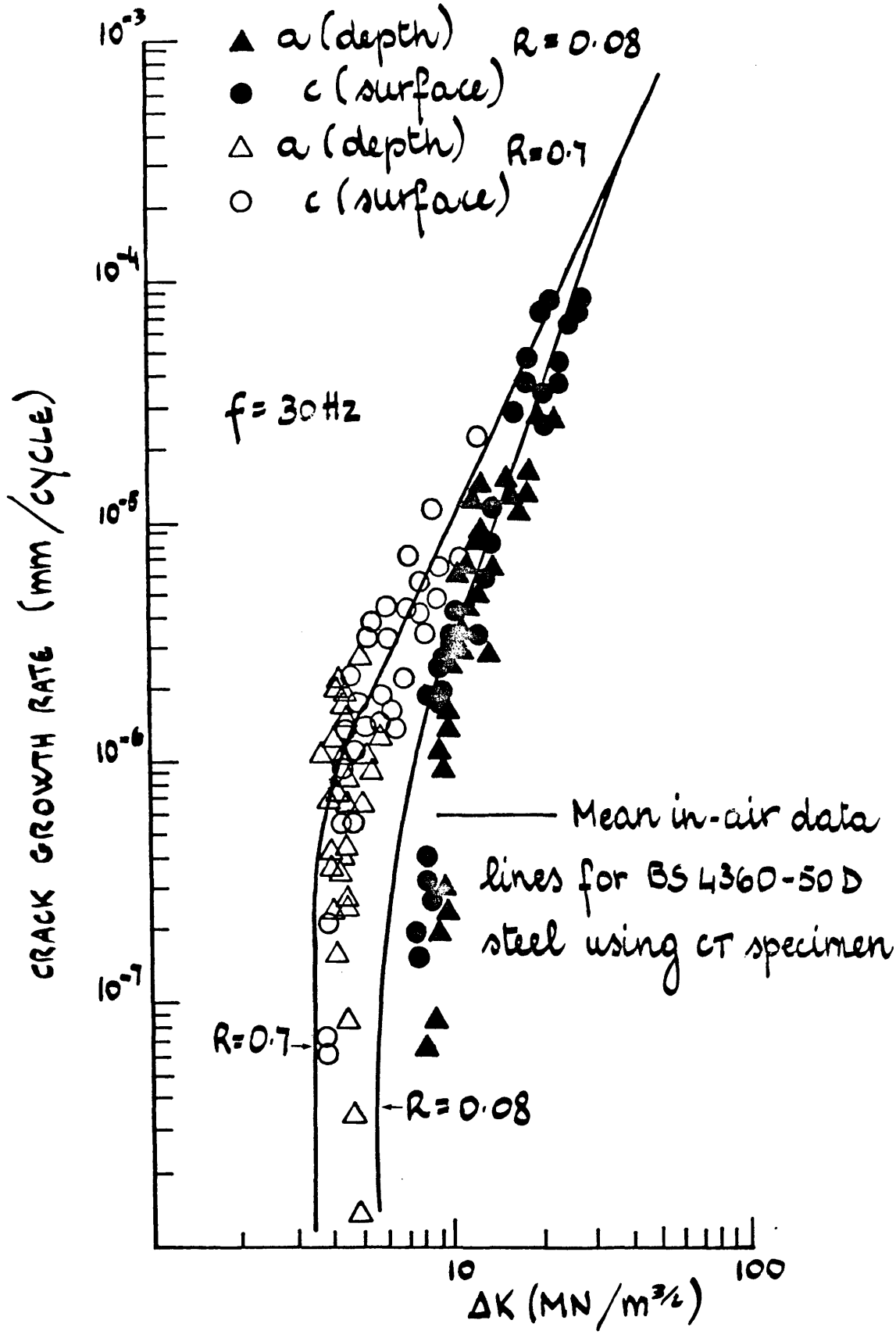


Figure 5.8 Comparison of results obtained for CT specimen and surface-notched plate in bending.

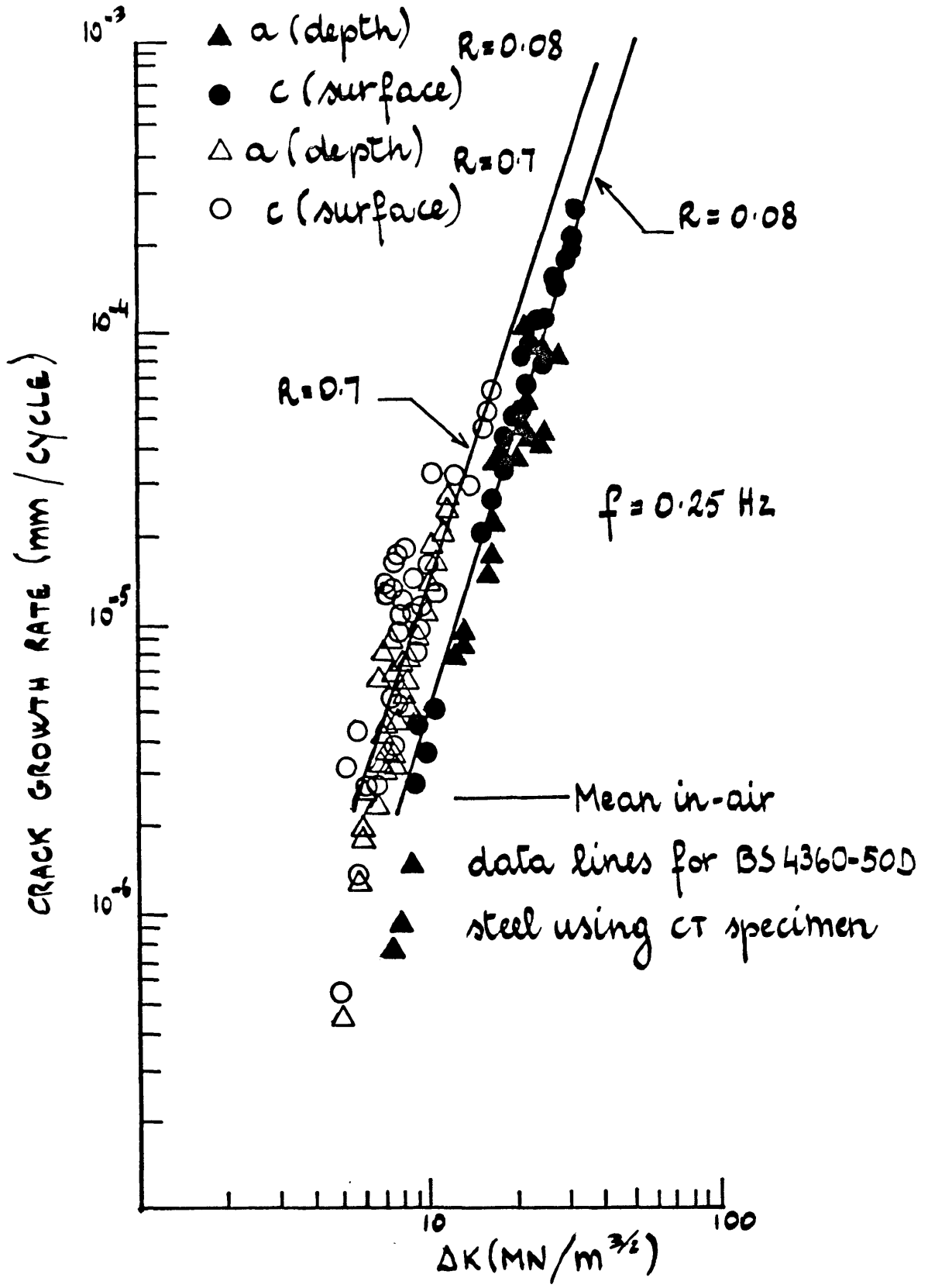


Figure 5.9 Comparison of results obtained for CT specimen and surface-notched plate in bending.

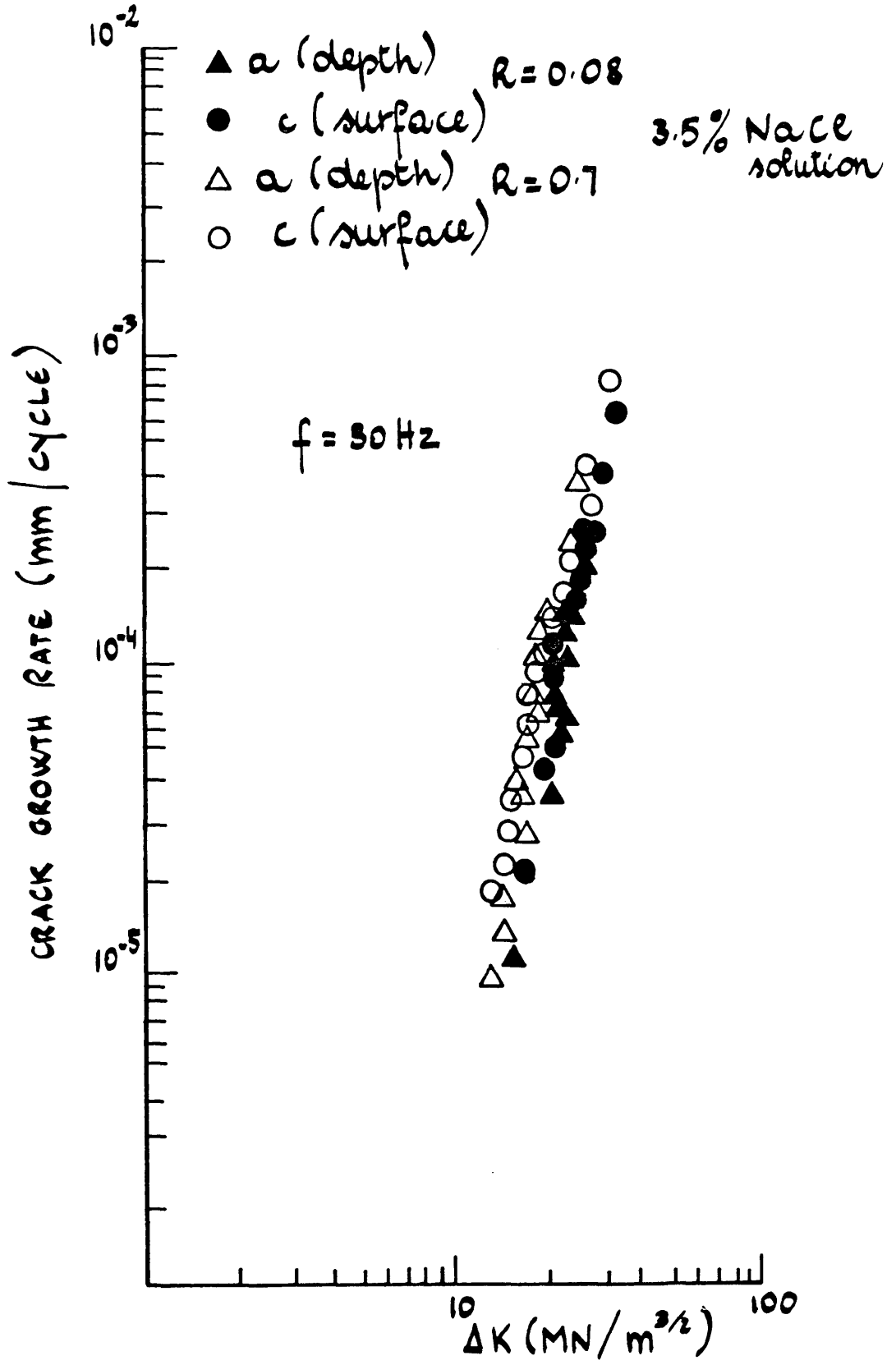


Figure 5.10 Effect of stress ratio on surface crack growth of BS4360-50D in salt solution.

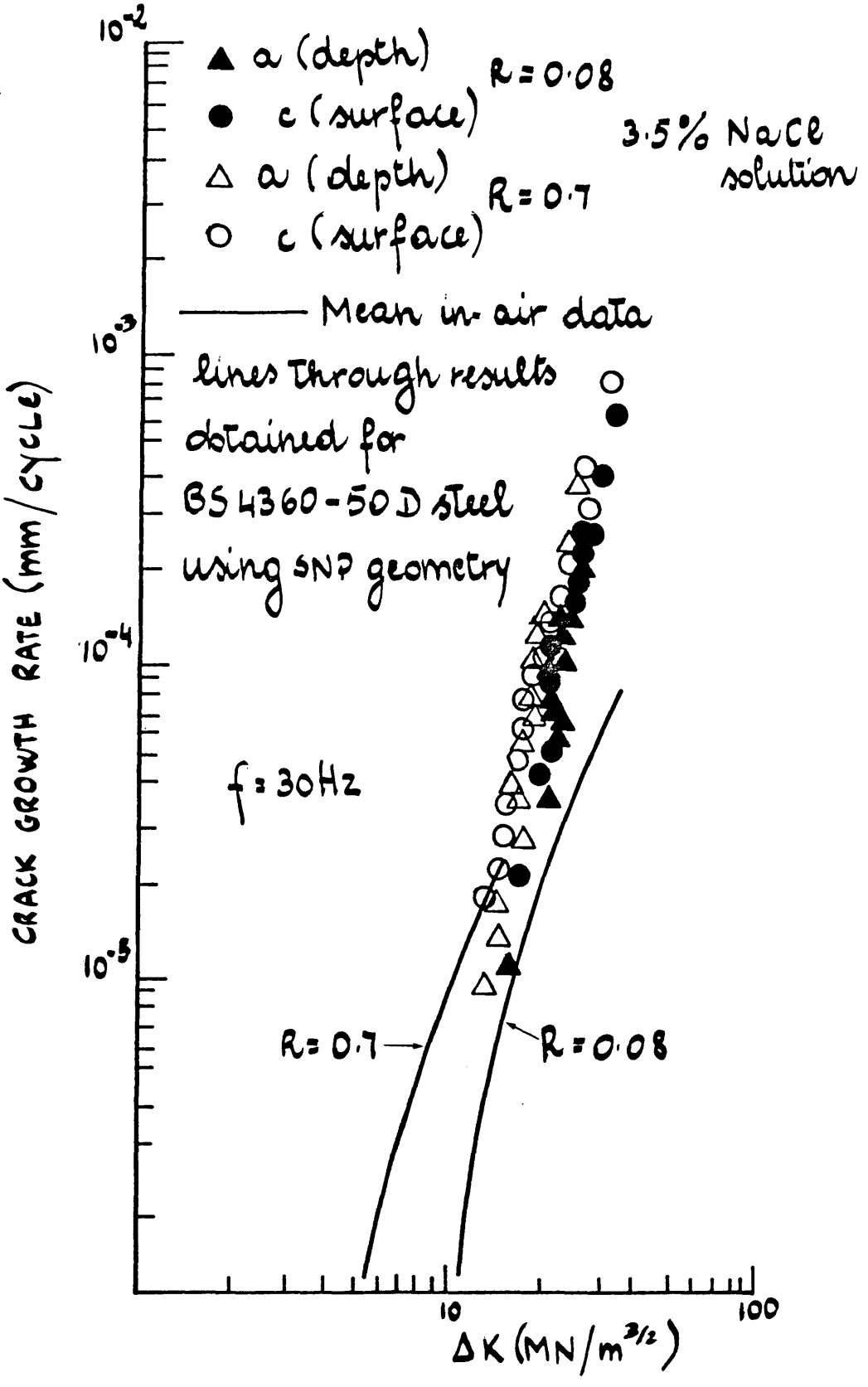


Figure 5.11 Comparison of results obtained for BS4360-50D steel using SNP geometry in air and in salt water solution.

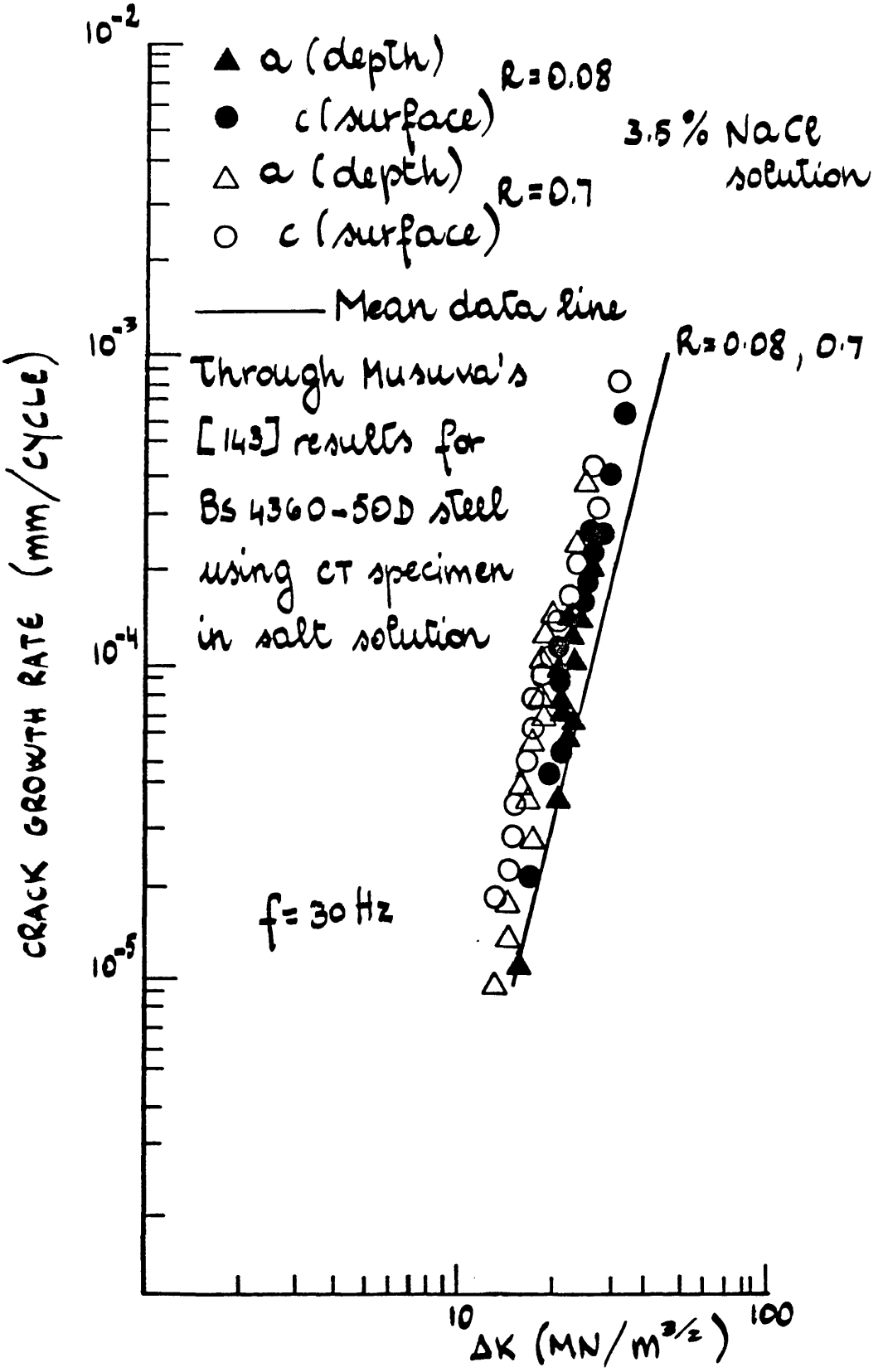


Figure 5.12 Comparison of results obtained for BS4360-50D steel using CT and SNP geometry in salt water solution.

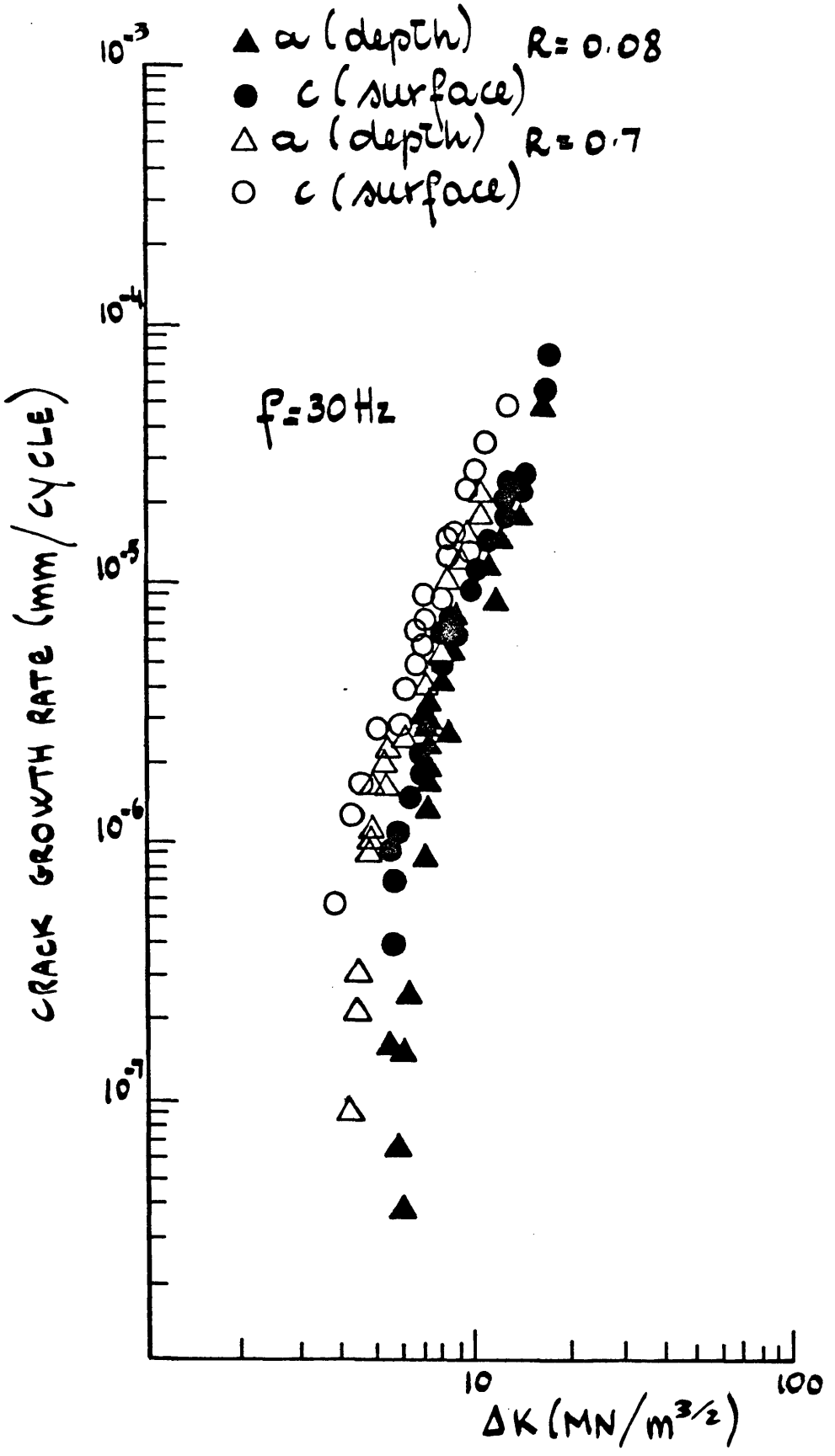


Figure 5.13 Effect of stress ratio on weldment using SNP geometry in air.

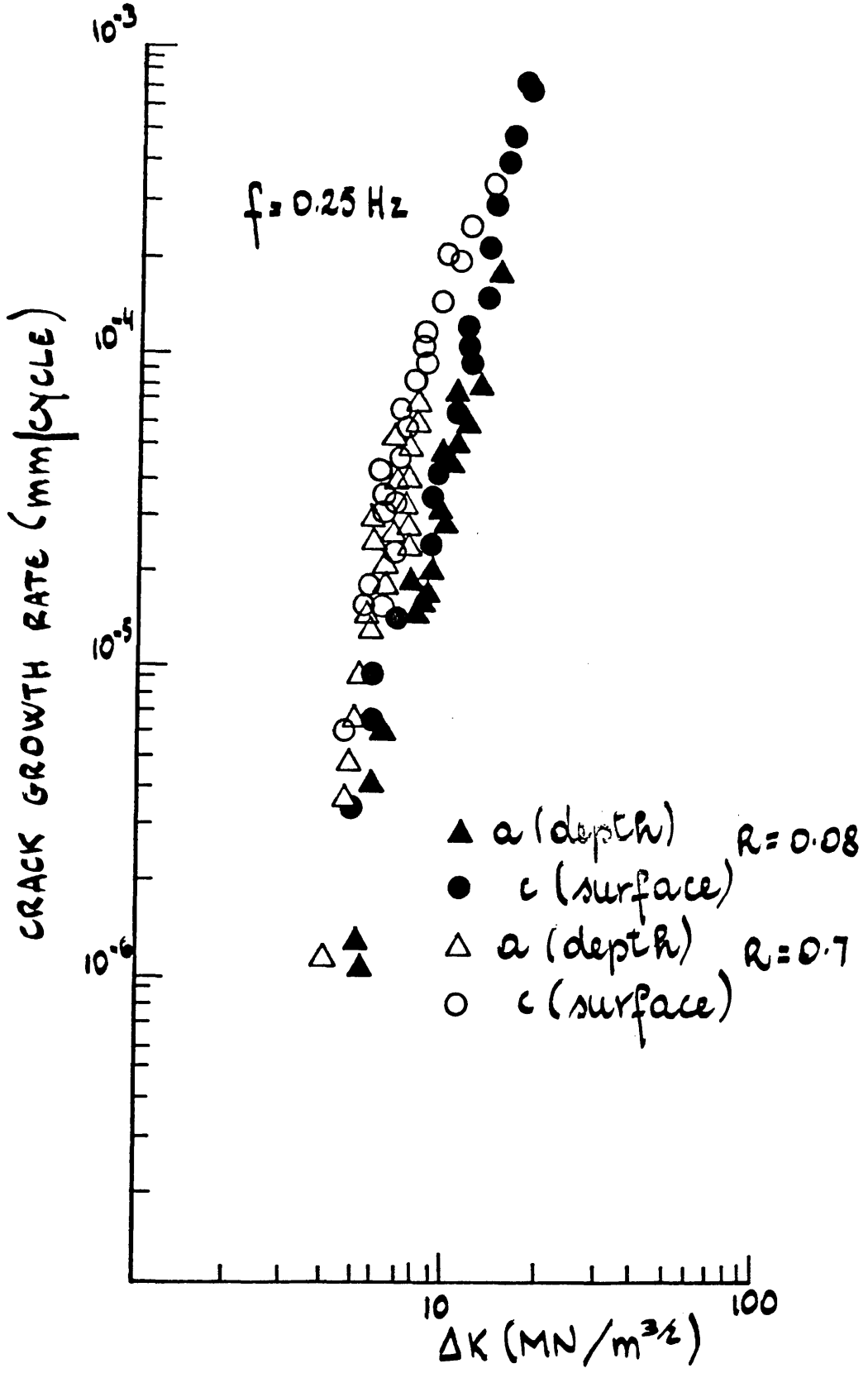


Figure 5.14 Effect of stress ratio on weldment using SNP geometry in air.

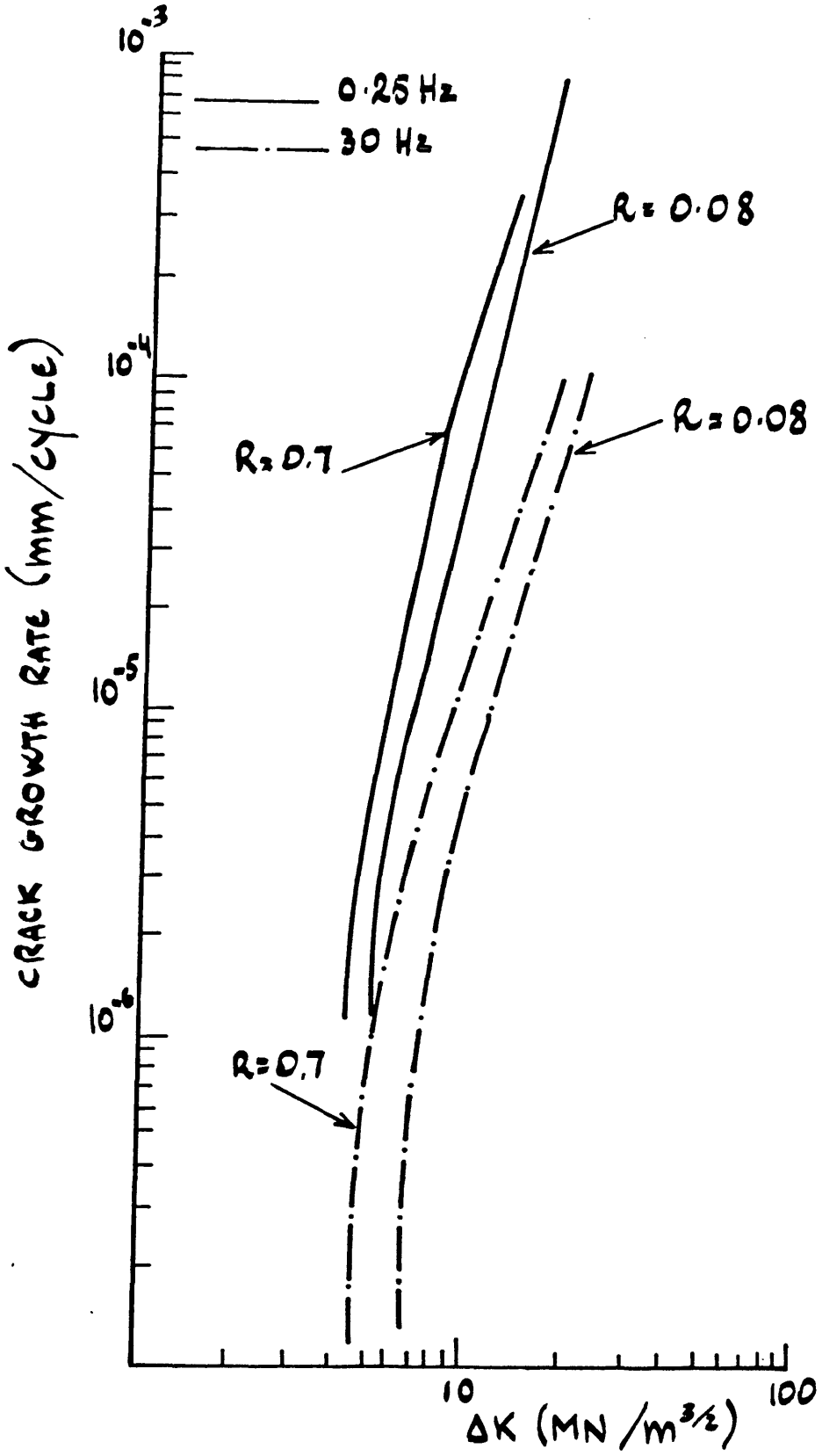


Figure 5.15 Effect of frequency on weldment using SNP geometry in air.

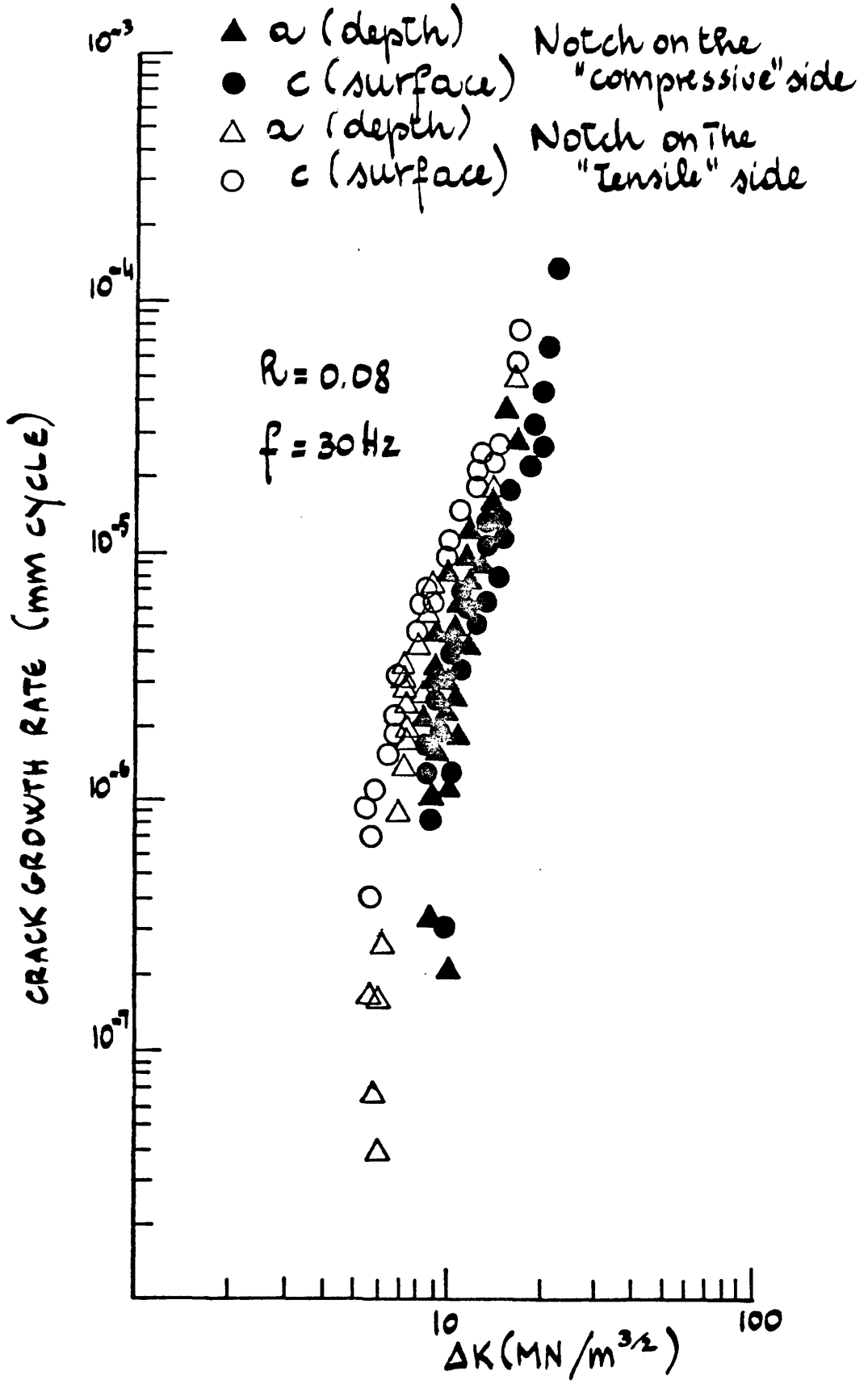


Figure 5.16 Comparison of the results obtained for weldment with the notch located on 'tensile' and 'compressive' sides of SNP geometry.

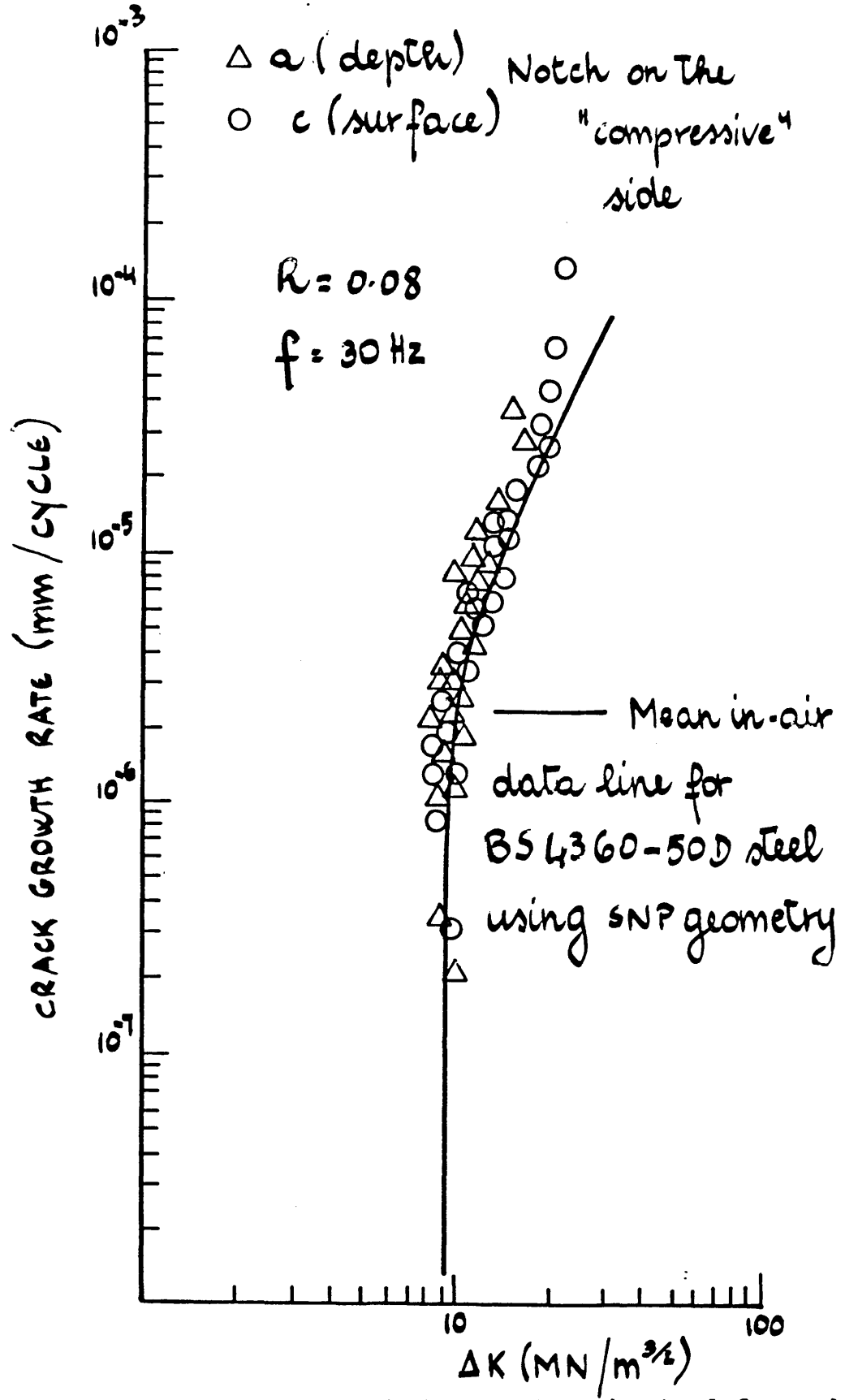


Figure 5.17 Comparison of the results obtained for weldment with the notch on "compressive" side and for parent metal using SNP geometry in air.

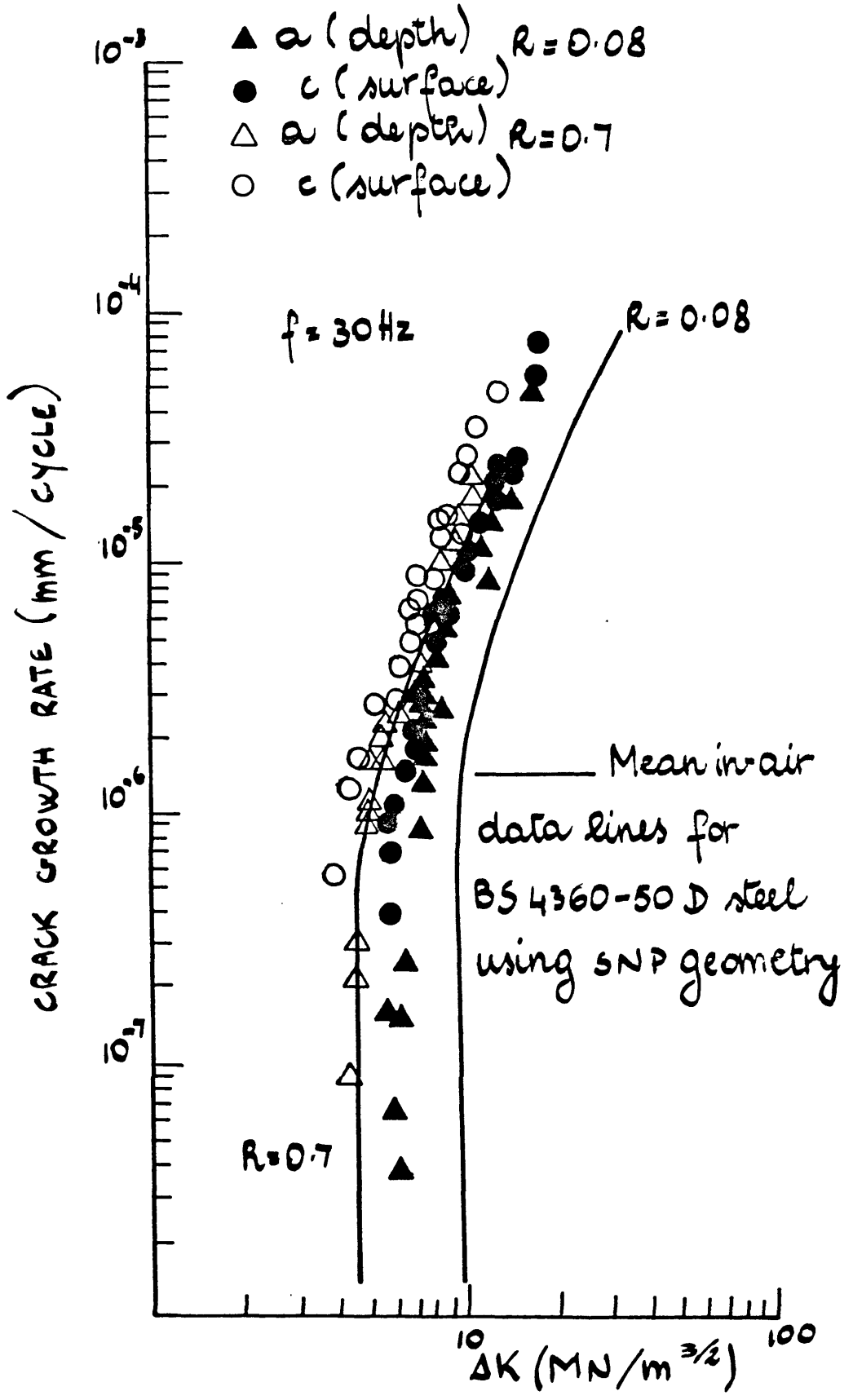


Figure 5.18 Comparison of results obtained for weldment and for parent metal using SNP geometry in air.

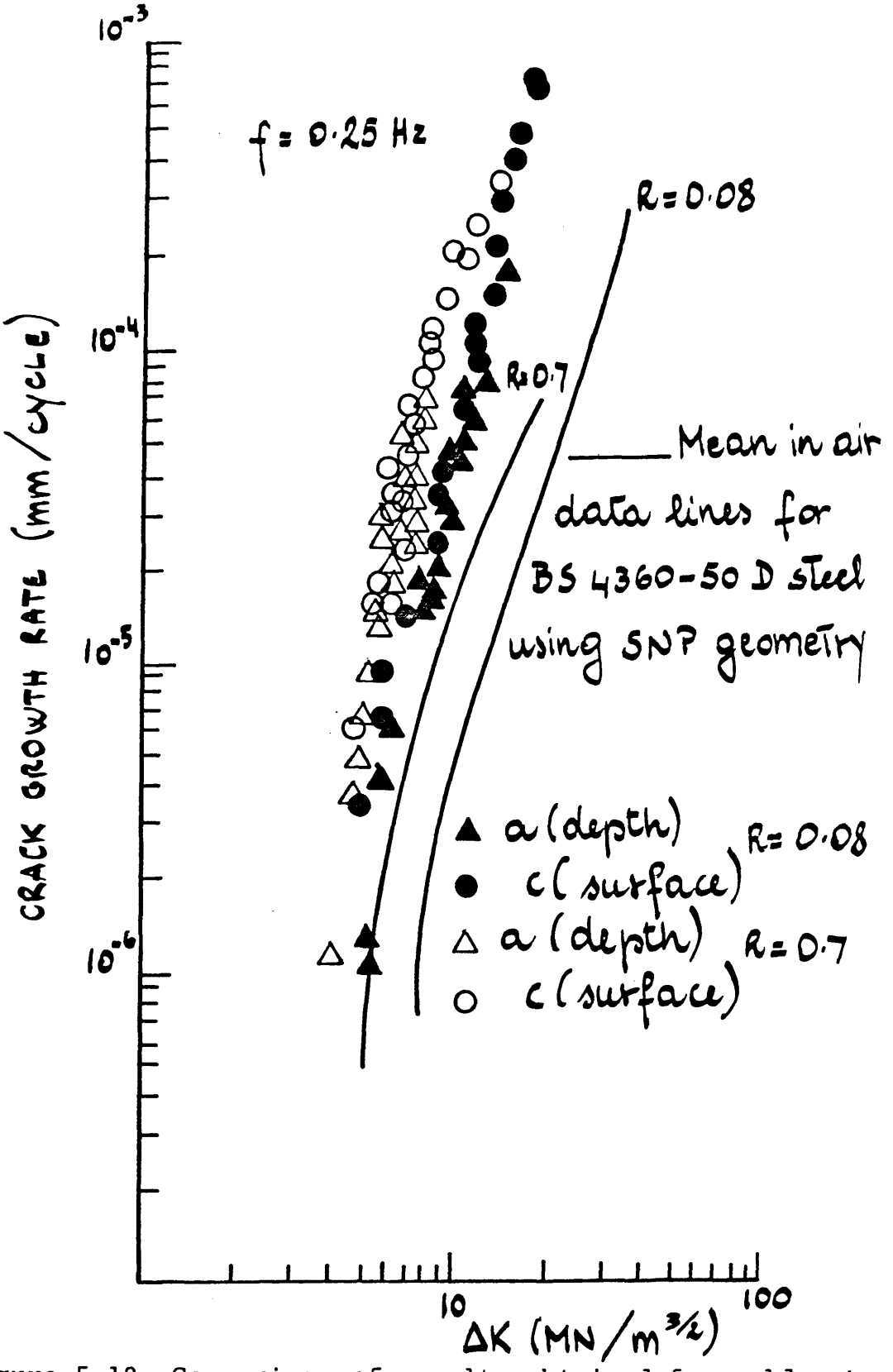


Figure 5.19 Comparison of results obtained for weldment and for parent metal using SNP geometry in air.

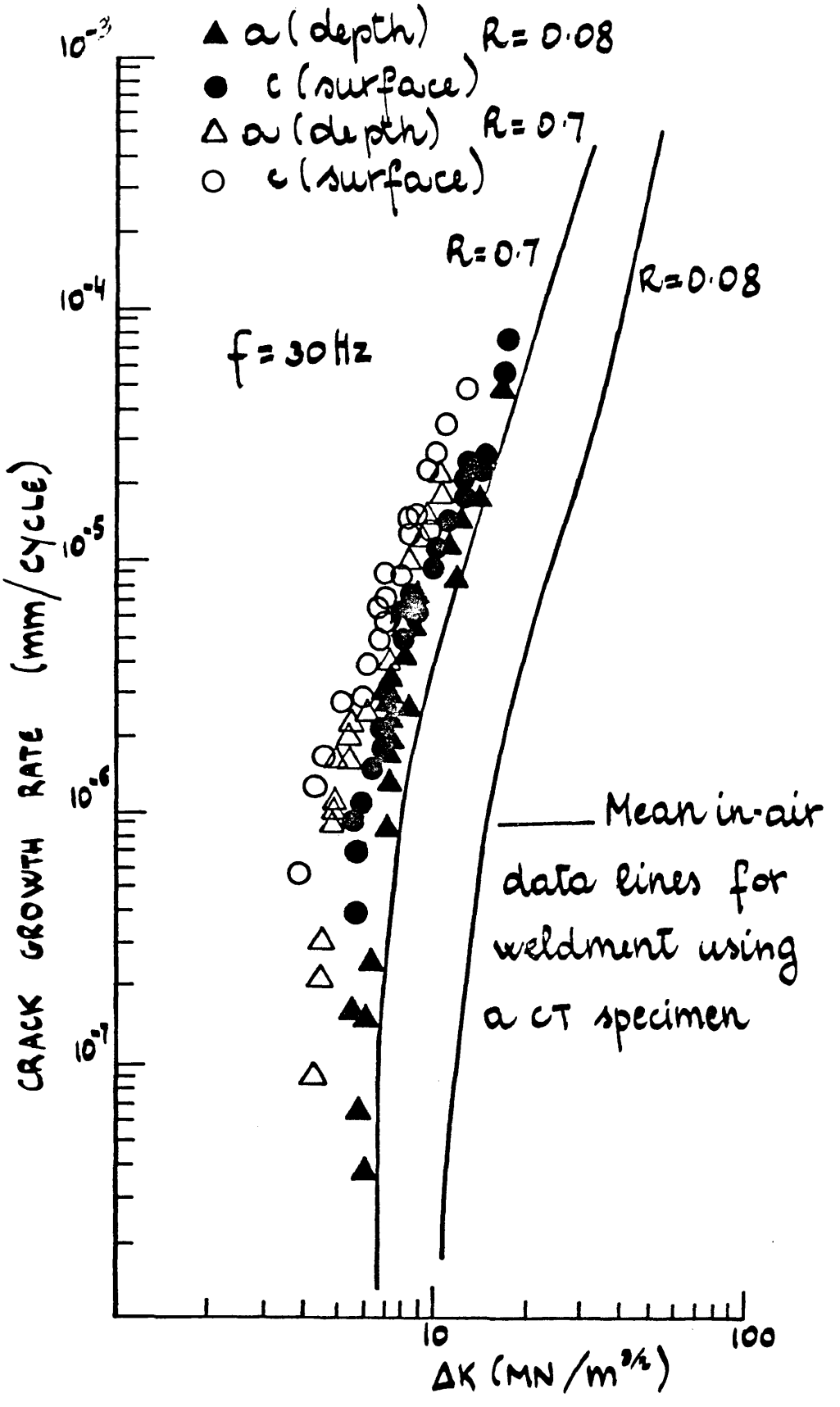


Figure 5.20 Comparison of results obtained for weldment using a CT specimen and a surface-notched plate in air.

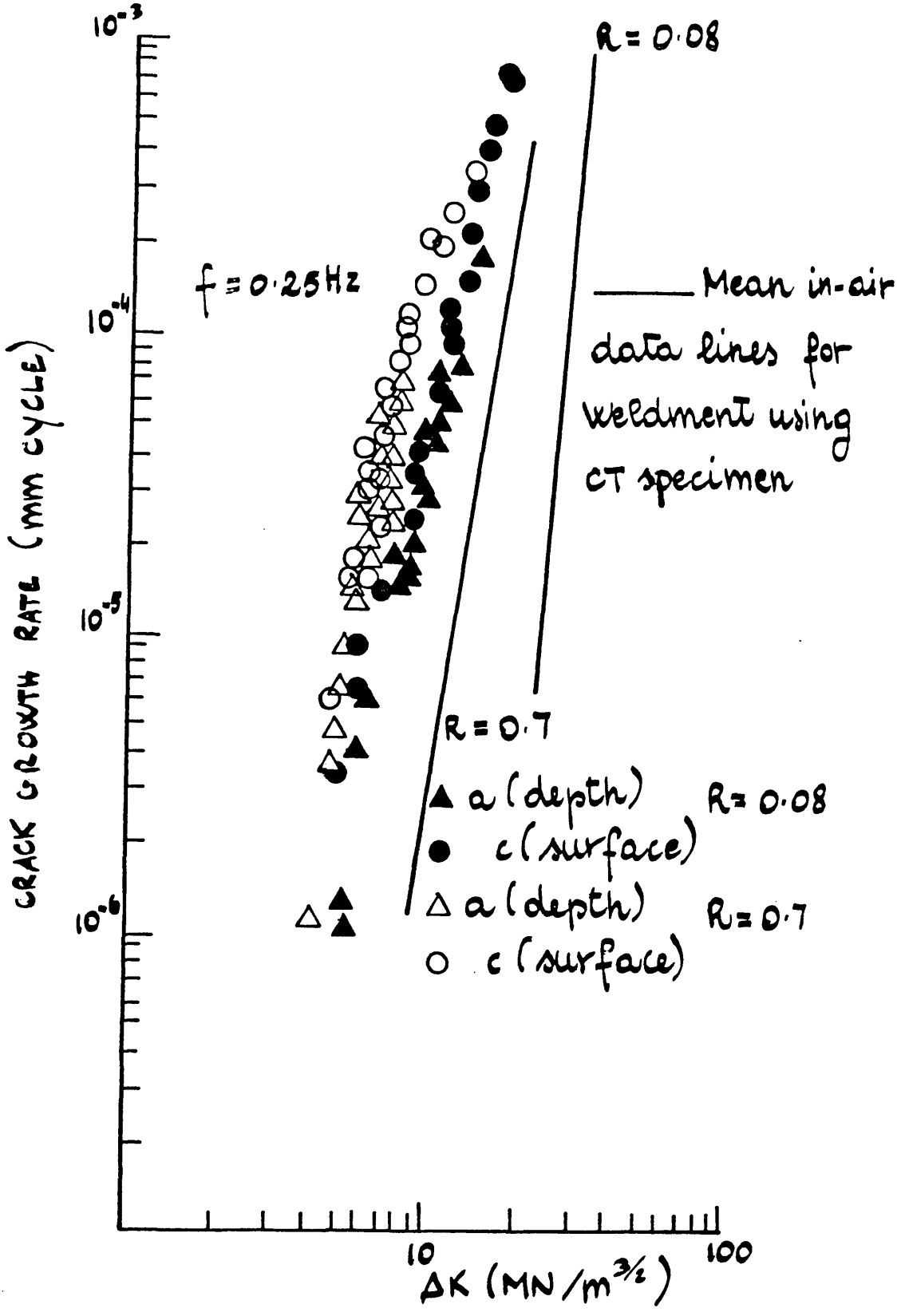


Figure 5.21 Comparison of results obtained for weldment using a CT specimen and a surface-notched plate in air.

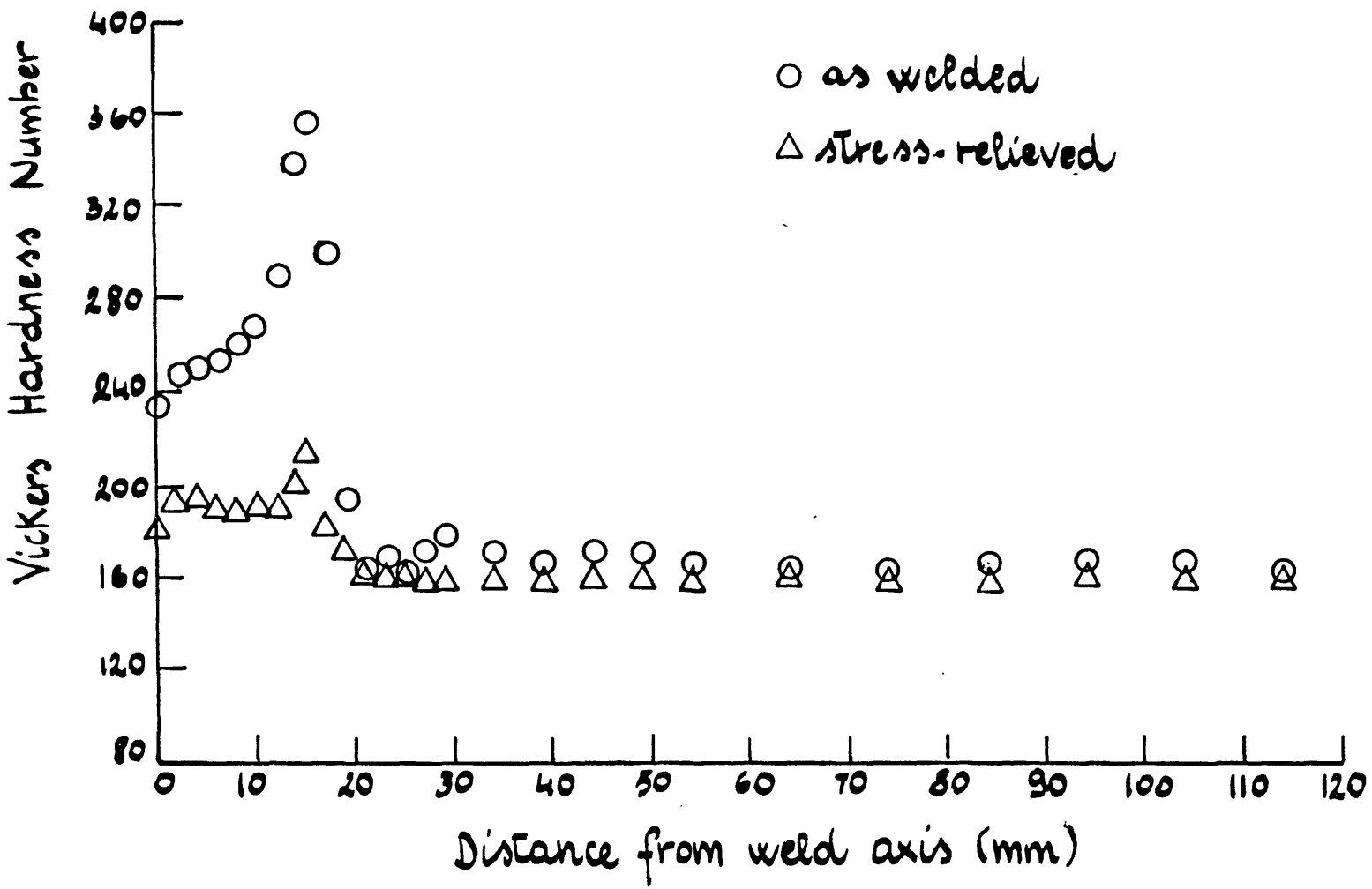


Figure 5.22 VHN hardness across 'as received' and 'stress-relieved' welds

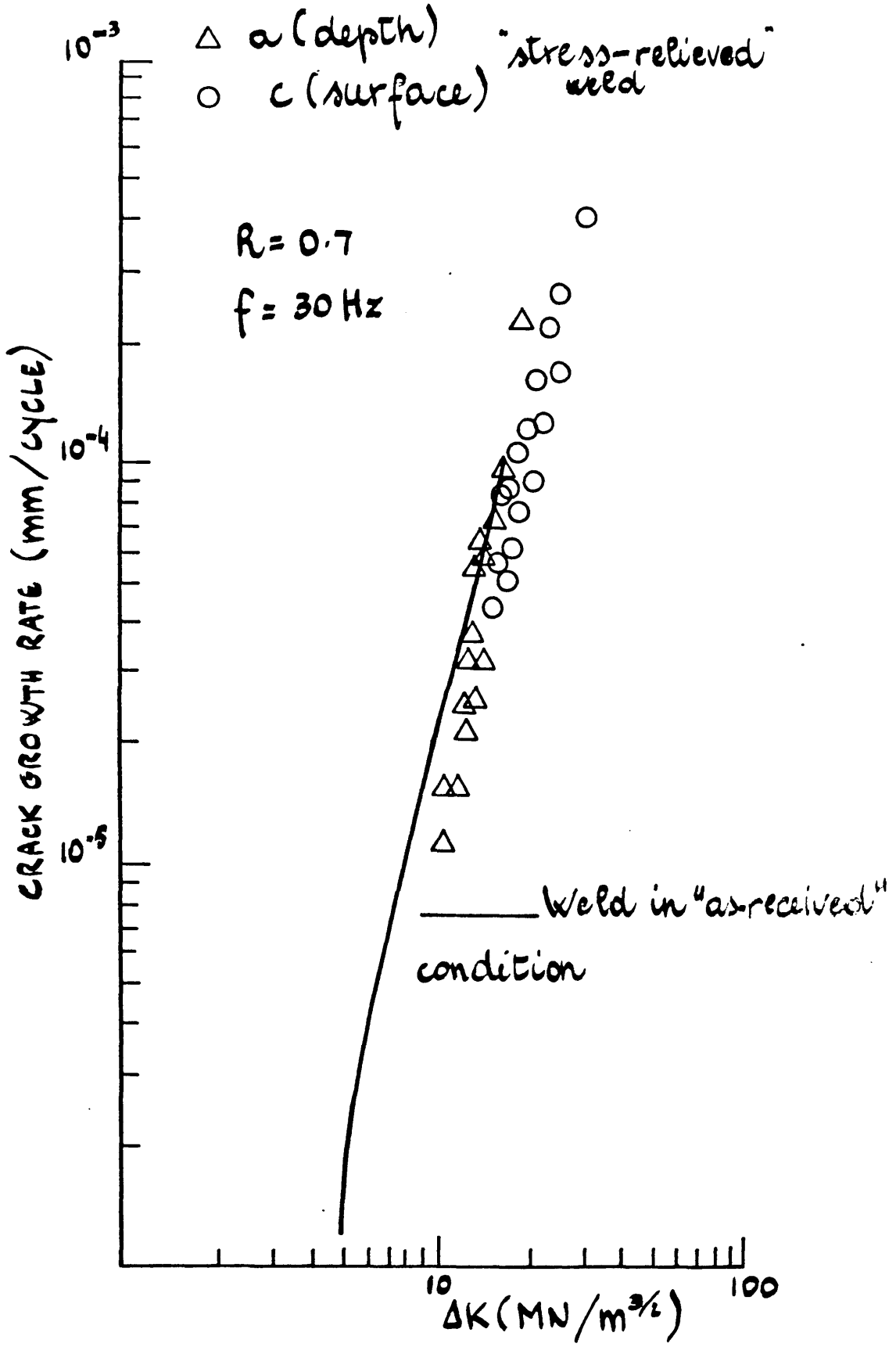


Figure 5.23 Effect of stress-relieving on crack propagation of butt-welded joints using SNP geometry in air.

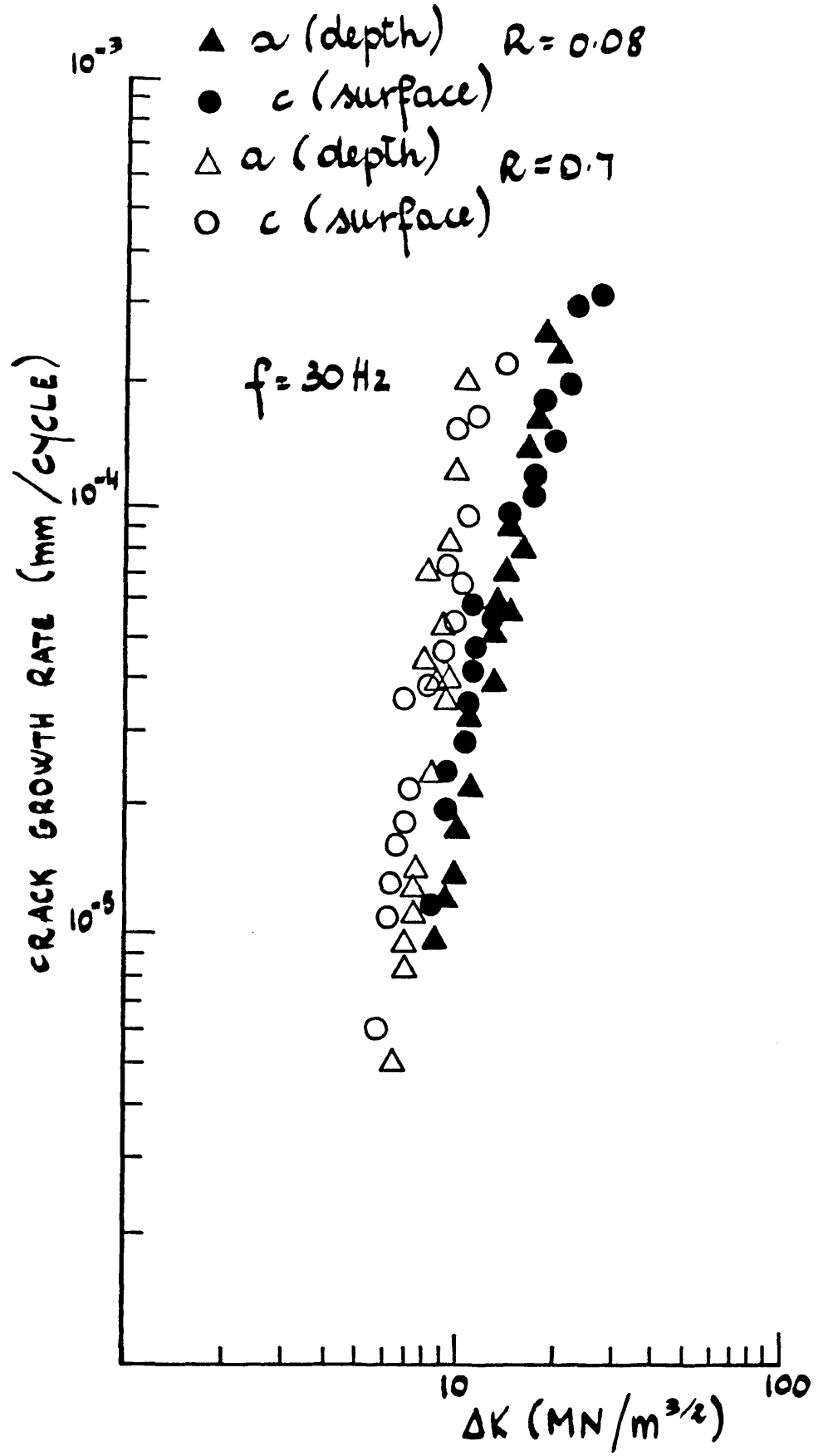


Figure 5.24 Effect of stress ratio on weldment in salt water environment.

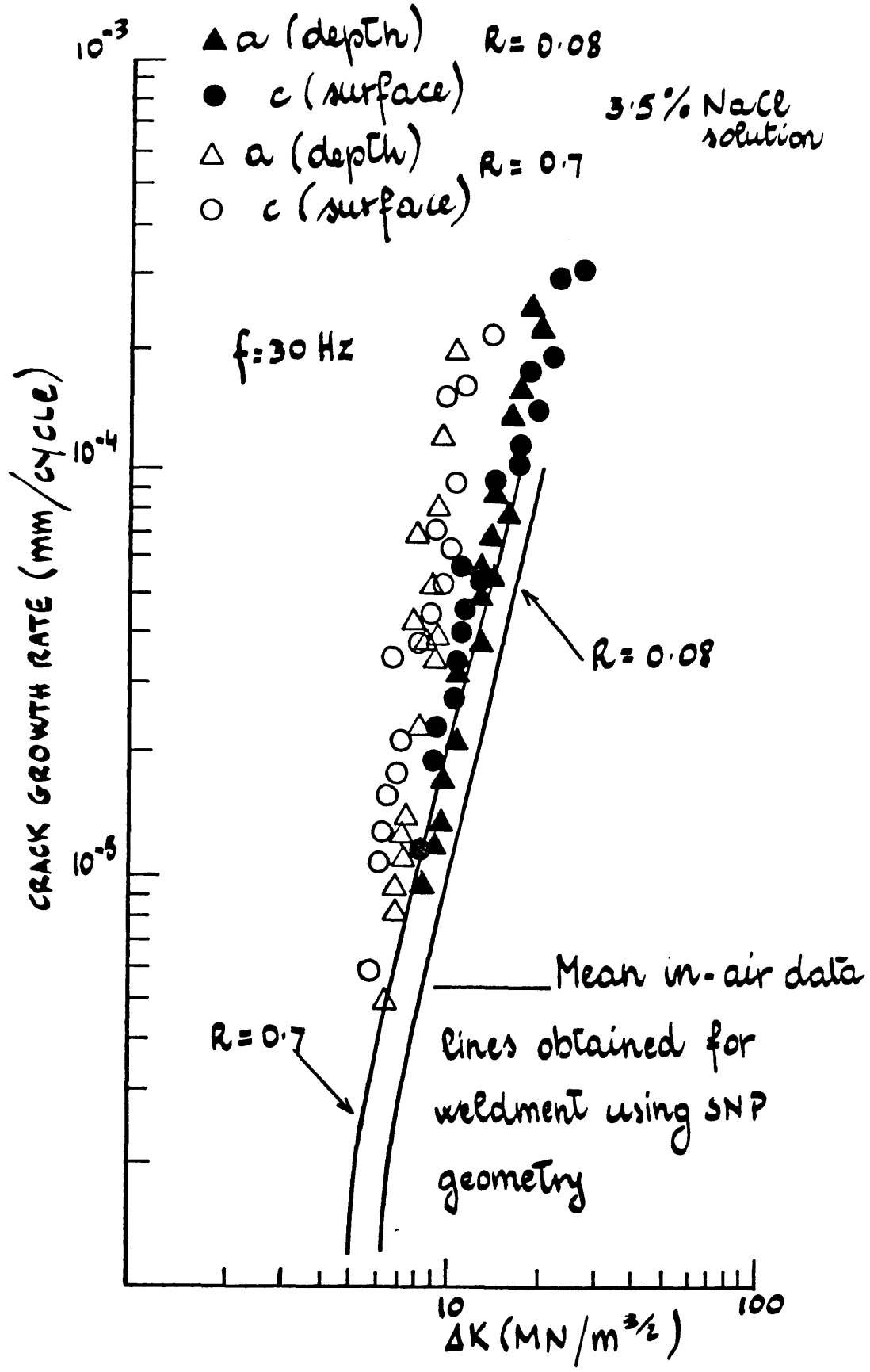


Figure 5.25 Comparison of results obtained for weldment in air and in salt water.

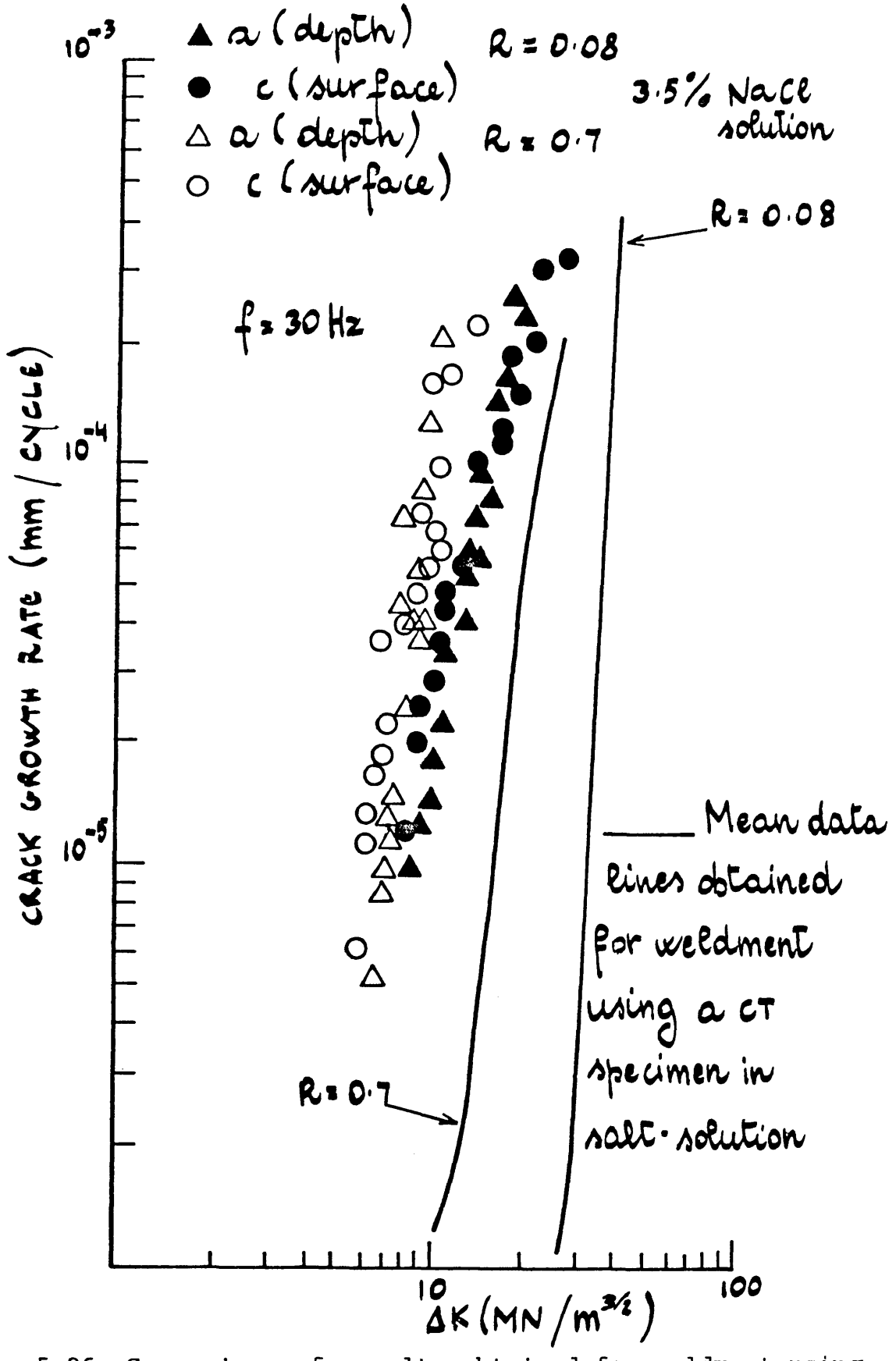


Figure 5.26 Comparison of results obtained for weldment using CT and SNP geometry in salt solution.

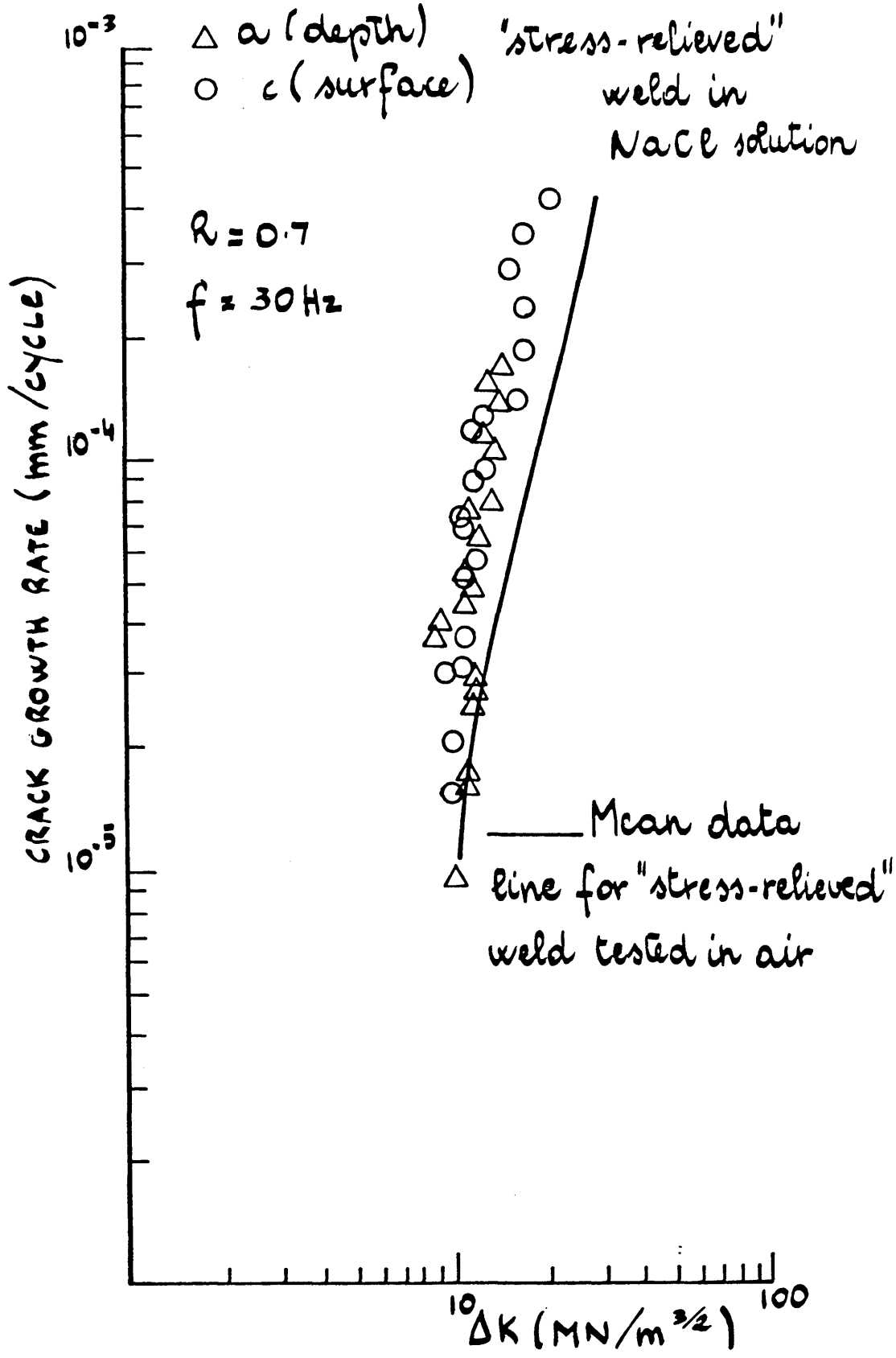


Figure 5.27 Effect of salt solution on 'stress-relieved' weld using SNP geometry.

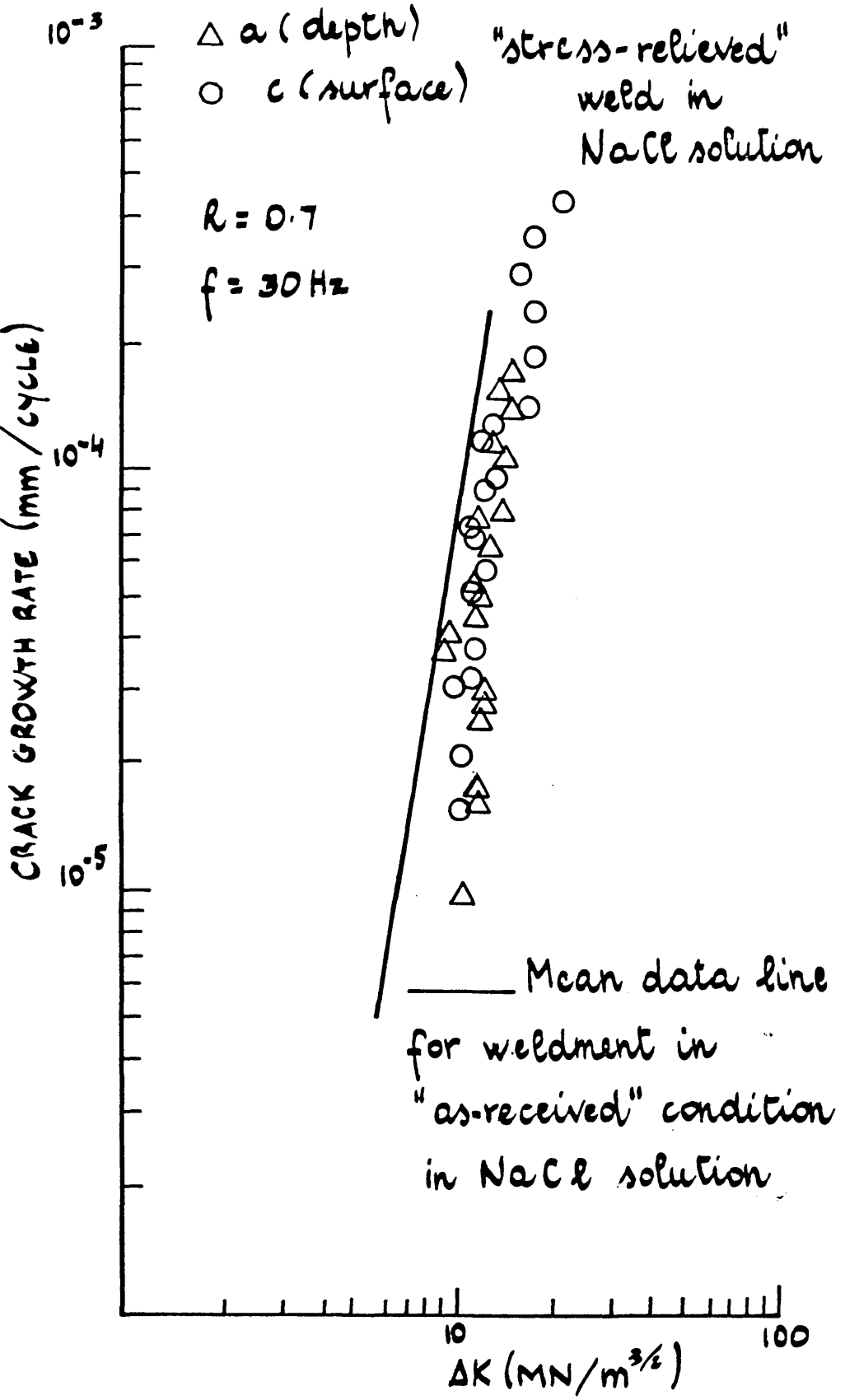


Figure 5.28 Effect of 'stress-relieving' on crack growth of weldments using SNP in salt solution.

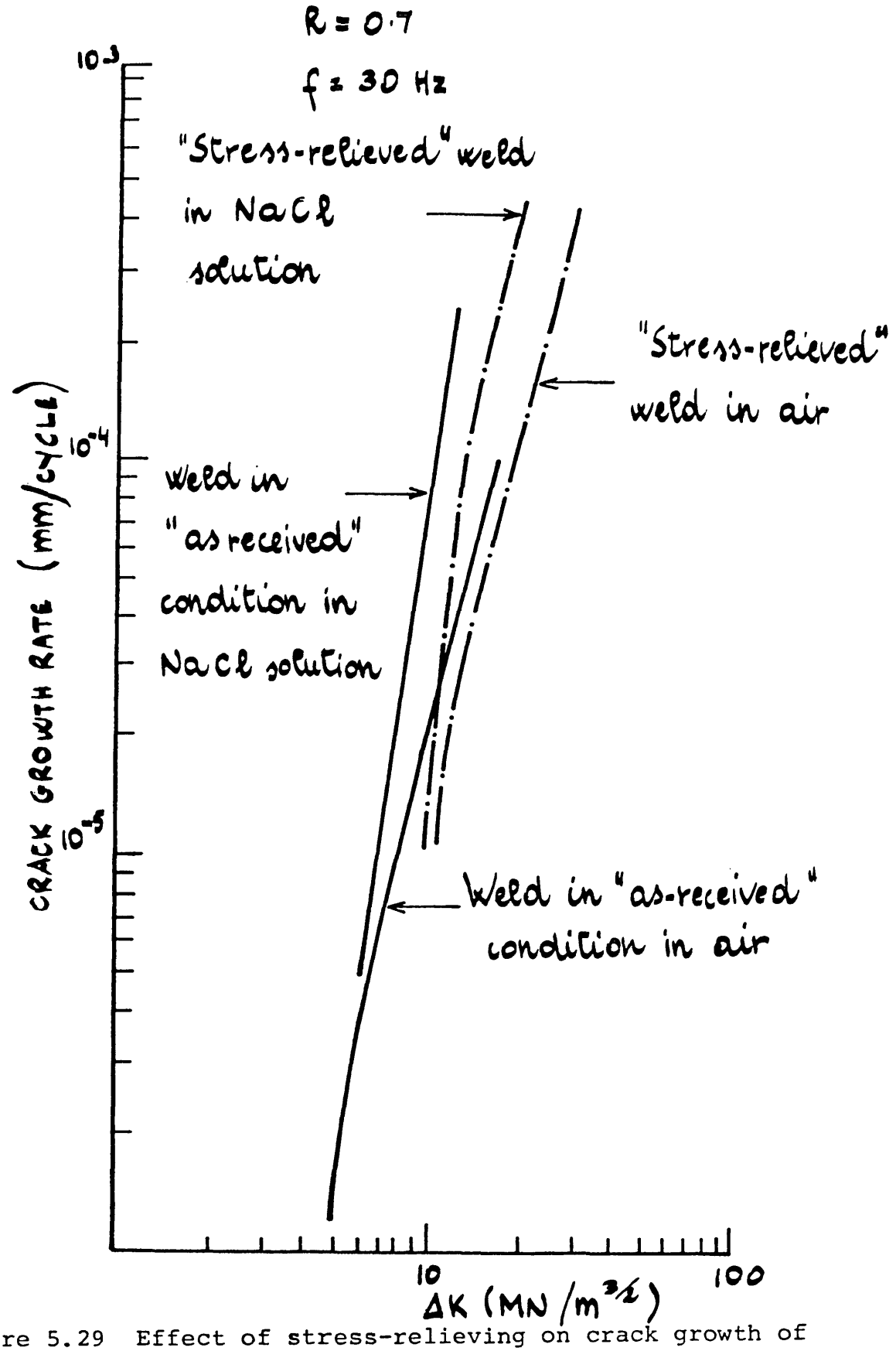


Figure 5.29 Effect of stress-relieving on crack growth of weldments in air and salt water environments using SNP geometry.

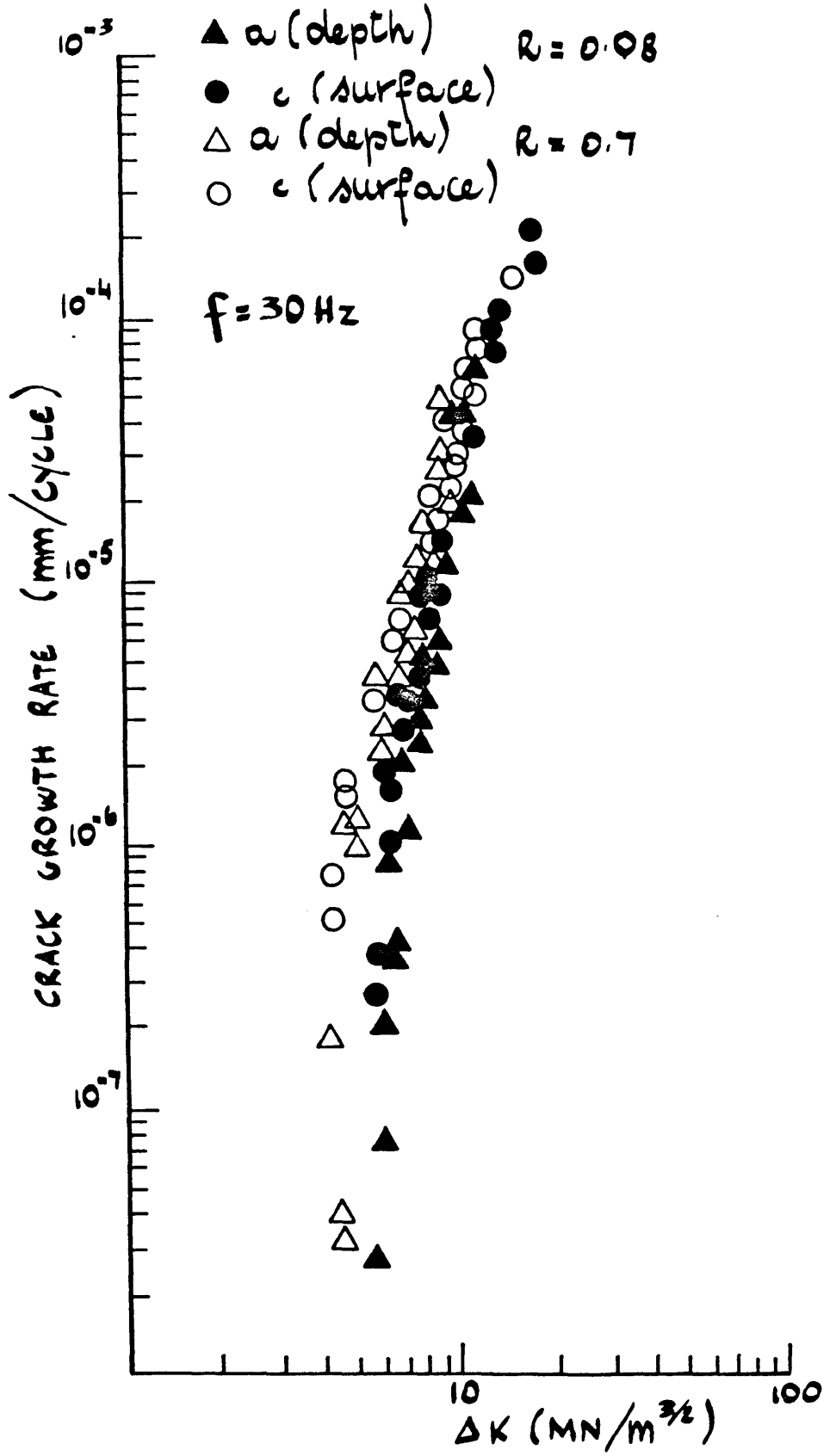


Figure 5.30 Effect of stress ratios on HAZ using SNP geometry in air.

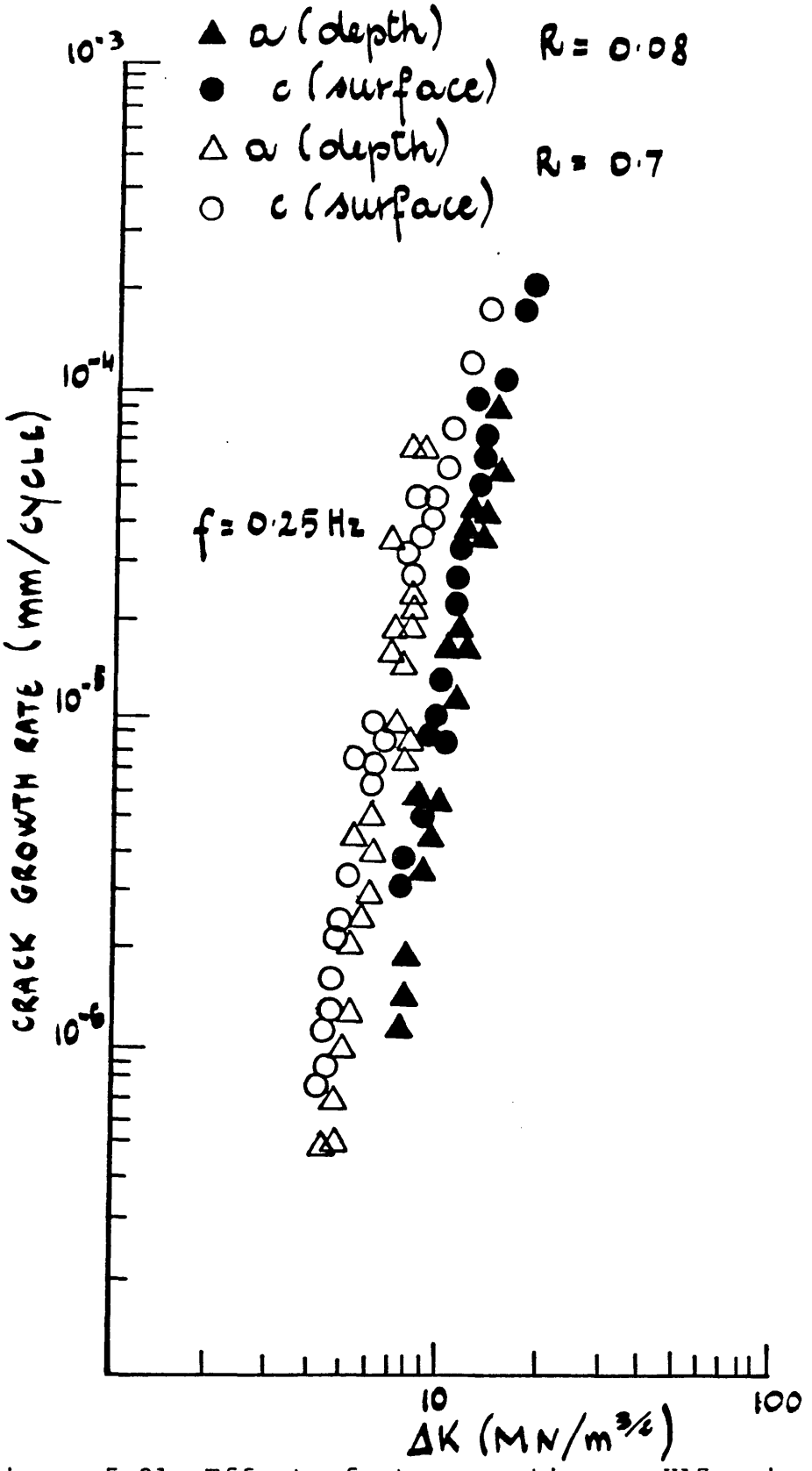


Figure 5.31 Effect of stress ratios on HAZ using SNP geometry in air.

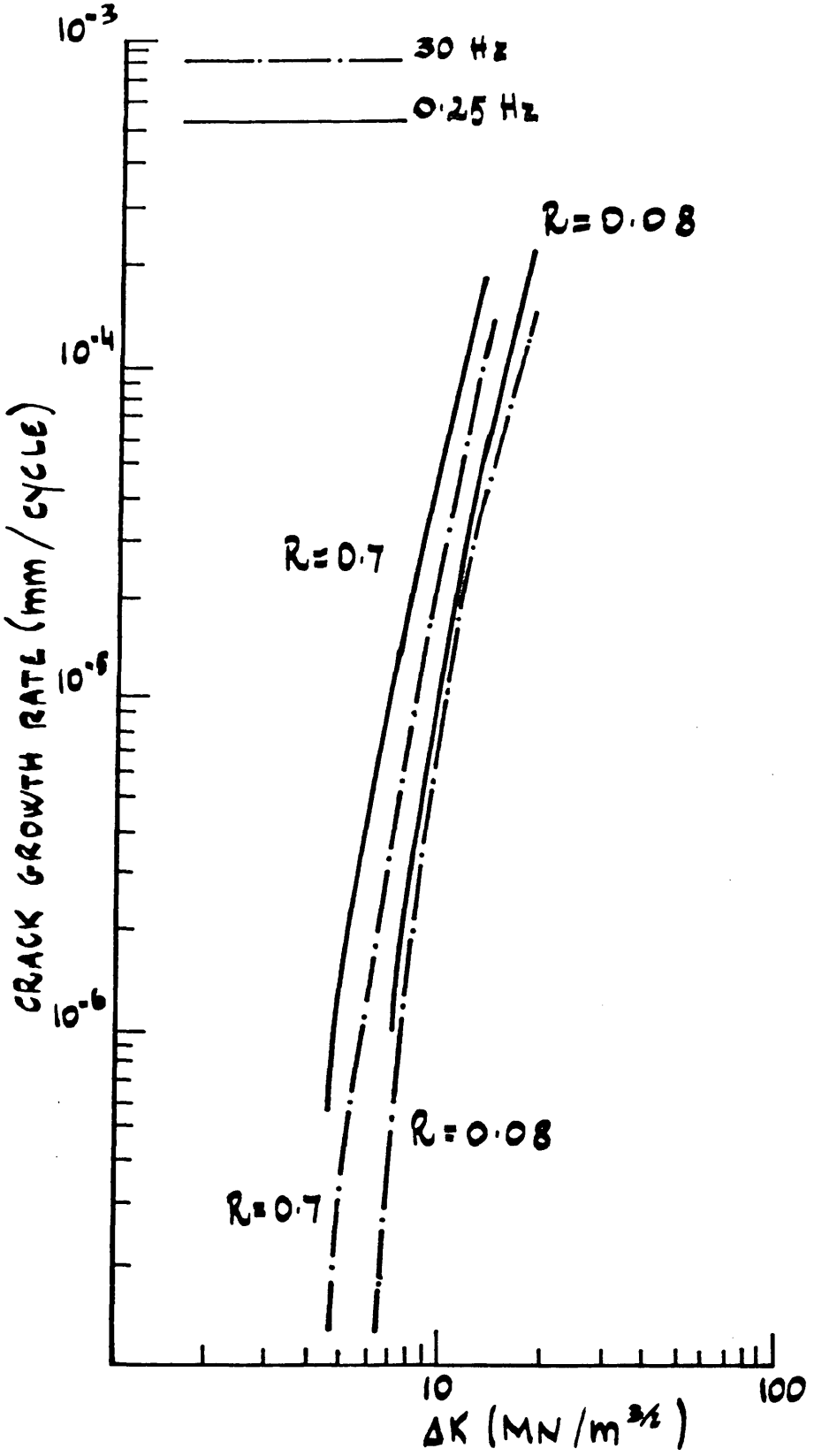


Figure 5.32 Effect of frequency on HAZ using SNP geometry in air.

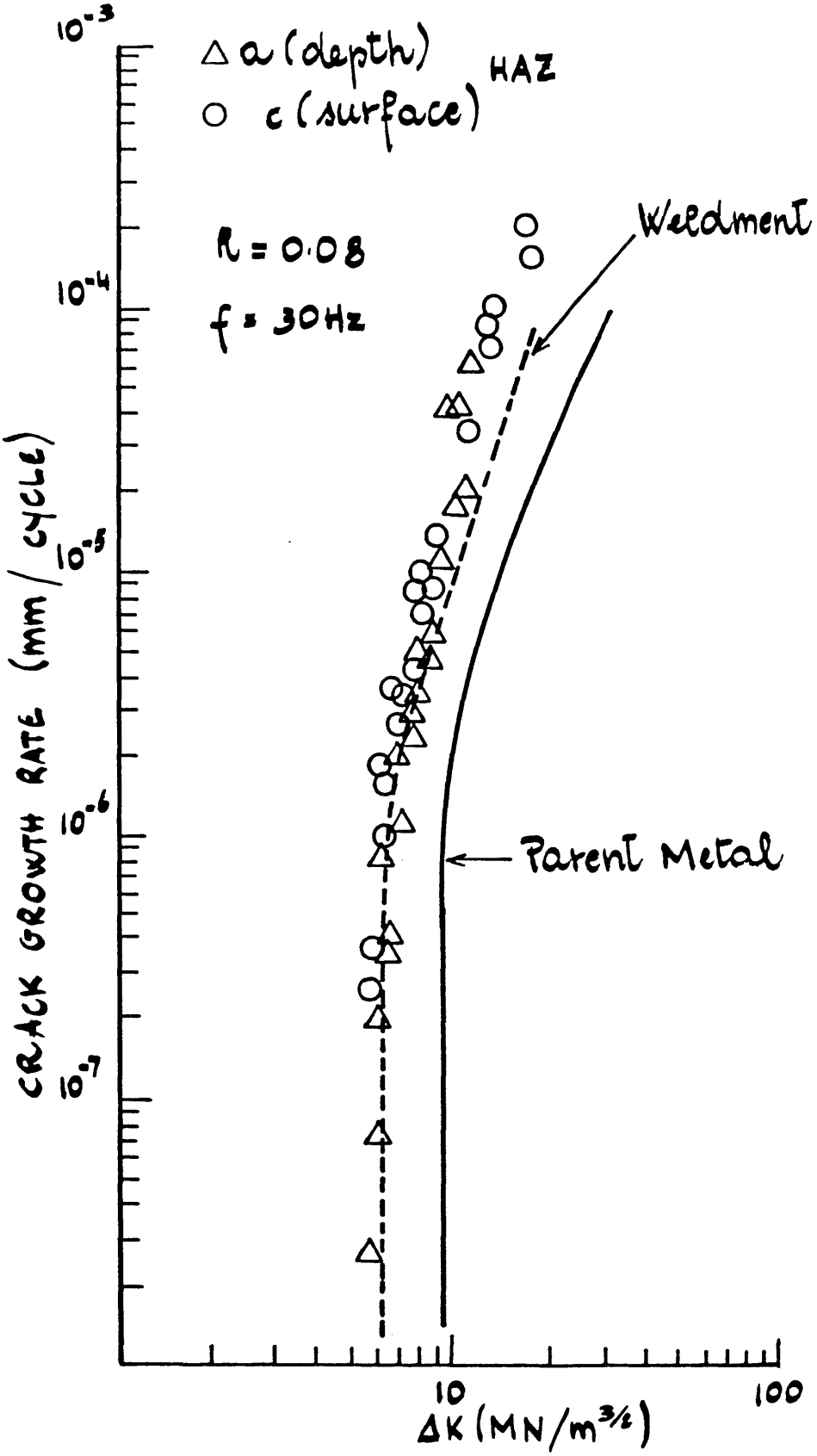


Figure 5.33 Comparison of the results obtained for HAZ, weldment and parent metal using SNP geometry in air.

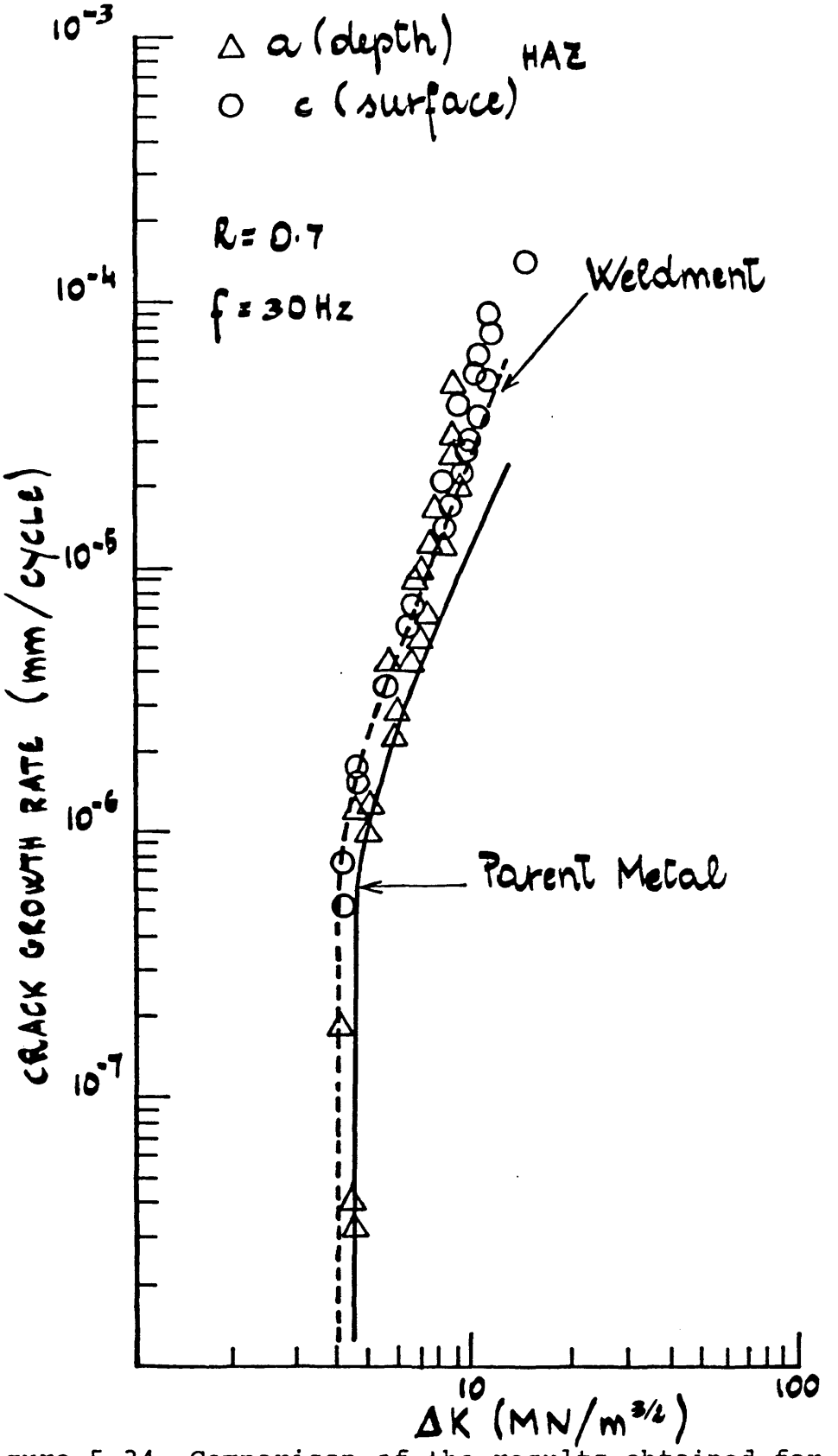


Figure 5.34 Comparison of the results obtained for HAZ, weldment and parent metal using SNP geometry in air.

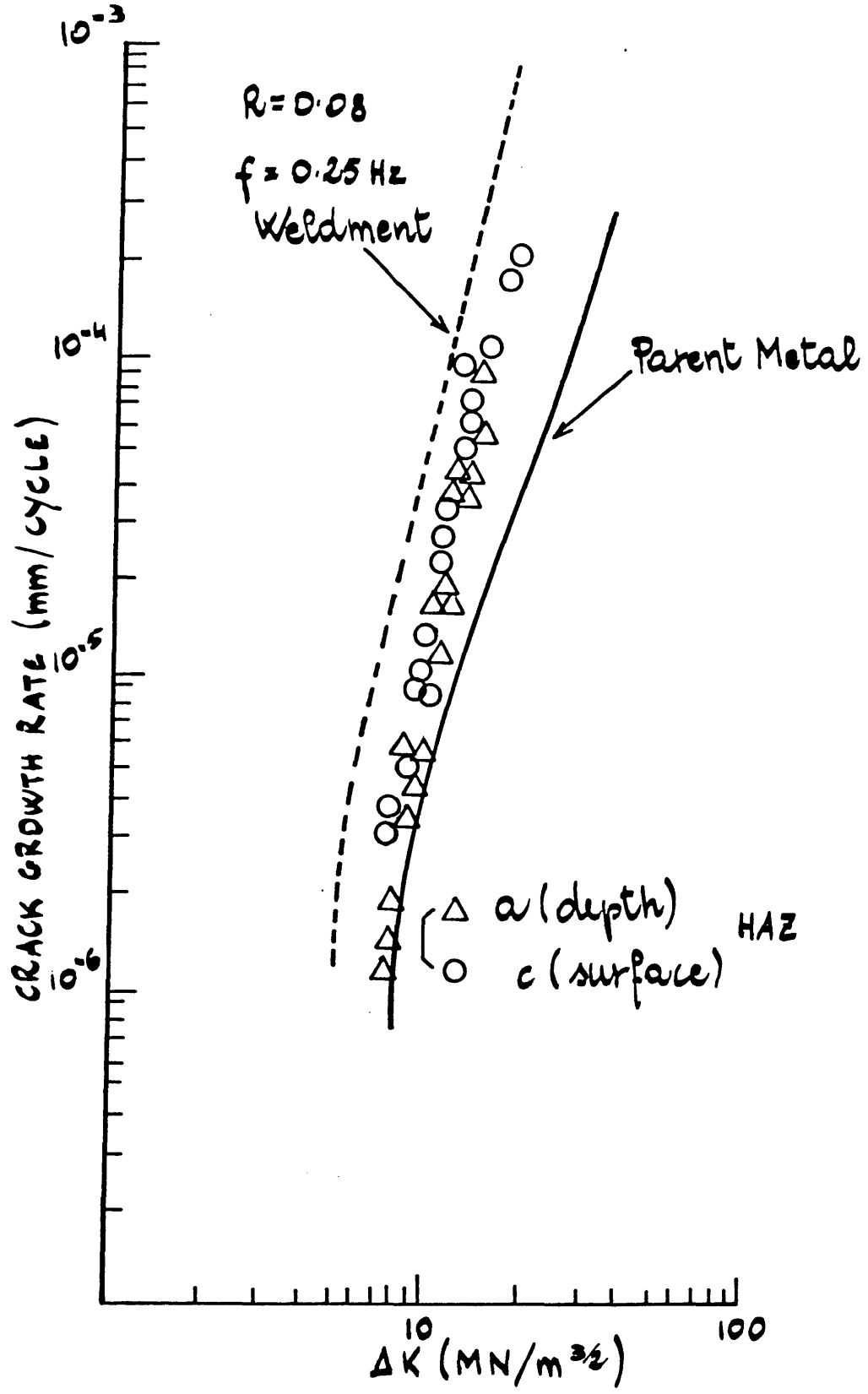


Figure 5.35 Comparison of the results obtained for HAZ, weldment and parent metal using SNP geometry in air.

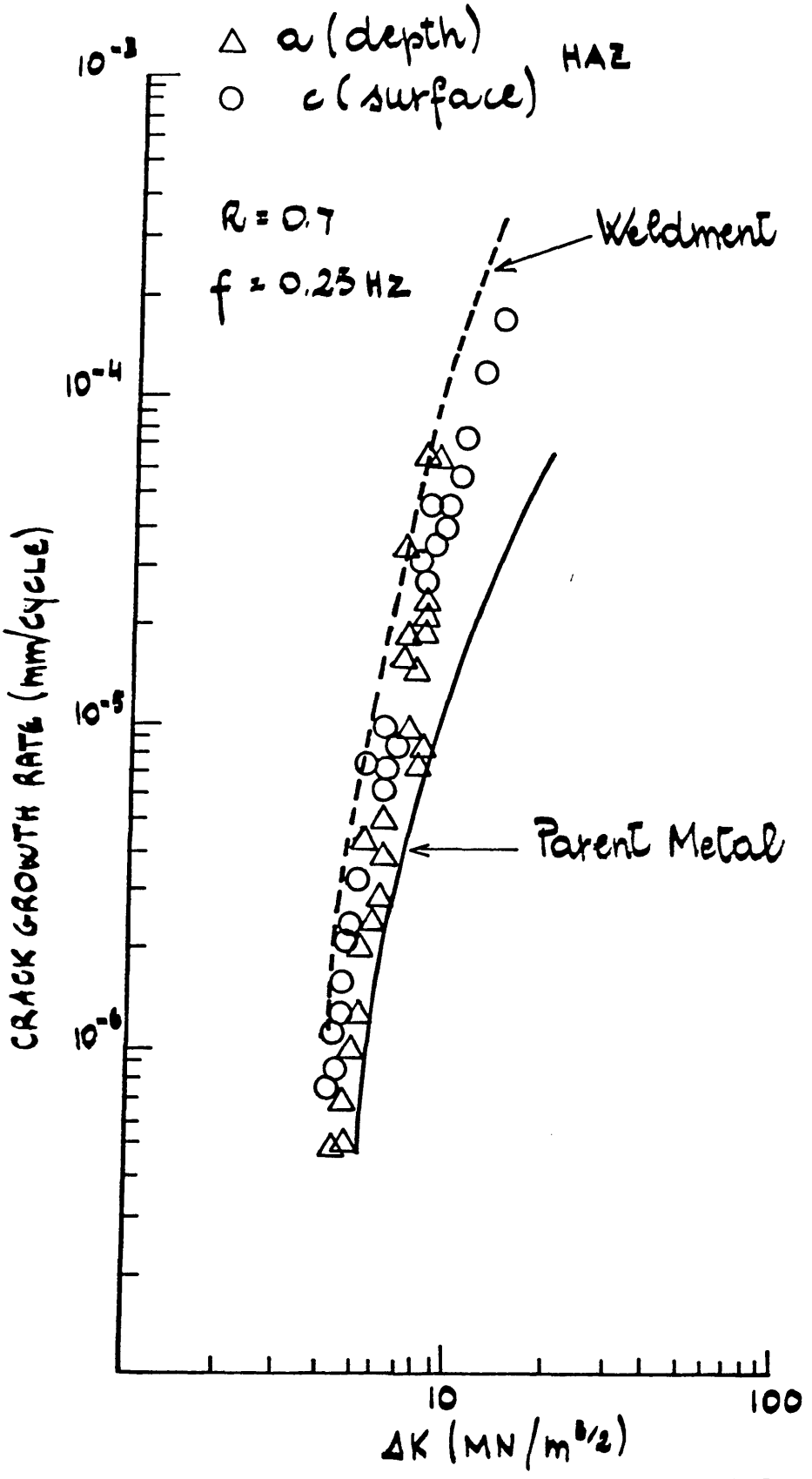


Figure 5.36 Comparison of the results obtained for HAZ, weldment and parent metal using SNP geometry in air.

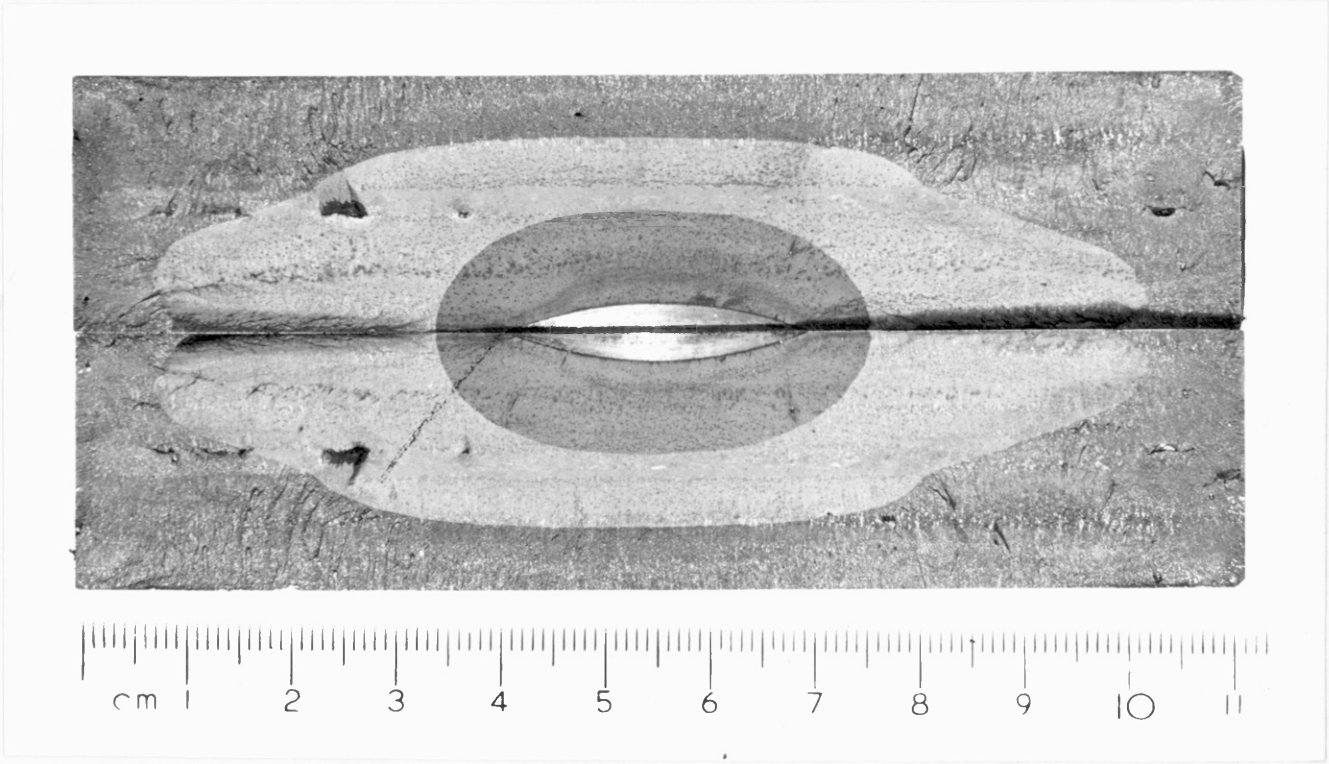


Figure 5.37 Cross-section of failed butt-welded specimen (mating halves) with notch located on compressive side showing "turn-back zone".

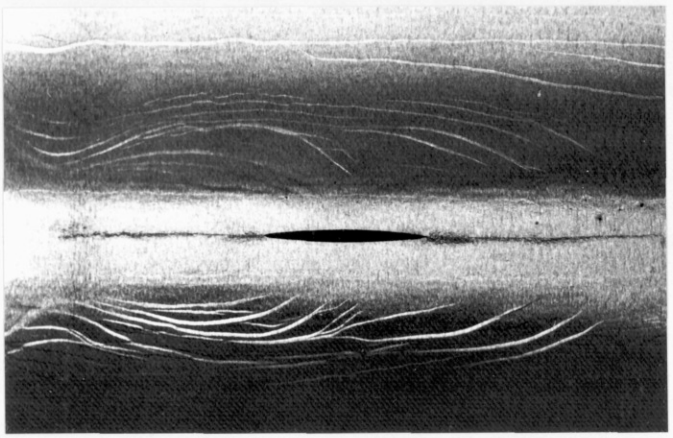


Figure 5.38 Local yielding on the surface of welded specimens as a result of high residual tensile stress

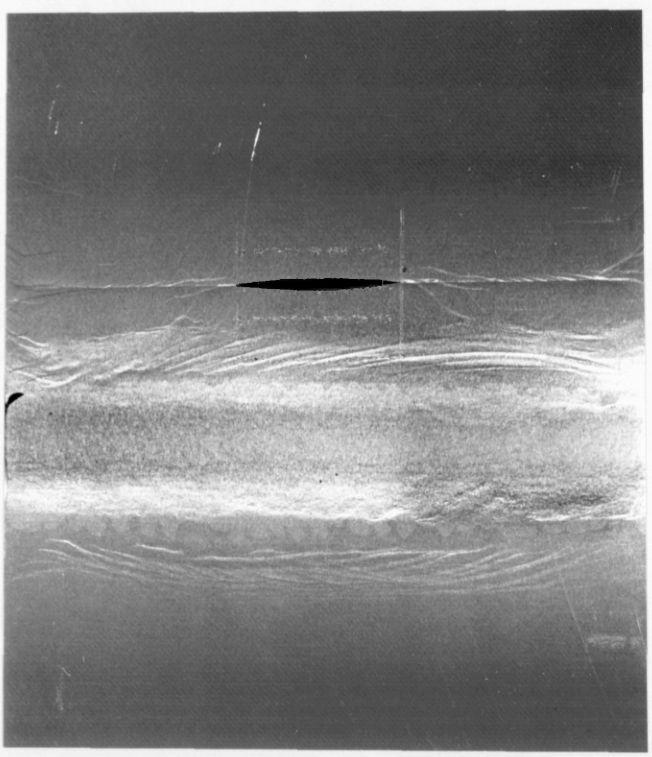


Figure 5.39 Local yielding around the weld in a specimen with the notch away from the weld

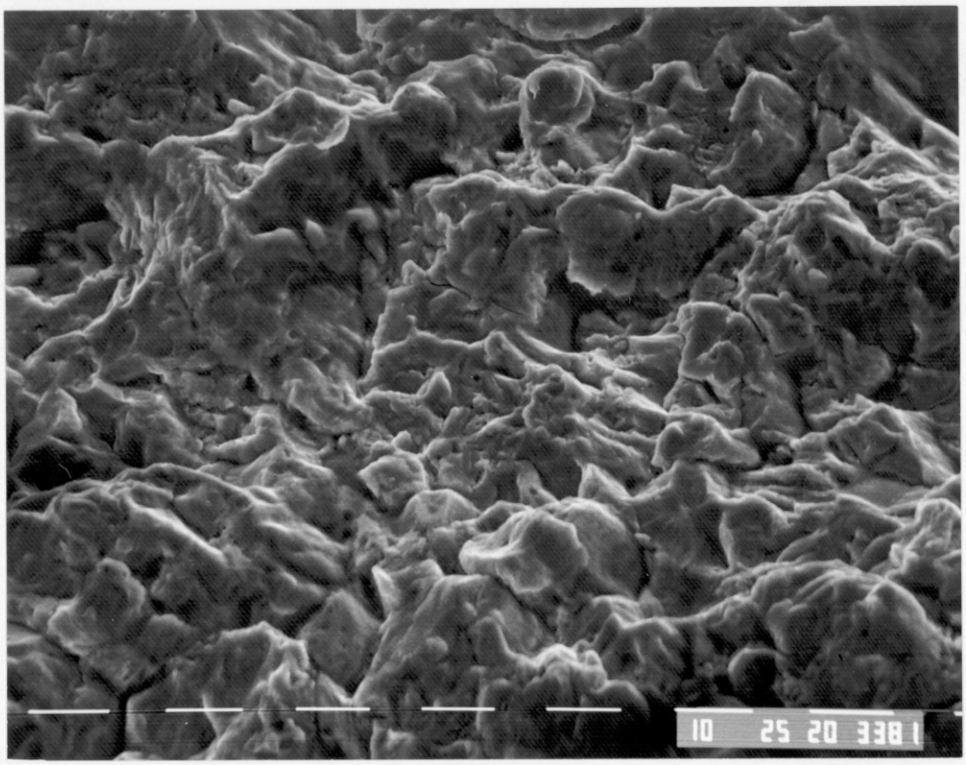


Figure 5.40 SEM photograph of HAZ illustrating intergranular fracture

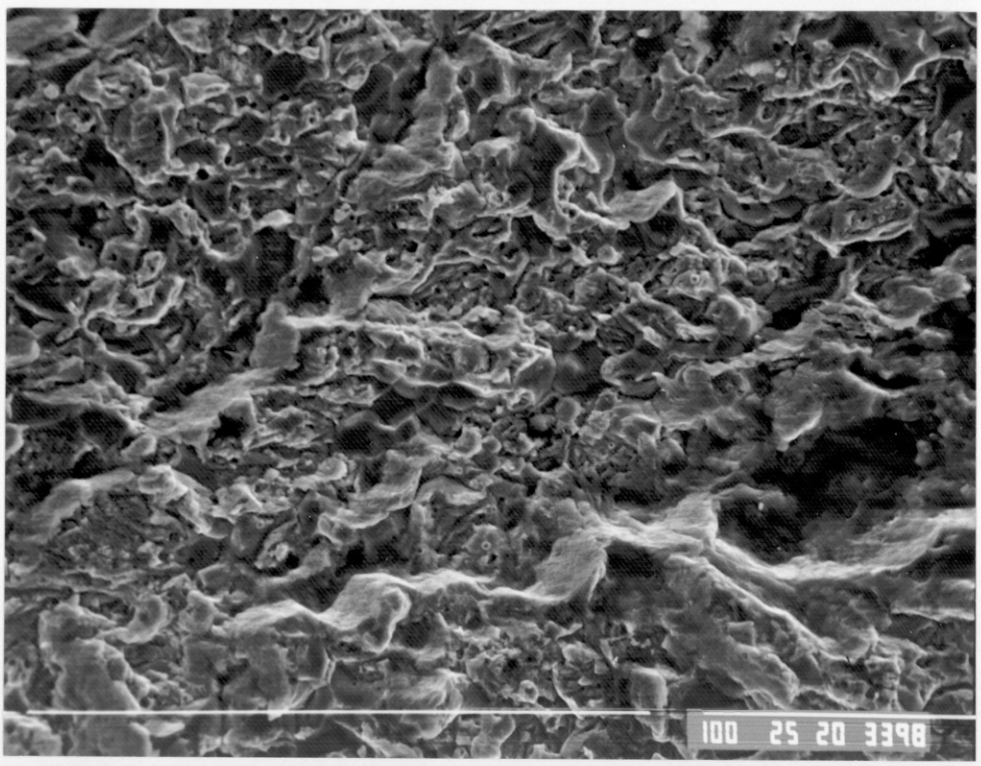


Figure 5.41 HAZ fracture surfaces showing transgranular fracture mechanism

CHAPTER 6

COMPUTER SIMULATION OF SURFACE CRACK PROPAGATION

6.1 INTRODUCTION

Surface notches and flaws in welded structures have long been recognised as major sources of potential failure. The subcritical or stable flaw growth stage usually involves complex geometric shapes and varying stress intensity levels along the flaw border, resulting in a very complex class of three-dimensional cracked body problems. However, progress in numerical methods of analysis and improved computer storage capacities are resulting in more powerful approximate methods.

In predicting crack growth, the linear elastic fracture mechanics approach is usually adopted. This approach is especially convenient if the stress intensity factor distribution along the surface crack perimeter has been established. As discussed in detail in Chapter 3, the solutions obtained for the stress intensity factor for a surface crack by different investigators disagree with each other, in some cases considerably. Therefore it can be concluded that a correct prediction of the growth of surface cracks depends on an exact calibration of stress intensity as well as on the uniformity of the material resistance to cracking. If crack growth is estimated under these conditions, the results are more likely to agree with experimentally observed crack development.

Surface cracks are known to change shape as they grow, under certain conditions. Thus it is desirable to be able to predict the changes of shape, as related to flaw shape, width and thickness, in order to determine if fracture will occur either as a part-through crack or as a through crack.

Analysing the fatigue data obtained during this investigation for surface cracks, it was shown that the stress intensity calibration (Equations (3.12) and (3.13)) correlated well with the results obtained for CT geometry. This foundation gives confidence in predicting the growth of surface cracks.

6.2 FATIGUE CRACK GROWTH MODEL

Paris [8] first proposed a fatigue crack propagation law as:-

$$\frac{da}{dN} = C\ (\Delta K)^m \qquad .(2.12)$$

Subsequent investigators [32-36] have modified Equation (2.12) to take account of a variety of factors including stress ratio, crack closure, threshold stress intensity and the critical stress intensity of fracture. One of these modifications, proposed by Branco et al [32], is given by:-

$$\frac{da}{dN} = A\,\phi^{\alpha} \qquad ,(6.1)$$

$$\phi = \frac{(1-R^2)(\Delta K^2 - \Delta K\ \Delta K_{th})}{K_{1c}^2\ (1-R)^2 - \Delta K^2} \qquad ,(6.2)$$

where A and α are constants.

Equation (6.1) is used in the present investigation to predict crack growth and propagation life. This is achieved by a computer program that numerically integrates the equation cycle by cycle to obtain the crack increment and hence the crack length. The constants used in Equations (6.1) and (6.2), A, α, and ΔK_{th}, were determined empirically from the results of the fatigue tests on the base metal and weldment described in the previous chapter; K_{1c} for base metal is given by Radon [202] but was estimated for the weldment. It was assumed that the threshold values of stress intensity for 0.25Hz and 30Hz are the same.

As discussed in Chapter 5 there was a slight difference in the slope of the growth rate curves for the crack at the free surface and at the deepest point of the crack front, probably due to different states of deformation (i.e., plane stress and plane strain), resulting in slight differences in A and α. Equation (6.1), which was used to obtain the new crack shape and size at the (i+1)th increment of ΔN_i cycles crack growth, was expressed in the form of:-

$$a_{i+1} = a_i + A_a \Phi\ (a_i, c_i, \theta=0)^{\alpha_a} \Delta N_i \qquad ,(6.3)$$

$$c_{i+1} = c_i + A_c \Phi\ (a_i, c_i, \theta=\frac{\pi}{2})^{\alpha_c} \Delta N_i \qquad ,(6.4)$$

$$N_{i+1} = N_i + \Delta N_i \qquad ,(6.5)$$

where subscripts a and c denote fatigue crack properties through the thickness and at the free surface, respectively.

The use of Equation (6.1) implies a relationship between $\log(da/dN)$ and $\log(\Delta K)$ from a threshold stress intensity factor, ΔK_{th}, to fracture.

6.3 PREDICTION OF SURFACE CRACK GROWTH UNDER BENDING LOADS IN STEEL AND WELD METAL

Computer runs were made in which the crack growth rates for a given applied stress, plate geometry and initial crack configuration were simulated by allowing the crack to grow for between 100,000 and 200,000 cycles.

Figs. 6.1 to 6.4 compare experimentally determined relationships between c and a with the results obtained from computer simulation for both steel and the weldment. Predicted values of a and c were obtained from the numerical integration of Equation (6.1), and an applied bending stress

of approximately $0.4\sigma_y$ was applied to both steel and the weldment. The second order equations obtained in order to relate predicted a and c for different testing conditions are as follows:-

For BS4360-50D steel,

$$a = -6.79 + 0.87c - 0.90 \times 10^{-2}c^2 \quad ,(6.6) \text{ at } R=0.08$$
$$a = -7.66 + 0.92c - 0.93 \times 10^{-1}c^2 \quad ,(6.7) \quad R=0.7 \quad \Big\} \; f=30Hz$$

$$a = -5.79 + 0.79c - 0.81 \times 10^{-2}c^2 \quad ,(6.8) \text{ at } R=0.08$$
$$a = -6.95 + 0.87c - 0.89 \times 10^{-2}c^2 \quad .(6.9) \quad R=0.7 \quad \Big\} \; f=0.25Hz$$

For the weld metal,

$$a = -5.48 + 0.85c - 0.93 \times 10^{-2}c^2 \quad ,(6.10) \text{ at } R=0.08$$
$$a = -5.76 + 0.89c - 0.96 \times 10^{-2}c^2 \quad ,(6.11) \quad R=0.7 \quad \Big\} \; f=30Hz$$

$$a = -6.69 + 0.96c - 0.12 \times 10^{-1}c^2 \quad ,(6.12) \text{ at } R=0.08$$
$$a = -5.99 + 0.88c - 0.99 \times 10^{-2}c^2 \quad .(6.13) \quad R=0.7 \quad \Big\} \; f=0.25Hz$$

The correlation coefficient between the above equations and the experimental a and c is in excess of 0.98.

The predicted crack propagation contours are presented in Figs. 6.5 and 6.6 for the base plate and weldment, respectively. As can be seen in these figures, for the initial crack configuration used the crack growth rate appears to increase from the surface to the centre of the crack.

To investigate the behaviour of the crack when it penetrates across the width of the plate, the problem was treated as a single-edge cracked bend specimen using the appropriate stress intensity calibration recommended [203]:-

$$K = Y \frac{6Ma^{\frac{1}{2}}}{Bw^2} \qquad ,(6.14)$$

$$Y = 1.99 - 2.47(a/w) + 12.97(a/w)^2 - 23.17(a/w)^3 + 24.8(a/w)^4 \qquad ,(6.15)$$

where a/w is no greater than 0.6 and M is the bending moment in three-point or four-point bending. The results are presented in Fig. 6.7 for the base plate showing that when the crack on the surface penetrates the width it continues to grow on the sides of the plate until it is reasonably straightened. The final contours shown in Fig. 6.7 appear to be part of an ellipse, but more work is needed to come to any firm conclusion on this.

6.3.1 Effect of Geometry

Fatigue of surface crack propagation was predicted for two thicknesses, i.e., 19mm and 38mm sections. The crack propagation contours are shown in Fig. 6.8. It can readily be seen from this figure that the life of the plate is considerably reduced by increase in thickness. Comparing the life of the 38mm plate to that of the 24mm plate used in the experimental study, there is a reduction of approximately 15% in the total number of cycles to failure in identical mechanical conditions.

The effect of width on a surface crack was also predicted for three widths, i.e., 500mm, 1000mm and 1500mm. The surface crack propagation contours are presented in Fig. 6.9. A comparison of these results is especially interesting since they indicate that a surface crack in a bending stress field does not appear to transform to a through-thickness crack. The results also indicate that increase in width increases the life of the plate, for example, the total number of cycles to failure for widths of 1500mm and 1000mm are up by 69% and 44% respectively, than that for the 500mm-wide plate.

6.3.2 The Influence of Initial Flaw Size and Shape

The ratio of a/c can be controlled either by adjusting the crack length and keeping the crack depth constant or by changing the crack depth and keeping the crack length constant. Both procedures will yield the same values of a/c

but, as will be seen later, will result in considerably different crack growth rates and propagation profiles. This adjustment is referred to here as "fixed a" when c is changed, and "fixed c" when a is changed, to produce an initial crack configuration.

Two initial crack configurations were used in the simulation of fatigue crack growth, namely, a/c=0.1 and a/c=0.8. The crack propagation profiles are shown in Fig. 6.10 for fixed c and in Fig. 6.11 for fixed a for the case of parent plate. The equivalent results for weldment are shown in Figs. 6.12 and 6.13, respectively. A considerable difference in crack growth rates can be observed between the initial crack configurations produced by fixed a and fixed c, and there is also a significant difference in growth rates both in the through-thickness direction and at the free surface for a particular value of a/c produced by fixed a and fixed c. It is interesting to note that for a fixed value of a/c the life of the sections seems to increase at fixed c, for example, at a/c= 0.1, and that fixed c failure occurs at 1.4×10^6 cycles which is 71% higher than for the case of fixed a. Therefore it appears that elongated inclusions or a collection of round inclusions lying side-by-side may be particularly detrimental to the fatigue strength of butt-welded joints. Comparing initial a/c ratios of 0.1 and 0.8 at fixed c, it can be seen that the crack commences to grow in the through-thickness direction when a/c is small (i.e., 0.1). However, the variation in propagation of the deepest point at a/c=0.8 seems to be

minimal. This is probably due either to the large difference between the stress intensity factors experienced by the crack at the free surface and at the deepest point of the crack, or to the stress gradient due to bending, or a combination of both.

The prediction of the pattern of growth for any crack is defined by the initial crack configuration as shown in Figs. 6.14 and 6.15 for the base plate, and in Figs. 6.16 and 6.17 for the weldment, for fixed c and fixed a, respectively. An interesting feature of all growth curves at fixed a is their tendency to join a common curve. This trend has been observed previously by Corn [204] and Burk [205]. Corn has labelled it the "preferred propagation path". However, at fixed c, extrapolated growth curves tend to intersect at a point with a/B approximately equal to 0.65. The growth curves $a/c<0.5$ for fixed a and $a/c<0.3$ for fixed c appear to emanate from the origin.

The straight line result for $a/c=0.1$ at fixed a for the parent plate is due to the notch geometry used in the experimental part of this investigation, as at fixed a (i.e., a=5.5mm), the crack length at the free surface needed to produce an initial a/c of 0.1 would be 110mm. Therefore an elongated initial crack is produced which is analogous to the single-edge cracked plate.

Finally, a comparison of change in crack shape in the parent metal and weldment at a/c=0.4 was made and is presented in Fig. 6.18 for fixed c and in Fig. 6.19 for fixed a. The slight difference in crack shape observed is attributed to the material properties of the base plate and weld metal whose yield strengths varied by approximately 14%.

6.4 DISCUSSION

The model described in this chapter appears to provide reasonably accurate predictions for surface cracks. It is not exceptional in this respect since similar claims have been made in other studies reviewed in Chapter 2. However, due to its ability to accommodate fatigue crack propagation both at the free surface and in the through-thickness direction from threshold to fracture, the model is able to provide additional useful information. Recent analytical crack growth programs [206], in which the changing crack contour is taken into account, apply only to tension loading. Although some attempts have been made at the computer simulation of a surface flaw in a bending stress field [207,208], no current program takes account of complex shape changes in the transition from low growth rates to medium and high growth rates in such stress fields.

Comparisons between the predicted and experimental results were made on the basis of crack growth rate and c versus a curves. The results show an extremely good

correlation. The second-order equations for expressing the crack length in the through-thickness direction in terms of crack length at the free surface can be used for estimating the crack depth without the use of complex measuring devices which in turn involve lengthy mathematical processing of raw data.

With respect to the effect of geometry there is little guidance in the literature as to the real effect of thickness on fatigue crack growth; what there is, is contradictory. Despite this shortcoming, design engineers performing growth analysis tend to extrapolate the growth rate data to thicker or thinner sections as a routine engineering approximation. The wisdom of this practice is doubtful judging from the conflicting results reported in the literature on thickness effects on growth rates. Three types of thickness effect have been reported by previous investigators: (i) no effect due to thickness [209]; (ii) growth rates accelerated by increase in thickness [210]; (iii) growth rates accelerated by decrease in thickness [211]. The present results concerning the effect of thickness predict that growth rates increase with increase in thickness, and cast some doubt on the results obtained by Thorpe et al [175] whose work was described in the previous chapter.

The thickness effect observed seems to be reasonable since the effect of the stress gradient on the deepest point

of the crack would be less for a thicker section than for a thinner section containing a flaw with an identical initial a/c ratio. Since, for a thin section in a bending stress field, the position of the neutral axis, being closer to the deepest point of the initial flaw than in a thicker section, would restrict the growth in the through-thickness direction, it will take a longer time for the crack to take up stable shape. It is therefore proposed that the observed effect of thickness could be explained in terms of steady load cracking which favours the thicker specimens as explained above.

The effect of width was investigated to see whether a surface crack can transform into a through-thickness crack, as was suggested by Pierce and Shannon [212]. They proposed that the through-crack produced by the extension of a surface crack in a bending stress field would have a length ten times the section thickness. However, the crack growth simulated for sections having upto 1500mm width did not show any tendency to transform to a through-thickness crack. To ensure that this was the case the crack growth was simulated for a section having 2500mm width, although the results are not separately presented because of the unrealistic proportions of such a section. The maximum crack depth obtained was 24.14mm in a section having a 25.4mm thickness and initial a/c=0.28; the final aspect ratio was 0.02. A simplified model of bending stress distribution would predict that the deepest point of the crack would asymptotically approach the mid-thickness where the stress

is zero and compressive beyond it. However, this does not appear to be the case as the data obtained here indicate that the thickness will be penetrated by the crack to a depth of approximately five-eighths of the thickness. Therefore it can be concluded that increasing the width does result in an increase in crack depth, but, for the cases predicted here, as well as for realistic geometric ratios, a part-through surface crack does not appear to penetrate the thickness in a bending stress field.

Initial crack configurations with a low aspect ratio at fixed a are liable to cause earlier failure since they appear to be able to develop to a stable shape more quickly. From this point onward the number of cycles to failure is about the same irrespective of initial crack configuration. However, when c is fixed the behaviour of the surface crack seems to be the opposite of that described above: the low aspect ratio cracks appear to have longer lives. All the growth curves for this case appear to intersect at one point when extrapolated, implying that the appearance of the fracture surface tends to a common shape irrespective of initial flaw geometry.

There are common factors for growth behaviour at both fixed a and fixed c. For small crack depths ($a/B<0.5$) crack growth at the free surface, dc/dN, appears to predominate over crack growth at the deepest point, da/dN (i.e., $da/dc>1$). For large crack depths ($0.5<a/B<0.8$) the converse

behaviour seems to occur (i.e., da/dc<1).

The shape change curves obtained are of considerable significance regarding the production of surface cracks for laboratory specimens and in fracture mechanics analysis of structural life based on the growing surface crack. The initial crack configuration required for a given terminal crack profile may be determined by tracing backward along the curve which contains the profile. Crack shapes are easier to produce if they are based on fixed c. The growth curves for all initial configurations appear to produce slightly different final crack profiles at failure, whereas in the case of fixed a the growth curves for all initial aspect ratios join together on a common curve. This curve, which is observed by Corn [205] and named as the "preferred propagation path", is important since a crack whose initial aspect ratio does not lie on the preferred propagation path will still tend towards it. Furthermore the rate of approach to the preferred propagation path appears greater for initial cracks having a low aspect ratio.

It would be desirable to compare these results with experimental results, but, unfortunately, experimental results of this kind cannot be obtained over a wide range of aspect ratios due to difficulties involved in producing such a crack configuration, and also to the high experimental cost which this would necessitate.

It is apparent from the present results that a realistic analysis of surface-initiated fatigue crack growth in a bending stress field depends on the substantial changes of shape of the crack. Such an analysis must explicitly consider the initial crack aspect ratio to be a function of both the crack length and crack depth.

6.5 CONCLUSIONS

The main conclusion drawn from these simulations is that initial elliptical flaws with low aspect ratio will cause earlier failure, since they appear to develop to a stable crack more quickly. This is the case assuming the initial aspect ratio is a function of the crack depth, a, only. Considering the case in which the aspect ratio is a function of the crack length, 2c, the converse is true.

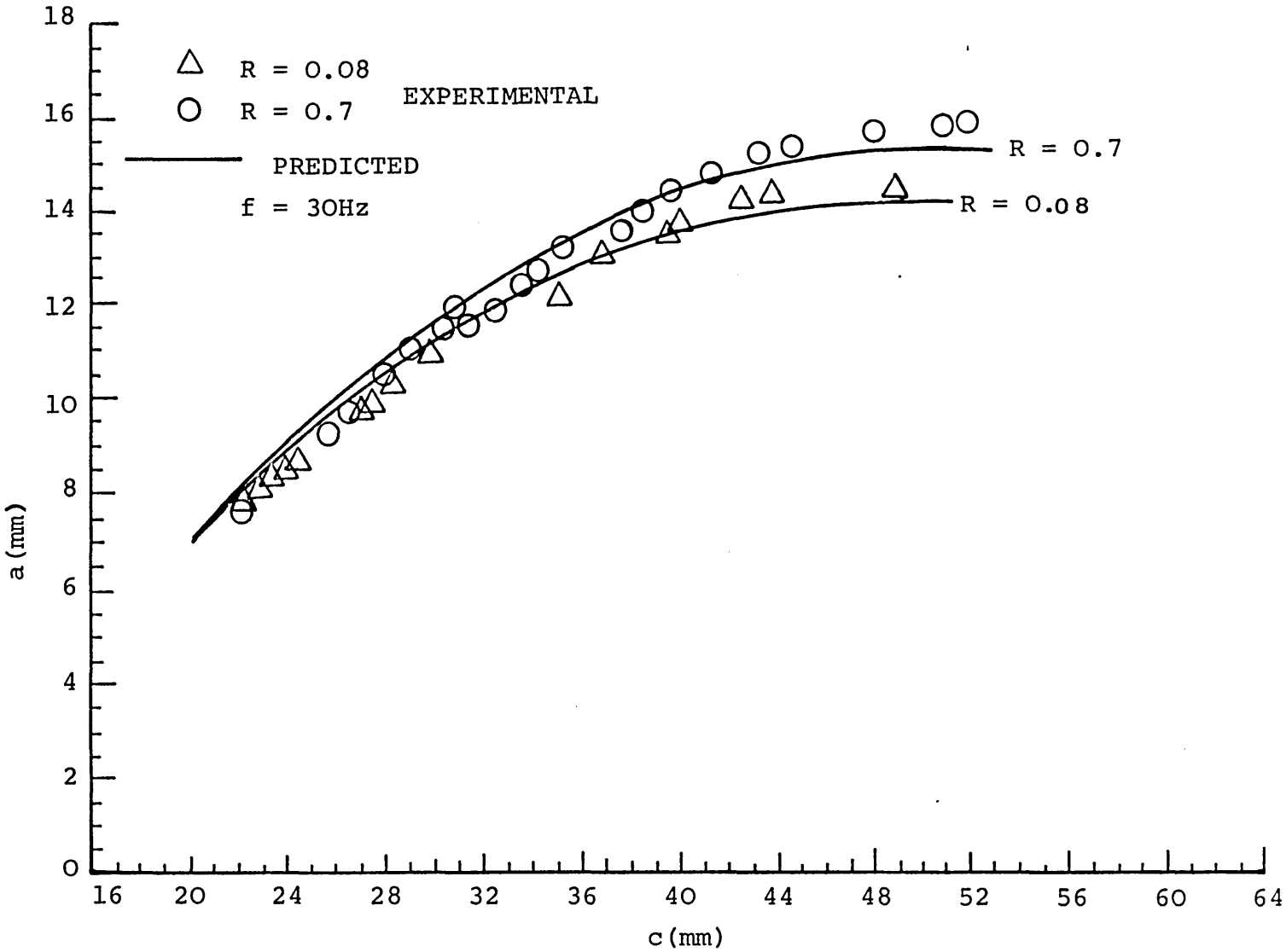


Figure 6.1 Crack depth versus half crack length for parent plate.

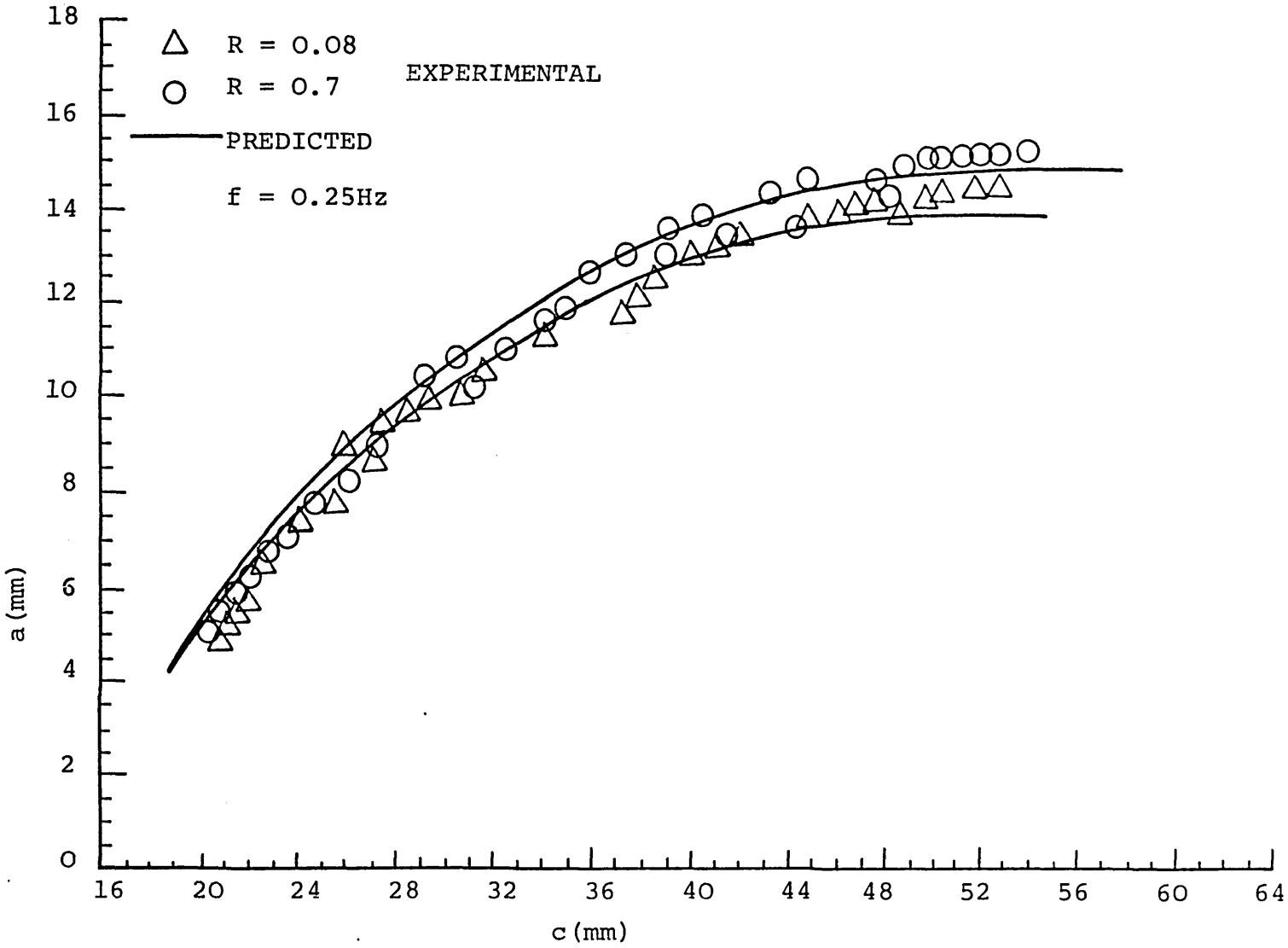


Figure 6.2 Crack depth versus half crack length for parent plate

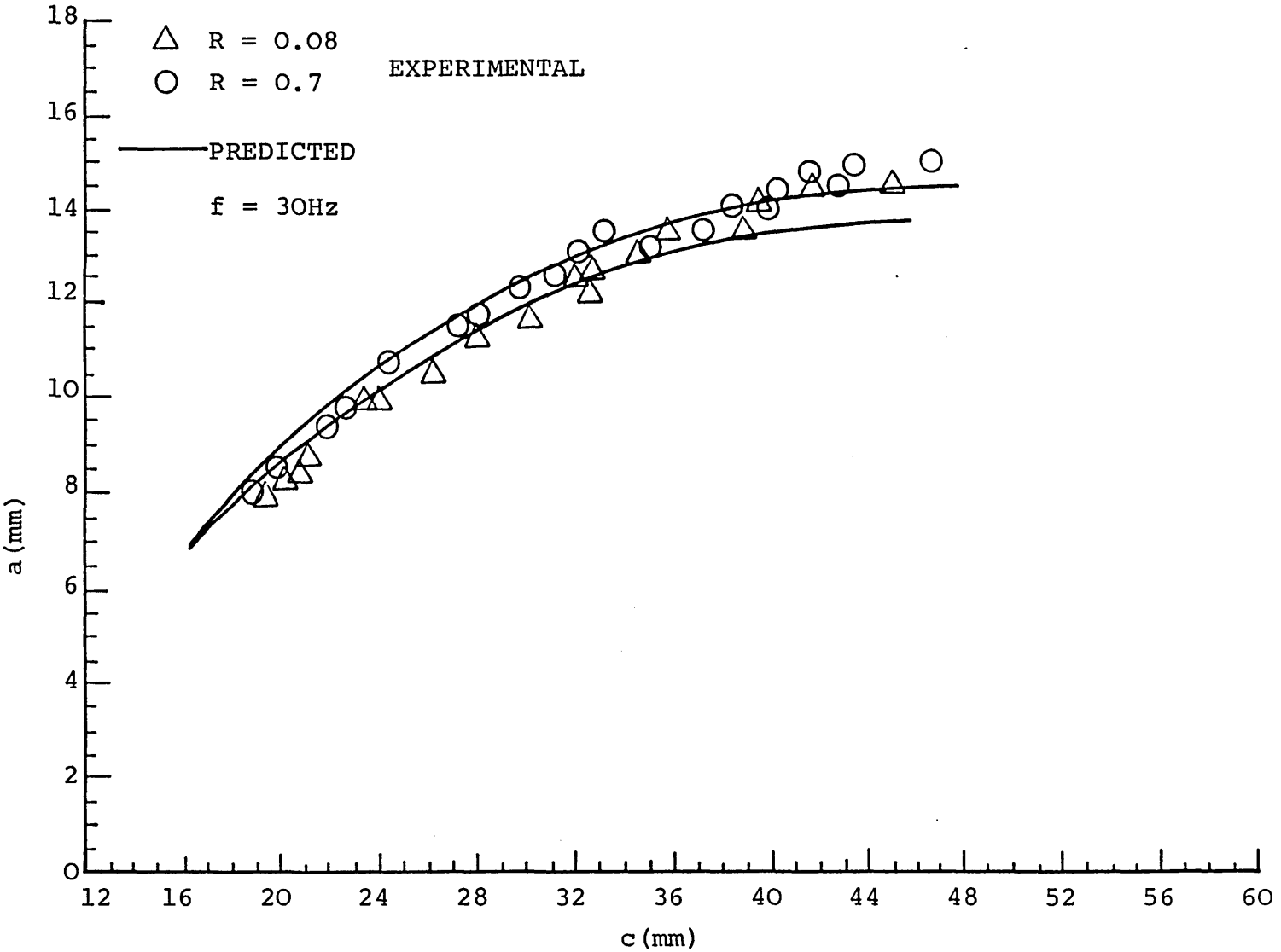


Figure 6.3 Crack depth versus half crack length for weldment.

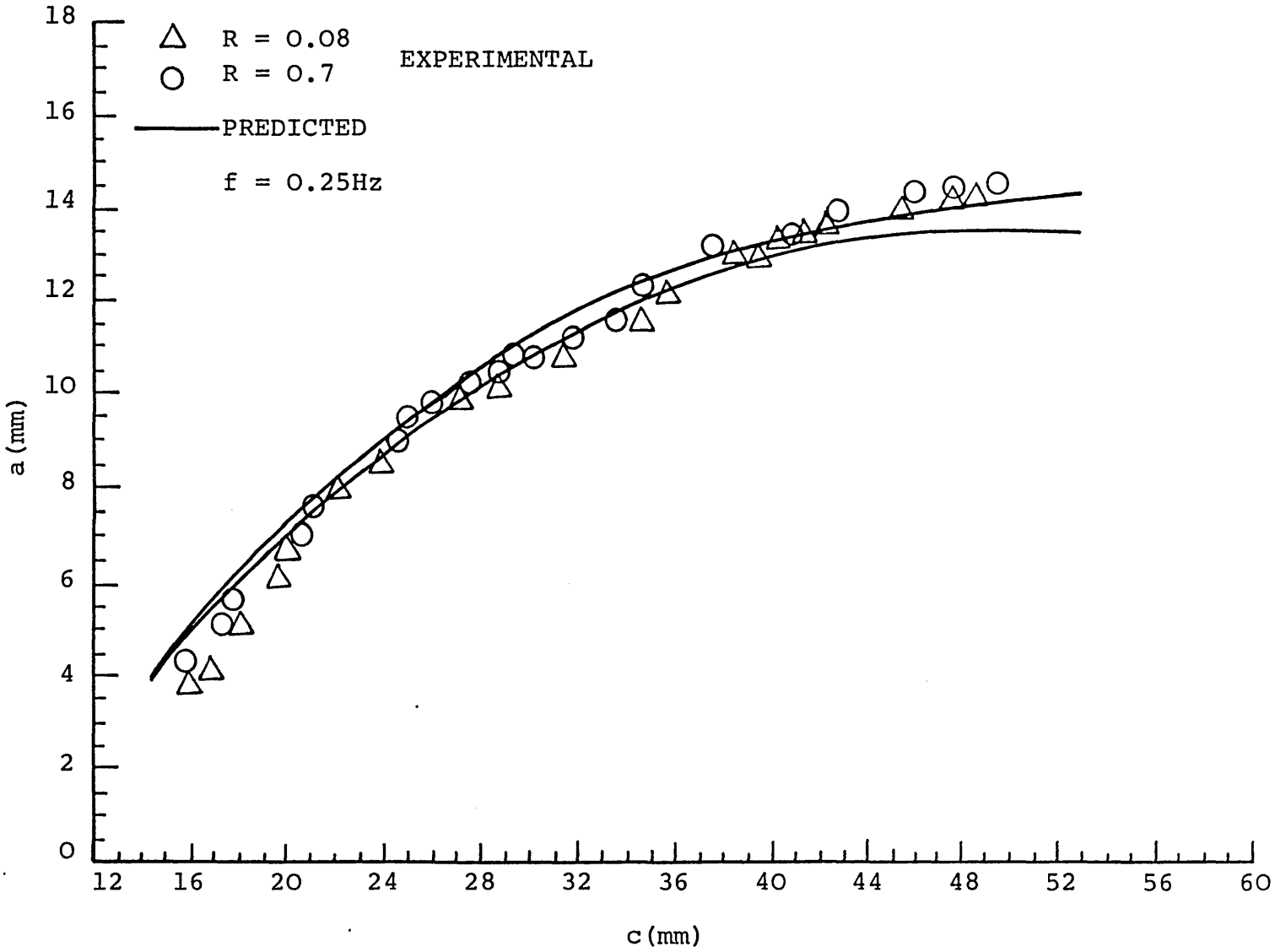
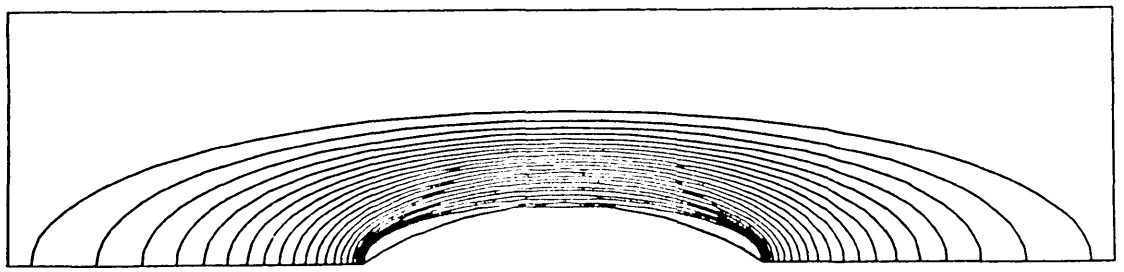
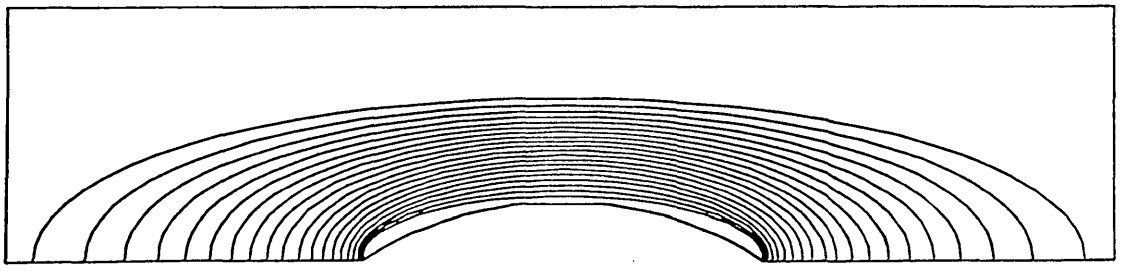


Figure 6.4 Crack depth versus half crack depth for weldment.



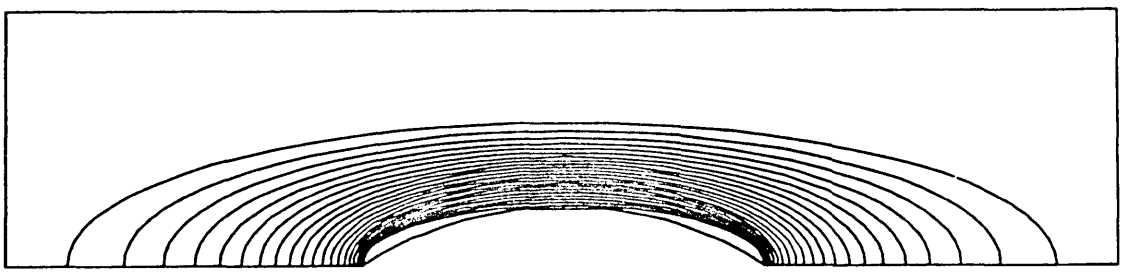
R = 0.08
f = 30Hz

N_t= 3.85x10^6 CYCLES



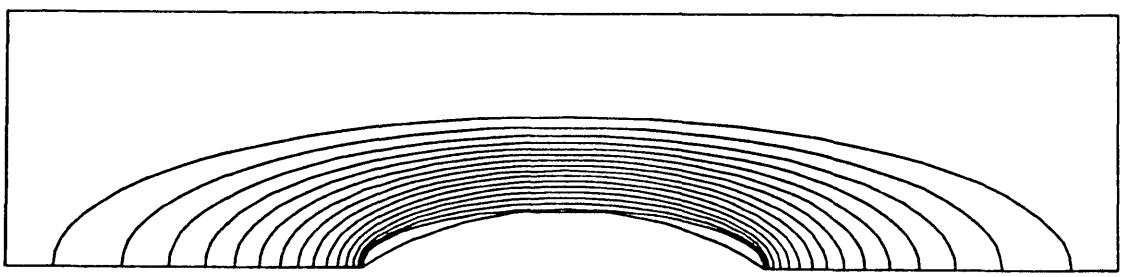
R = 0.7
f = 30Hz

N_t= 10.0x10^6 CYCLES



R = 0.08
f = 0.25Hz

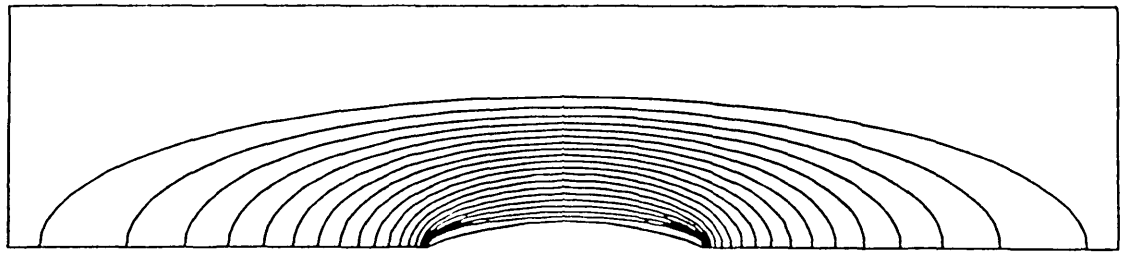
N_t= 2.2x10^6 CYCLES



R = 0.7
f = 0.25Hz

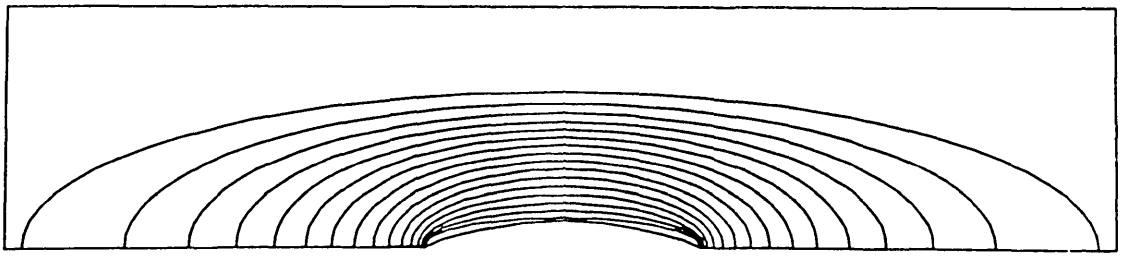
N_t= 6.2x10^6 CYCLES

Figure 6.5 Surface crack propagation profile for BS4360-50D steel, a/c = 0.28.



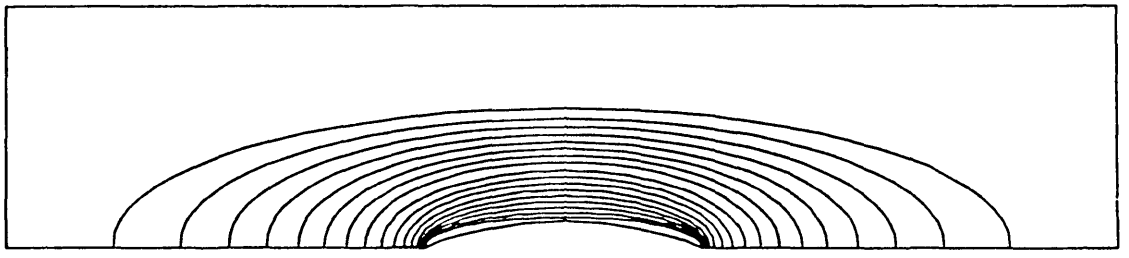
R = 0.08
f = 30Hz

N_t = 0.95x10^6 CYCLES



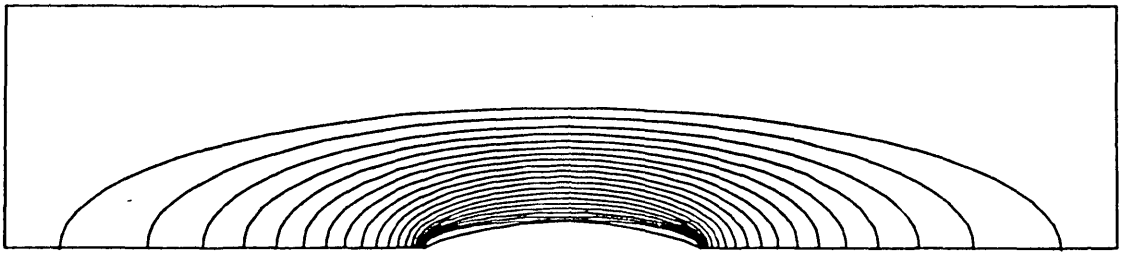
R = 0.7
f = 30Hz

N_t = 1.55x10^6 CYCLES



R = 0.08
f = 0.25Hz

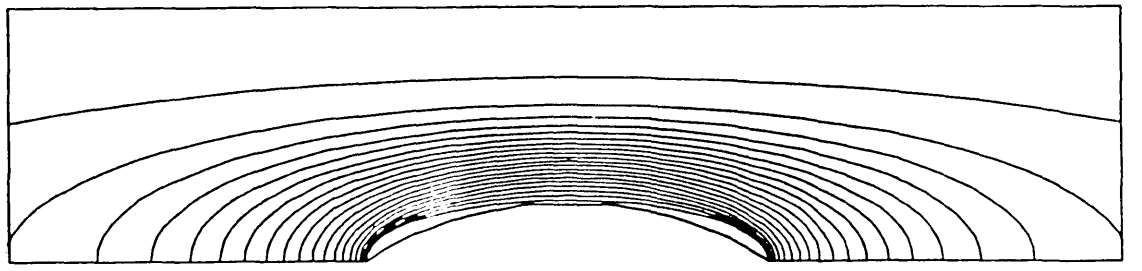
N_t = 0.17x10^6 CYCLES



R = 0.7
f = 0.25Hz

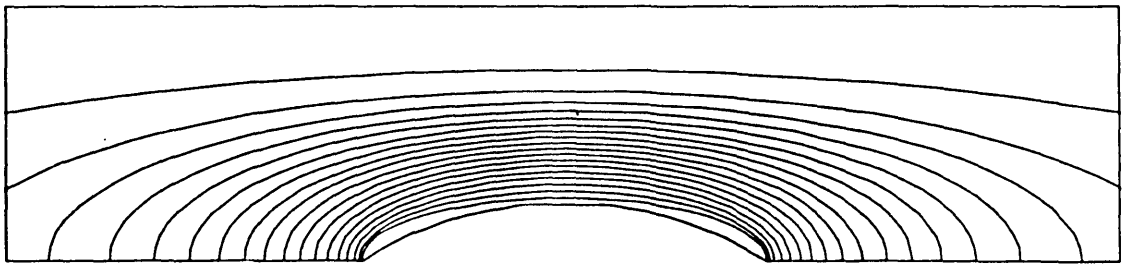
N_t = 0.39x10^6 CYCLES

Figure 6.6 Surface crack propagation profile for weldment, a/c = 0.18.



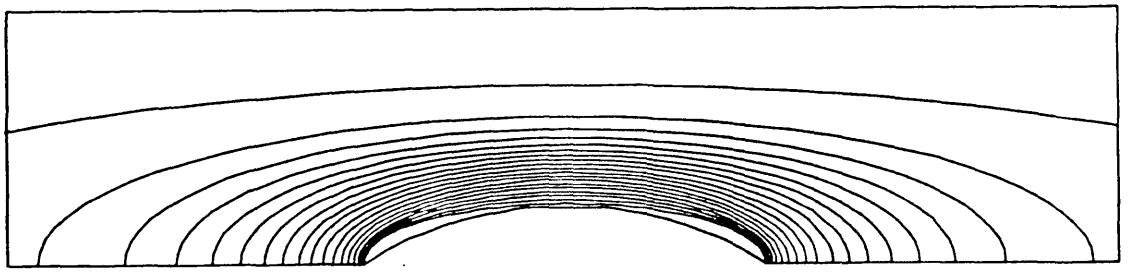
R = 0.08
f = 30Hz

$N_t = 4.0 \times 10^6$ CYCLES



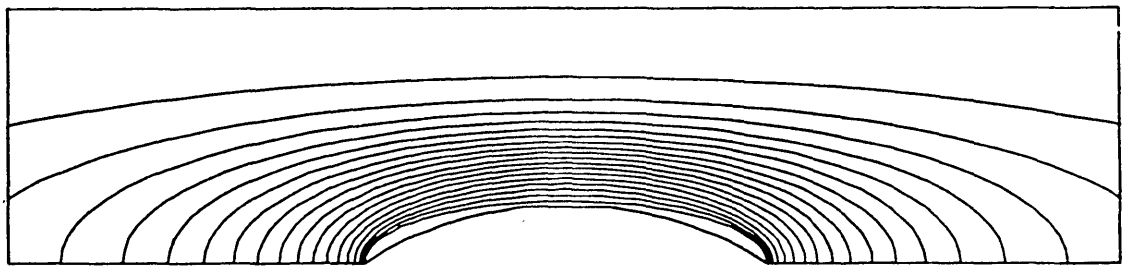
R = 0.7
f = 30Hz

$N_t = 10.8 \times 10^6$ CYCLES



R = 0.08
f = 0.25Hz

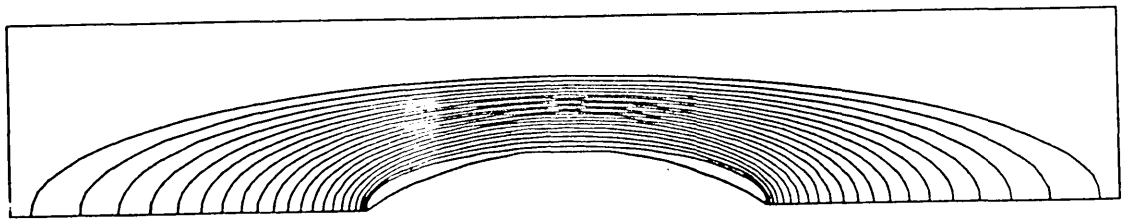
$N_t = 2.28 \times 10^6$ CYCLES



R = 0.7
f = 0.25Hz

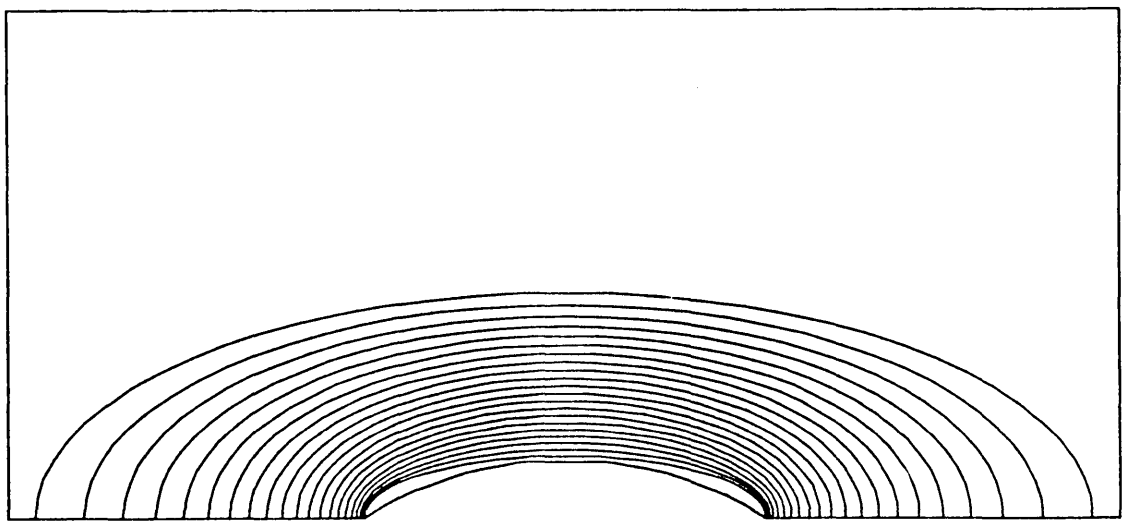
$N_t = 7.2 \times 10^6$ CYCLES

Figure 6.7 Surface crack propagation behaviour of steel after penetration of the crack at the free surface to the width of the specimen, a/c = 0.28.



B = 19mm

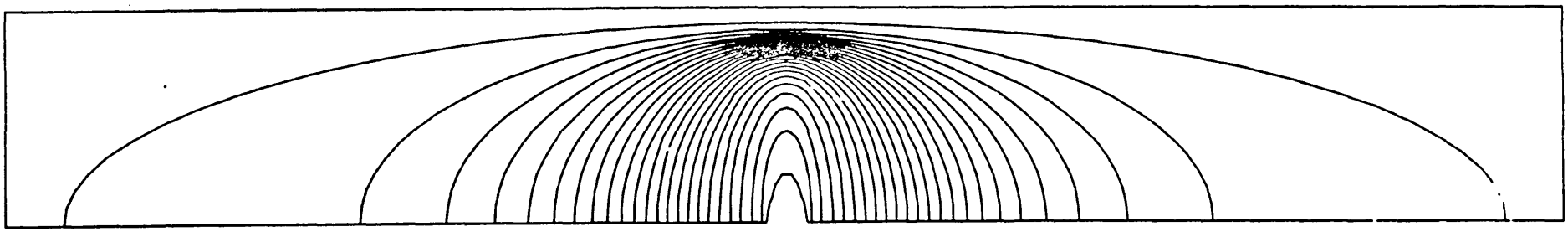
$N_t = 12.6 \times 10^6$ CYCLES



B = 38mm

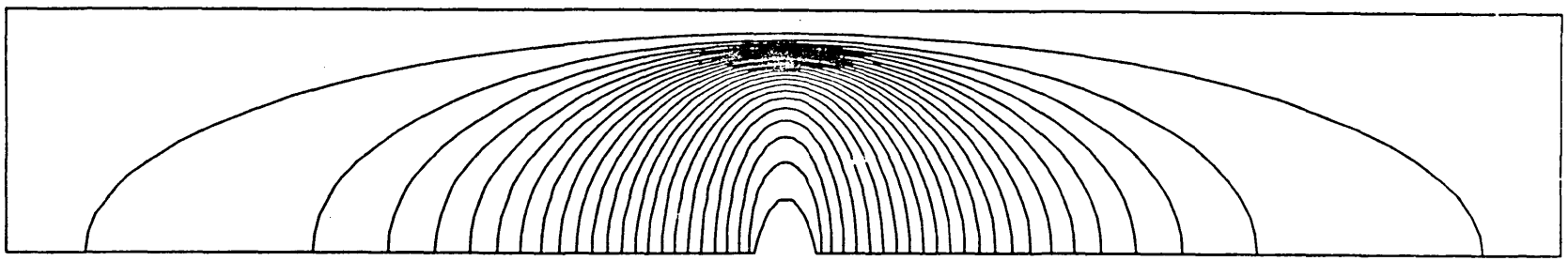
$N_t = 8.4 \times 10^6$ CYCLES

Figure 6.8 Effect of thickness on surface crack propagation profile of steel, R = 0.7, f = 30Hz, a/c = 0.28.



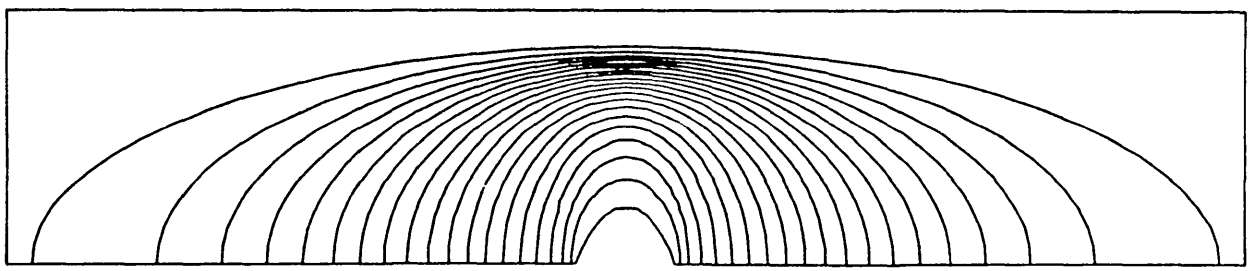
W = 1500mm

$N_t = 92.0 \times 10^6$ CYCLES



W = 1000mm

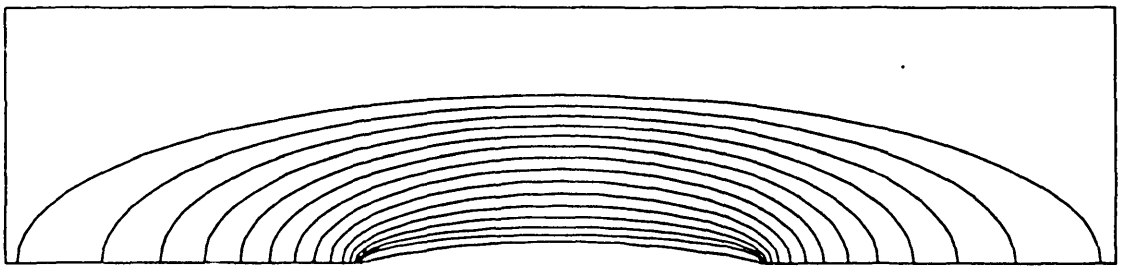
$N_t = 69.0 \times 10^6$ CYCLES



W = 500mm

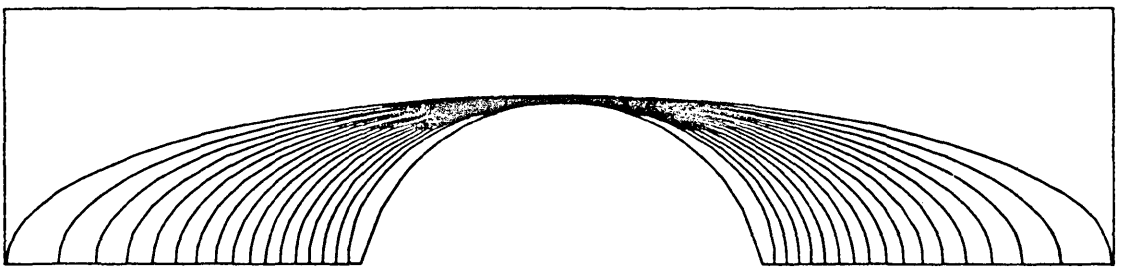
$N_t = 38.0 \times 10^6$ CYCLES

Figure 6.9 Effect of width on surface crack propagation profile of steel, R = 0.7, f = 30Hz, a/c = 0.28.



a/c = 0.1

$N_t = 1.4 \times 10^6$ CYCLES



a/c = 0.8

$N_t = 0.34 \times 10^6$ CYC_ES

Figure 6.10 Effect of initial crack configuration at " fixed c" on surface crack growth of steel, R = 0.7, f = 30Hz.

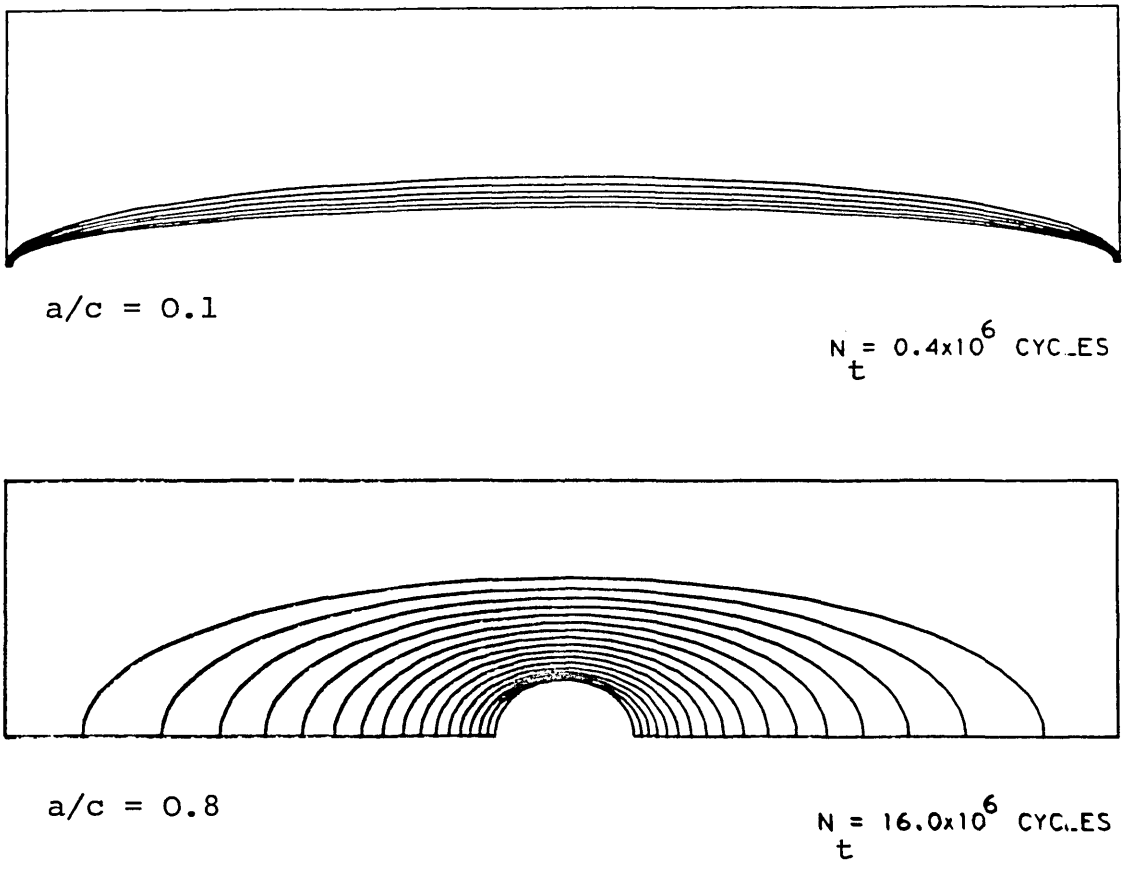
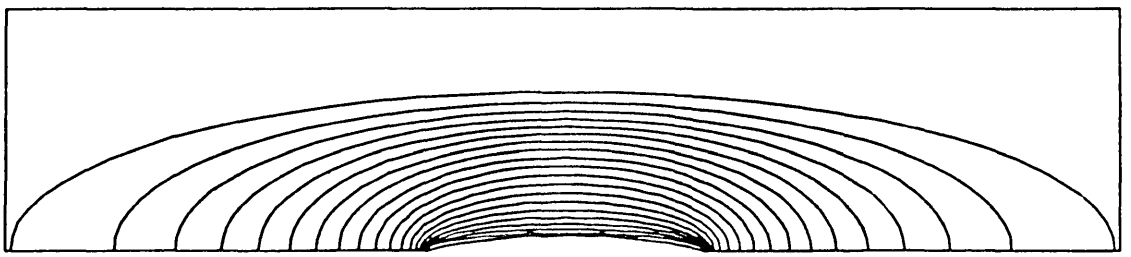
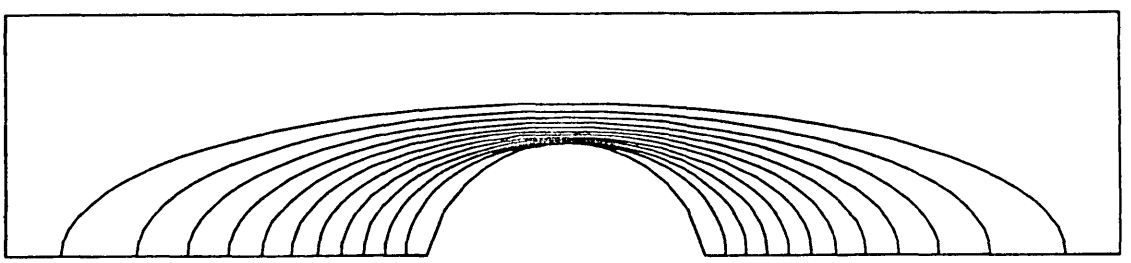


Figure 6.11 Effect of initial crack configuration at "fixed a" on the surface crack growth of steel, R = 0.7, f = 30Hz.



a/c = 0.1

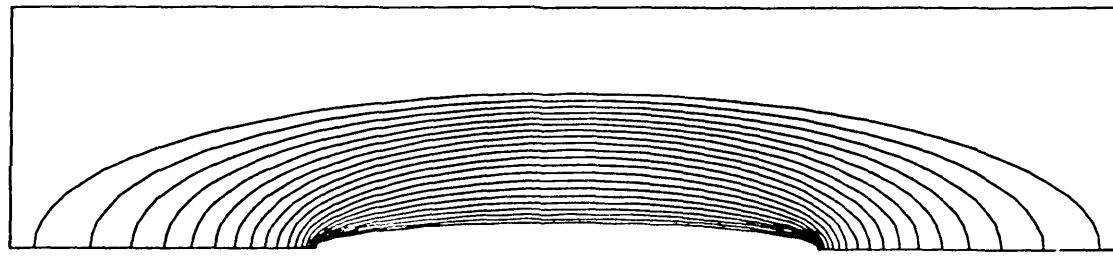
$N_t = 0.37 \times 10^6$ CYCLES



a/c = 0.8

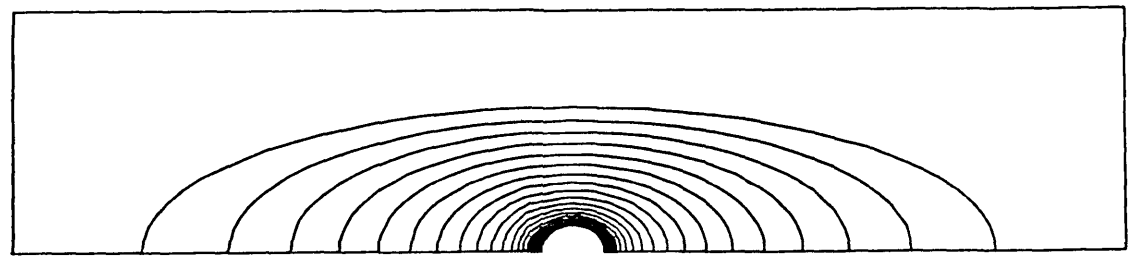
$N_t = 0.22 \times 10^6$ CYCLES

Figure 6.12 Effect of initial crack configuration at "fixed c" on surface crack growth of weldment, R = 0.7, f = 30Hz.



a/c = 0.1

$N_t = 0.5 \times 10^6$ CYCLES



a/c = 0.8

$N_t = 7.6 \times 10^6$ CYCLES

Figure 6.13 Effect of initial crack configurations at "fixed a" on surface crack growth of weldment R = 0.7, f = 30Hz.

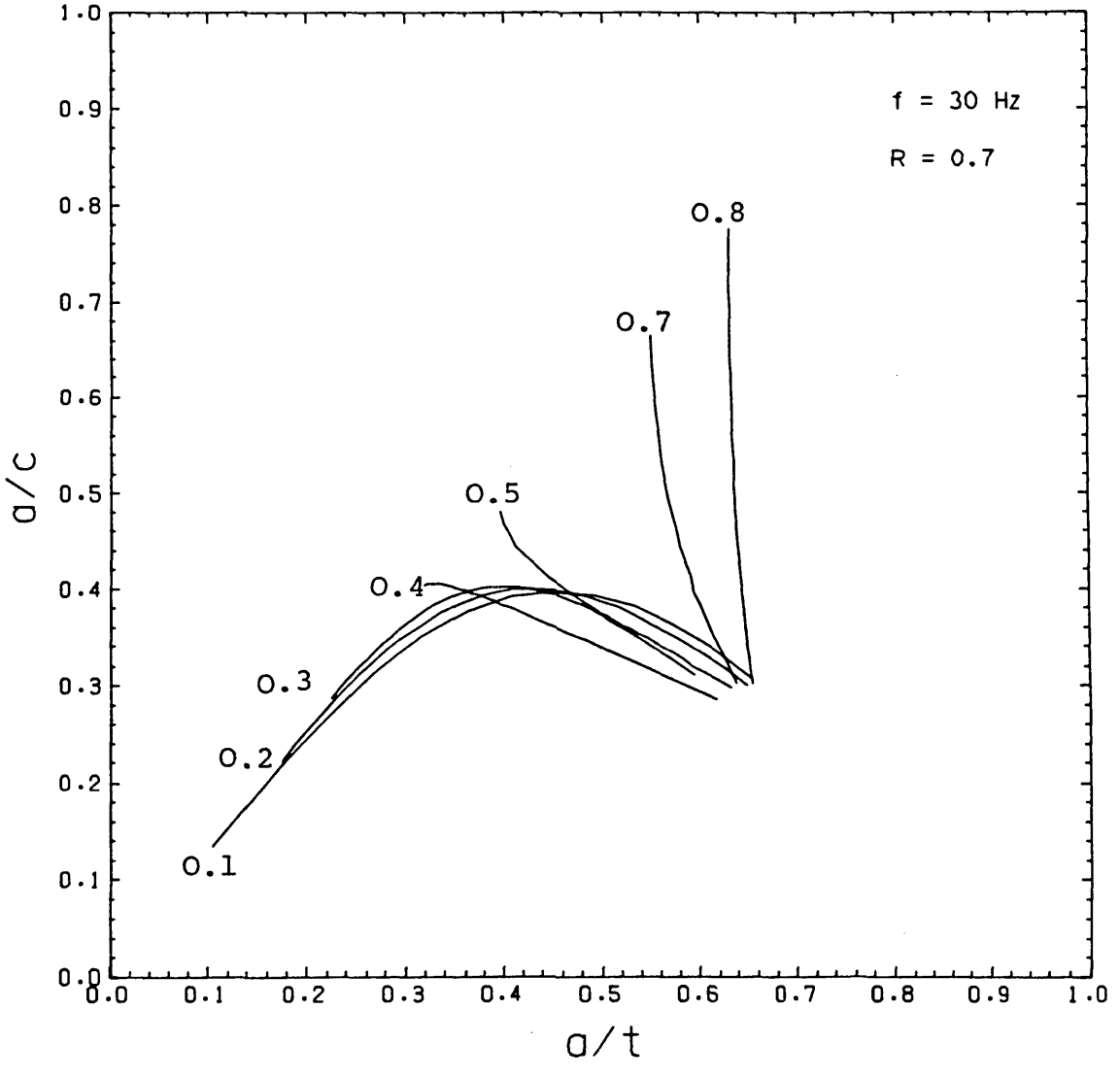


Figure 6.14 Change in surface crack shape as a function of initial crack configuration at "fixed c" in BS4360-50D steel.

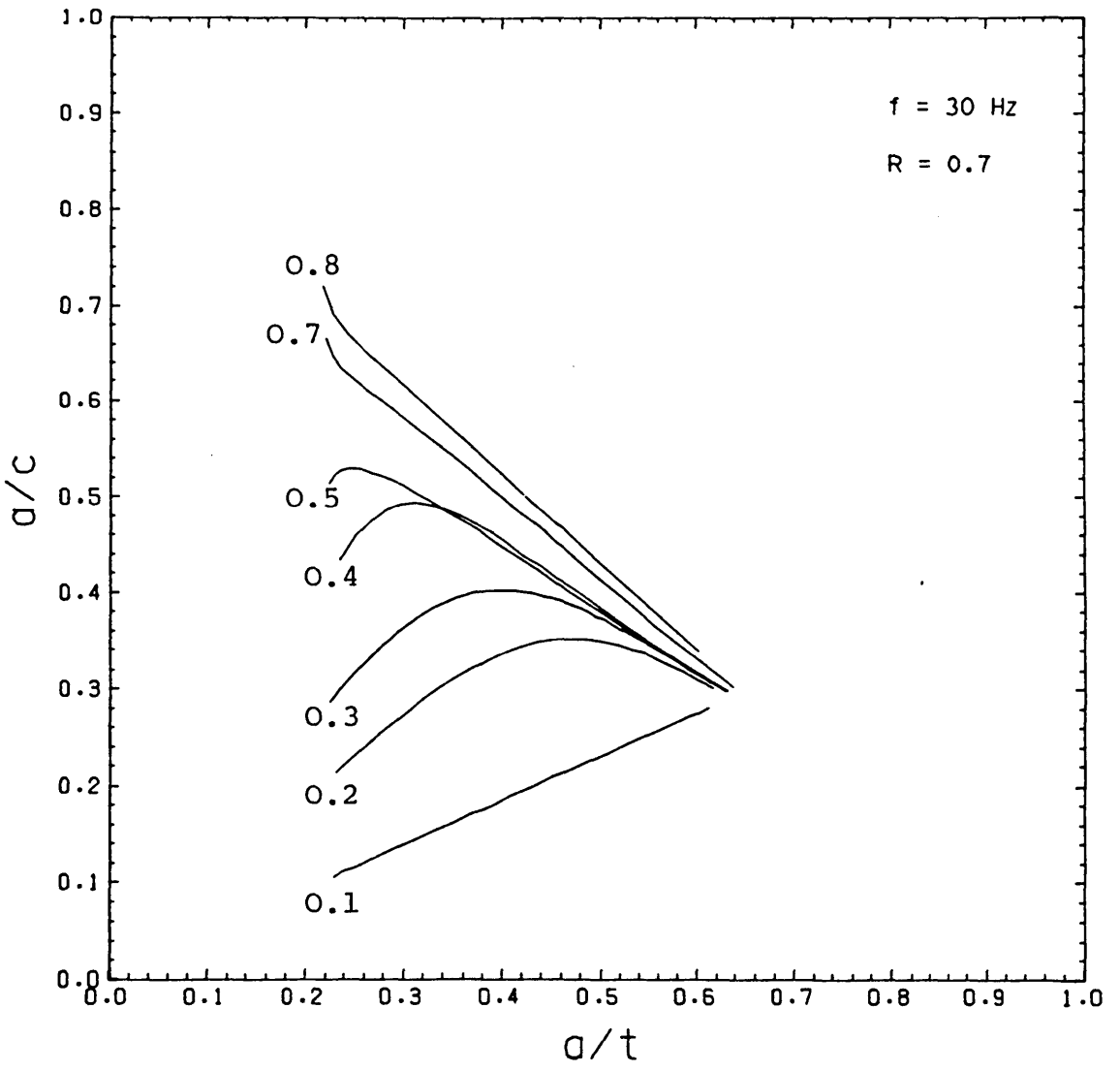


Figure 6.15 Change in surface crack shape as a function of initial crack configuration at "fixed a" in BS4360-50D steel.

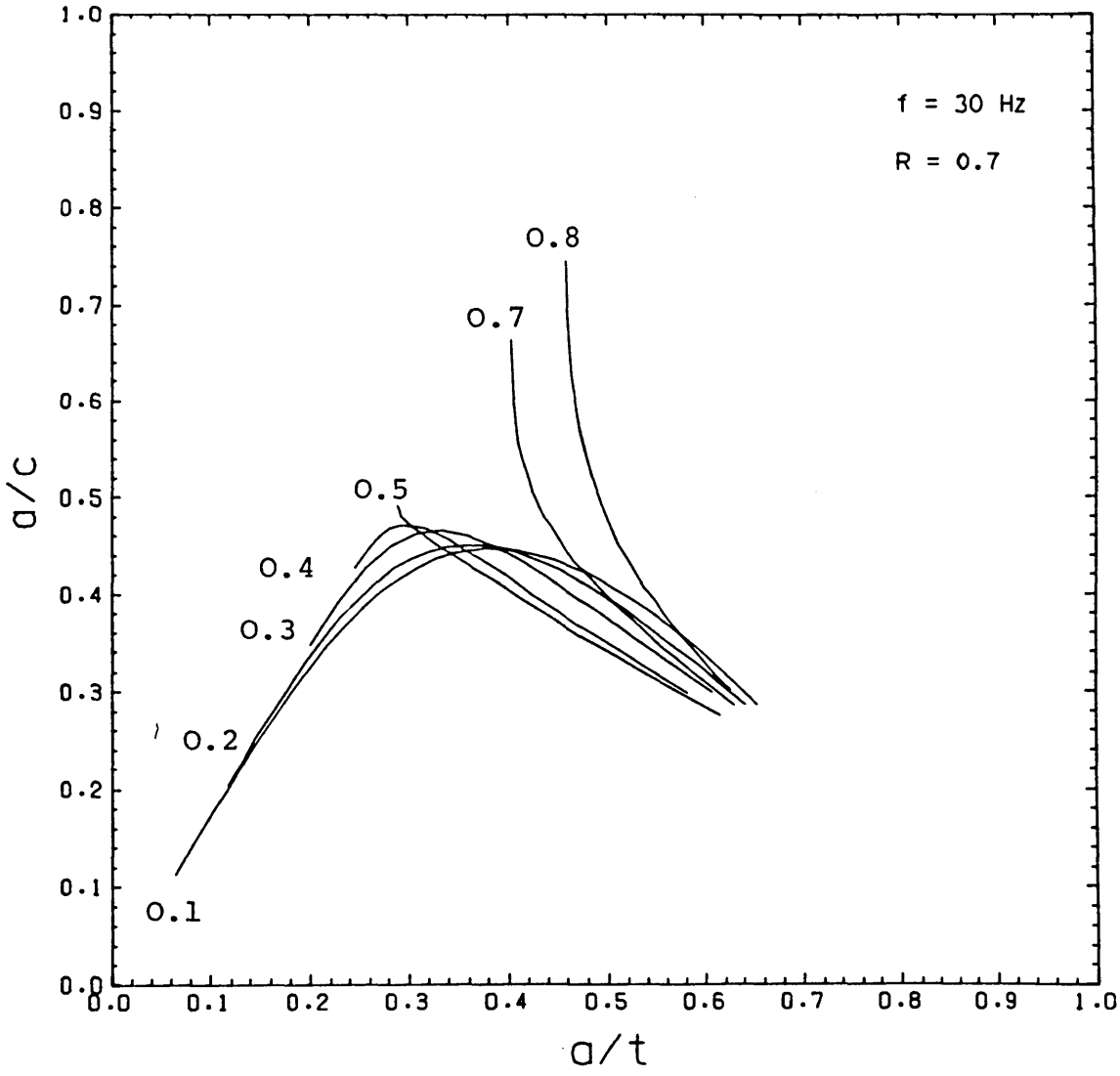


Figure 6.16 Change in surface crack shape as a function of initial crack configuration at "fixed c" in weldment.

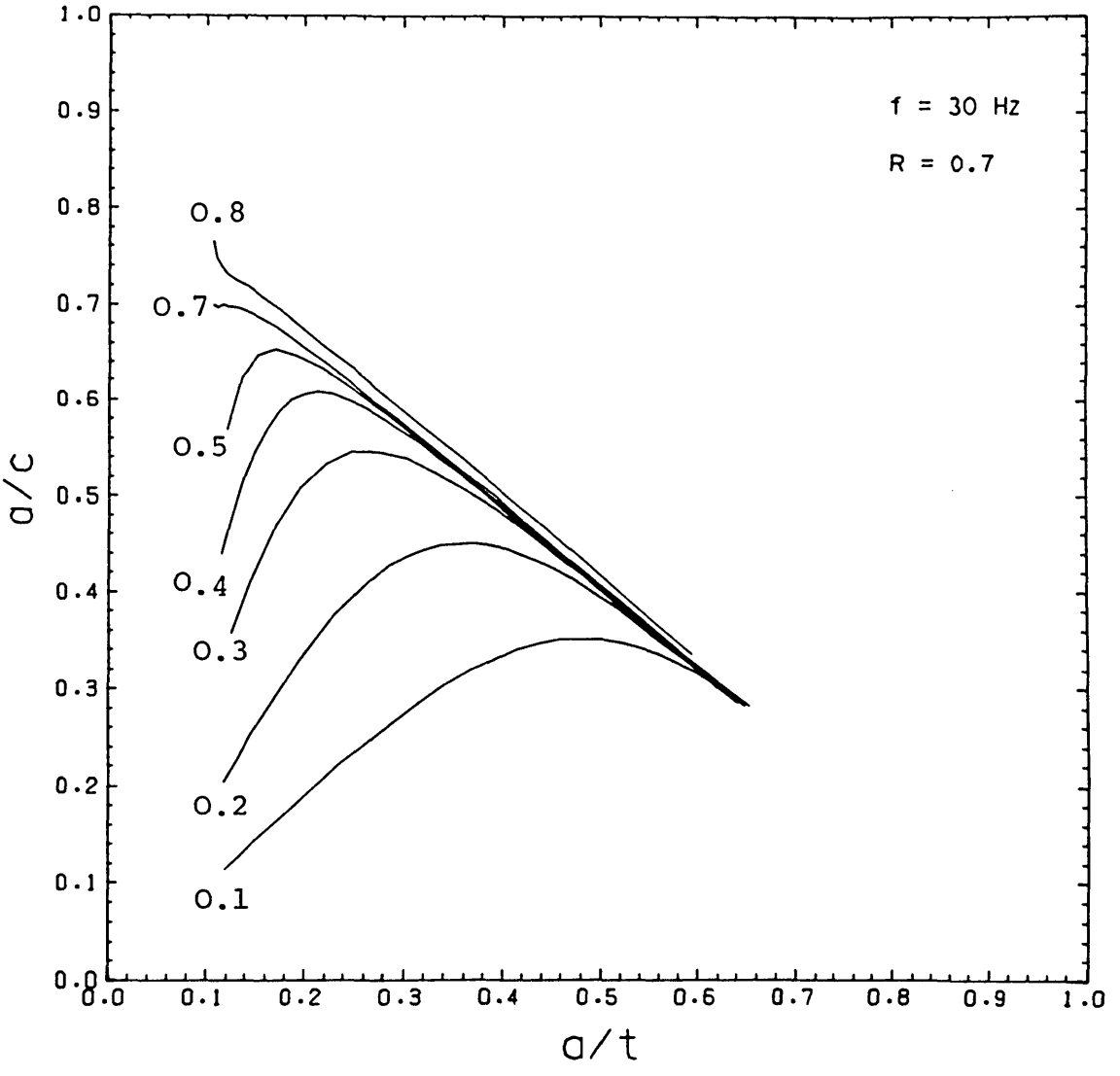


Figure 6.17 Change in surface crack shape as a function of initial crack configuration at "fixed a" in weldment.

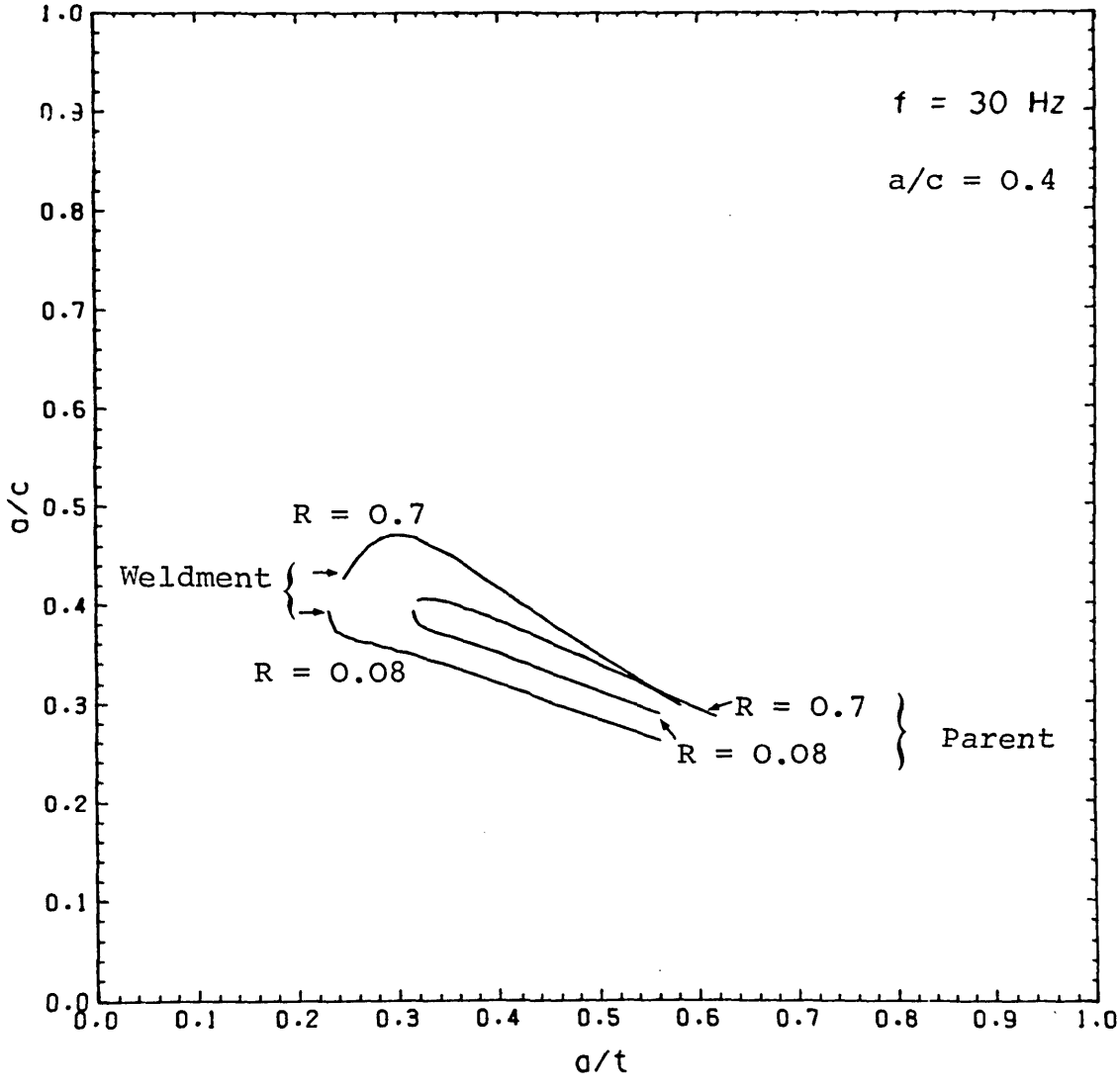


Figure 6.18 Comparison of change in crack shape at "fixed c" in parent metal and in weldment.

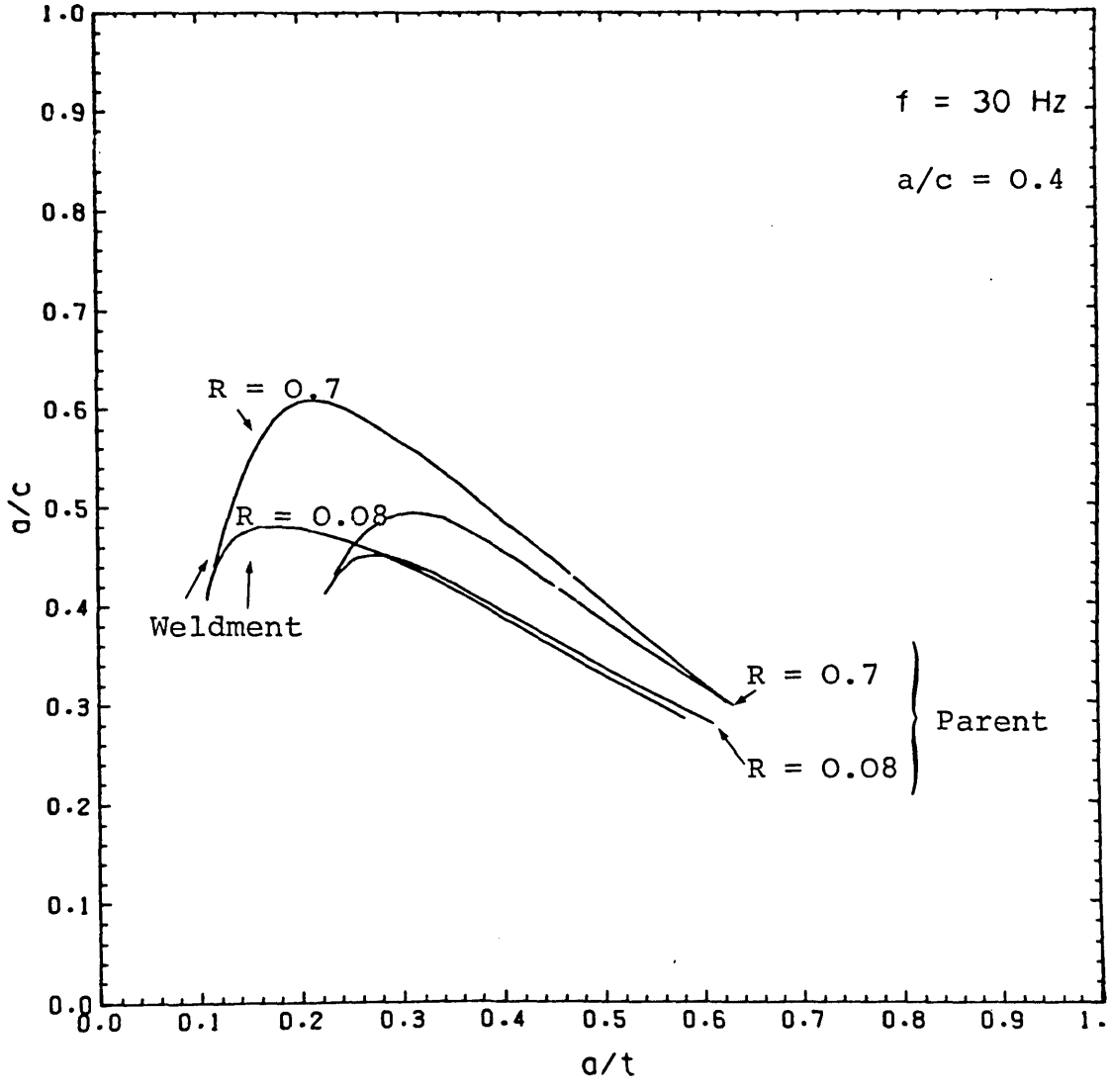


Figure 6.19 Comparison of change in crack shape at "fixed a" in parent metal and in weldment.

CHAPTER 7

IMPROVEMENT OF FATIGUE STRENGTH OF BUTT-WELDED JOINTS

7.1 INTRODUCTION

The fatigue strength of butt-welded joints in structural steel is generally low, but there are nevertheless growing requirements for improved fatigue strength. Peening, prior overloading, spot heating [93], etc., have been used to improve the fatigue life of welded joints and some attempts have been made to assess the comparative costs of such techniques. Also, improvement of the types of electrode used in welding has been sought in order to produce better weld profiles [213].

It is difficult to compare results from different investigators since the welding details as well as the material may vary considerably. However, since the above-mentioned procedures, though effective, are expensive, employing an alternative technique to produce a better weld is a more desirable means of achieving higher fatigue strength.

It is generally accepted that the fatigue properties of welded joints are virtually independent of the mechanical characteristics of the parent material. This is because of stress concentrations due to the joint geometry and to weld bead defects. Such defects can be divided into two groups:

those which arise from the design of the weldment (i.e., partial penetration); and those which arise from poor material properties or inadequate welding procedures (i.e., lack of inter-run fusion, etc.).

The present investigation was therefore undertaken in an attempt to improve the fatigue life of weldments by using a completely new method. This method, which is named sandwich welding, consists of using welding rods which have different mechanical properties for each pass and stacking up a sandwich in which the outer layers are made of the same material but having different mechanical properties from the middle layer.

7.2 SOME METHODS OF IMPROVING THE FATIGUE STRENGTH OF WELDMENTS

The fatigue strength of weldments can be improved in number of ways. Text books by Munse [84] and Gurney [93] discuss the subject in detail. The following sections discuss the use of a re-distribution of residual stress to improve the fatigue strength of weldments. It is possible to improve fatigue strength by creating residual compressive stresses at locations where fatigue cracks are likely to be initiated. The following sections also discuss how prior overloading, peening and spot heating can affect the fatigue strength of some welded specimens. The information is taken primarily from the book by Gurney.

7.2.1 Prior Overloading

If a specimen containing a stress concentration is loaded until yielding occurs at the notch, and the load is then removed, residual stresses will remain in the specimen. The sign of residual stress adjacent to the notch is opposite to that of overload. In order to create compressive residual stresses adjacent to a notch it is necessary to apply a tensile overload.

Several investigators [214] have reported that fatigue strength increased when they applied tensile prior loading. Harrison [214], who studied how the fatigue strength of fillet-welded steel specimens could be increased by prior overloading, found that the S-N curves for specimens preloaded at various levels of overload stress were approximately parallel to each other.

7.2.2 Peening

Peening is a cold-working process that consists either of bombarding the surface of a component with a high-velocity stream of metal particles, or battering with a tool operated by a pneumatic hammer, with the object of inducing a compressive residual stress in the surface layer.

Gurney [93] prepared a table which summarised the fatigue strength of non-load carrying fillet-welds, as

recorded by several investigators. He stated that peening would increase the strength in load-carrying fillet-welds in a way similar to that found in non-load carrying fillet-joints, at least for failures initiating at the weld toe.

Maddox [215] has recently studied how peening affects the fatigue strength of fillet-welds. The results showed that peening was more effective for transverse welds than for longitudinal; also, the preliminary tests indicated that shot-peening was still beneficial under variable amplitude loading. The benefit of shot-peening varied with peening conditions and even under nominally identical conditions.

7.2.3 Spot Heating

In spot heating, the structure is heated locally, usually with a gas torch, so as to produce local yielding, resulting in compressive thermal stresses. When locally heated metal cools, it shrinks, causing residual stresses. These residual stresses can be used for improving the fatigue properties of weldments. The basic principle is to produce compressive residual stresses in those local areas, especially near notches, where fatigue cracks are likely to initiate. Several investigators [216] have conducted extensive studies on this subject. By spot heating in selected parts, compressive residual stresses were induced at the notch and at the ends of the weld, and a 53% increase in strength was obtained. But when spot heating was done at the centre-line of the specimen, even though the distance

from the notch was the same and the heating thus had the same metallurgical effect, the residual stresses produced were tensile, and the fatigue strength measured was the same as for an untreated specimen. This indicated that the strength increase was due to the residual stresses.

7.3 EXPERIMENTAL PROCEDURES

Fatigue tests were carried out on sandwich weldments using a Dowty electrohydraulic fatigue machine at R-values of 0.08 and 0.7 with loading frequecies of 0.25Hz and 30Hz. Two types of specimen were used in this investigation, namely, compact type and surface notched plate, details of which are given in Chapter 3.

All the tests were performed in laboratory air, in ambient conditions and at room temperature.

7.4 RESULTS

Fig. 7.1 shows a typical crack length, a, versus number of cycles, N, curve for conventional and sandwich weldments using CT specimens.

The result of tests on CT specimens at cyclic frequencies of 30Hz and 0.25Hz and stress ratios of 0.08 and 0.7 is presented in Figs. 7.2 and 7.3. These figures show the general effect of stress ratio observed on weldment

using CT geometry, that is, crack growth rate increases with increase in stress ratio but decreases with increasing rates of growth.

The effect of frequency is illustrated in Fig. 7.4. This again shows the general trend observed in this investigation.

A comparison was made on data obtained for sandwich weldment, conventional weldment and the base material. The results are presented in Figs. 7.5 and 7.6 for a loading frequency of 30Hz, and R-values of 0.08 and 0.7, respectively, and in Figs. 7.7 and 7.8 for a cyclic frequency of 0.25Hz, and two stress ratios (i.e., 0.08 and 0.7). In general all these results show that the crack growth rate is lower in sandwich weldment than in conventional weldment and the base metal.

At a cyclic frequency of 30Hz the crack growth rates in conventional weldments at high values of ΔK (>20 $MN/m^{3/2}$) tend to approach the growth rates in parent material, while at lower frequency (0.25Hz), the growth rates in conventional weldments for ΔK values above 30 $MN/m^{3/2}$ at R=0.08, and 15 $MN/m^{3/2}$ at R=0.7, are higher than the crack growth rates in the base plate. However, from the results obtained for sandwich weldments it appears that the crack growth rates, being always lower than in parent metal, may

be due to favourable compressive residual stresses.

The results for sandwich welded plates are presented in terms of dc/dN or da/dN versus ΔK_c and ΔK_a, respectively. The effect of stress ratio at 30Hz is illustrated in Fig. 7.9, from which it can be seen that the stress ratio does not have a significant effect over the range investigated.

It was shown in Chapter 5 that butt-welded plates contained a tensile residual stress field which caused a higher stress intensity at the crack tip and hence higher growth rates as compared to the base plate. The sandwich welded plate in this study did not show any deterioration when compared to the conventional welded plate of the previous study. These results are shown in Figs. 7.10 and 7.11.

7.5 FRACTOGRAPHY

Examination of the fatigue fracture surfaces of sandwich weldments produced by CT specimens was made by means of a scanning electron microscope.

Fig. 7.12 illustrates a typical example of low growth rates at ΔK values of approximately 8 $MN/m^{3/2}$. With the crack maintained near threshold, facets were a common feature of fracture surfaces. The facets were rounded rather

than planar, indicative of intergranular fracture as the principle mechanism operating in this region. Some patches of faint striations were also observed at slightly higher values of ΔK(10 $MN/m^{3/2}$), as shown in Fig. 7.13. The presence of striation patches is believed to be due to the sensitivity of the grain orientation of the weld metal. Surface damage as a result of fatigue, and porosity were the remaining common features observed in low crack growth rate regions (see Fig. 7.14).

Under intermediate ΔK conditions (15 $MN/m^{3/2} < \Delta K <$30 $MN/m^{3/2}$) slag entrapment was evident, as shown in Figs. 7.15 and 7.16, and typical fatigue surfaces were observed (see Fig. 7.17).

At higher values of ΔK (>30 $MN/m^{3/2}$) fracture surfaces manifested four distinct features:

1) 100-percent microvoid coalescence, as shown in Fig. 7.18;

2) inclusions and striations (see Fig. 7.19); the chemical composition of the inclusions showed significant traces of manganese, silicon, phosphorus and sulphur.

3) Transgranular cleavage-like fracture (see Fig. 7.20);

4) microvoid, porosity and striations (see Fig. 7.21).

Figs. 7.22 and 7.23 shows the fractograghs taken at the boundary of the two weld metals in the low ΔK region (9 $MN/m^{3/2}$) and the high ΔK region (>30 $MN/m^{3/2}$), respectively. They reveal two different regions, namely, those of smooth and rough fatigue fracture. The outer layer of weld metal shows a superior resistance to crack propagation by exhibiting a smoother surface while the layer of weld metal adjacent to it shows a coarser structure. This suggests that the mechanism of fracture was not the same in each material and, noting that their mechanical properties were similar, they have not resulted in similar growth rates.

7.6 DISCUSSION

Fatigue cracks usually initiate from a weld defect in the weldments due to embrittlement of the regions adjacent to it and to stress concentrations arising from it. It follows that an increase in fatigue strength can be obtained if the stress intensity at the crack site can be lowered. One way of doing this is by the introduction of compressive residual stresses which counteract the applied load, thus decreasing the stress intensity at the crack tip; this was discussed in the previous sections. However, Chen and Sih [217] analytically found that for a three-layered plate, it was beneficial to have the modulus of elasticity of the middle layer kept lower than that of the outer layers: this appeared to decrease the crack border stress intensity by a significant amount. However, the author's own mathematical analysis for two-layer spherical laminates failed to come to

any firm conclusion, as the final equations obtained represented only one medium. This was because the material constants such as Young's modulus, shear modulus, etc., for the weld metals considered were almost the same.

The results obtained for the two geometries indicate that the improvement was considerably greater in CT specimens when compared to the base plate. The average crack growth retardation was approximately three times compared with that for conventional weldment for both geometries tested.

Although no attempt was made to measure the residual stresses in the weldment fabricated by this process, due to the complexity of such residual fields (i.e., different heat input, welding rod, etc.), it appeared that this welding process introduced some compressive residual stresses in both geometries. In the case of SNP geometry, which was shown in Chapter 5 to contain tensile residual stresses, there was still some improvement and crack growth was about two times slower than in welds produced by conventional methods. A possible explanation for this difference is that the tensile residual stresses produced by conventional welding would have been higher except that employing this technique either inhibited the introduction of tensile residual stresses or reduced their deleterious effect. The observed effect of stress ratio (see Fig. 7.9) also confirms the above hypothesis in that if tensile residual stresses

are present their magnitude should be smaller than for the previous case. It was feared in the case of SNP geometry that the magnitude of the tensile residual stress would be higher than that produced in conventional weldment, but it was encouraging to find that this does not necessarily happen.

Metallurgically, in sandwich weldments the cyclic work-hardening appears to be smaller near the surface than in the volume of weaker material, since using a stronger material raises the yield stress of the surface, thereby reducing the total plastic slip, thus supressing both the rate and the amount of surface hardening. The tests performed did not throw much light on the relative importance of the mechanical inhibition of surface deformation in improving the fatigue properties; however, the mechanism by which the improvement in fatigue properties occurs appears to be partly controlled primarily by the supression of surface hardening, hence choosing a stronger material for the surface seems to restrict slip-band formation and surface crack propagation correspondingly. Furthermore, since the crack in any one grain is parallel to the slip plane, then, as the crack propagates to an adjacent grain or medium, it changes its direction to be parallel to the slip planes of the new grains or medium. However, when it reaches the grain boundary it may, in fact, be stopped if the orientation of the slip planes of the adjacent grain or that of the grains in the adjacent medium is not such as to favour propagation. While this is not the last word on the fatigue mechanism in

sandwich weldments, some progress has been made in explaining the details of hardening and crack propagation.

7.7 CONCLUSIONS

This work shows that under certain conditions the fatigue properties of butt-welded joints can be improved using the new sandwich welding technique. It is also shown that the degree of improvement varies, depending on the specimen geometry. The welding process is easy to control and, considering its economic aspect, the sandwich weldment does not involve any higher cost. However, more work is required before firm conclusions can be drawn.

To sum up, it can be stated that in general the fatigue properties are evidently improved by the sandwich welding technique. As the test results showed, this is not only valid for CT specimens, which were shown to contain compressive residual stresses, but also for SNP geometry, which contains tensile residual stresses.

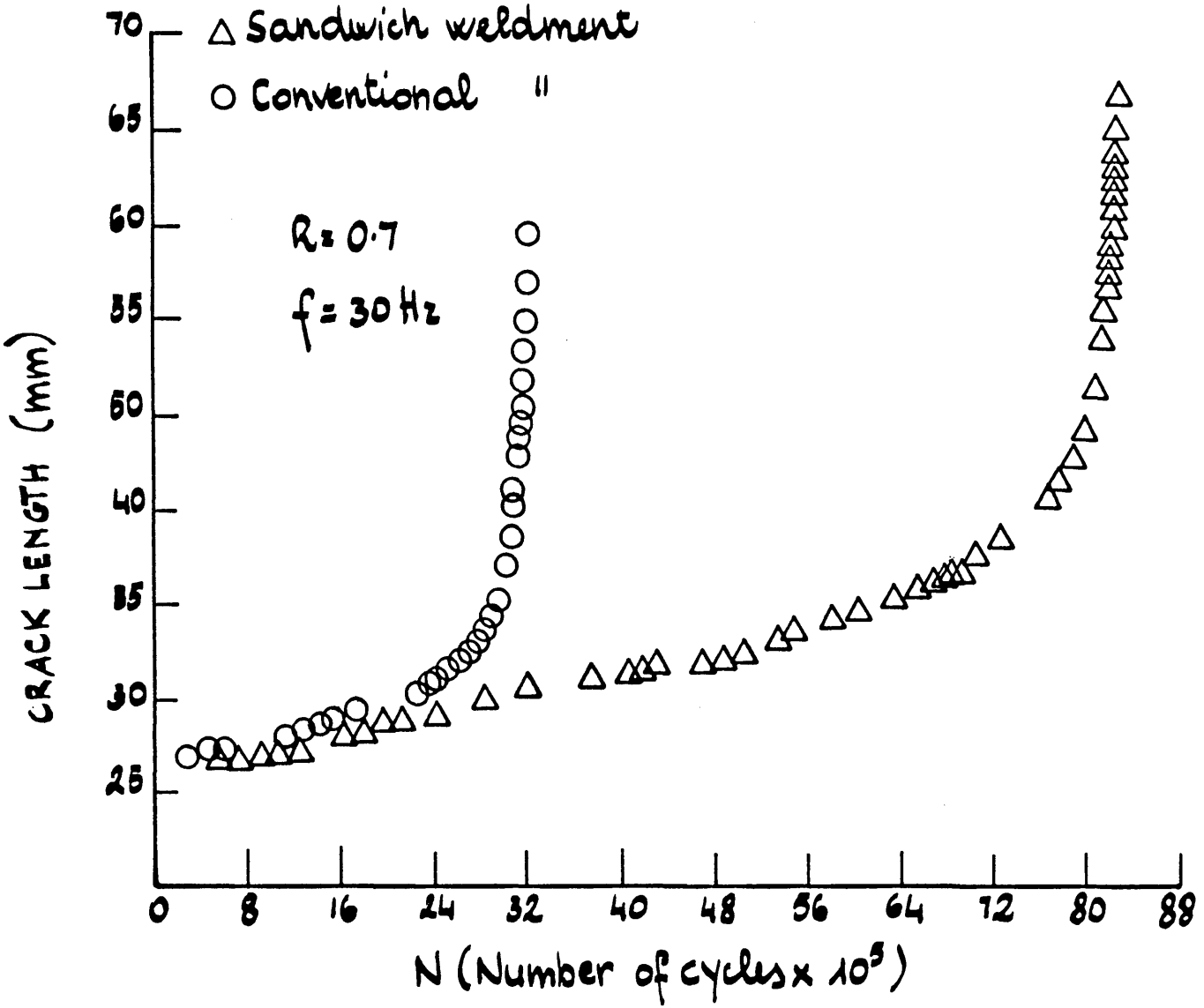


Figure 7.1 a versus N for conventional and sandwich weldments.

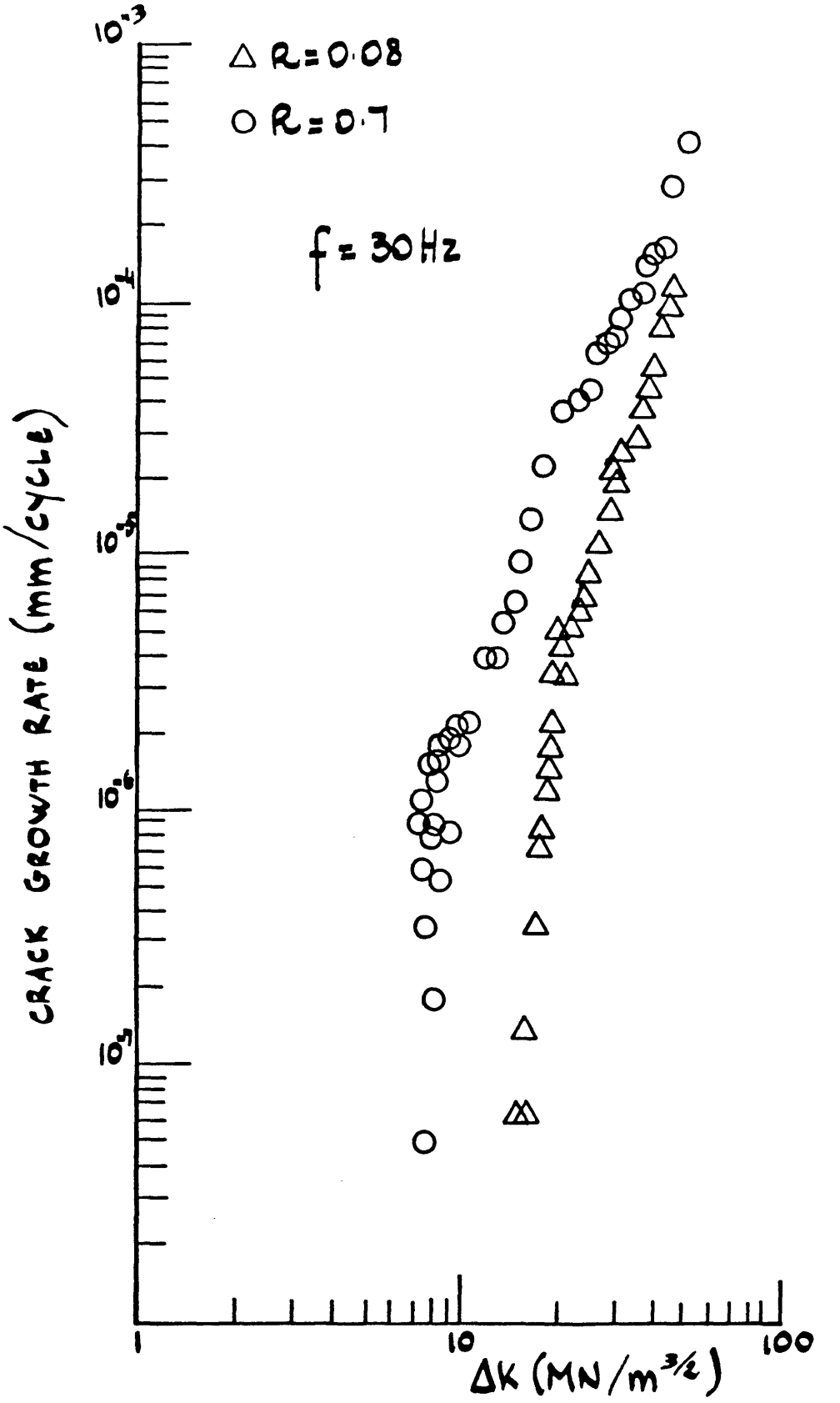


Figure 7.2 Effect of stress ratio on sandwich weldment using a CT specimen.

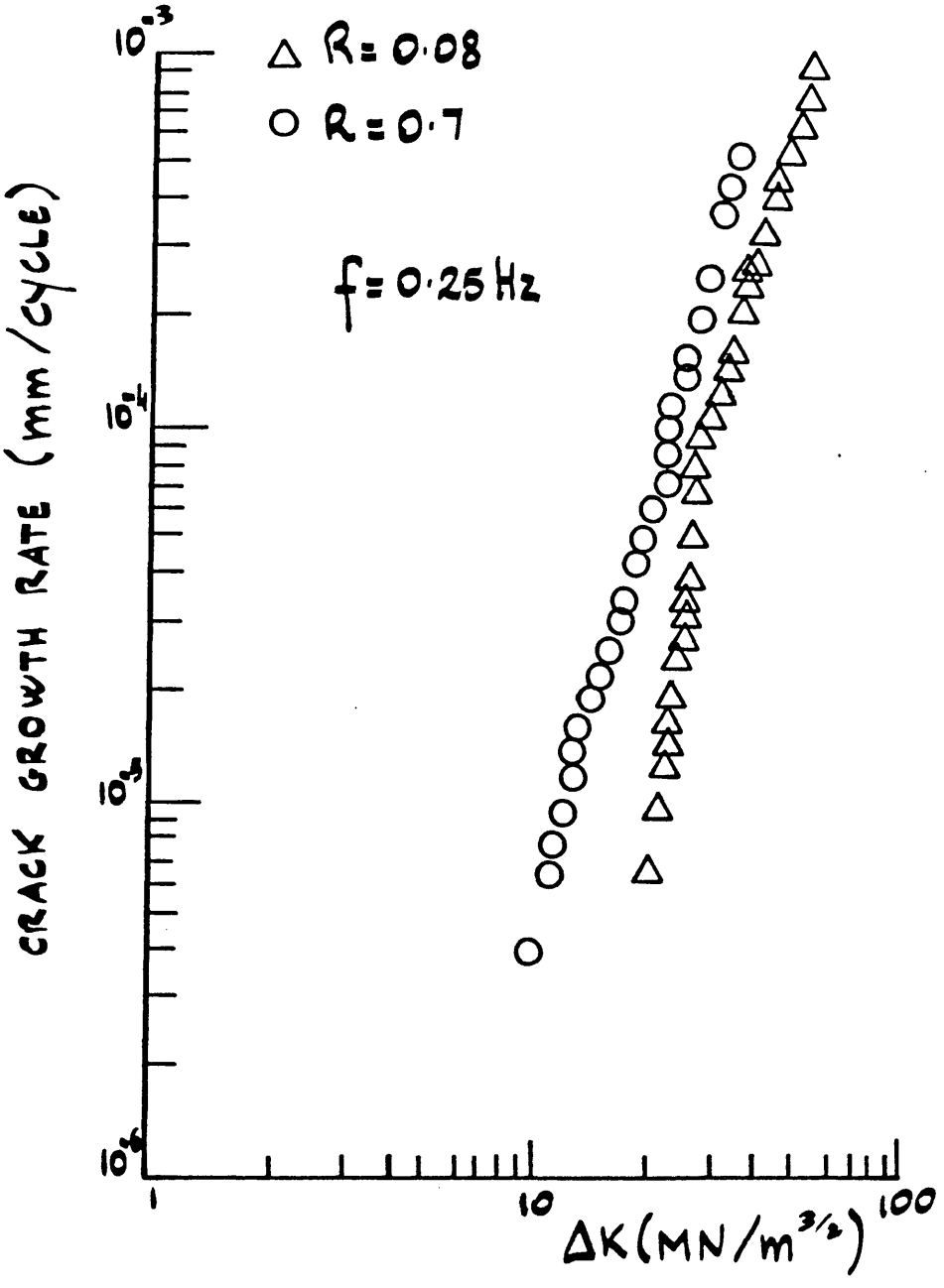


Figure 7.3 Effect of stress ratio on sandwich weldment using a CT specimen.

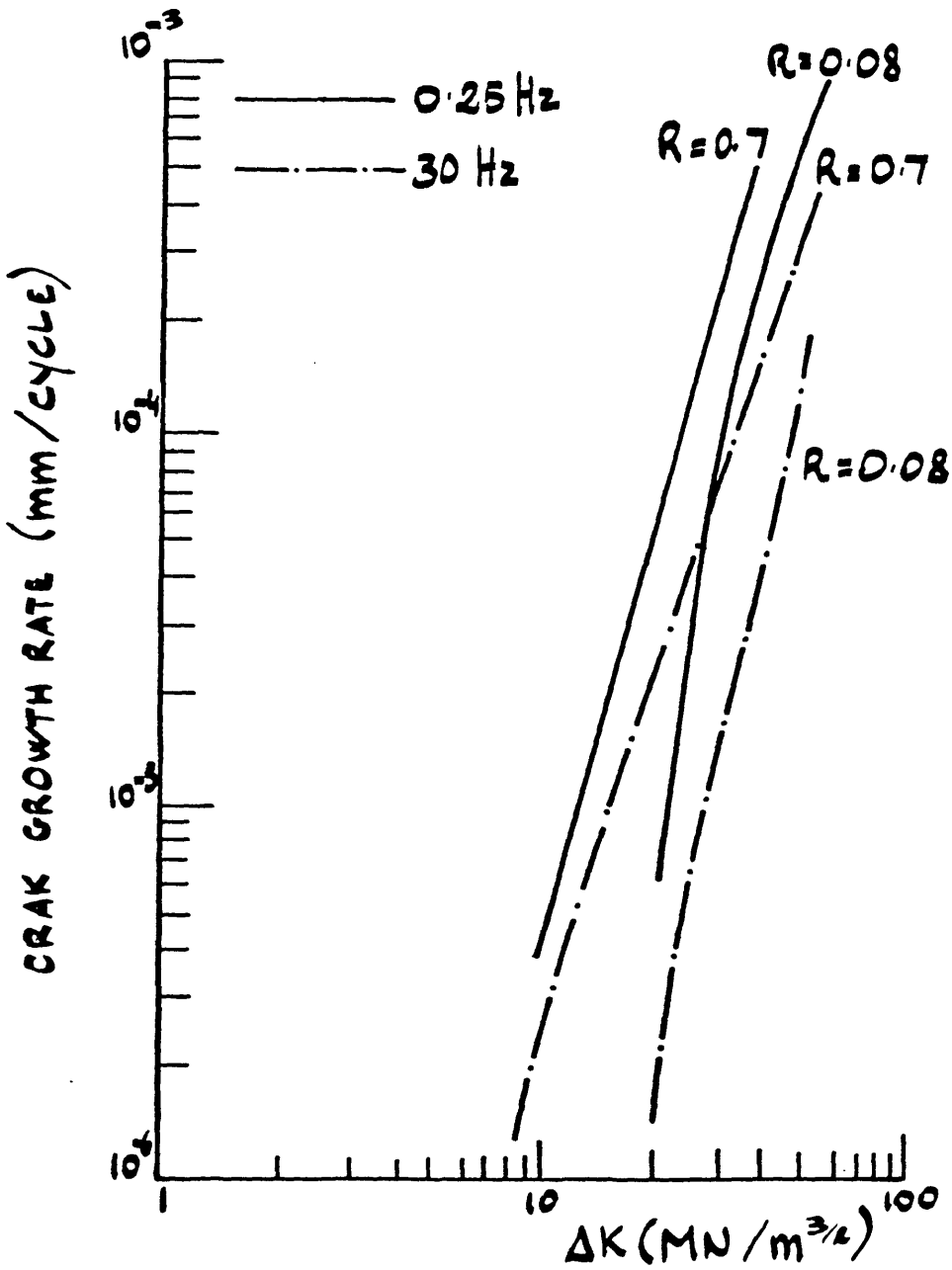


Figure 7.4 Effect of frequency on sandwich weldment using a CT specimen.

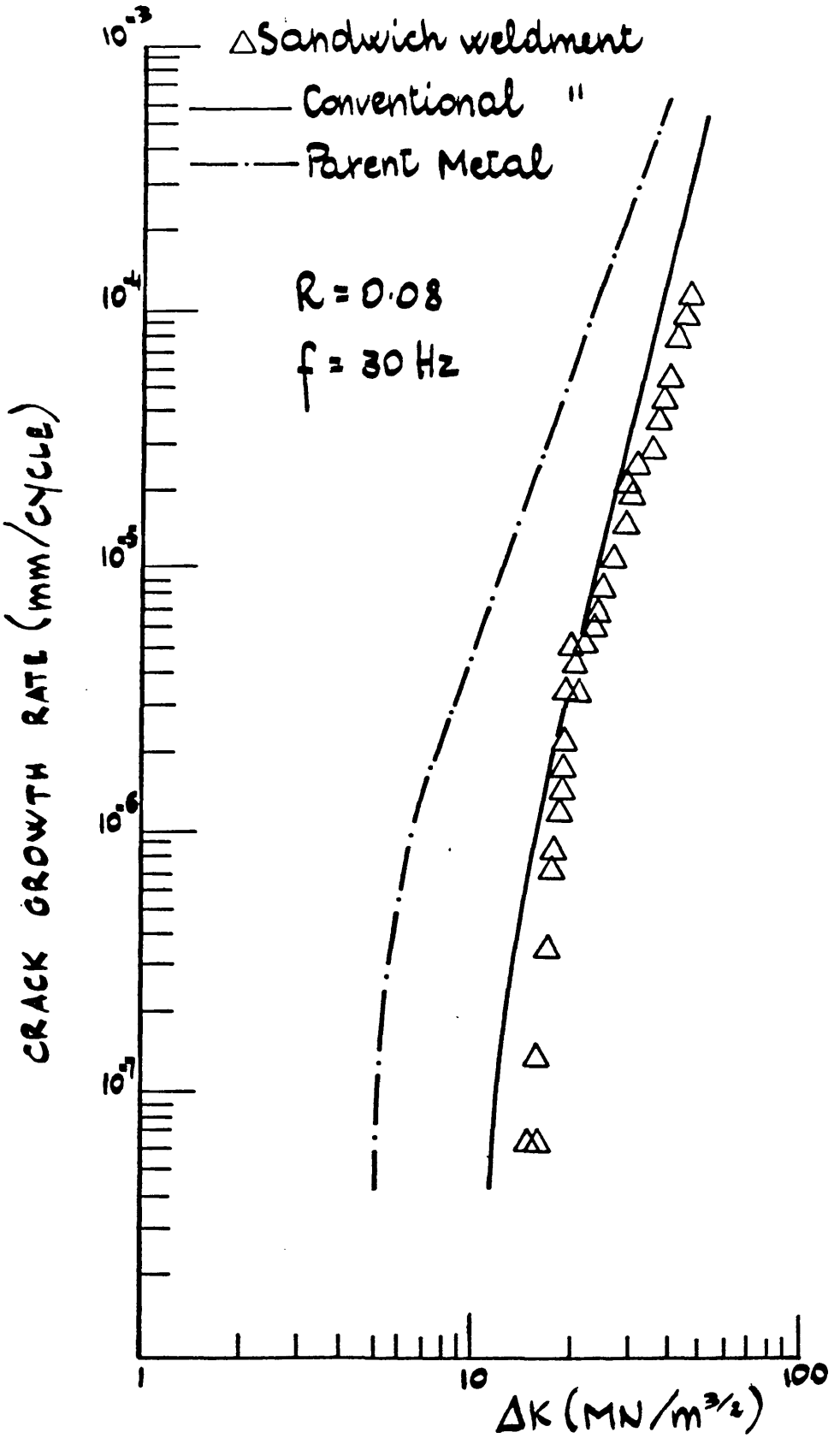


Figure 7.5 Comparison of results obtained for sandwich weldment, conventional weldment and parent material using a CT specimen.

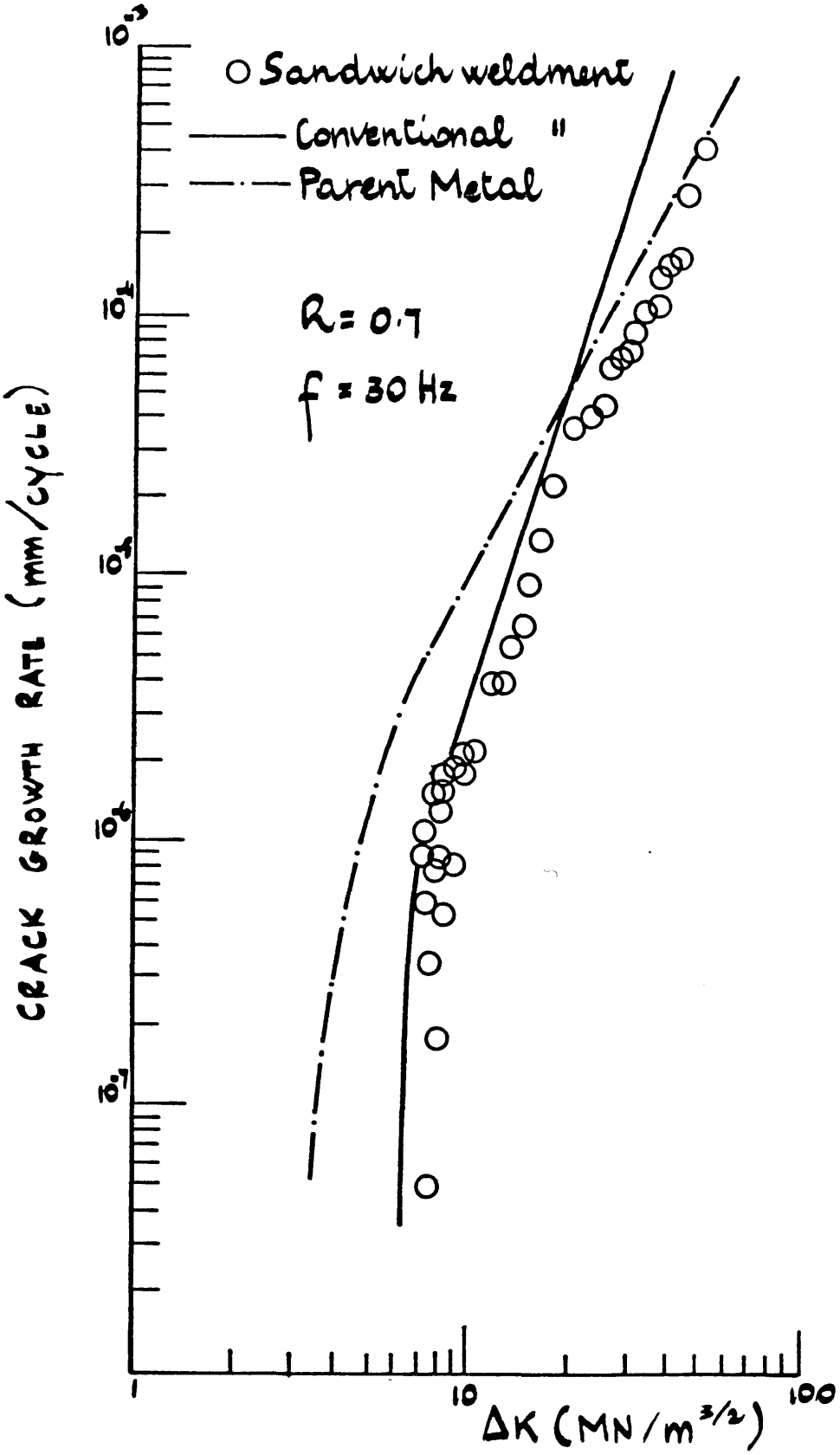


Figure 7.6 Comparison of results obtained for sandwich weldment, conventional weldment and parent material using a CT specimen.

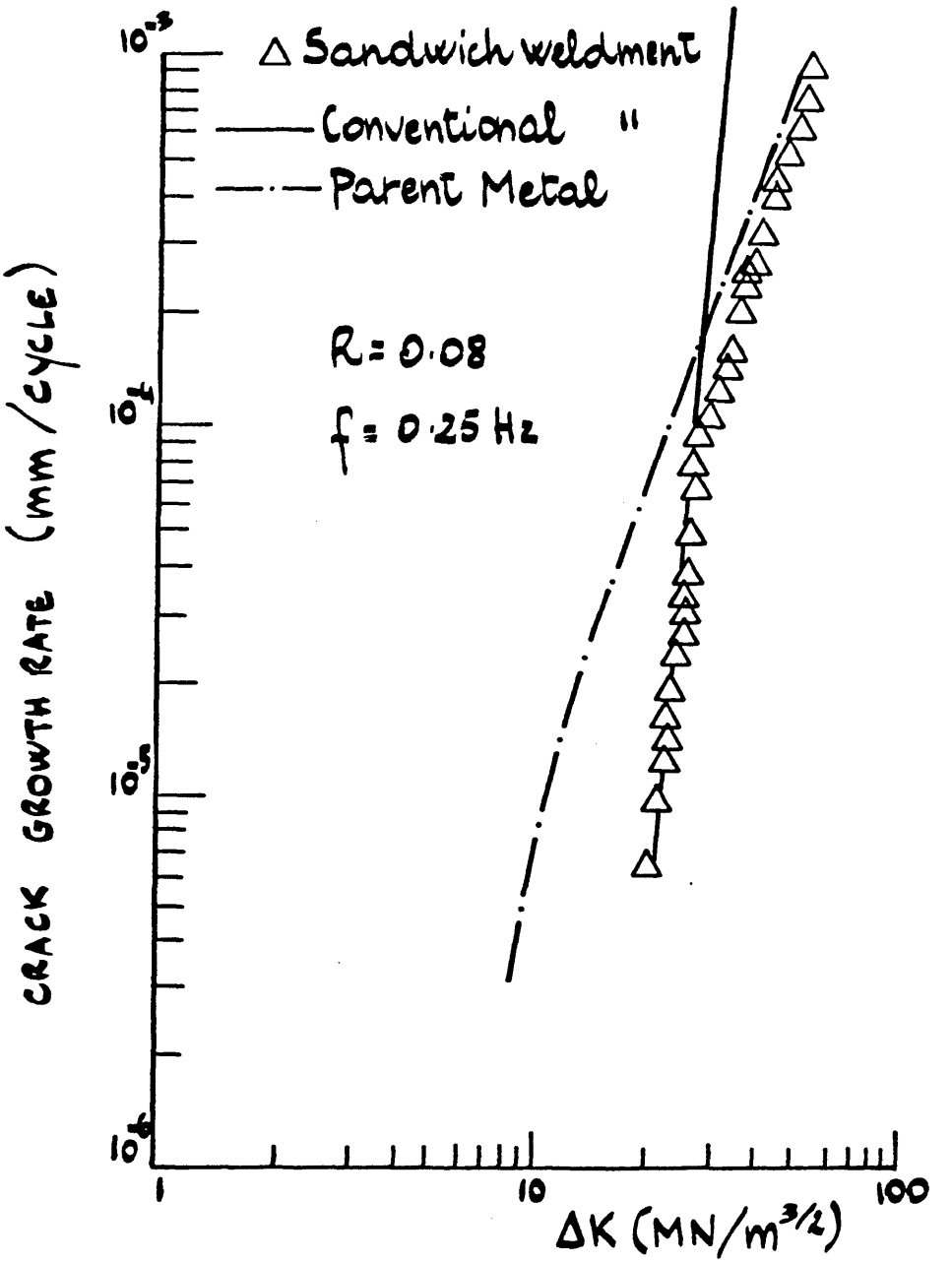


Figure 7.7 Comparison of results for sandwich weldment, conventional weldment and parent material using a CT specimen.

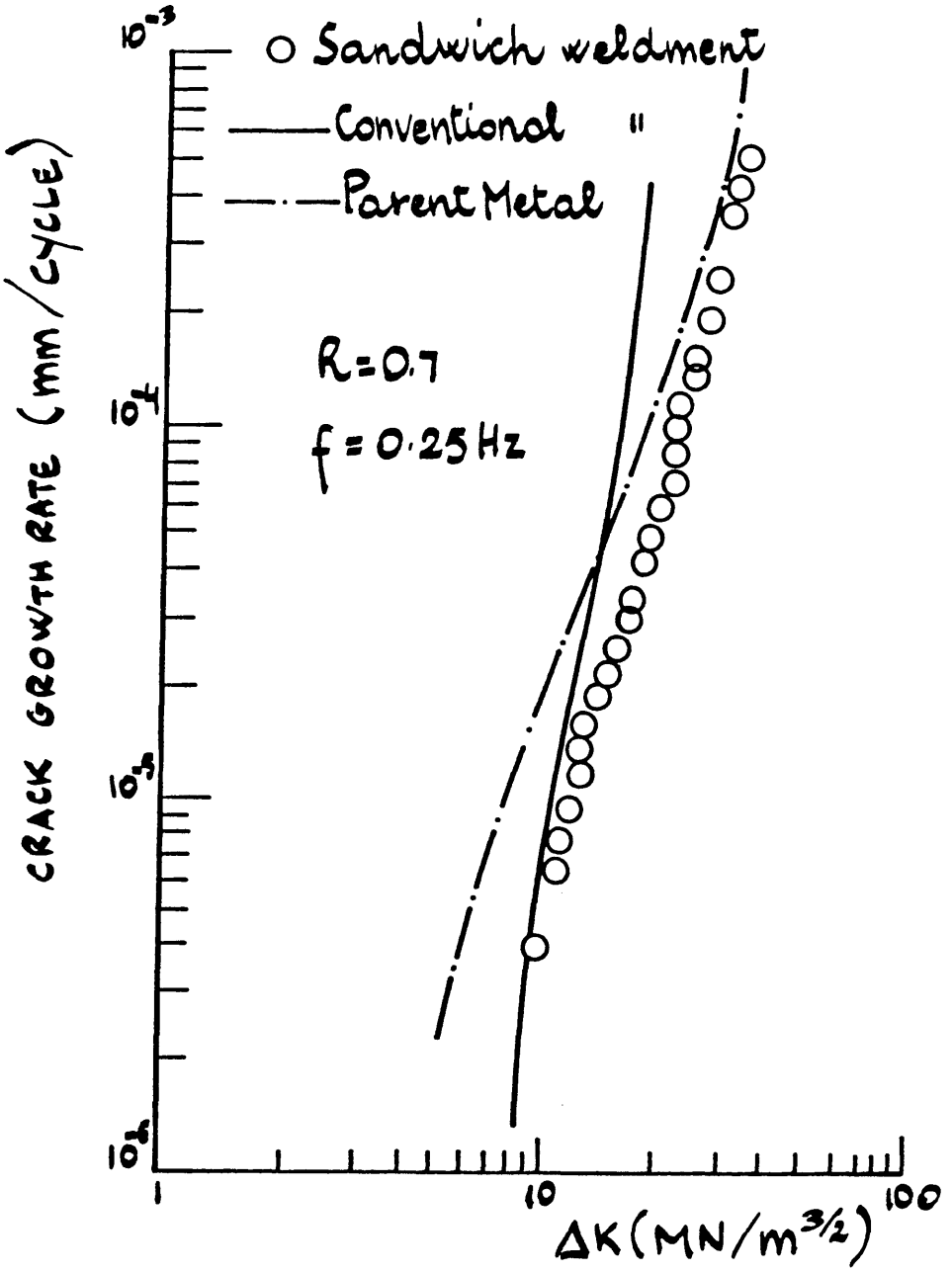


Figure 7.8 Comparison of results for sandwich weldment, conventional weldment and parent material using a CT specimen.

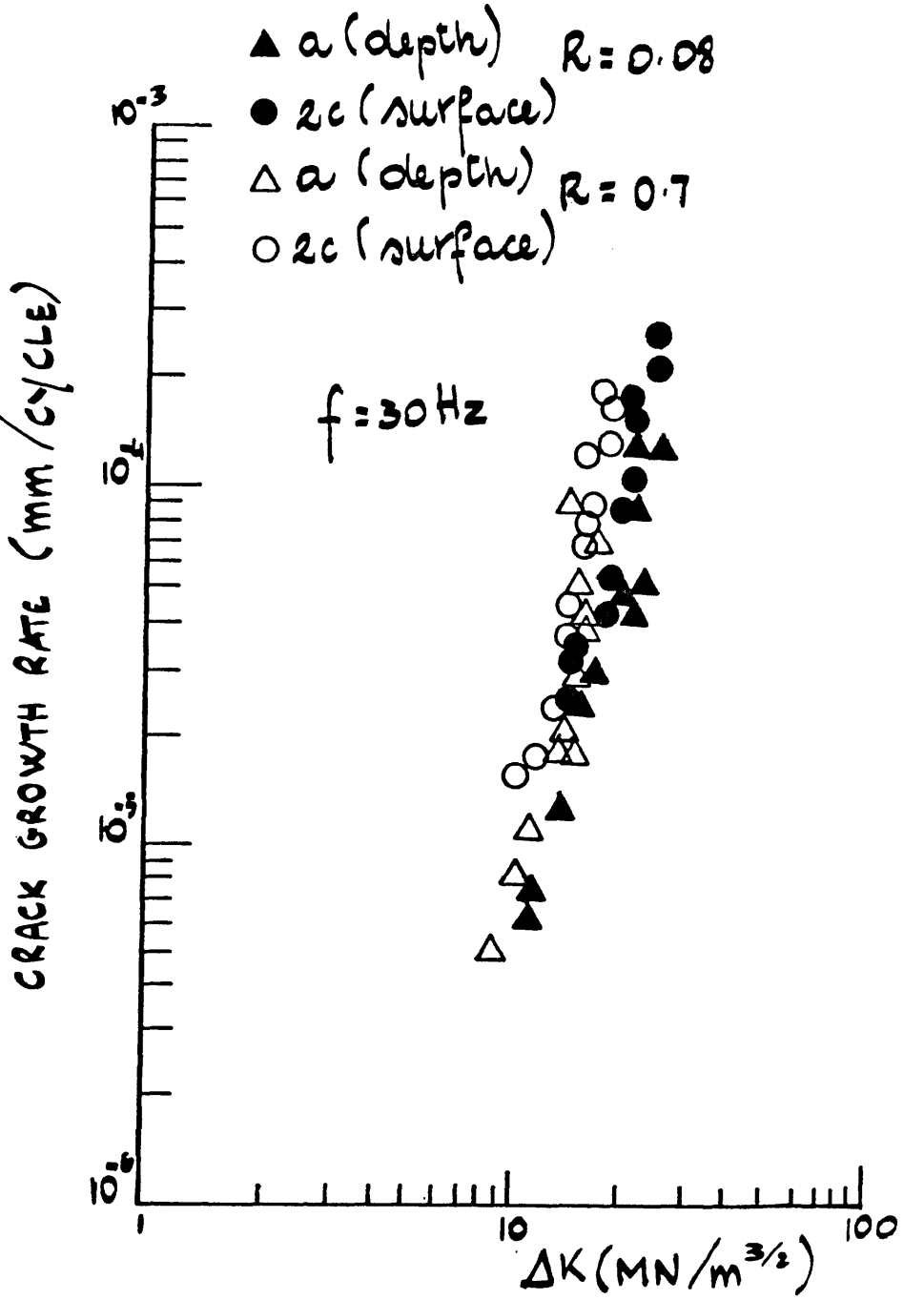


Figure 7.9 Effect of stress ratio on sandwich weldment using SNP geometry.

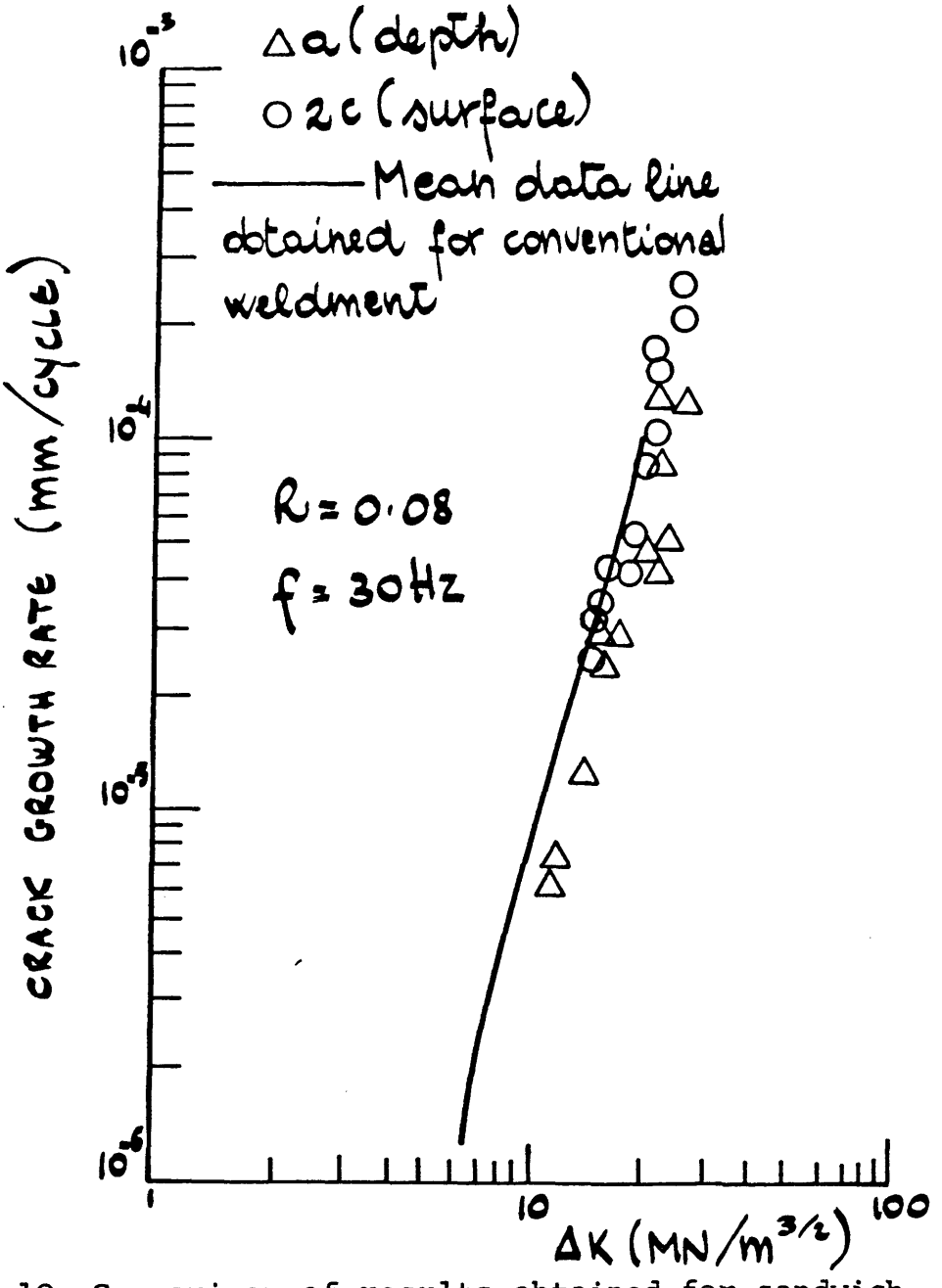


Figure 7.10 Comparison of results obtained for sandwich weldment and conventional weldment using SNP geometry.

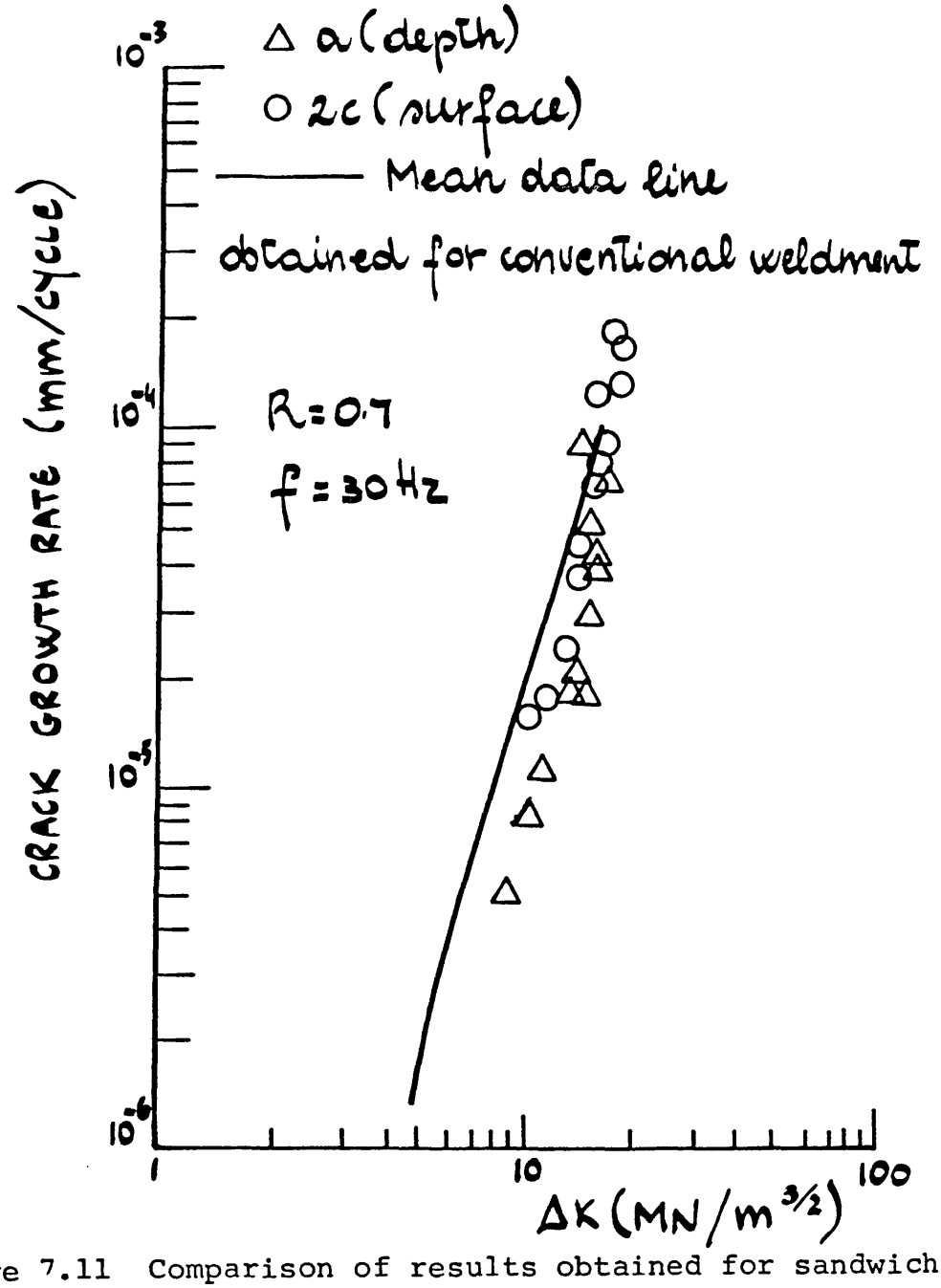


Figure 7.11 Comparison of results obtained for sandwich weldment and conventional weldment using SNP geometry.

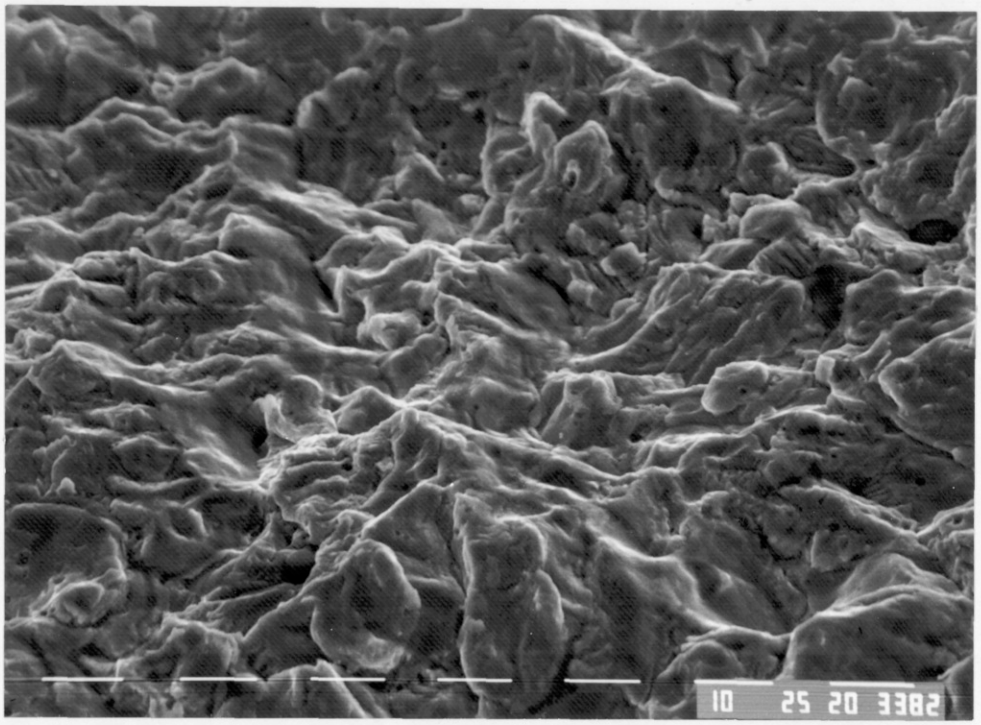


Figure 7.12 SEM photograph of sandwich weldment in the threshold region illustrating intergranular fracture, $\Delta K=8$ MN/m$^{3/2}$

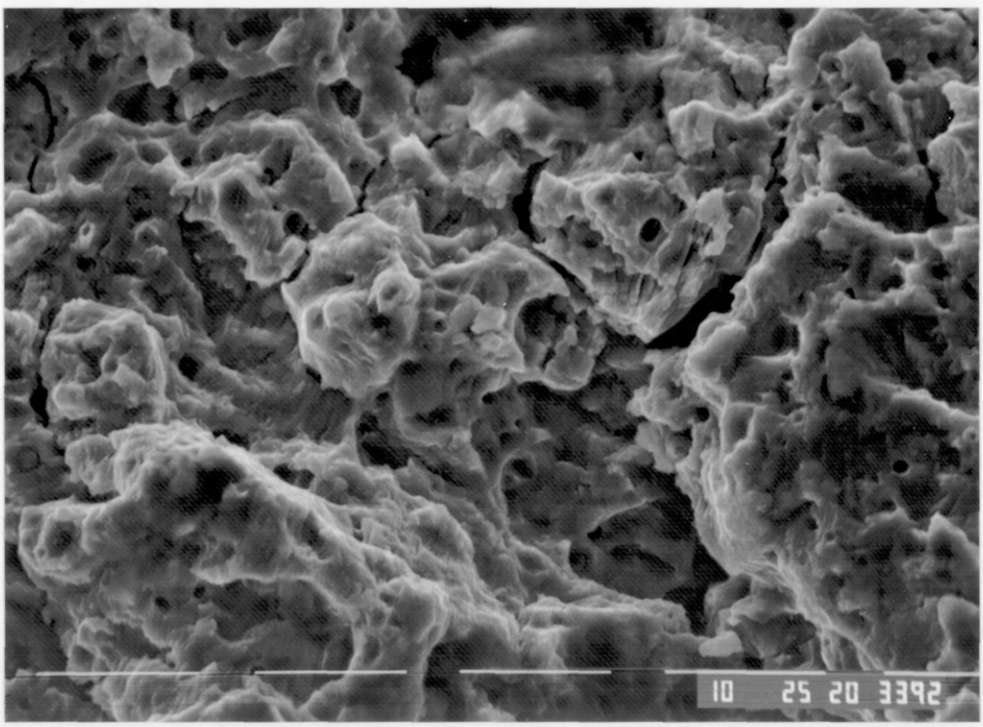


Figure 7.13 Fracture surface of sandwich weldment at $\Delta K=10$ MN/m$^{3/2}$ showing striation patches

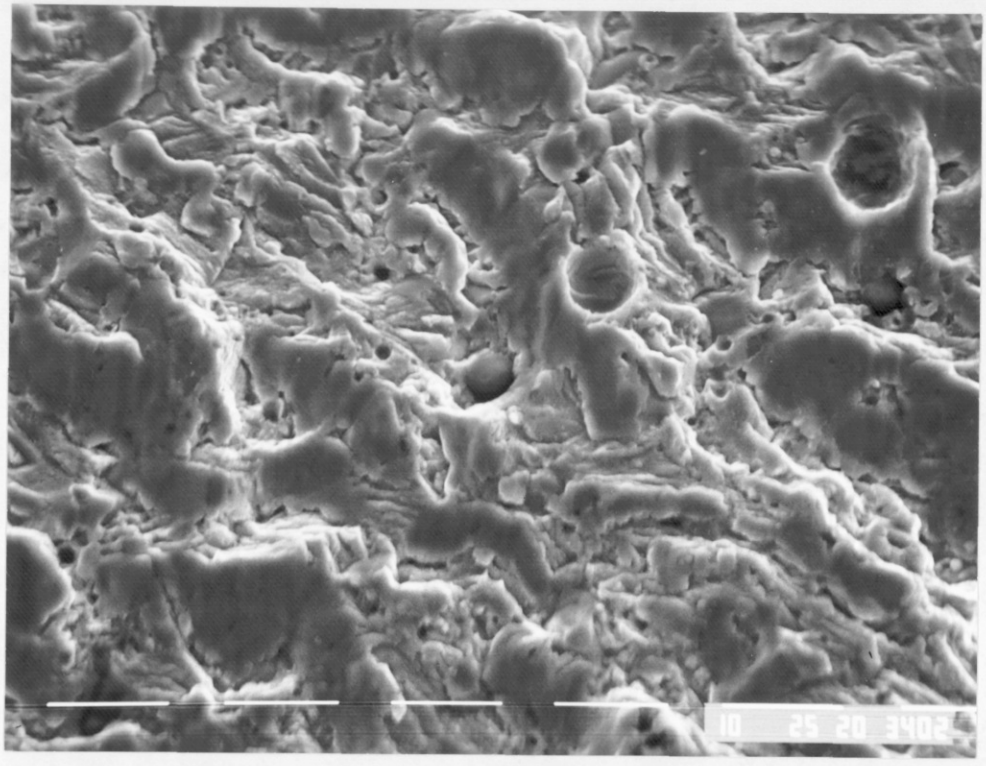


Figure 7.14 Fatigue fracture in sandwich weldment across low ΔK region region with mechanical damage and porosity

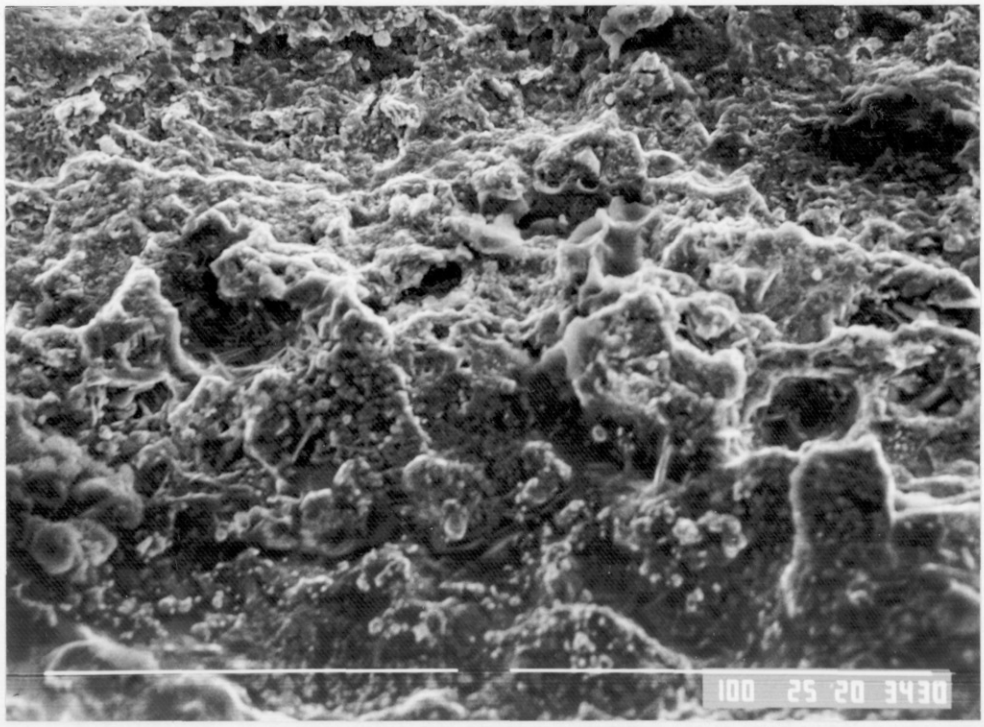


Figure 7.15 A typical area containing slag entrapment

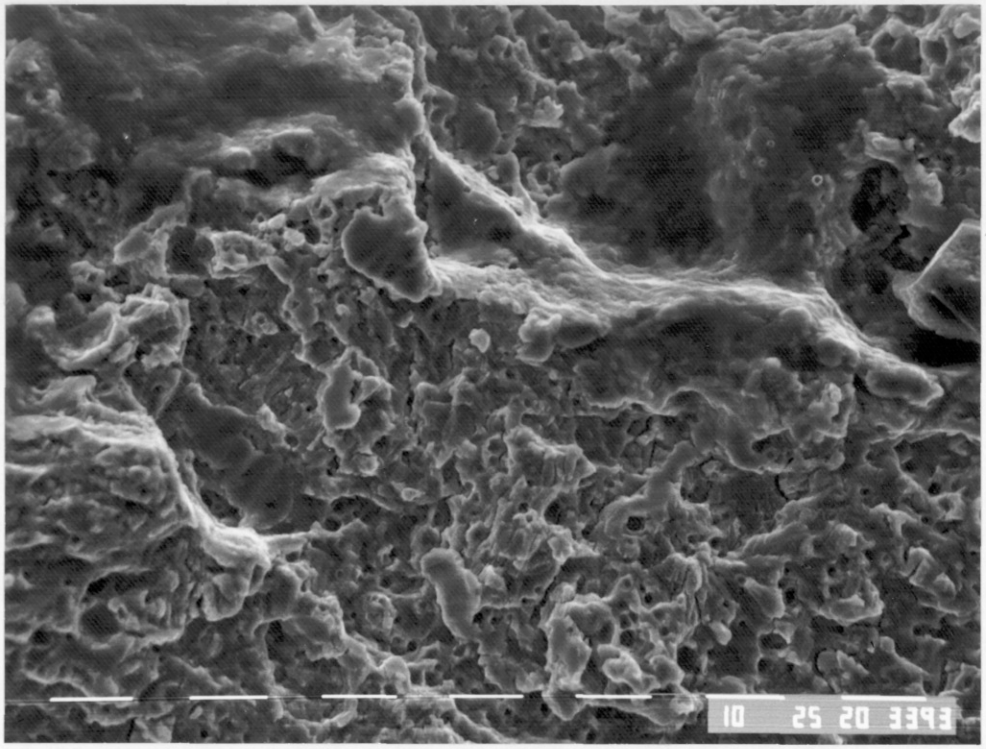


Figure 7.16 Slag entrapment in sandwich weldment

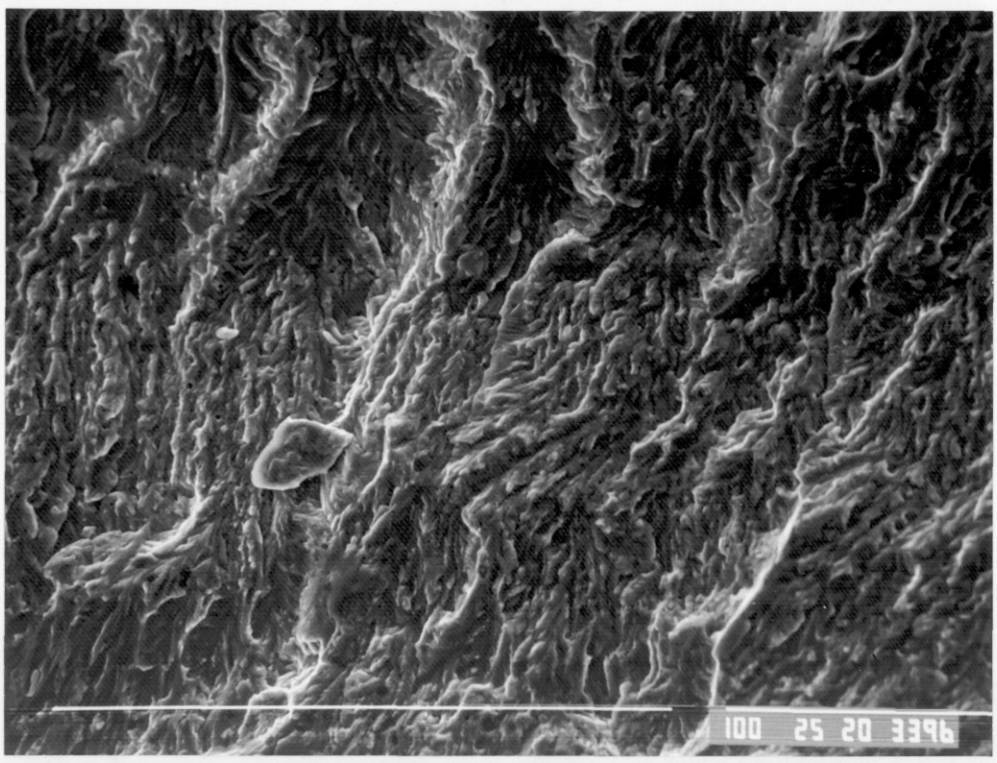


Figure 7.17 SEM photograph showing typical fatigue surfaces in sandwich weldment

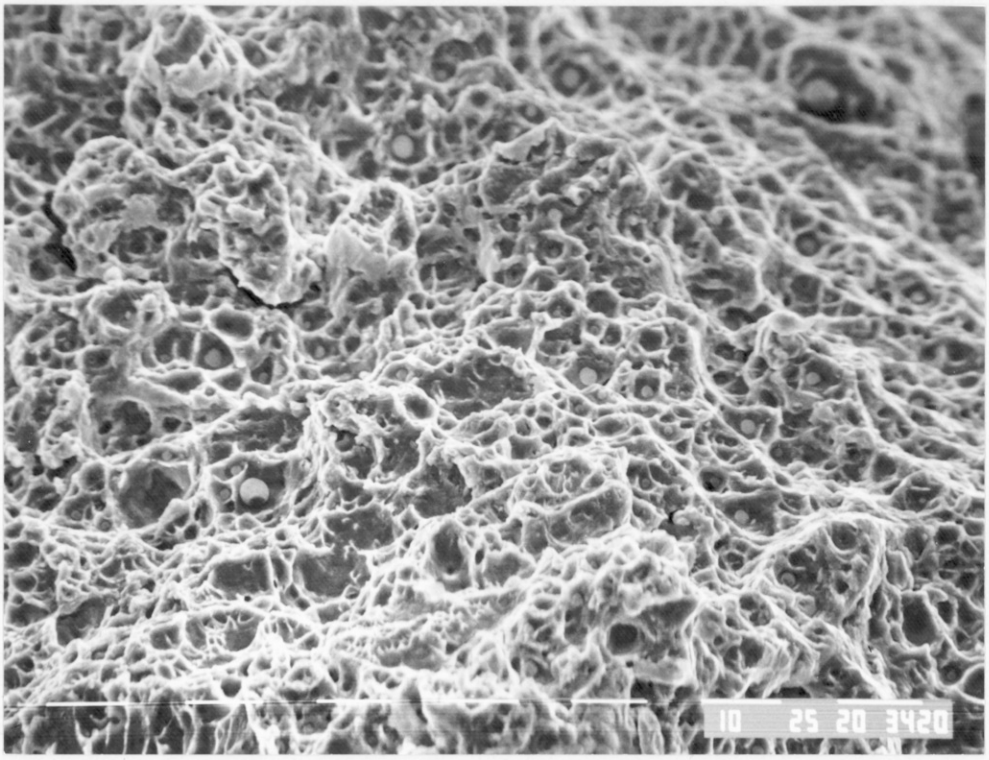


Figure 7.18 Sandwich weldment fracture surfaces showing an area of 100% microvoid coalescence

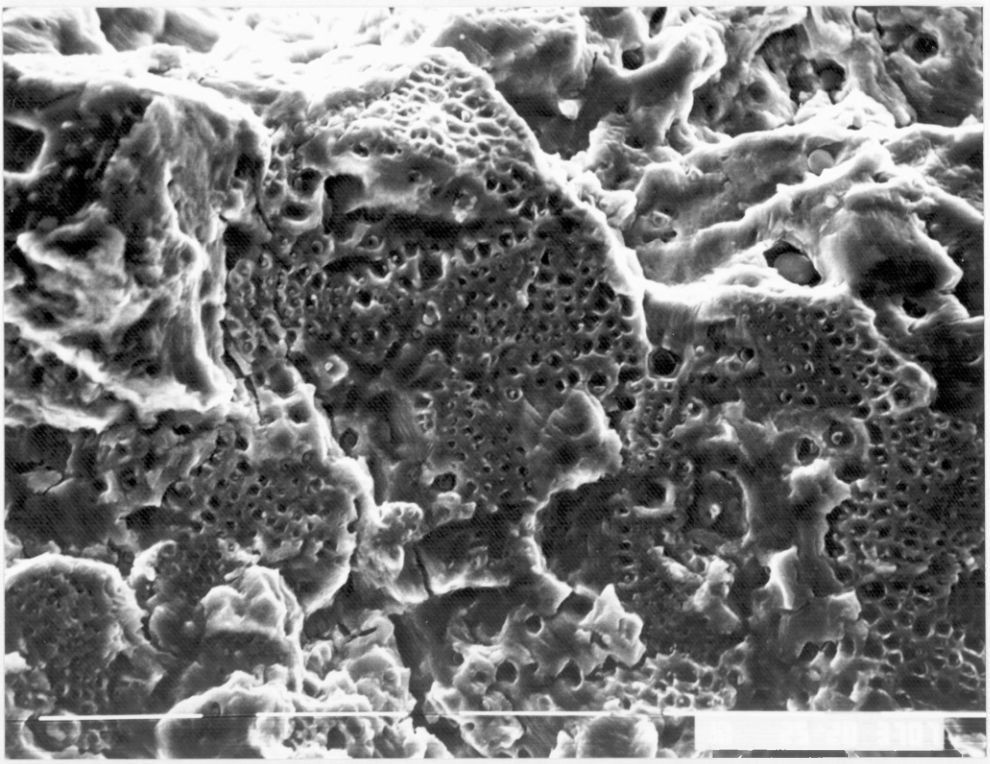


Figure 7.19 SEM photograph of sandwich weldment showing inclusion and striation in the Paris regime

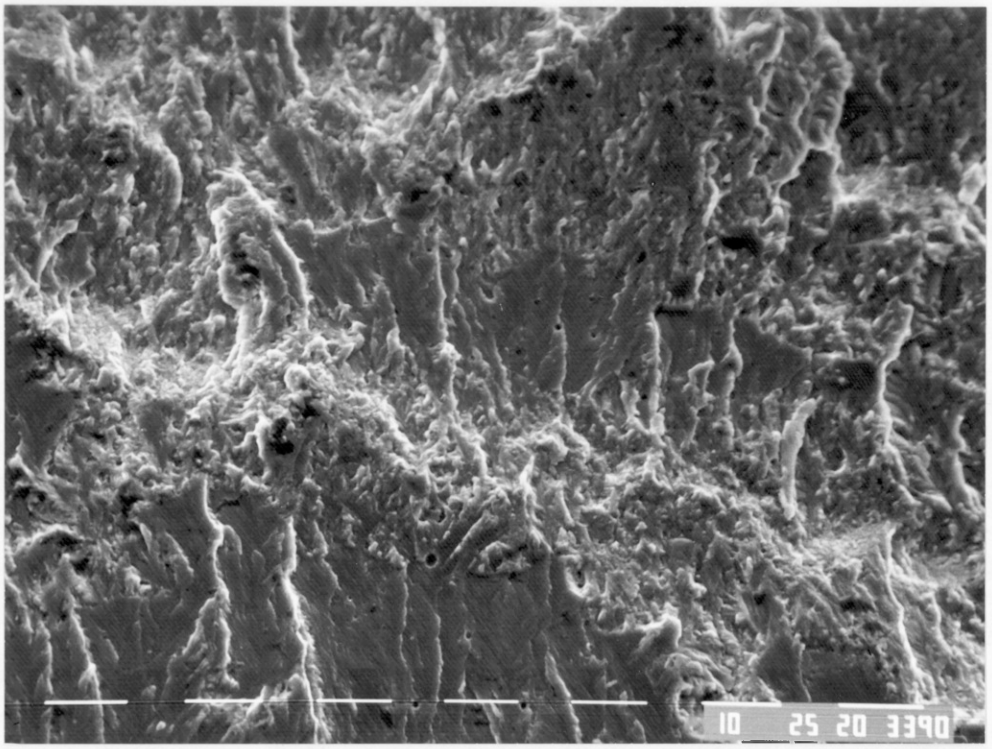


Figure 7.20 SEM photograph of sandwich weldment illustrating transgranular cleavage-like fracture in the Paris regime

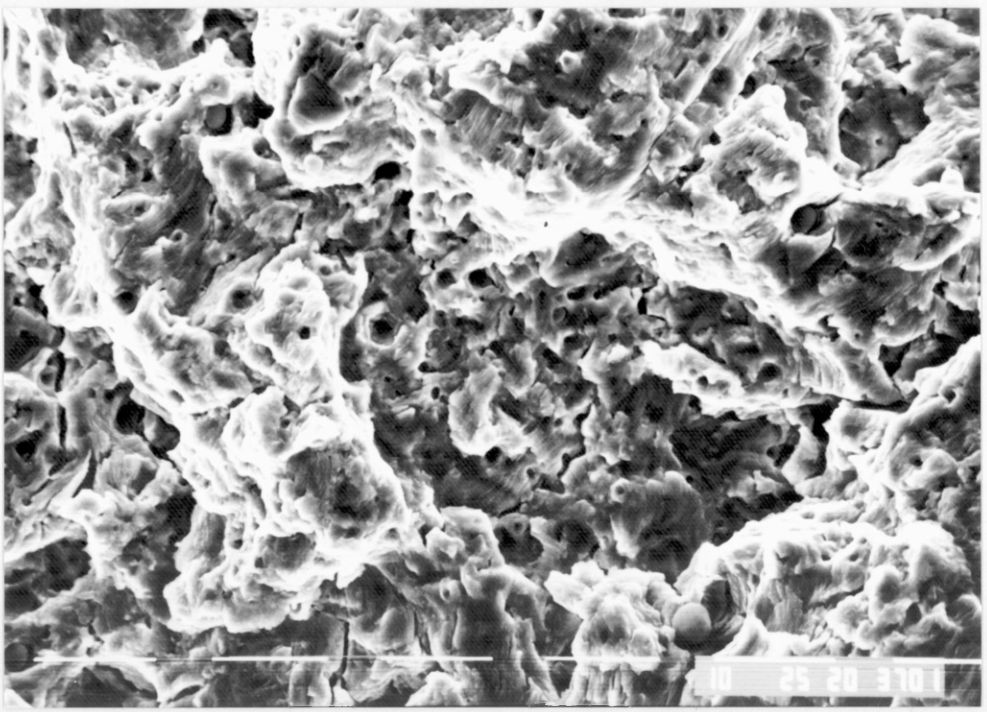


Figure 7.21 Microvoid, porosity and striation on the surface of a sandwich weldment at $\Delta K > 30$ MN/m$^{3/2}$

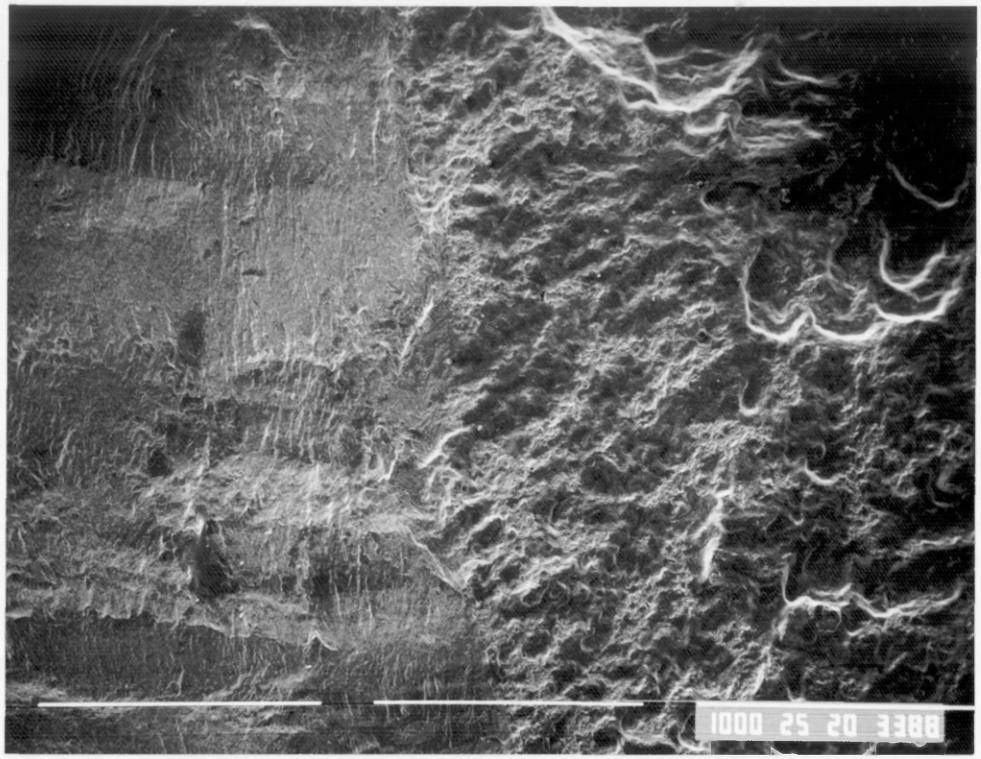


Figure 7.22 SEM photograph taken at the boundary of two weld metals at $\Delta K=9$ MN/m$^{3/2}$

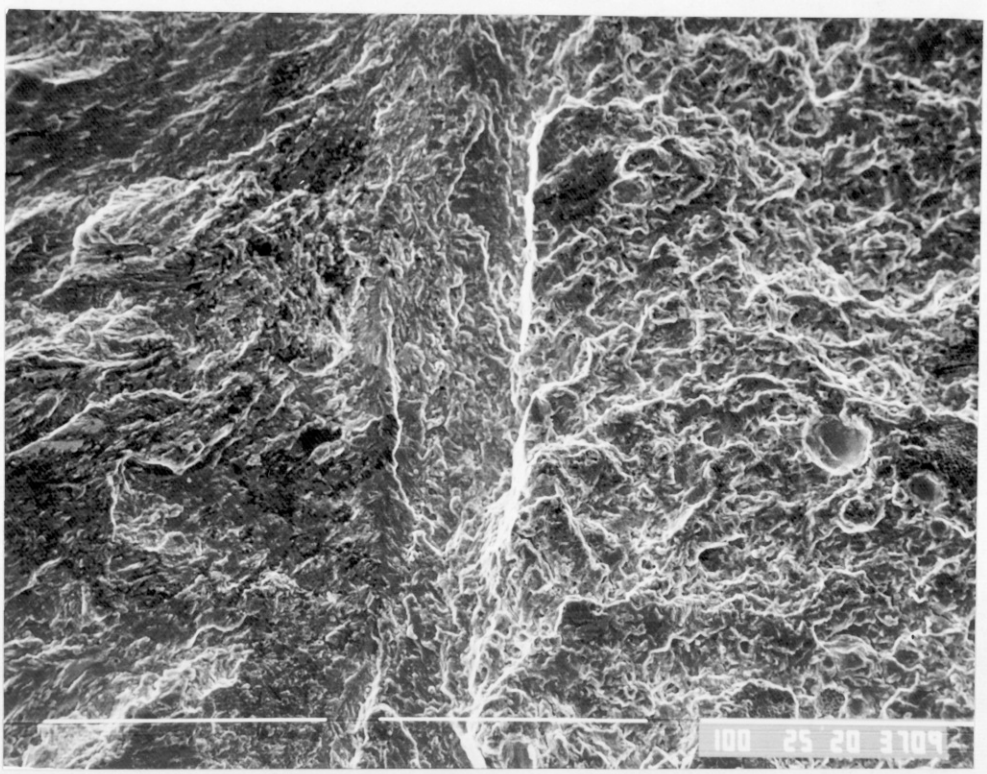


Figure 7.23 SEM photograph taken at the boundary of two weld metals at $\Delta K>30$ MN/m$^{3/2}$

CHAPTER 8

CONCLUSIONS AND RECOMMENDATIONS

8.1 INTRODUCTION

A fracture mechanics approach was successfully applied in the investigation of surface crack growth in BS4360-50D low alloy structural steel and class 6 weld metal. This investigation differed from its predecessors in a number of ways. Both for the through-thickness direction and at the free surface, crack growth rates were obtained, the model proposed not being limited to fatigue crack propagation of the deepest point alone; the crack both in the through-thickness direction and across the width can be accommodated.

Although the fields of fracture mechanics and of failure in thick plates have both been the subjects of active research at Imperial College for some years, attempts to describe the behaviour of surface cracks more accurately have been made only very recently. This investigation is one of the first and may perhaps be viewed as a forerunner in this field. Nevertheless, when compared with previous work on fatigue properties of low alloy structural steel, this investigation has provided considerable data on the surface crack behaviour of steel and weld metal used in the fabrication of North Sea oil platforms. This chapter draws together the main conclusions of the investigation, followed by recommendations of areas in which further work may be

beneficial.

8.2 GENERAL CONCLUSIONS

The main conclusions drawn from this investigation are as follows:-

1) The A.C. potential drop microgauge is suitable for crack depth measurements in a bending stress field. The main advantages of the microgauge are that it can measure the crack depth along the crack front for the surface notched plates tested and that its accuracy can be varied for different positions of the crack front by varying the gain value. Increasing the gain was found to increase the sensitivity of the microgauge without affecting the linearity of the digital voltage with the crack depth.

2) Fatigue crack growth rates are generally found to increase with increase in stress ratio and decrease in frequency. The effect of stress ratio is most pronounced at low growth rates, especially in the base metal and welded joints containing compressive residual stresses (i.e., CT geometry). At high growth rates and frequencies, however, no appreciable effect of stress ratio was observed for both HAZ and weldment. The effect of frequency in general was most significant at high stress ratios for a given frequency.

3) The stress intensity factor solution proposed by Koterazawa and Minamisaka [138] for semi-elliptical surface cracks in a bending stress field was demonstrated to be a

simple and fast way of finding the stress intensity factor range, ΔK, and was found to yield accurate data when compared with data obtained from compact-type specimens. However, the disagreement between the results for weldments obtained from different types of specimen tested was due to the different residual stress distributions produced by welding. When the sign and magnitude of the welding residual stresses around the crack tip are unknown, the data obtained for surface-notched welded plates will be conservative, and no further deterioration factor need be considered to account for tensile mean stresses. However, if the welding residual stresses are compressive, the fatigue data for the base metal will be conservative. In this case it will be necessary to take into account the deterioration of these properties at high growth rates ($>10^{-4}$mm/cycle) due to the existence of the tensile mean stress.

4) A salt-water environment was found to enhance crack growth rates only after a certain stress intensity factor range, ΔK, was reached. Below this ΔK -value the crack growth rate is the same as or lower than in air. This ΔK -value, beyond which rapid growth ensues, varies with the material, and also with the residual stress distribution for the case of welded joint specimens.

5) Stress-relieving does not change the shape of the curves in air and salt-water environments, but reduces only the stress intensity factor range, ΔK, for welded joints containing compressive residual stresses (i.e., CT geometry) and increases this ΔK value for welded joints with tensile

residual stresses (i.e., SNP geometry).

6) The following expressions were obtained and can be used to express the crack growth rate for BS4360-50D steel, and the weldment and HAZ associated with that steel, under various mechanical and environmental conditions:-

BS4360-50D Steel

i) Upper bound for growth rates in air -

$$\frac{da}{dN} = 9.0 \times 10^{-8} (\Delta K)^{3.0} \qquad \text{at 30Hz,}$$

$$\frac{da}{dN} = 4.9 \times 10^{-9} (\Delta K)^{3.6} \qquad \text{at 0.25Hz.}$$

ii) Upper bound for growth rates in 3.5% NaCl solution -

$$\frac{da}{dN} = 6.5 \times 10^{-11} (\Delta K)^{5.4} \qquad \text{at 30Hz.}$$

Weldment

i) Upper bound for growth rates using CT specimen in air -

$$\frac{da}{dN} = 5.0 \times 10^{-11} (\Delta K)^{4.85} \qquad \text{at 30Hz,}$$

$$\frac{da}{dN} = 5.0 \times 10^{-11} (\Delta K)^{5.15} \qquad \text{at 0.25Hz.}$$

ii) Upper bound for growth rates using SNP geometry in air -

$$\frac{da}{dN} = 2.3 \times 10^{-8} (\Delta K)^{3.2} \qquad \text{at 30Hz,}$$

$$\frac{da}{dN} = 1.35 \times 10^{-8} (\Delta K)^{4.2} \qquad \text{at 0.25Hz.}$$

iii) Upper bound for growth rates using CT specimen in 3.5% NaCl solution -

$$\frac{da}{dN} = 1.0 \times 10^{-10} (\Delta K)^{5.67} \qquad \text{at 30Hz,}$$

$$\frac{da}{dN} = 3.1 \times 10^{-11} (\Delta K)^{5.8} \qquad \text{at 0.25Hz.}$$

iv) Upper bound for growth rates using SNP geometry in 3.5% NaCl solution -

$$\frac{da}{dN} = 2.5 \times 10^{-10} (\Delta K)^{5.67} \qquad \text{at 30Hz.}$$

HAZ

i) Upper bound of growth rate data for HAZ using SNP geometry in air -

$$\frac{da}{dN} = 2.0 \times 10^{-10} (\Delta K)^{5.15} \qquad \text{at 30Hz,}$$

$$\frac{da}{dN} = 1.6 \times 10^{-10} (\Delta K)^{5.67} \qquad \text{at 0.25Hz.}$$

7) Crack growth rates can also be modelled from threshold to the high crack growth rate regime in terms of material fatigue properties:

$$\frac{da}{dN} = A \left\{ \frac{(1-R^2)(\Delta K^2 - \Delta K . \Delta K_{th})}{K_{1c}^2 (1-R)^2 - \Delta K^2} \right\}^{\alpha}$$

for BS4360-50D where $A_c=4.69\times10^{-4}$, $A_a=2.49\times10^{-4}$ and $\alpha_c=1.00$, $\alpha_a=0.94$ at 30Hz, and $A_a=2.02\times10^{-3}$, $A_c=1.43\times10^{-3}$ and $\alpha_c=1.17$, $\alpha_a=1.19$ at 0.25Hz; for weldment using SNP geometry, $A_c=5.22\times10^{-3}$, $A_a=3.34\times10^{-3}$ and $\alpha_c=1.26$, $\alpha_c=1.23$ for 30Hz, and $A_c=7.08\times10^{-2}$, $A_a=3.34\times10^{-2}$ and $\alpha_c=1.48$, $\alpha_a=1.65$ for 0.25Hz. These results are confined to an air environment.

8) For the initial crack configuration tested, the crack depth in air can be found using the following equations:

BS4360-50D Steel

at 30Hz -

$a = -6.79 + 0.87c - 0.90 \times 10^{-2}c^2$ R=0.08,

$a = -7.66 + 0.92c - 0.93 \times 10^{-1}c^2$ R=0.7;

at 0.25Hz -

$a = -5.79 + 0.79c - 0.81 \times 10^{-2}c^2$ R=0.08,

$a = -6.95 + 0.87c - 0.89 \times 10^{-2}c^2$ R=0.7.

Weldment

at 30Hz -

$a = -5.48 + 0.85c - 0.93 \times 10^{-2}c^2$ R=0.08,

$a = -5.76 + 0.89c - 0.96 \times 10^{-2}c^2$ R=0.7;

at 0.25Hz -

$a = -6.69 + 0.96c - 0.12 \times 10^{-1}c^2$ R=0.08,

$a = -5.99 + 0.88c - 0.99 \times 10^{-2}c^2$ R=0.7.

9) Using assumed values of initial flaw size, a prediction of the development of the shape of the surface crack in a bending stress field was made; differing values for initial flaw size and shape, and geometric variables, were considered. The main conclusion drawn from these simulations is that initial elliptical flaws with low aspect ratio will cause earlier failure since they appear to develop to a stable crack shape more quickly. This is the case assuming the initial aspect ratio is a function of crack depth, a, only. Considering the case in which the aspect ratio is a function of crack length, 2c, the converse is true.

8.3 RECOMMENDATIONS FOR FUTURE WORK

The present study has indicated a number of areas which require further work and more detailed investigation:-

1) The crack microgauge system with standard probe performed very well but, due to lengthy procedures of processing the raw data, further attention should be given to fixed probes along the crack line at the surface which are interfaced to a micro-computer. Also, using a micro-computer system for control of the machine and for analysis of the fatigue data during fatigue testing should be explored.

2) The present results for the weldment indicate the importance of welding residual stresses, which is reflected in the data obtained for laboratory specimens of different

geometries. Therefore, it is recommended that in the first instance the welding residual stresses should be measured and taken account of in calculations in an attempt to describe the results of tests more comprehensively, and where possible the tests should be carried out on test-pieces of the same geometry and the full-scale size for which the data is required.

3) The threshold region of crack growth at low frequency has not been the subject of an experimental study. Extrapolation of the low frequency results point to the fact that the threshold region of growth is not affected by the frequency. The significance of this region in respect of life-expectancy in relatively high stress situations makes a detailed investigation necessary.

4) The results of tests in air and salt-water environments indicate that in the latter, where crack growth continues at a reduced rate, a critical value of ΔK exists beyond which rapid growth ensues. This value of ΔK appeared to be a function of residual stresses, and to be independent of frequency as far as weldments are considered. Further work is required to assess this phenomenon.

5) The model for predicting the shape development of surface cracks, as described in Chapter 6, should be modified to include life prediction. The accuracy of the model when using different aspect ratios should be determined by experiments in which it is possible to produce initial crack configurations of the required size.

6) Interesting results have been obtained from sandwich weldments but considerably more work is required in this field. The fatigue properties of sandwich weldments produced by different combinations of welding rods and/or more layers (i.e., seven-layer sandwich) should be explored.

REFERENCES

1) Knott, J.F. "Fundamentals of Fracture Mechanics", Butterworth [1973]

2) Broek, D. "Elementary Engineering Fracture Mechanics", Noordhoff Int. Publishing [1974]

3) Griffith, A.A. "Phenomena of Rupture and Flow in Solids", Phil. Trans. Vol. 221, Series A, pp. 163-198 [1921]

4) Irwin, G.R. "Fracture Dynamics in Fracture of Metals", ASME. J. App. Mech. Vol. 14, p.152 [1948]

5) Irwin, G.R. "Analysis of Stresses and Strains Near the End of a Crack Traversing a Plate", J. App. Mech., Vol. 24, pp.361-364 [1957]

6) Williams, M.L. "On the Stress Distribution at the Base of a Stationary Crack", J. app. Mech., Vol. 24, pp. 109-114 [1957]

7) Westergaard, H.M. "Bearing Pressure and Cracks", J. App. Mech., Vol. 6, p. A49 [1939]

8) Paris, P.C. and Edrogan, F. "A Critical Analysis of Crack Propagation Laws", J. Basic Eng. Trans. ASME, Series D, Vol. 85, pp.528-539 [1963]

9) Lindley, T.C., Richard, C.E., Ritchie, R.O. "The Mechanics and Mechanism of Fatigue Crack Growth in Metals",

Conf. on the Mechanics & Physics of Frac., Churchill College, Cambridge [1975]

10) Pelloux, R.M.N. "Mechanism of Formation of Ductile Fatgue Striations", Trans. ASME, Vol. 63, pp. 281-285 [1969]

11) Pelloux, R.M.N. "Crack Extension by Alternating Shear", Eng. Frac. Mech., Vol. 1, pp. 697-704 [1970]

12) Richard, C.E. and Lindley, T.C. "The Influence of Stress Intensity and Microstructure on Fatigue Crack Propagation in Ferritic Materials" Eng. Frac. Mech., Vol. 4, pp. 951-978 [1972]

13) Ritchie, R.O. and Knott, J.F. "Mechanisms of Fatigue Crack Growth in Low Alloy Steels", Acta Metallurgica, Vol. 21, pp. 639-648 [1973]

14) Ritchie, R.O. "Near-Threshold Fatigue Crack Propagation in Ultra-High Strength Steels: Influence of Load Ratio and Cyclic Strength", J. Eng. Mater. & Tech., Vol. 99, pp. 195-204 [1977]

15) Barsom, J.M. "The Influence of Fatigue Crack Propagation on Strain Energy Release Rate and Crack Opening Displacement", ASTM, STP 486 [1970]

16) Liu, H.W. "Fracture Crack Propagation and Applied Stress Range - An Energy Approach", J. Basic Eng. Trans. ASME, Vol. 83, pp. 23-31 [1961]

17) Weertman, J. "Rate of Growth of Fatigue Cracks Calculated from the Theory of Infinitesimal Dislocations Distributed in a Plane", Proc. Int. Conf. on Frac., Sendai, Japan, p. 153 [1965]

18) Bilby, B.A., Cottrell, A.H. and Swinden, K.H. "The Spread of Plastic Yield from a Notch", Proc. Roy. Soc., Vol. A272, pp. 304-314 [1973]

19) Rice, J.R. "Mechanism of Crack Tip Deformation and Extension by Fatigue", ASTM, STP 415, p. 247 [1967]

20) McCartney, L.N. "The Effect of Periodic-Random Loading on Fatigue Crack Growth", Int. J. Frac. Mech., Vol. 12, pp. 273-288 [1976]

21) Lardner, R.W. "A Dislocation Model for Fatigue Crack Growth in Metals", Phil. Mag. Vol. 17, pp. 71-82 [1968]

22) Schwalbe, K.H. "Some Aspects of Crack Propagation Under Monotonic and Cyclic Load", Eng. Frac. Mech., Vol. 9, pp. 547-556 [1977]

23) Majumdar, S. and Morrow, J. "Correlation Between Fatigue Crack Propagation and Low Cycle Fatigue Properties", ASTM, STP 559, pp. 159-182, [1974]

24) Antolovich, S.D., Saxena, A. and Chanani, G.R. "A Model for Fatigue Crack Propagation", Eng. Frac. Mech., Vol. 7,

pp. 649-652 [1975]

25) Duggan, T.V. "A Theory for Fatigue Crack Propagation", Eng. Frac. Mech., Vol. 9, pp. 735-747 [1977]

26) Roberts, R. and Edrogan, F. "The Effect of Mean Stress on Fatigue Crack Propagation in Plates Under Extension and Bending", J. Basic Eng., Trans. ASME, Vol. 89, pp. 885-892 [1967]

27) Forman, R.G., Kearney, V.E. and Engle, R.M. "Numerical Analysis of Crack Propagation in Cyclic Loaded Structures", J. Basic Eng., Trans. ASME, Vol. 89, pp. 459-464 [1967]

28) Mukherjee, B. and Burns, D.J. "Regression Models For the Effect of Stress Ratio on Crack Growth Rates" ASTM STP 511, p.43 [1972]

29) Hudson, C.M., Scardina, J.T. "Effect of Stress Ratio on Fatigue Crack Growth in 7075-T5 Aluminium Alloy Sheet", Eng. Frac. Mech., Vol. 1, pp. 429-446 [1969]

30) Pearson, S. "Effect of Mean Stress in 12.6mm Aluminium Alloy of High and Low Fracture Toughness", Eng. Frac. Mech., Vol. 4, pp. 9-24 [1972]

31) Nordmark, G. and Kaufman, J.G. "Fatigue Crack Propagation Characteristics of Aluminium Alloys in Thick Sections", Eng. Frac. Mech., Vol. 4, pp.193-204, [1972]

32) Branco, C.M., Radon, J.C. and Culver, L.E. "Growth of Fatigue Cracks in Steels", Metal Sciece, Vol. 10, pp. 149-155 [1976]

33) Maddox, S.J., Gurney, T.R., Mummery, A.M. and Booth, G.S. "An Investigation of the Influence of Applied Stress Ratio on Fatigue Crack Propagation in Structural Steel", Weld. Inst. Res. Rep. 72/1978/E [1978]

34) Klesnil, M. and Lukas, P. "Effect of Stress Cycle Asymmetry of Fatigue Crack Growth", Mat. Sci. Eng., Vol. 9, p. 231 [1972]

35) Dover, W.D., and Hibberd, R.D. "The Infuence of Mean Stress and Amplitude Distribution on Random Load Fatigue Crack Growth" Eng. Frac. Mech., Vol. 9, p.251 [1977]

36) Elber, W. "The Significance of Fatigue Crack Closure", ASTM STP 486, pp. 230-242 [1971]

37) Ogura, K., Ohji, K. and Honda, K. "Influence of Mechanical Factors on Fatigue Crack Closure", 4th Int. Conf. on Fracture, Vol. 2, Waterloo, Canada, p. 1035 [1977]

38) Ohta, A., Kosuge, M. and Sasaki, E. "Fatigue Crack Closure Over the Range of Stress Ratios from -1 to 0.8 Down to Stress Intensity Threshold Level in HT80 Steel and SUS304 Stainless Steel", Int. J. Frac. Mech., Vol. 14, pp. 251-269 [1978]

39) Schmidt, R.A. and Paris, P.C. "Threshold for Fatigue Crack Propagation and Effects of Load Ratio and Frequency", ASTM STP 536, p. 79 [1973]

40) Schijve, J. "Fatigue Crack Propagation in Light Alloy Sheet Materials and Structures", Nat. Aero.'& Astr. Res. Inst. Amsterdam, Rep. No. MP195 [1960]

41) Hertzberg, R.W. and Paris, P.C. "Application of Electron Fractography and Fracture Mechanics to Fatigue Crack Propagation", Proc. Int. Conf. on Frac., Sendai, Japan, Vol. 1, p. 459 [1965]

42) Yokobori, T. and Sato, K. "The Effect of Frequency on Fatigue Crack Propagation Rate and Striation Spacing in 2024-T3 Aluminium Alloy and SM-50 Steel", Eng. Frac. Mech., Vol. 18, pp. 81-88 [1976]

43) Musuva, J.K. and Radon, J.C. "The Effect of Stress Ratio and Frequency on Fatigue Crack Growth", Fatigue of Eng. Mater. & Struc., Vol. 1, pp. 457-470, [1979]

44) McEvily, A.J. and Wei, R.P. "Fracture Mechanics and Corrosion Fatigue", Proc. Int. Conf. on Corrosion Fatigue, Univ. of Connecticut, p. 381 [1972]

45) Radon, J.C. "Effect of Environment on Cyclic Crack Growth in Metals", Recent Research on Mechanical Behaviour of Solids, Univ. of Tokyo Press, pp. 359-387 [1979]

46) McAdam, D.J.,Jr., and Geil, G.W. "Pitting and its Effect on the Fatigue Limit of Steels Corroded Under Various conditions", Proc. ASTM, Vol. 41, pp. 696-732 [1941]

47) Duquette, D.J. "An Historical Review of Corrosion Fatigue", Proc. Int. Conf. on Corrosion Fatigue, Univ. of Connecticut, p. 33 [1971]

48) Evans, W.R. "The Corrosion and Oxidation of Metals", Edward Arnold, London [1960]

49) Oriani, R.A. and Josephic, P.H. "Equilibrium Aspects of Hydrogen Induced Cracking in Steels", Acta Metallurgica, Vol. 22, pp. 1065-1074, [1974]

50) Barsom, J.M. "Corrosion Fatigue Crack Propagation Below K_{ISCC}", Eng. Frac. Mech., Vol. 3, pp. 15-26 [1971]

51) Vosikovsky, O. "Fatigue Crack Growth in X-65 Line Pipe Steel at Low Cyclic Frequencies in Aqueous Environments", Trans. ASME, Vol. 97, pp. 298-304 [1975]

52) Austen, I.M. and Waker, E.F. "Quantitative Understanding of the Effects of Mechanical and Environmental Variables on Corrosion Fatigue Crack Growth Behaviour", Conf. on Influence of Env. on Fatigue, Paper No. C98/77, Inst. of Mech. Engs. [1977]

53) Atkinson, J.D. and Lindley, T.C. "The Effect of Frequency and Temperature on Environmentally Assisted

Fatigue Crack Growth Below K_{ISCC} in Steels", Conf. on Influence of Env. on Fatigue, Paper No. C109/77, Inst. of Mech. Engs. [1977]

54) Scott, P.M. and Silvester, D.R.V. "The Influence of Mean Stress on Corrosion Fatigue Crack Growth in Structural Steel Immersed in Sea Water", UKOSRP Report, 3/02 [1977]

55) Bamford, W.H. "The Effect of Pressurised Water Reactor Environment on Fatigue Crack Propagation on Pressure Vessel Steel", Proc. Conf. on Influence of Env. on Fatigue, Inst. of Mech. Engs., London [1977]

56) Bamford, W.H. "Application of Corrosion Fatigue Crack Growth Rate Data to Integrity Analysis of Nuclear Reactor Vessels", Trans. ASME, J. Press. Vess. Tech., Vol. 101, pp. 182-190 [1979]

57) Bamford, W.H. "Fatigue Crack Growth of Stainless Steel Piping in a Pressurised Water Reactor Environment", J. Press. Vess. Tech., Vol. 101, pp. 73-79 [1977]

58) Hibberd, R.D. and Dover, W.D. "The Influence of a Sea Water Environment on Random Load Fatigue Crack Growth in Two Low Alloy Steels", Conf. on Influence of Env. on Fatigue, Inst. of Mech. Engs., London, pp. 145-159, [1977]

59) Frost, N.E. "Notch Effects and the Critical Alternating Stress Required to Propagate a Crack in an Aluminium Alloy Subjected to Fatigue Loading", J. Mech. Eng. Sci., Vol. 2,

p. 109 [1960]

60) Frost, N.E., Pook, L.P. and Denton, K. "A Fracture Mechanics Analysis of Fatigue Crack Growth Data for Various Materials", Eng. Fract. Mech., Vol. 3, p. 109 [1971]

61) Sadananda, K. and Shahinian, P. "Prediction of Threshold Stress Intensity for Crack Propagation Using a Dislocation Model", Int. J. Fract. Mech., Vol. 13, pp. 585-594 [1977]

62) Ritchie, R.O. "Influence of Microstructure on Near Threshold Fatigue Crack Propagation in Ultra High Strength Steel", Metal Sci., Vol. 11, pp. 368-381 [1977]

63) Cooke, R.J. and Beevers, C.J. "Slow Fatigue Crack Propagation in Pearlitic Steels", Mater. Sci.& Eng., Vol. 13, pp. 201-210 [1974]

64) Masounave, J. and Bailon, J.P. "The Dependence of the Threshold Stress Intensity Factor on Cyclic Stress Ratio of Fatigue of Ferritic-Pearlitic Steels", Scripta Metall., Vol. 9, pp. 723-730 [1975]

65) Vosikovsky, O. "Frequency, Stress Ratio and Potential Effects on Fatigue Crack Growth of HY130 Steel in Salt Water", J. Testing & Eval., Vol. 6, pp. 175-182 [1977]

66) Vosikovsky, O. "The Effect of Stress Ratio on Fatigue Crack Growth Rates in Steels", Eng. Fract. Mech., Vol. 11, pp. 595-603 [1979]

67) McEvilly, A.J. "Current Aspects of Fracture", Proc. Conf. on Fatigue, Cambridge, U.K., pp. 1-9 [1977]

68) Davenport, R.T. and Brook, R. "The Threshold Stress Intensity Range in Fatigue", Fatigue of Eng. Mater. & Struct., Vol. 1, pp. 151-158 [1979]

69) Radon, J.C. "Influence of Environment on Threshold in Fatigue Crack Growth", Metal Sci., Vol. 13, pp. 411-419 [1979]

70) Pook, L.P. and Greenman, A.F. "Various Aspects of Fatigue Crack Growth Threshold in Mild Steel", Proc. of Fatigue Testing & Design Conf., City University, London, Vol. 2, pp. 301-303 [1976]

71) Frost, N.E., Marsh, J.K. and Pook, L.P. "Metal Fatigue", Clarendon Press [1974]

72) Paris, P.C., Bucci, R.J., Wessel, E.T., Clark, W.G. and Morgan, T.R. "Extensive Study of Low Fatigue Crack Growth Rates in A533 and A508 Steels", ASTM STP 513, pp. 141-176 [1972]

73) Bucci, R.J., Clark, W.G. and Paris, P.C. "Fatigue Crack Propagation Rates Under a Wide Variation of ΔK for ASTM A517 Grade F(T-1) Steel", ASTM STP 513, pp. 177-195 [1972]

74) Mantz, J. and Weiss, V. "Mean Stress and Environmental

Effects on Near Threshold Fatigue Cracks and Fracture", ASTM STP 601, pp. 154-168, [1976]

75) Usami, S. and Shida, S. "Elastic-Plastic Analysis of the Fatigue Limit for a Material With Small Flaws", Fatigue of Eng. Mater.& Struct., Vol. 1, pp. 471-481 [1979]

76) Cooke, R.J., Irwing, P.E., Booth, B.S. and Beevers, C.J. "The Slow Fatigue Crack Growth and Threshold Behaviour of Medium Carbon Alloy Steel in Air and Vacuum", Eng. Fract. Mech., Vol. 7, pp. 69-77 [1975]

77) Irving, P.E. and Kurzfeld, A. "Measurement of Intergranular Failure Produced During Fatigue Crack Growth in Quenched and Tempered Steels", Metal Sci., Vol. 12, pp. 495-502 [1978]

78) Kirby, B.R. and Beevers, C.J. "Slow Fatigue Crack Growth and Threshold Behaviour in Air and Vacuum of Commercial Aluminium Alloys", Fatigue of Eng. Mater. & Struct., Vol. 1, pp. 203-215 [1979]

79) Ritchie, R.O. "Near Threshold Fatigue-Crack Propagation in Steels", Int. Metals Review, Nos. 5 and 6, pp. 205-230 [1979]

80) Newman, R.P. "Significance of Weld Defects in Relation to Fatigue Fracture", Br. J. of NDT., Vol. 7, pp. 90-96 [1965]

81) Newman, R.P. and Dawes, M.G. "Exploratory Fatigue Tests on Transverse Butt Welds Containing Lack of Penetration", Br. Weld. J., Vol. 12, pp. 117-120 [1965]

82) Mindlin, H. "Influence of Details on Fatigue Behaviour of Structures", ASCE, J. of Struct. Division, Vol. 94, No. ST12, pp. 2679-2697 [1968]

83) Welter, G. and Choquet, J.A. "Variable Stress Cycle Fatigue of Large Butt Welded Specimens", Weld. Res. Suppl., Vol. 46, pp. 395-485 [1967]

84) Munse, H.J. "Fatigue of Welded Steel Structures", Welding Research Council, New York [1964]

85) Newman, R.P. and Gurney, T.R. "Fatigue Tests on Plain Plate Specimens and Transverse Butt Welds", Br. Weld. J., Vol. 6, pp. 569-594 [1959]

86) Signes, E.G., Baker, R.G., Harrison, J.D. and Burdekin, F.M. "Factors Affecting the Fatigue Strength of Welded High Strength Steels", Br. Weld. J., Vol. 14, pp. 108-116 [1967]

87) Clough, R. "Application of Weld Performance Data", Br. Weld. J., Vol. 15, pp. 319-325 [1968]

88) Munse, W.H., Comment on Fatigue Properties of Materials", Ocean Eng. Vol. 1, pp. 189-195 [1968]

89) Warren, W.G. "Fatigue Tests on Defective Butt Welds",

Weld. Res. Suppl., Vol. 6, pp. 112r-117r [1952]

90) Newman, R.P. and Gurney, T.R. "Fatigue Tests on 1/2 in. Transverse Butt Welds Containing Slag Inclusions", Br. Weld. J., Vol. 11, pp. 341-352 [1964]

91) Harrison J.D. "Further Fatigue Tests on 1½ in. Thick Butt Welds Containing Slag Inclusions", Br. Weld. J., Vol. 15, pp. 85-94, [1968]

92) Osgood, W.R. "Residual Stresses in Metal and Metal Construction", Reinhold Publ. Co., New York [1954]

93) Gurney, T.R. "Fatigue of Welded Structures", Cambridge University Press [1968]

94) Masubushi, K. "Analysis of Welded Structures", Pergamon Press Ltd. [1980]

95) Cordiano, H.V. "Effect of Residual Stresses on Low Cycle Fatigue Life For Large Scale Weldments in High Strength Steel", Trans. ASME, J. Eng. for Indust., Vol. 92, pp. 86-92 [1970]

96) Wirsching, P.H. and Kempert, J.E. "Design Codes That Fight Fatigue", Machine Design, Vol. 48, pp. 108-113 [1976]

97) Gurney, T.R. and Maddox, S.J. "Reanalysis of Fatigue Data for Welded Joints in Steel", Weld. Res. Int., Vol. 3, pp. 1-54 [1973]

98) Booth, G.S. "The Effect of Mean Stress on Fatigue Lives of Ground or Peened Fillet Welded Steel Joints", The Weld. Inst., 34(1977) [1977]

99) Pisarski, H.G. "Fatigue Crack Propagation in Aluminium Alloy Weldment", Weld. Res. Int., Vol. 6, pp. 28-39 [1976]

100) Underwood, J.H., Pook, L.P. and Sharples, J.K. "Fatigue Crack Propagation Through a Measured Residual Stress Field in Low Alloy Steel", ASTM STP 631, pp. 402-415 [1977]

101) Glinka, G. "Effect of Residual Stresses on Fatigue Crack Growth in Steel Weldment Under Constant and Variable Loads" ASTM STP 677, pp. 198-214 [1979]

102) Kanazawa, T., Oba, H. and Machida, S. Soc. of Naval Arch. of Japan J., Vol. 109, pp. 359-369 [1961] (in Japanese)

103) Baxter, D.E. and Madlen, G.F. "Some Factors Affecting the Fatigue Strength of Fillet Welds", Br. Weld. J., Vol. 13, pp. 184-188 [1966]

104) Dawse, K.R. and Richards, C.E. "Fatigue Crack Propagation Through Weld Heat Affected Zone", Metall. Trans, Vol. 2, pp. 599-603 [1971]

105) Griffiths, J.C., Mogford, I.L. and Richards, C.E. "The Influence of Mean Stress on Fatigue Crack Propagation in a

Ferritic Weld Metal", Metal Sci., Vol. 5, pp. 145-149 [1971]

106) Parry, M., Nordberg, H. and Hertzber, R.W. "Fatigue Crack Propagation in A514 Base Plate and Welded Joints", Weld. Res. Suppl., Vol. 51, pp. 485s-490s [1972]

107) Shahinian, P., Smith, H.H. and Hawthorne, J.R. "Fatigue Crack Propagation in Stainless Steel Weldment at High Temperature", Weld. Res. Suppl., Vol. 51, pp. 527s-532s [1972]

108) Poon, C.J. and Hoeppner, D.W. "The Effect of Frequency and Environment on Fatigue Behaviour of ASTM A533 Grade B Class 1 Weldment Material", Int. J. of Fract. Mech., Vol.1, pp. 141-152 [1979]

109) Ohta, A., Sasaki, E., Nihei, M., Kanao, M. and Inagaki, M. "Fatigue Crack Propagation Rates and Threshold Stress Intensity Factors for Welded Joints of HT80 Steel at Several Stress Ratios", Int. J. Fatigue, Vol. 4, pp. 233-237 [1982]

110) Lloyd, G.J. and Walls, J.D. "Propagation of Fatigue Cracks From Surface Flaws in Austenitic Type 316 Butt Welds", Eng. Fract. Mech., Vol. 13, pp. 897-911 [1980]

111) Kenyon, N., Morrison, W.B. and Quarrell, A.G. "The Fatigue Strength of Welded Joints in Structural Steel", Br. Weld. J., Vol. 13, pp. 123-137, [1965]

112) Ishihara, M., Hiraishi, S. and Sugimoto, T. "Fatigue

Ferritic Weld Metal", Metal Sci., Vol. 5, pp. 145-149 [1971]

106) Parry, M., Nordberg, H. and Hertzber, R.W. "Fatigue Crack Propagation in A514 Base Plate and Welded Joints", Weld. Res. Suppl., Vol. 51, pp. 485s-490s [1972]

107) Shahinian, P., Smith, H.H. and Hawthorne, J.R. "Fatigue Crack Propagation in Stainless Steel Weldment at High Temperature", Weld. Res. Suppl., Vol. 51, pp. 527s-532s [1972]

108) Poon, C.J. and Hoeppner, D.W. "The Effect of Frequency and Environment on Fatigue Behaviour of ASTM A533 Grade B Class 1 Weldment Material", Int. J. of Fract. Mech., Vol.1, pp. 141-152 [1979]

109) Ohta, A., Sasaki, E., Nihei, M., Kanao, M. and Inagaki, M. "Fatigue Crack Propagation Rates and Threshold Stress Intensity Factors for Welded Joints of HT80 Steel at Several Stress Ratios", Int. J. Fatigue, Vol. 4, pp. 233-237 [1982]

110) Lloyd, G.J. and Walls, J.D. "Propagation of Fatigue Cracks From Surface Flaws in Austenitic Type 316 Butt Welds", Eng. Fract. Mech., Vol. 13, pp. 897-911 [1980]

111) Kenyon, N., Morrison, W.B. and Quarrell, A.G. "The Fatigue Strength of Welded Joints in Structural Steel", Br. Weld. J., Vol. 13, pp. 123-137, [1965]

112) Ishihara, M., Hiraishi, S. and Sugimoto, T. "Fatigue

Crack Growth Rate in Base Plate and Welded Joints of High Strength Steel", 3rd Int. Symp. of the Japan Weld. Soc., Tokyo, pp. 239-244 [1978]

113) Kitsunai, Y. "Fractographic Study of Fatigue Crack Propagation in a Mild Steel Butt Welded Joint", 3rd Int. Symp. of the Japan Weld. Soc., Tokyo, pp. 233-238 [1978]

114) Maddox, S.J. "Fatigue Crack Propagation in Weld Metal and HAZ", Metal Const. & Br. Weld. J., Vol. 2, pp. 285-289 [1970]

115) Pook, L.P. "Analysis and Application of Fatigue Crack Growth Data", J. Strain analysis, Vol. 10, pp. 242-250 [1975]

116) "Tentative Test Method for Constant Load Amplitude Fatigue Crack Growth Rates Above 10^{-8} m/cycle", ASTM Standard, E647-78T [1978]

117) Dover, W.D., Charlesworth, F.D.W., Taylor, K.A., Collins, R. and Micheal, D.H. "The Use of A.C. Field Measurement to Determine the Shape and Size of a Crack in a Metal", Measurement of Crack Length and Shape During Fracture and Fatigue, Ed. Beevers, C.J., Eng. Mater. Advisory Services Ltd [1980]

118) Dover, W.D. "The Use of A.C. Field Measurements to Detect and Size Surface Breaking Cracks", Conf. Insp., Repair, Maitenance, IRM81, Edinburgh [1981]

119) Clark, W.G.,Jr., and Hudak, S.J.,Jr. "Variability in Fatigue Crack Growth Rate Testing", J. Test. & Eval., Vol. 3, pp. 454-475 [1975]

120) Gurney, T.R. "The Effect of Mean Stress and Material Yield Stress on Fatigue Crack Propagation in Steels", Metal Const., Vol. 1, pp. 91-99 [1969]

121) Davis, K.B. and Fedderson, C.E. "Evaluation of Fatigue Crack Growth Rates by Polynomial Curve Fitting", Int. J. Fract. Mech., Vol. 19, pp. 116-118 [1973]

122) Mc Cartney, L.R. and Cooper, P.M. "A Numerical Method of Processing Fatigue Crack Growth Data", Eng. Fract. Mech., Vol. 9, pp. 265-272 [1977]

123) Wei, R.P., Wei, W. and Miller, G.A. "Effect of Measurement Precision and Data Processing Procedures on Variability in Fatigue Crack Growth Rate Data", J. Test.& Eval., Vol. 7, pp. 90-95 [1979]

124) Wessel, E.T. "State of the Art of WOL Specimen for K_{1c} Fracture Toughness Testing", Eng. Fract. Mech., Vol. 2, pp. 77-103 [1968]

125) Wilson, W.K. "Stress Intensity Factors for Deep Cracks in Bending and Compact Tension Specimens", Eng. Fract. Mech., Vol. 2, pp. 169-171, [1971]

126) Srawley, J.E. "Wide Range of Stress Intensity Factor Expressions for ASTM E399 Standard Fracture Toughness Specimen", Int. J. Fract. Mech., Vol. 12, pp. 475-476 [1976]

127) Irwin, G.R. "Crack Extension Force for a Part Through Crack in a Plate", Trans ASME, J. App. Mech., Vol. 29, pp. 651-654 [1962]

128) Newman, J.C.,Jr. "A Review and Assessment of the Stress Intensity Factors for Surface Cracks", ASTM STP 687, pp. 16-42 [1979]

129) Shah, R.C. and Kobayashi, A.S. "On Surface Flaw Problem", The Surface Crack: Physical Problems and Computational Solutions, J.L. Swedlow Ed., pp. 79-124 [1972]

130) Smith, F.N. and Sonersen, D.R. "The Semi-Elliptical Surface Crack a Solution by Alternating Method", Int. J. Fract. Mech., Vol. 12, pp. 47-57 [1976]

131) Raju, I.S. and Newman, J.C.,Jr. "Stress Intensity Factors For a Wide Range of Semi-Elliptical Surface Cracks in Finite-Thickness Plates", Eng. Fract. Mech., Vol. 11, pp. 817-829 [1979]

132) Green, A.E. and Sneddon, I.N. "The Distribution of Stress in the Neighbourhood of a Flat Elliptical Crack in an Elastic Solid", Proc. Camb. Phil. Soc., Vol. 46, pp. 159-164 [1950]

133) Newman J.C.,Jr. and Raju, I.S. "Analysis of Surface Cracks in Finite Plates Under Tension or Bending Loads" NASA Tech. Paper 1578 [1979]

134) Hayashi, K. and Abe, H. "Stress Intensity Factors for a Semi-Elliptical Crack in the Surface of a Semi-Infinite Solid", Int. J. Fract., Vol. 16, pp. 275-285 [1980]

135) Smith, F.W., Emery, A.F. and Kobayashi, A.S. "Stress Intensity Factors for Semi-Circular Cracks Part 2 - Semi-infinite solid", Trans ASME J. App. Mech., Vol. 89, pp. 953-959 [1967]

136) Hartranft, R.J. and Sih, G.C. "On Methods of Analysis of Crack Problems", Noordhoff Int. Pub., pp. 179-238 [1973]

137) McGowan, J.J. "A Critical Evaluation of Numerical Solutions to the 'Benchmark' Surface Flaw Problem", Exp. Mech., Vol. 20, pp. 253-264 [1980]

138) Koterazawa, R. and Minamisaka, S. "Stress Intensity Factor of Semi-Elliptical Cracks in Bending", Japan J. Soc. Mater. Sci., Vol. 26, Part 289, pp. 915-921 [1979] (In Japanese)

139) Shah, R.C. and Kobayashi, A.S. "Stress Intensity Factors for an Elliptical Crack Approaching The Surface of a Plate in Bending", ASTM STP 513, pp. 3-21 [1972]

140) Holdbrook, S.J. and Dover, W.D. "The Stress Intensity

Factor for a Deep Surface Crack in a Finite Plate", Eng. Fract. Mech., Vol. 12, pp. 347-364 [1979]

141) Scott, P.M. and Thorpe, T.W. "A Critical Review of Crack Tip Stress Intensity Factors for Semi-Elliptical Cracks", Fatigue of Eng. Mater.& Struct., Vol. 4, pp. 291-301 [1981]

142) "Standard Test Method for Constant Load Amplitude Fatigue Crack Growth Rates Above 10^{-8} m/cycle", ASTM E647-81 [1981]

143) Musuva, J.K. "Fatigue Crack Growth in Low-Alloy Steel", PhD Thesis, Dept. of Mech. Eng., Imperial College, University of London [1980]

144) Musuva, J.K. and Radon, J.C. "Threshold of Fatigue Crack Growth in a Low Alloy Steel", Adv. in Fract. Mech., 5th Int. Conf. on Fract., Ed. D. Francois, Cannes, France, pp. 1365-1372 [1981]

145) Pook, L.P. "Fatigue Crack Propagation", In Developments in Fract. Mech. 1, App. Sci. Pub., London [1979]

146) Sullivan, A.M. and Crooker, T.W. "Analysis of Fatigue Crack Growth in High Strength Steels Part I: Stress Level and Stress Ratio Effects at Constant Amplitude", Trans ASME J. Press. Vess. Tech., Vol. 98, p. 179, [1976]

147) James, L.A. "Fatigue Crack Propagation Behaviour in

Inconel 600", Int. J. Press. Vess.& Piping, Vol. 5, p. 241 [1977]

148) Crooker, T.W. "Effect of Tension-Compression on Fatigue Crack Growth in High-Strength Alloys", Trans ASME, J. Eng. in Ind., Vol. 93, p. 893, [1971]

149) Mackay, T.L., Alperin, B.J., Bhatt, D.D. "Near-Threshold Fatigue Crack Propagation of Several High Strength Steels", Eng. Fract. Mech., Vol. 18, pp. 403-416 [1983]

150) El Haddal, M.H., Topper, T.H. and Smith, K.N. "Prediction of Non-Propagating Cracks", Eng. Fract. Mech. Vol. 11, pp. 573-584 [1979]

151) Roberts, R. and Schmidt, R.A. "Observation of Crack Closure", Int. J. Fract. Mech., Vol. 8, pp. 469-474 [1972]

152) Lindley, T.C. and Richards, C.E. "The Influence of Crack Closure and Plastic Zone Geometry on Fatigue Crack Propagation", 3rd Int. Conf. on Fract., Munich [1973]

153) Fleck, N.A. and Smith, R.A. "Crack Closure - is it just a Surface Phenomenon?", Int. J. Fatigue, Vol. 4, pp. 157-160 [1982]

154) Stewart, A.T. "The Influence of Environment and Stress Ratio on Fatigue Crack Growth at Near Threshold Stress Intensities in Low Alloy Steels", Eng. Fract. Mech., Vol. 13, pp. 463-478 [1980]

155) Reemsnyder, H.S. "Development and Application of Fatigue Data for Structural Steel Weldments", ASTM STP 648, pp. 3-21 [1978]

156) Gurney, T.R. and Maddox, S.J. "Determination of Fatigue Design Stresses for Welded Structures from an Analysis of Data", Met. Const. & Br. Weld. J., Vol. 4, pp. 418-422 [1972]

157) Blacktop, J. and Brook, R. "Compodium", Eng. Fract. Mech., Vol. 12, pp. 619-620 [1979]

158) Adams, N.J.I. "Crack Growth in the Vicinity of Welds", Weld. J., Vol. 52, pp. 508s-514s [1973]

159) Kapadia, B.M. "The Role of Residual Stresses in Fatigue Crack Propagation in Weldments", ASTM STP 648, p. 244 [1974]

160) Miller, K.J., Kfouri, A.P. "An Elastic-Plastic Finite Element Analysis of Crack Tip Fields Under Biaxial Loading Conditions", Int. J. Fract. Mech., Vol. 10, pp. 393-404 [1974]

161) Bradshaw, F.J. and Wheeler, C. "The Influence of Gaseous Environments and Fatigue Frequency on the Growth of Fatigue Cracks in Some Aluminium Alloys", Int. J. Fract. Mech., Vol. 5, pp. 255-268 [1969]

162) Nix, K.J. "The Metallography of Fatigue in High

Strength Aluminium Alloys", PhD Thesis, Dept. of Metallurgy and Material Science, Imperial College, University of London [1980]

163) Wheeler, Q.E. "Spectrum Loading and Crack Growth", General Dynamics Report FZM-5602, Forth Worth [1970]

164) Rhodes, D. and Radon, J.C. "Environmental Effects on Crack Propagation in Aluminium Alloys", Fatigue of Eng. Mater. & Struct., Vol. 1, pp. 383-393 [1979]

165) Barsom, J.M. and Novak, S.R. "Subcritical Crack Growth in Steel Bridge Members", Final Report, NCHRP, Nat. Cooperative Highway Res. Prog., Washington, pp. 12-14 [1974]

166) Johnson, R., Bretherton, J., Tomkins, B., Scott, P.M. and Silvester, D.R.V. "The Effect of Sea-Water Corrosion on Fatigue Crack Propagation in Structural Steel", Europ. Offshore Steel Res. Sem., Cambridge, U.K., [1978]

167) Morgan, H.G. and Bretherton, I. "The Influence of Intermittent Immersion on Fatigue Crack Propagation in BS4360 Grade 50D Structural Steel in Natural Sea-Water", Interim Tech. Rep. UKOSRP 3/08, Dept. of Energy, U.K. [1980]

168) Hodgkiess, T. "The Effect of Periods of Stress-Free-Corrosion on the Fatigue Behaviour of Structural Steel in Sea-Water", Europ. Offshore Steel Res. Sem., Cambridge, U.K. [1978]

169) Hartt, W.H., Tennant, J.S. and Hopper, W.C. "Solution Chemistry Modification with Corrosion Fatigue Cracks" ASTM STP 642, pp. 5-18, [1978]

170) Tu, L.K. and Seth, B.B. "Threshold Corrosion Fatigue Crack Growth in Steels", J. Test. & Eval., Vol. 6, pp. 66-74 [1978]

171) Radon, J.C., Branco, C.M. and Culver, L.E. "Crack Blunting and Arrest in Corrosion Fatigue of Mild Steel", Int. J. Fract. Mech., Vol. 12, pp. 467-469 [1976]

172) Cruse, A., Meyers, G.J. and Wilson, R.B. "Fatigue Growth of Surface Cracks", ASTM STP 631, pp. 174-189 [1977]

173) Sommer, E., Hodulak, L., Kordisch, H. "Growth Characteristic of Part Through Cracks in Thick Walled Plates and Tubes", Trans ASME, J. Press. Vess. Tech., Vol. 99, pp. 106-111 [1977]

174) Hodulak, L., Kordisch, H., Kunzelmann, S. and Sommer, E. "Influence of the Load Level on the Development of Part-Through Cracks", Int. J. Fract. Mech., Vol. 14, pp. R35-R38 [1978]

175) Thorpe, T.W., Morgan, H., Rance, A., Silvester, D.V.R., Scott, O.M. "The Effect of North Sea Service Conditions on Fatigue Crack Growth in Structural Steel", Fatigue in Offshore Structural Steel, ICE, London, pp. 29-36 [1981]

176) Francis, P.H., Davidson, D.L. and Forman, R.G. "An Experimental Investigation into the Mechanics of Deep Semi-Elliptical Surface Cracks in Mode I Loading", Eng. Fract. Mech., Vol. 4, pp. 617-635 [1972]

177) Rice, R.J. "Mathematical Analysis in the Mechanics of Fracture", Fracture, Ed. Liebowitz, H., Vol. 2, Math. Fund., Academic Press, New York [1968]

178) Keer, L.M. and Mura, T. "Stationary Crack and Continuous Distributions of Dislocations", Proc. 1st Conf. Fract., Sendai, Vol. 1, pp. 99-116 [1965]

179) Irwin, G.R. "Dimensional and Geometric Aspects of Fracture", Proc. of Conf. on Fract. of Eng. Mater. New York, ASM, pp. 211-231 [1964]

180) Liu, H.W. "The Effect of Size and Stress History on Fatigue Crack Initiation and Propagation", Proc. Cranfield Crack Propagation Symp., Vol. 2, p. 514 [1962]

181) Ayres, D.J. "A Numerical Procedure for Calculating Stress and Deformation Near a Slit in a Three Dimensional Elastic-Plastic Solid", Eng. Fract. Mech., Vol. 2, pp. 87-106 [1970]

182) Sadananda, K. and Shahinian, P. "Analysis of Crystallographic High Temperature Fatigue Crack Growth in Nickel Based Alloy", Metall. Trans. Vol. 12A, pp. 343-351 [1981]

183) Walker, N. and Beevers, C.J. "A Fatigue Crack Closure Mechanism in Titanium", Fatigue of Eng. Mater. & Struct., Vol. 1, pp. 135-148 [1979]

184) Suresh, S., Zamiski, G.F. and Ritchie, R.O. "Oxide Induced Crack Closure: An Explanation for Near Threshold Corrosion Fatigue Crack Growth Behaviour", Metall. Trans., Vol. 12A, pp. 1435-1443 [1981]

185) Wadsworth, N.J. and Hutchings, J. "The Effect of Atmospheric Corrosion on Metal Fatigue", Phil. Mag., Vol. 3, 8th Series, p. 1154 [1958]

186) Clark, W.G.Jr. "Effect of Hydrogen Gas on the Fatigue Crack Growth Rate Behaviour of HY-80 and HY-130 Steels", Proc. of Int. Conf. on the Effects of Hydrogen on Materials Properties and Selection and Structural Design, Hydrogen in Metals, Champion, Pennsylvania, ASM Special Publication 2, pp. 149-164 [1973]

187) Bennett, J.A. "Evidence Regarding Mechanism of Fatigue from Studies of Evnironmental Effects", Acta Metall., Vol. 11, pp. 799-806 [1963]

188) Holder, R. "Environmental Effects on Fatigue Crack Initiation and Propagation in a Cast Steel", Conf. on the Influ. of Envir. on Fatigue, IME, London, pp.37-41 [1977]

189) Bradshaw, F.J. "The Effect of Gaseous Environment on

Fatigue Crack Propagation", Scripta Metall., Vol. 1, pp. 41-47 [1967]

190) Harrison, J.D. "The Effect of Residual Stresses on Fatigue on Fatigue Behaviour", Residual Stresses and Their Effect, Weld. Inst. Pub., pp. 9-16 [1981]

191) Allen, J.S. "The Effect of Residual Stresses on Distortion", Residual Stresses and Their Effect, Weld. Inst. Pub., pp. 5-8 [1981]

192) Burk, J.D. and Lawerence, F.V. "Influence of Bending Stresses on Fatigue Crack Propagation Life in Butt Joint Welds", Weld. J., Vol. 56, pp. 61s-66s [1977]

193) Milliken, K.S. and Mitchell, C.M. "Comparison of Strain Gauge and X-Ray Diffraction Measurements of Residual Stresses in a Weldment of HY130 Steel", Weldment: Physical Metallurgy and Failure Phenomenon, Proc. of The 5th Landing Conf., pp. 83-94 [1978]

194) Chrenko, R.M. "Residual Stress Studies of Austenitic and Ferritic Steels", Int. Conf. on Residual Stresses in Welded Const. and Their Effect, London, Weld. Inst., pp. 79-88 [1977]

195) Scott, P.M., Silvester, D.R.V. "The Influence of Mean Tensile Stress on Corrosion Fatigue Crack Growth in Structural Steel Immersed in Sea Water", UKOSRP Report, 3/02, Harwell [1977]

196) Bristoll, P. and Opdam, J.J.G. "Fatigue of Offshore Structures: The Prediction of Fatigue Crack Propagation Under Conditions of Random Loading", Oceanology Int. 75, Brighton, U.K., pp. 3-6 [1975]

197) Wildschutt, H., de Back, J., Dortland, W. and Van Leeuwen, J.L. "Fatigue Behaviour of Welded Joints in Air and Sea water", Europ. Offshore Steel Res., Cambridge, pp. 112-153 [1978]

198) Vosikovsky, O. "Fatigue Crack Growth in HY130 Steel Weldment in Air and Water", Weld. J., Vol. 59, pp. 255s-258s [1980]

199) Ivens, P.F. and Van den Bergh, A.A. "Impact Testing of the HAZ", Met. Const.& Br. Weld. J., Vol. 6, pp. 234-236 [1974]

200) El-Soudani, S.M., Pelloux, R.M. "Anisotropy of Fatigue Crack Propagation in Aluminium Alloy Butt Welded Joints", Weld. J., Vol. 54, pp. 144s-153s, [1975]

201) Maddox, S.J. "A Fracture Mechanics Analysis of the Fatigue Strength of Welded Joints", PhD Thesis, Dept. of Mech. Eng., Imperial College, University of London [1972]

202) Radon, J.C. "Determination of Critical Stress Intensity of Fracture", Unpublished Report, Dept. Mech. Eng., Imperial College, London [1981]

203) Brown, F.W.,Jr. and Srawley, J.E. "Plain Strain Crack Toughness Testing of High Strength Metallic Materials", ASTM STP 410, p. 13 [1966]

204) Corn, D.L. "A Study of Cracking Techniques for Obtaining Partial Thickness Cracks of Pre-Selected Depth and Shapes", Eng. Fract. Mech., Vol. 3, pp. 45-52 [1971]

205) Burk, L.H. "Fatigue Growth of Surface Cracks in Bending", Eng. Fract. Mech., Vol. 9, pp. 389-395 [1977]

206) Collipriest, J.E.,Jr. "An Experimentalist's View of the Surface Flaw Problem by the Alternating Method", The Surface Crack: Physical Problems and Computational Solution, Ed. Swedlow, J.L., ASME, pp. 125-152 [1972]

207) Nair, P.K. "Fatigue Crack Growth Model for Part Through Flaws in Plates and Pipes", J. Eng. Mater. & Tech., Trans ASME, Vol. 101, pp. 53-58 [1979]

208) Hodulak, L., Kordisch, H., Kunzelmann, S. and Sommer, E. "Growth of Part-Through Cracks", ASTM STP, 677, pp. 399-410 [1979]

209) Sullivan, A.M. and Crooker,T.W. "The Influence of Specimen Thickness and Stress Relief on Fatigue Crack Growth Rate in Ni-Co-Mo-V Steel", J. Test. & Eval., Vol. 5, p. 96 [1977]

210) Heiser,F.A. and Mortimer, W. "Effect of Thickness and Orientation on Fatigue Growth rate in 4340 Steel", Met. Trans., Vol. 3, p. 2119 [1972]

211) Dover, W.D. and Boutle, N.F. "The Influence of Mean Stress and Thickness on Fatigue Crack Growth Behaviour of Aluminium Alloy BS2 L71", J. Strain Anal., Vol. 13, pp. 129-140 [1978]

212) Pierce, W.S. and Shannon, J.L. "Surface Crack Shape Change in Bending Fatigue Using an Inexpensive Resonant Fatiguing Apparatus", J. Test. & Eval., Vol. 6, pp. 183-188 [1978]

213) Ikeda, K., Denoh, S., Godai, T. and Ogawa, T. "Improvement of the Fatigue Strength of Fillet Welded Joints in 780 N/mm^2 High Strength Steel", Weld. Res. Int., Vol. 8, No. 1, pp. 16-27 [1978]

214) Harrison, J.D. "Further Fatigue Tests on Fillet Welded Specimens Subjected to Prior Overloading", Br. Weld. J., Vol. 12, No. 5, pp. 225-258 [1965]

215) Maddox, S.J. "Improving the Fatigue Lives of Fillet Welds by Shot Peening", Proc. of Conf. on Fatigue of Steel Struct. Lausanne, Switzerland, pp. 377-384 [1982]

216) Gurney, T.R. "The Influence of Residual Stress on the Fatigue Strength of Plates With Fillet Welded Attachments", Br. Weld. J., Vol. 7, pp. 415-431 [1960]

217) Chen, E.P. and Sih, G.C. "Stress Intensity Factor for a Three-Layered Plate With a Crack in the Centre Layer", Eng. Fract. Mech. Vol. 14, pp. 195-214 [1981]

APENDIX 1

The mean line fitted to the results obtained by Musuva [143] on BS4360-50D steel in air was presented in Chapter 4. Musuva whose work was briefly discussed before performed threshold fatigue tests at stress ratios of -0.7, 0.0, 0.08 and 0.7 on 25.4mm-thick CT specimens.

He used two different methods for shedding the load to obtain low crack growth rates and thresholds. In the first technique, the value of ΔK was progressively reduced by steps of 10% or less (i.e., stepping down load). This procedure was continued until threshold conditions were attained. The second technique involved lowering ΔK by increasing the stress ratio. He started the test at some value of K_{max} and at a low stress ratio (preferably R=0.0) the maximum load, P_{max} , was kept constant, but minimum load increased in steps. He found that the value of $-\Delta K$ could be reduced by even larger steps than 30% without noticeable load history effects.

He also investigated the effect of frequency on crack propagation rate and performed tests at cyclic loading of 0.06Hz, 0.02Hz and 0.25Hz and two stress ratios (i.e., 0.08 and 0.7). In all the tests he used a combination of graphical curve-fitting and finite difference (secant) method to process the raw experimental data.

However, as the present investigation and that of Musuva were performed under identical mechanical and environmental conditions to that last detail (i.e., testing machines, crack length measuring equipment, etc.) it is important to see the scatter between the results obtained in the present work and those of Musuva. Therefore it was necessary to compare the data points rather than the mean line. This is shown in Figs. A.1 and A.2 for the tests at 30Hz and in Figs. A.3 and A.4 for the tests at 0.25Hz and R-values of 0.08 and 0.7, respectively. The correlation between the results is extremely good especially for threshold tests showing that although different techniques were employed to determine the threshold stress intensity factor, both techniques yield accurate data.

The work of Thorpe et al [175] which was reviewed in Chapter 5 showed some discrepancy with the present investigation especially in the case of crack growth rates in the through-thickness direction and at stress ratio of 0.7. However, in a recent publication by Thorpe et al [1A] on corrosion fatigue of BS4360-50D steel in seawater, they conducted research on through-thickness defects in BS4360-50D steel in air and in seawater, and have presented results on semi-elliptic flaws under three-point bend loading. Like their previous investigation (i.e., [175]) they performed tests on 38mm-thick SNP geometry specimen at a cyclic frequency of 0.1Hz and stress ratios, R, of 0.1 and 0.7. The starter notches were spark machined with initial aspect

ratios of 1.0, 0.5, 0.33 and 0.25. The cyclic crack tip stress intensity factor was calculated using stress intensity factor solution proposed by Koterazawa and Minamisaka [138] together with finite area correction factor of Dover and Holdbrook [140]. Surface crack lengths were measured by direct visual observation and crack depths were measured by AC resistance and also after the test, by inspection of fracture surfaces's beach marks.

Their investigation showed that each experiment could yield up to sixteen readings of crack length and crack depth, and a study of various data-processing techniques showed that accurate measures of surface crack growth rates could be obtained by fitting a polynomial curve through the plot of surface crack length vs elapsed cycles. Through-thickness crack growth rates were determined in one of two ways: (i) if sufficient in-depth reading exited (i.e., >10) then the above polynomial method was used; (ii) if less than ten crack depths reading were available, then crack depth growth rate, da/dN, was determined from the surface crack length growth rate, dc/dN, and the slope of the plot of crack depth against length, da/dc (i.e., da/dN = da/dc x dc/dN).

The result of the present investigation when compared to the data obtained by Thorpe et al explained above showed a very good correlation. They measured growth rates higher than $1x10^{-5}$ mm/cycle at R=0.1 and $3x10^{-6}$ mm/cycle at R=0.7

and only over one order of magnitude as is shown in Figs. A.5 and A.6. Although, the specimen's thickness used in these investigations varied by about 50%, it has been reported by the above authors that crack propagation rates in air are independent of specimen thickness is further comfirmed as is shown in Figs. A.5 and A.6.

REFERENCES

1A) Thorpe, T.W., Scott, P.M., Rance, A. and Silvester, D. "Corrosion Fatigue of BS4360:50D Structural Steel in Seawater", Int. J. Fatigue, Vol. 5, No. 3, pp. 123-133 [1983]

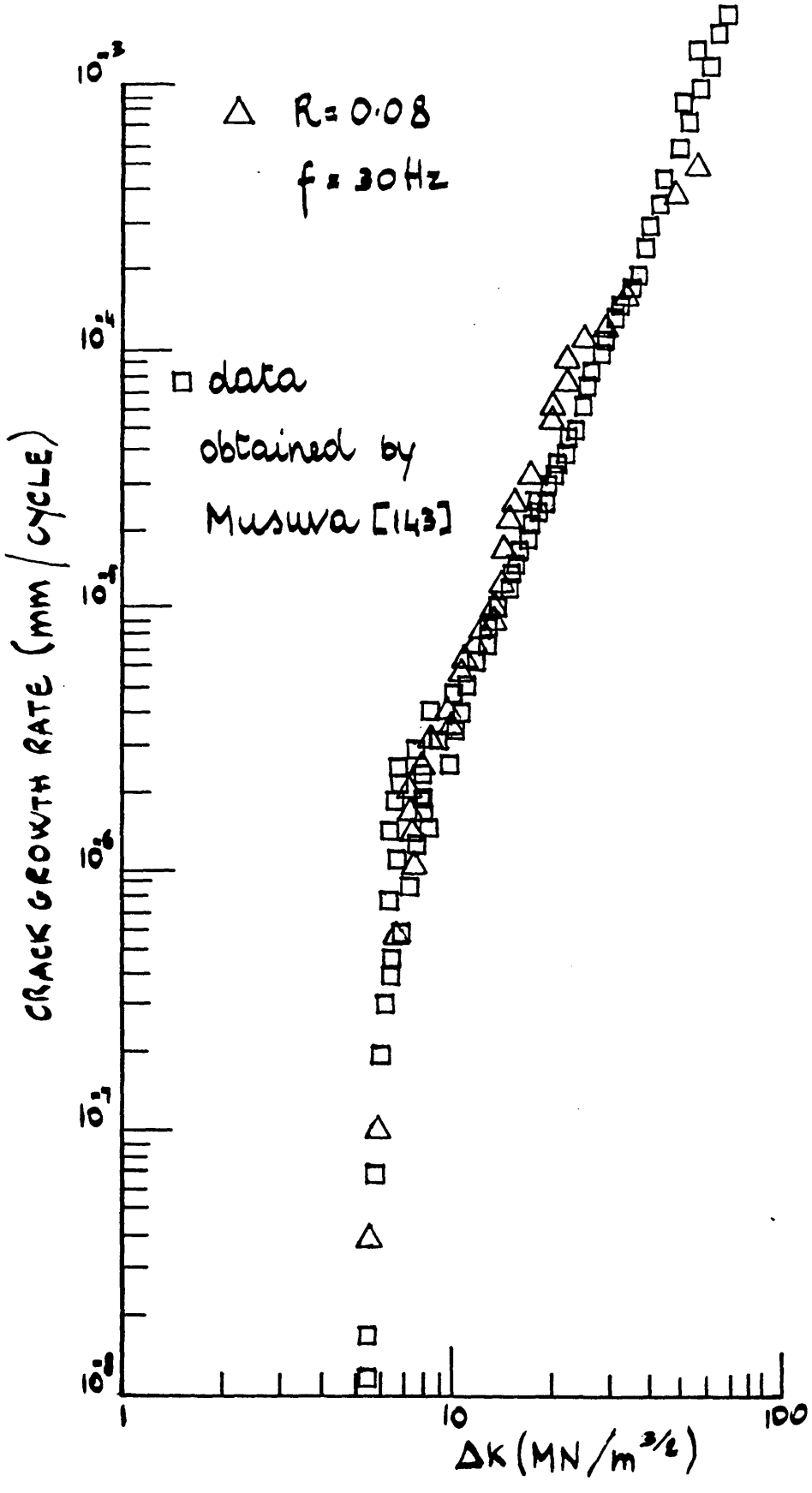


Figure A.1 Comparison of results obtained from the present study and those of Musuva [143].

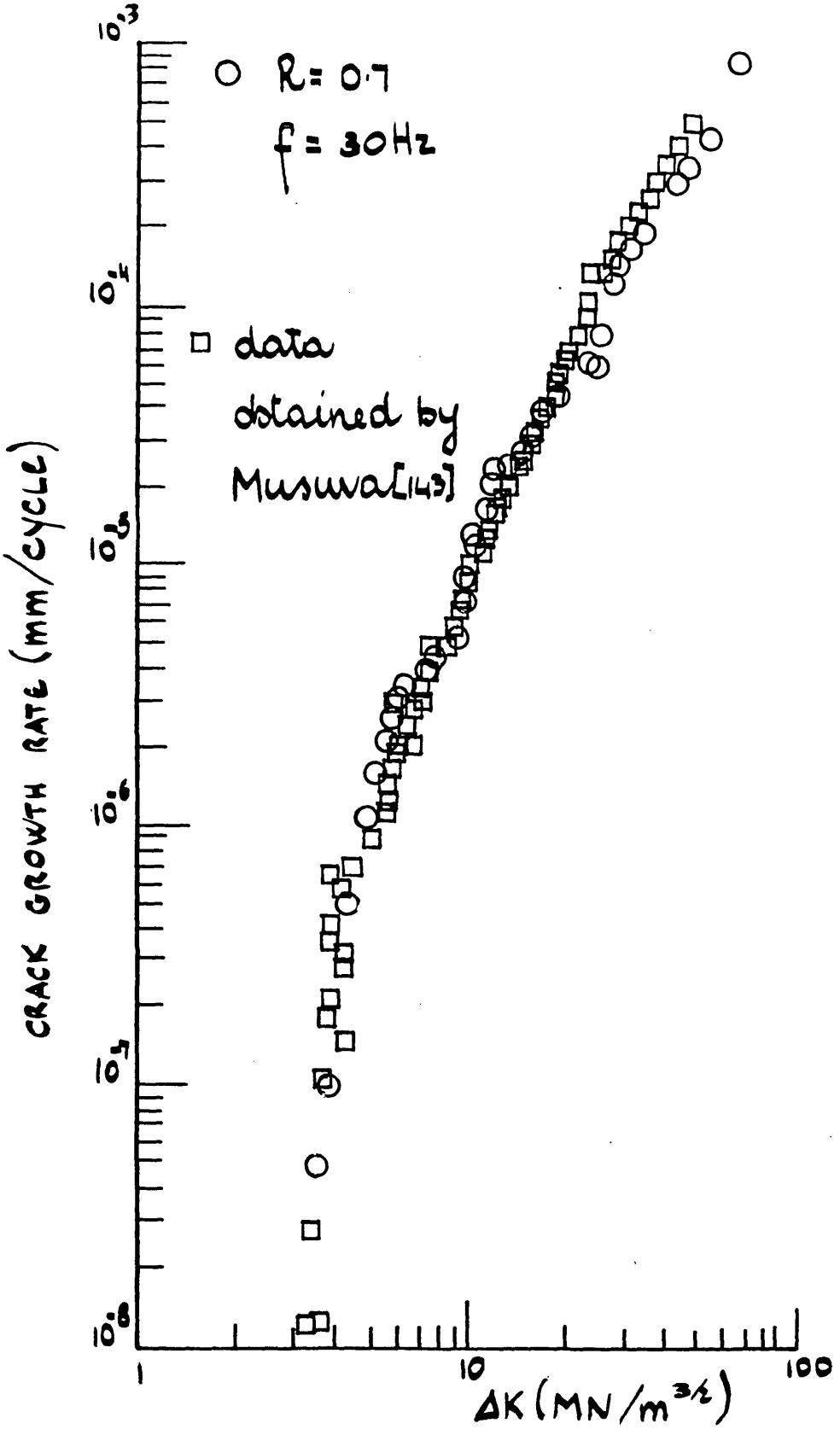


Figure A.2 Comparison of results obtained from the present study and those of Musuva [143].

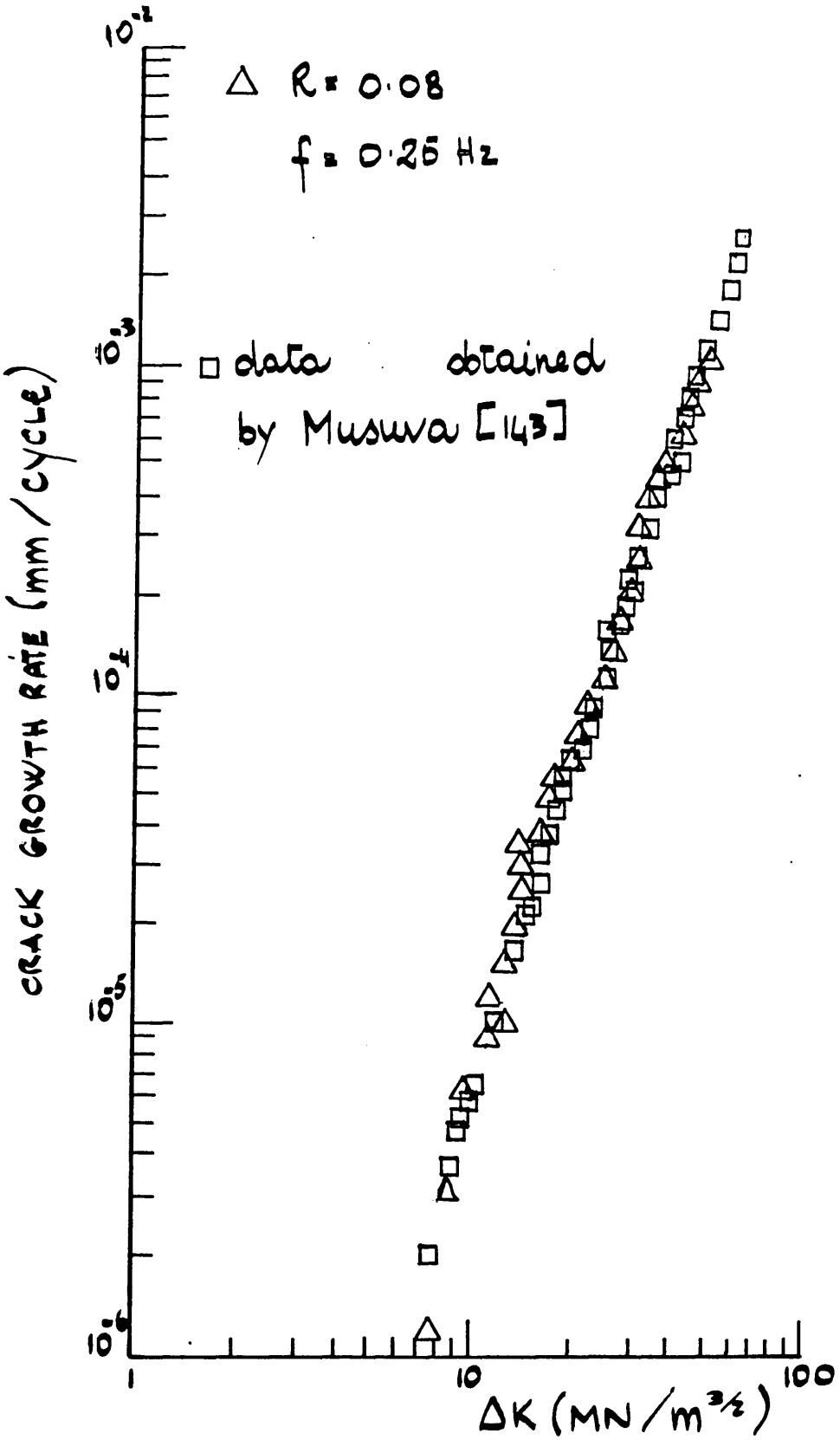


Figure A.3 Comparison of results obtained from the present study and those of Musuva [143].

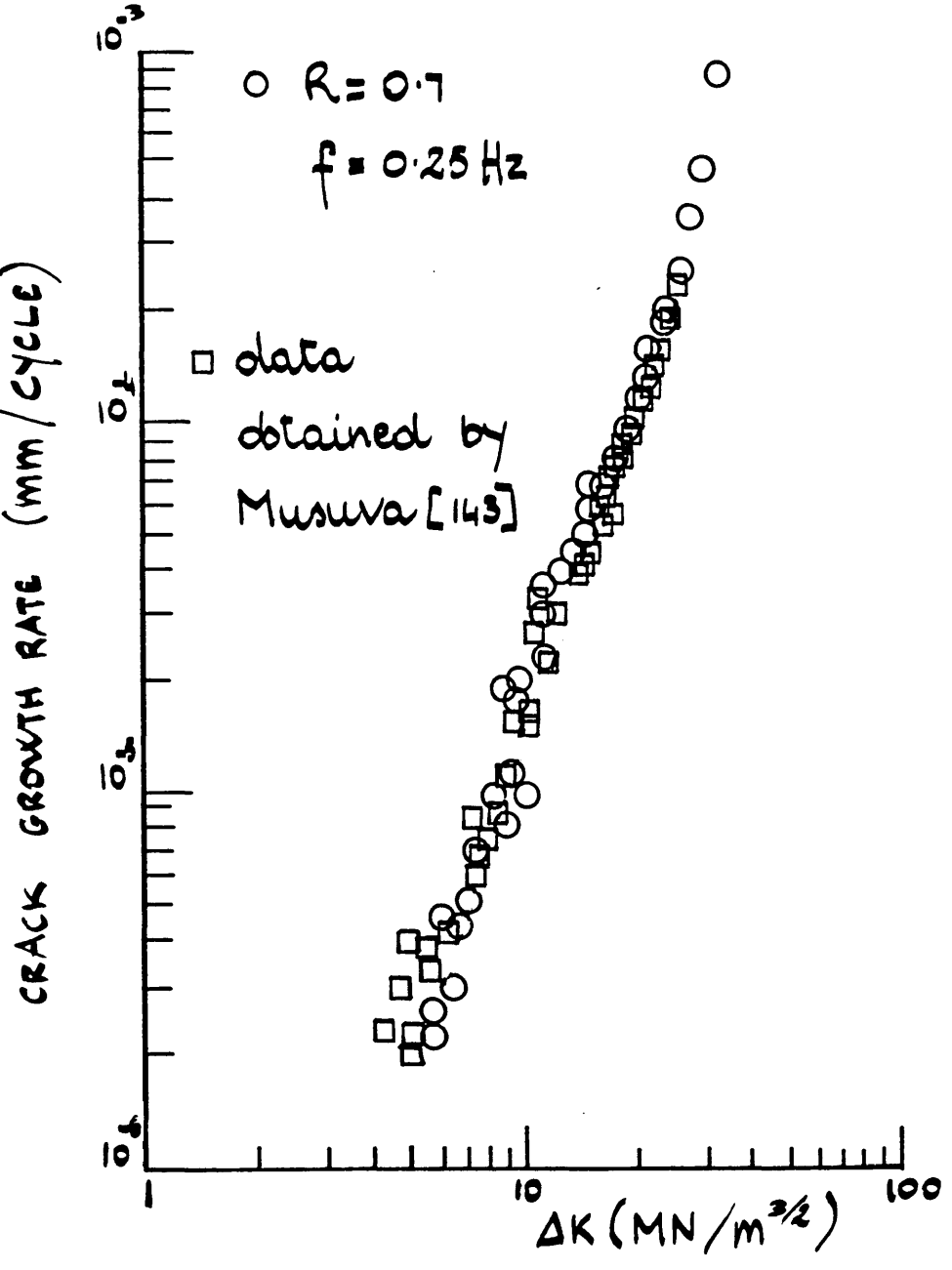


Figure A.4 Comparison of results obtained from the present study and those of Musuva [143].

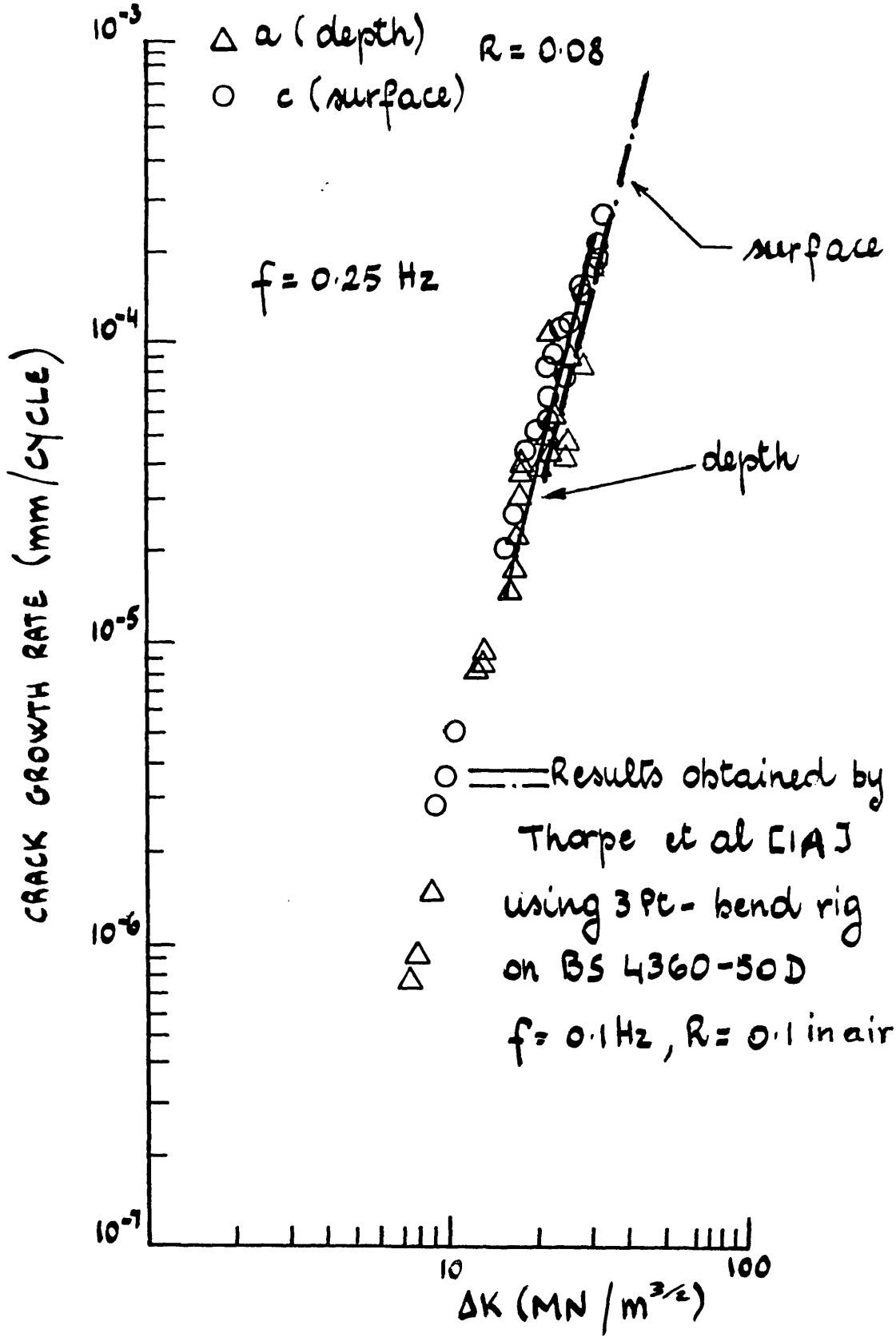


Figure A.5 Comparison of results obtained in the present investigation with those obtained by Thorpe et al.

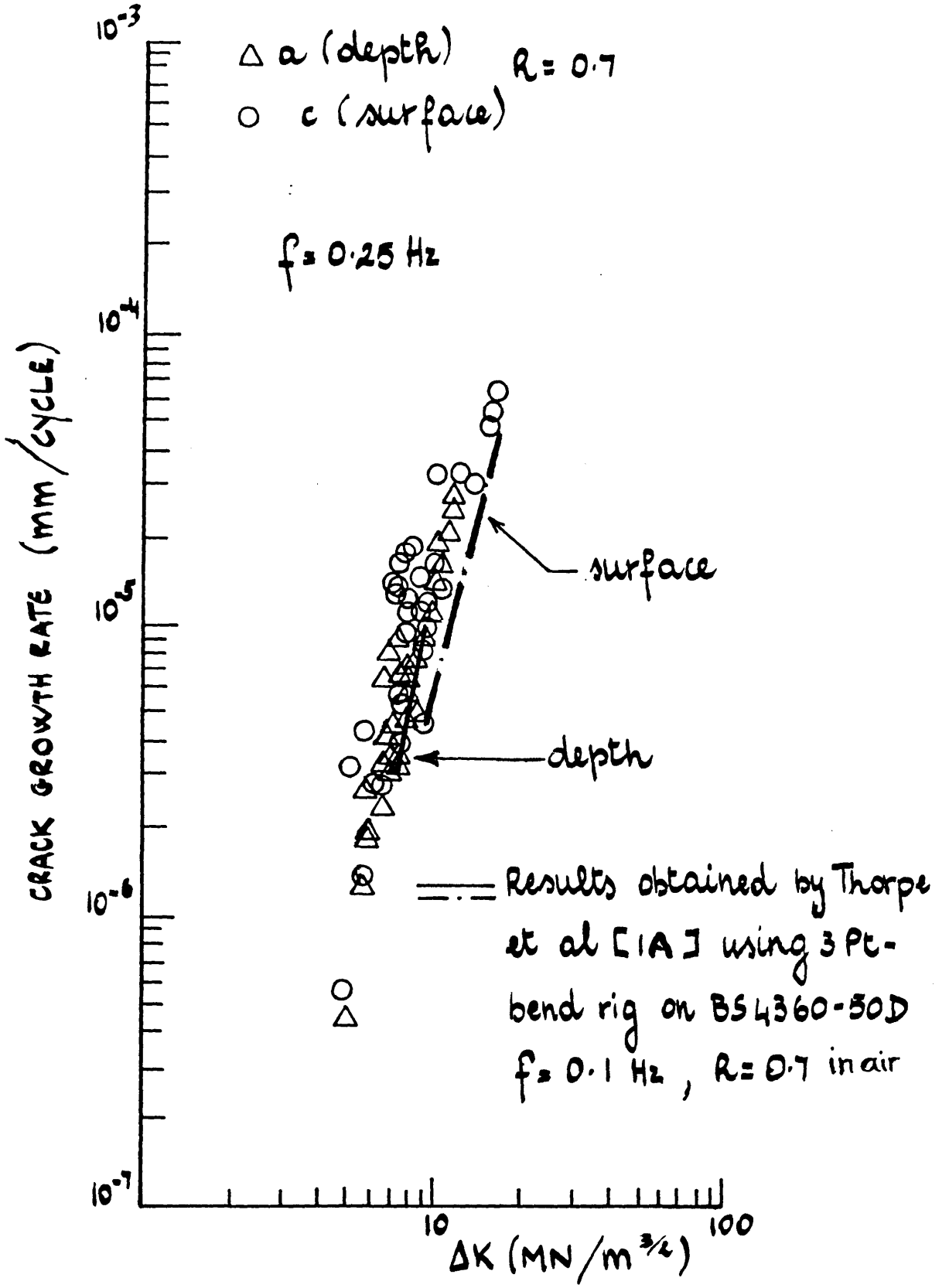


Figure A.6 Comparison of results obtained in the present investigation with those obtained by Thorpe et al.